Strategies to improve the biological performance of protein therapeutics

Dissertation zur Erlangung des naturwissenschaftlichen Doktorgrades der

Julius-Maximilians-Universität Würzburg

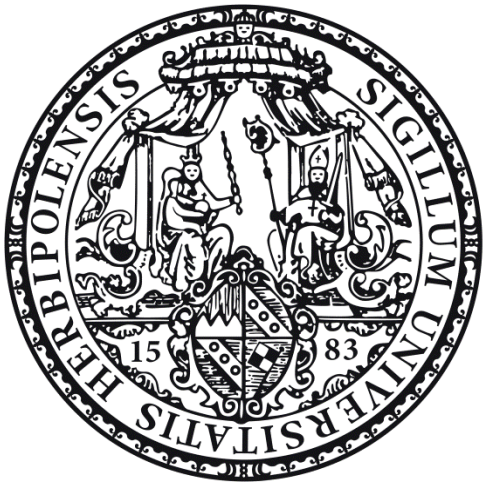

vorgelegt von

Eva Gador

aus Würzburg

Würzburg 2017

Eingereicht bei der Fakultät für Chemie und Pharmazie am

_____

Gutachter der schriftlichen Arbeit

1. Gutachter: _____

2. Gutachter: _____

Prüfer des öffentlichen Promotionskolloquiums

1. Prüfer: _____

2. Prüfer: _____

3. Prüfer: _____

Datum des öffentlichen Promotionskolloquiums

_____

Doktorurkunde ausgehändigt am

_____

Die vorliegende Arbeit wurde in der Zeit von März 2012 bis Dezember 2017

am Institut für Pharmazie und Lebensmittelchemie

der Bayerischen Julius-Maximilians-Universität Würzburg

unter der Anleitung von

Prof. Dr. Dr. Lorenz Meinel

und

PD Dr. Tessa Lühmann

angefertigt.

Table of contents

1 Introduction

Biopharmaceutical drugs such as peptides, therapeutic proteins, hormones, enzymes, vaccines, monoclonal antibodies and antibody-drug conjugates have conquered the global market since the early 1980s [1]. Biopharmaceuticals also known as biologics are produced by living organisms and are mostly used as therapeutics, *in vivo* diagnostics or vaccines. The approval of recombinant human insulin (Humulin®, Eli Lilly,) in the United States by the Food and Drug Administration (FDA) to treat diabetes mellitus in 1982 was the beginning for the development of new biopharmaceutical drugs against a variety of indications such as rheumatoid arthritis, multiple sclerosis, cancer or anemia [2]. Until now about 239 therapeutic proteins and peptides have been approved by the FDA for treating several diseases and numerous biologics are in clinical development [2, 3]. Beside the recombinant versions of natural proteins, new therapeutic proteins have been engineered with increased therapeutic potential such as insulin analogs. By replacing one to three amino acids the rapid-acting analogs insulin lispro (Humalog®, Eli Lilly, 1996), insulin aspart (NovoRapid® (1999) and Novolog® (2001), Novo Nordisk) and insulin glulisine (Apidra®, Aventis, 2004) as well as the long acting analogs insulin glargine (Optisulin® and Lantus®, Aventis, 2000) and insulin detemir (Levemir®, Novo Nordisk, 2004) have been created [4]. Insulin lispro approved in 1996 was the first genetic altered biologic with varied biological performance on the market [2]. Since 2007 such modified biopharmaceuticals with improved pharmacological properties or additional characteristics aiming at the same target are called “Biobetters” [5].
In contrast to small molecules, biologics benefit by high specificity and potency as well as decreased side effects and toxicity because of their structural complexity [1]. However, the complex three-dimensional structure of such biological macromolecules is the reason why the formulation and the delivery of biopharmaceutical drugs is still a challenge. During production and storage of biopharmaceutical therapeutics the preservation of potential physical degradation processes such as unfolding, misfolding and aggregation that can lead to immune responses by the development of tailor-made protein formulations is of paramount importance [6]. Moreover, the large molecular mass and the short serum half-life of biologics pose hurdles for their administration requiring delivery systems adapted for the protein of interest and its application [7].

1.1 Overview of different delivery technologies for protein therapeutics

Intravenous, intramuscular and subcutaneous injections are the administration routes of choice but due to limitations of injections such as the required sterility, the discomfort for patients and the fast renal clearance, alternative delivery routes have been proposed including buccal, nasal (Fortical®, salmon calcitonin, Upsher-Smith Laboratories/Unigene), ocular (Lucentis®, ranibizumab, Roche/Genentech; Eylea®, aflibercept, Regeneron/Bayer), oral, pulmonary (Pulmozyme®, dornase-α, Roche/Genentech; Exubera®, insulin, Pfizer, withdrawn 2008; Afrezza®, insulin,

MannKind), rectal, transdermal and vaginal (**Figure 1**) [1]. Until now just few alternatives to injections are on the market demonstrating the hardness of adequate alternative delivery routes for biopharmaceuticals because of biophysical properties as well as biological barriers.

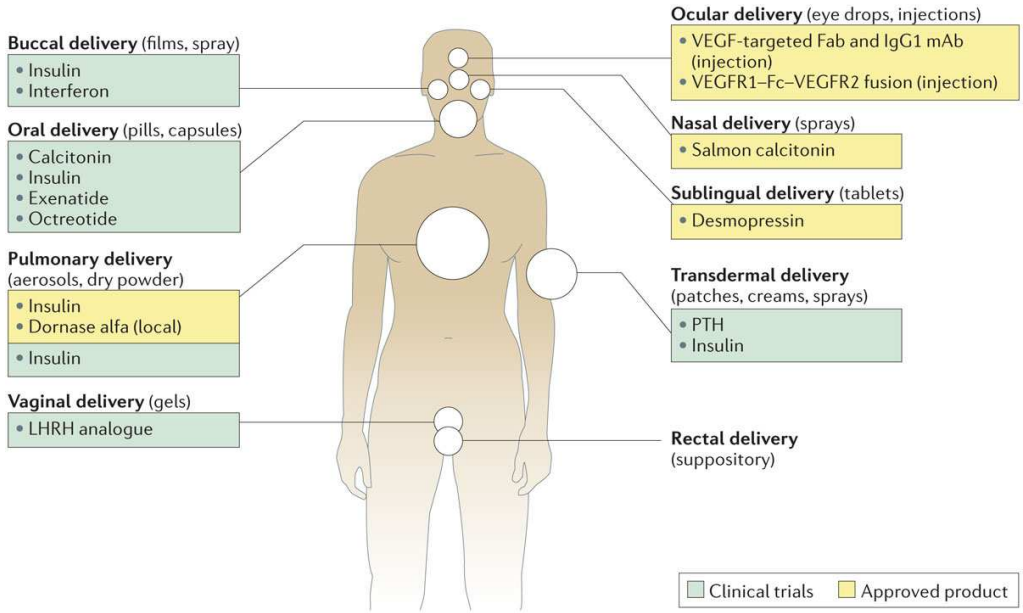

Figure 1: Alternative routes of biopharmaceutical delivery**.** Reprinted by permission from Macmillan Publishers Ltd: Nature Reviews Drug Discovery [1], copyright (2014).

Via the oral administration route, the most convenient way to administer drugs, biopharmaceuticals are degraded via enzymes and hydrolysis in the gastrointestinal tract (GIT) and absorption is hindered due to their size, their low lipophilicity and charged functional groups [8].

Transdermal delivery of biologics circumvents degradation in the GIT as well as the hepatic first-pass metabolism of short half-life drugs. However, the skin has to be passed, a barrier that allows diffusion of lipophilic molecules smaller than 500 Dalton and seems to be impenetrably for large biopharmaceutical drugs of hydrophilic nature [9].

The administration of biologics via mucosal membranes in the mouth, the buccal route, has the advantage of avoiding GIT and the first pass effect as well, but the surface area for absorption is low and the permeability of the buccal mucosa is as low as in the GIT for proteins. In addition, the constant flow of saliva and its containing enzymes further reduce the ability of proteins to permeate buccal mucosa [10].

Via the vaginal route the first pass metabolism is bypassed, too, and the large surface area as well as the rich blood supply are advantageous, but in common with other mucosal sites the permeability of vaginal mucosa is low for macromolecular drugs [11]. Besides, cyclic changes in histology and physiology of the vagina are disadvantageous for consistent drug absorption and even vaginal enzyme activity alters with the menstrual cycle [11].

The pulmonary route of administration offers a large surface area for absorption as well as good vascularization optimal for a rapid systemic uptake and a high bioavailability. But therefore an

appropriate formulation and delivery system is needed to reach the alveolar epithelium deep in the lung where absorption takes place [12]. For instance, Schultz et al. successfully developed a pulmonary insulin-like growth factor I delivery system using silk fibroin (SF) as well as trehalose as carriers [13].

Less technologically demanding than the pulmonary route is the nasal delivery of biopharmaceuticals where the site of absorption is reached easily but the mucosal membrane permeability is low and enzymatic degradation has to be circumvented as well [14].

The rectal administration is a favored route for drugs with low molecular mass especially for babies and young children to avoid first pass metabolism. The low enzymatic activity and the neutral pH is advantageous compared to buccal, nasal, pulmonary or vaginal protein administration, however, the bioavailability is similarly low and limited surface area and dissolution problems are disadvantages [15].

As mentioned above all alternative routes have their limitations, especially peptide degrading enzyme activity and the low permeability of the respective barrier for macromolecular drugs of hydrophilic nature impede the boost of bioavailability. However, clinical trials are going on in order to find formulation-based approaches to overcome these drawbacks.

Another way to circumvent frequent injections, rapid renal clearance and low *in vivo* stability of proteins are sustained release systems. The development of such drug delivery systems began in the 1970s with the encapsulation of large molecular weight compounds in polymers. In 1972 Davis [16] reported of polyacrylamide implants containing insulin that were able to control diabetes over a few weeks after subcutaneously deposition by injection and in 1976 Langer et al. [17] showed that several biocompatible polymers are suitable for sustained release of proteins and peptides over 100 days if used in the appropriate concentration and formulation. Until now several controlled release systems have been studied such as implants, microspheres, nanoparticles, liposomes or in situ injectable gels triggered by pH, temperature or ions [18]. Poly(lactic-co-glycolic acid) (PLGA) is widely used for the encapsulation of macromolecular drugs because of its biocompatibility and biodegradability. The encapsulation process, the lactic acid to glycolic acid ratio of the PLGA polymer, the porosity, the protein loading, the size of the drug and in the case of particles the size of the micro- or nanoparticles play a crucial role for the drug release rate and have to be adjusted in order to find the desired release profile for the drug of interest [1]. Several PLGA based controlled release pharmaceutical formulations are approved by the FDA and/or EMA as for example the implant Zoladex® (goserelin acetate / PLGA, AstraZeneca, 1989) for the goserelin delivery over a period of 1 to 3 months or Bydureon® (exenatide / PLGA, Eli Lilly, 2012) containing encapsulated exenatide in PLGA microspheres that has to be injected subcutaneously once a week compared to Byetta® (exenatide, Eli Lilly, 2005) that has to be injected twice a day [1, 19]. Despite these great achievements for controlled protein delivery in the last decades, there are still some hurdles to take to retain protein stability during encapsulation process as well as during

degradation under physiological conditions. The formation of lactic and glycolic acid during PLGA degradation results in an acidic microenvironment that is harmful for protein stability. Hydrolysis or aggregation of the protein can be the consequence and result in loss of activity. The incorporation of the antacid magnesium hydroxide has been shown to buffer the releasing acids and protect the protein from hydrolysis and aggregation [20].

Liposomes were first mentioned in 1964 by Bangham et al. [21]. Until now several liposomal drug delivery systems including small molecular drugs are on the market as vaccine adjuvants, anti-infective agents and for the treatment of cancer but none with a therapeutic protein [22, 23]. Liposomes are able to encapsulate lipophilic drugs in the bilayer membrane as well as hydrophilic drugs such as therapeutic proteins in the aqueous core. Moreover, therapeutic proteins can be covalently conjugated to or adsorbed on the surface of the liposomes. A sucrose-formulated Factor VIII product (rFVIII-FS; Kogenate® FS, Bayer), that is already FDA approved since 1993 for the treatment of hemophilia A, is now under clinical investigation again in combination with PEGylated liposomes (BAY 79-4980) [2, 24]. After reconstitution, factor VIII is adsorbed to the PEGylated liposomes leading to a prolonged bleeding free interval compared to Kogenate® alone as well as a decreased detection by the immune system [24, 25].

The first *in situ* injectable gel was developed by Dunn et al. in 1990 [26] based on polymer precipitation and was later called Atrigel® technology (Atrix Laboratories). Biodegradable, biocompatible FDA approved polymers like poly (dl-lactide), lactide/glycolide copolymers or lactide/caprolactone copolymers are dissolved in a biocompatible organic solvent such as N-methyl-2-pyrrolidone (NMP) [27, 28]. Directly before injection the drug of interest is suspended in the polymer solution forming a suspension. In situ a solid implant is formed releasing the drug in a controlled manner. The release interval can be adjusted by modifying the molecular weight and/or the composition of the polymer [28]. For instance, Eligard® (Astellas Pharma, 2002) contains leuprolide acetate in a depot formulation based on this Atrigel® technology allowing sustained release of leuprolide acetate after subcutaneous application over 1, 3 or 4 months [29]. Recent studies show the success of developing a drug delivery system for insulin by incorporating insulin complexed with zinc and chitosan in a thermosensitive poly(lactic acid)-poly(ethylene glycol)-poly(lactic acid) (PLA-PEG-PLA) polymer that forms a gel at physiological temperature of 37 °C [30]. Various delivery systems exist for small and hydrophobic molecules and progress has been made over the last decades to develop delivery systems for biopharmaceuticals. However, there is a still a need to improve such systems in order to remain their biological activity because each delivery system bears its own advantages and limitations (**Table 1**).

Method	Advantages	Limitations
Microparticles	• Controlled release can be achieved • Delivery is possible using subcutaneous injections	• Burst release can occur, which causes the potential for local toxicity and wastage • Burst release can be associated with adverse events related to peak serum exposure
Depot injections	• The same parent drugs can be formulated in several dosage forms (such as weekly, monthly, quarterly or semi-annual formulations) • The delivery technology can be applied to a large number of compounds • Lower burst release (in implants) • Avoids the requirement for reconstitution and/or suspension (in implants)	• Larger gauge needle can be required (for injections), or incisions need to be made into the skin (for implants)
Nanoparticles	• Targeted delivery: small size allows enhanced permeation into tumours and retention in tumours • Has high adjuvancy for vaccine applications	• Non-specific uptake in reticuloendothelial system (RES) organs • Immunotoxicity can occur
Jet injections	• Allows a needle-free approach • Has a long history of use • Works with injectable formulations • Broad applicability without the need to modify the design of injectors • Rapid systemic absorption	• Cause occasional pain and bruising • Inconsistent delivery of drug
Pumps	• Precise control over rates of delivery • Long duration of delivery	• Implanted devices are invasive • Infection can occur with patch pumps
Transdermal delivery	• Painless and sustained delivery • Allows for active control and discontinuation of delivery • High patient compliance	• Low bioavailability (potentially addressable with advanced technologies) • Some devices are bulky and expensive
Pulmonary delivery	• High bioavailability • Rapid systemic uptake • Ease of use	• Some devices are bulky • Potential for local toxicity and immunogenicity
Oral delivery	• Ease of use • High patient compliance	• Low bioavailability (potentially addressable with advanced technologies) • Enzymatic degradation in the stomach or liver • Variable absorption • Interference in absorption rates from food
Other mucosal routes (vaginal, nasal and buccal)	• Non-invasive • Ease of use	• Low bioavailability (potentially addressable with advanced technologies) • Enzymatic degradation • Variable absorption

*The summary presented in this table offers a generalized description of several delivery methodologies. Exceptions to generalized descriptions exist in certain cases and ongoing research is actively addressing the limitations discussed throughout the main text.

Table 1: Comparison of different delivery technologies for biopharmaceutical drugs. Reprinted by permission from Macmillan Publishers Ltd: Nature Reviews Drug Discovery [1], copyright (2014).

1.2 Protein modification to improve biological performance

Most biologics have a very fast *in vivo* clearance upon intravenous injection limiting their therapeutic potential [31]. Possible ways to improve their biological and pharmacological properties are the conjugation to polyethylene glycol (PEG) in order to increase the size of the protein and decrease glomerular filtration by the kidney, or the fusion of the protein to a naturally long half-life protein such as human serum albumin (HSA) [32], transferrin [33] or the Fc domain of human immunoglobulin G (IgG) [34, 35].

The modification of therapeutic proteins by PEGylation was first reported by Abuchowski et al. [36] in 1977 and has become a popular method to improve pharmacokinetic properties of therapeutic proteins. Linear as well as branched PEG polymers exist with various chain lengths selectable compliant with the pharmacokinetic requirements of the target protein. PEG is described as non-toxic, non-immunogenic and non-degradable and according to the FDA PEG can be generally regarded as safe (GRAS) [37, 38]. As a result, many PEGylated proteins conquered the global market over the last 25 years and numerous protein-PEG conjugates are still under clinical investigation. Adagen® (PEGylated adenosine deamidase, Enzon, 1990 (USA)) was the first

PEGylated protein on the market approved by the FDA in 1990 [39]. Until now several PEGylated proteins are approved by the FDA and/or EMA such as Adynovate® (PEGylated Factor VIII, Baxter, 2015 (USA)) and Plegridy® (PEGylated interferon-β-1a, Biogen, 2014 (EU)) [40]. In 2013 Neulasta® (Pegfilgrastim, PEGylated G-CSF, Amgen, 2002 (USA)) was one of the top 10 product sales of biopharmaceutical products generating 4.39 billion US dollar [2]. Besides the prolonged half-lives resulting from increased molecular mass and increased stability towards enzymatic degradation, immune response is decreased through PEGylation due to steric hindrance [41, 42].

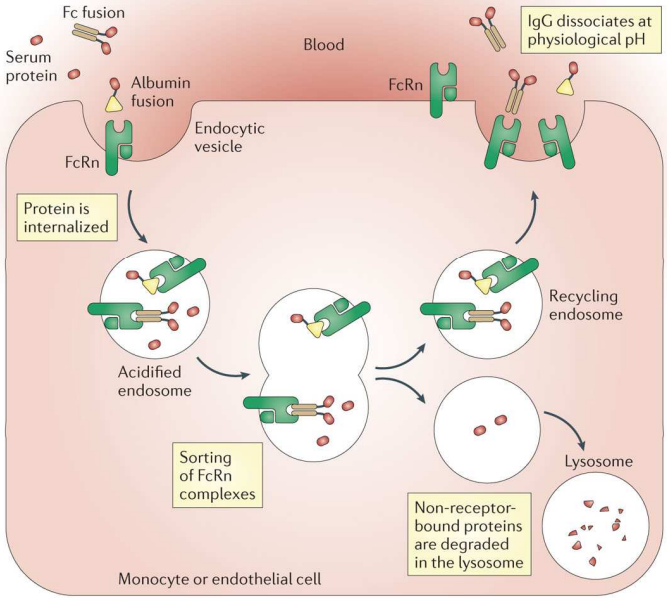

Figure 2: FcRn recycling mechanism**.** Reprinted by permission from Macmillan Publishers Ltd: Nature Reviews Drug Discovery [1], copyright (2014).

The so-called Fc-fusion proteins consist of the crystallizable fragment (Fc) of an antibody and the protein of interest which is directly attached to the flexible hinge region via a specific linker [35]. The fusion to the Fc fragment drastically increases serum half-life due to its interaction with the salvage neonatal Fc-receptor (FcRn) (**Figure 2**) [43] as well as due to decreased renal clearance rate because of the larger size of the molecule [44].

Moreover, the stability as well as solubility is improved by fusion to Fc domain [45]. In 1989, the first Fc-fusion protein, CD4-Fc-fusion protein for treating HIV, was described by Capon et al. [46]. This was the beginning for the development of novel approaches in order to improve safety and efficacy of Fc-fusion proteins [35]. Until now eleven Fc-based fusion proteins are on the market such as the blockbuster Enbrel® (Etanercept, Amgen/Pfizer, 1998), the first Fc-fusion protein on the US market in 1998, consisting of the extracellular domain of TNF receptor II and the Fc domain of IgG1 or Eloctate® (Biogen, 2014), containing coagulation Factor VIII (antihemophilic factor) fused to Fc part of IgG1 (**Table 2**), and several Fc-fusion proteins are still in clinical trials

such as Revacept® (PR-15, advanceCOR) consisting of extracellular domain of glycoprotein VI (GPVI) and Fc part of IgG1 (**Table 3**) [1, 2, 47].

Parent drug	*Drug*	*Indication*	*Commercial Stage*
TNF receptor 2 (TNFR75) + IgG1 Fc	Etanercept (Enbrel®, Amgen/Pfizer)	Rheumatoid arthritis, ankylosing spondylitis, polyarticular juvenile idiopathic arthritis, psoriatic arthritis, plaque psoriasis	Approved 1998 USA 2000 EU
LFA-3 + IgG1 Fc	Alefacept (Amevive®, Astellas Pharma/Biogen Idec)	Severe chronic plaque psoriasis	Approved 2003 Withdrawn 2011
CTLA-4 + IgG1 Fc	Abatacept (Orenica®, Bristol-Myers Squibb)	Rheumatoid arthritis, juvenile idiopathic arthritis, psoriasis	Approved 2005 2007 EU
IL-1R + IgG1 Fc	Rilonacept (Arcalyst®, Regeneron)	Cryopyrin-associated periodic syndromes (CAPS)	Approved 2008 USA 2009 EU withdrawn 2012 EU
Thrombopoietin binding peptide + IgG1 Fc	Romiplostim (Nplate®, Amgen)	Chronic idiopathic thrombocytopenia purpura	Approved 2008 2009 EU
VEGF receptor 1 + 2 + IgG1 Fc	Aflibercept (Eylea®, Regeneron/Sanofi)	Neovascular (wet) age-related macular degeneration	Approved 2011 USA, 2012 EU
VEGF receptor 1 + 2 + IgG1 Fc	ziv-aflibercept (Zaltrap®, Regeneron/Sanofi)	Metastatic colorectal cancer	Approved 2012 USA, 2013 EU
CTLA-4 + IgG1 Fc	Belatacept (Nulojix®, Bristol-Myers Squibb)	Prophylaxis of organ rejection in adults receiving a kidney transplant	Approved 2011 USA and EU
Factor IX + IgG1 Fc	rFIXFc (Alprolix®, Biogen Idec)	Hemophilia B	Approved 2014 USA 2016 EU
Factor VIII + IgG1 Fc	rFVIII-Fc (Eloctate® (USA) Elocta® (EU), Biogen Idec)	Hemophilia A	Approved 2014 USA 2015 EU
GLP-1 + IgG4 Fc	Dulaglutid (Trulicity®, Eli Lilly and Company)	Diabetes, Type 2	Approved 2014 USA and EU
TNF receptor 2 (TNFR75) + IgG1 Fc	Etanercept (Benepali®, Biogen/Samsung Bioepis) 1st Biosimilar	Moderate to severe rheumatoid arthritis, psoriatic arthritis, non-radiographic axial spondyloarthritis and plaque psoriasis in adults	Approved 2016 EU

Table 2: Fc-fusion proteins approved by FDA and/or EMA. Adapted by permission from Macmillan Publishers Ltd: Nature Reviews Drug Discovery [1], copyright (2014).

Parent drug	*Drug*	*Indication*	*Commercial Stage*
sIL-4R	Altrakincept (Nuvance)	Asthma	Phase III
Angiopoietin 1 and 2 binding peptide	Trebananib (AMG386)	Cancer (various)	Phase III
B cell activating factor	Blisibimod, A-623	Systemic lupus erythematosus	Phase III
TNFR55	Lenercept	Rheumatoid arthritis, severe sepsis	Phase III
Tumor necrosis factor receptor superfamily member 13B (TACI)	Atacicept	Systemic lupus erythematosus; multiple sclerosis	Phase II/III
VEGFR 1 + 2	KH902	AMD-associated choroidal neovascularization	Phase II
CD4	PRO542	HIV	Phase II
Activin Receptor IIA extracellular domain	Sotatercept, ACE-011	Anemia	Phase II
Soluble activin type IIB receptor	ACE-031	Duchenne muscular dystrophy	Phase II
Cytotoxic T-lymphocyte antigen 4 (CTLA-4)	ASP2408	Rheumatoid arthritis	Phase II
Lymphotoxic-beta receptor	Baminercept alfa, BG-9924	Sjögren's syndrome rheumatoid arthritis	Phase II
Activin receptor-like kinase 1 (ALK1)	Dalantercept, ACE-041	Advanced renal cell carcinoma; advanced hepatocellular carcinoma; recurrent endometrial carcinoma	Phase II
Recombinant P-selectin glycoprotein ligand	YSPSL, TS-1	Ischemia reperfusion injury	Phase II
Fibroblast growth factor receptor 1c	FP-1039, GSK3052230	Squamous non-small cell lung cancer; mesothelioma	Phase I
CD95 receptor extracellular domain	APG101	Myelodysplastic syndromes Glioblastoma	Phase I
extracellular domain of human glycoprotein VI + IgG1 Fc	PR-15 (Revacept®, advanceCOR)	Inhibitor of platelet adhesion in symptomatic carotid stenosis	Phase II

Table 3: Fc-fusion proteins in clinical development. Adapted by permission from Macmillan Publishers Ltd: Nature Reviews Drug Discovery [1], copyright (2014).

Human serum albumin has a molecular mass of 67 kDa and a serum half-life of 19 days making it suitable as fusion partner in order to extend serum half-life of smaller proteins through neonatal Fc receptor (FcRn) recycling (**Figure 2**) [34]. In 1992, the first fusion protein with human serum albumin and CD-4 as fusion partner was described by Yeh et al. [48]. In addition to Alprolix® (eftrenonacog alfa, Biogen, 2014), a fusion protein of factor IX and the Fc part of IgG1 that is marketed since 2014 with a serum half-life of 82 h [49], another factor IX drug with prolonged serum half-life of 92 h, Idelvion® (albutrepenonacog alfa, CSL Behring, 2016), a fusion protein of factor IX and albumin was approved by the FDA [50] and EMA [51] in 2016 for the treatment of hemophilia B [52]. Both fusion proteins need less frequent dosing compared to currently available factor IX products with serum half-lives between 17–19 hours such as BeneFix® (Nonacog alfa, Pfizer/Wyeth, 1997) [49]. In 2014 Tanzeum® (albiglutide, GSK, 2014) an albumin fusion protein with glucagon-like peptide 1 (GLP-1) was approved by the FDA for the therapy of type-2-diabetes.

In contrast to Victoza® (liraglutide, Novo Nordisk, 2010) containing a GLP-1 analog with attached fatty acid, which has to be administered daily, Tanzeum® has just to be injected subcutaneously once a week [2, 34].

The long persistence of transferrin in human serum is caused by its molecular weight (80 kDa) as well as a clathrin-dependent transferrin receptor-mediated recycling of transferrin and amounts to 12 days [34, 53]. A transferrin fusion protein platform was established in 2002 from BioRexis® Technologies (acquired by Pfizer in 2007) in order to focus on research for protein engineering technologies based upon transferrin. Their fusion product of transferrin with GLP-1 for the treatment of type 2 diabetes reached a significantly elongated serum half-life compared to GLP-1, however, clinical trials are still expected [34, 54]. Until now no transferrin fusion protein is on the market, but several are under preclinical investigation such as exendin-4-transferrin fusion protein [54], proinsulin-transferrin fusion protein [55] or G-CSF-transferrin fusion protein [56].

1.3 Challenges in the development of injectable protein formulations

Regardless whether the biopharmaceutical drug is administered intravenous, subcutaneous or intramuscular, there is a need for the development of a formulation that prevents the loss of biological activity of the therapeutic protein during filling, shipment, storage and the appropriate administration. Light exposure, temperature changes as well as freeze-thaw cycles can influence protein stability during all these steps and the primary packaging material or the application device might interact with the protein [57]. This has to be considered and even examined in accelerated stability and forced degradation studies. In such studies the protein is exposed to conditions that are harsher than in reality in order to produce degradation products and to predict degradation kinetics in a short period of time [58]. In order to develop the optimal formulation, it is advantageous to know physico-chemical characteristics and potent degradation pathways of the protein of interest making it possible to add specific agents to prevent or at least minimize these degradation mechanisms. Important herein is the chemical and physical stability, however, immunogenicity has to be taken into account as well. Instabilities caused by aggregation, oxidation, deamidation, hydrolysis, protein fragmentation or denaturation may lead to loss of activity and therefore have to be prevented. Therefore, some additives can be added such as reducing agents to prevent oxidation or polysorbates in order to avoid the formation of aggregates. It is recommended to use additives that are already used in marketed products for the same route of administration and with a similar application profile in order to avoid additional pre-clinical and clinical studies [58]. Moreover, the stability of the protein depends on its concentration, pH and ionic strength of the formulation as well as on the storage temperature [59].

1.4 The role of protein delivery in tissue engineering

Tissue engineering uses living cells and biocompatible biomaterials, sometimes in combination with certain growth factors in order to create functional biological constructs that can help to repair or even replace tissues damaged by disease, injury or age. Despite the term “tissue engineering” being born in the 20th century, even ancient Egyptians used elements of tissue engineering. The Papyrus of Ebers from 1500 B.C. describes the use of lint as fibrous scaffold, grease as barrier against pathogens and honey as antibiotic for wound healing [60]. Wolter and Meyer [61] were the first who used the term “tissue engineering” in a publication about the formation of a endothelium-like membrane on the inside of a successful keratoprosthesis. Just few years later Langer and Vacanti [62] made the field of tissue engineering as we know it today popular and aroused the interest of many researches. Until now, promising results are primarily obtained in the area of bone [63] and cartilage repair [64] as well as skin replacement [65], but research is done for nerve regeneration [66], blood vessel formation [67], engineering of liver [68] and even the heart [69] as well.

Growth factors are naturally secreted from cells and regulate many cellular activities such as proliferation, differentiation, migration, adhesion, division as well as gene expression. Hence, growth factors play a pivotal role in the field of tissue engineering. Several growth factors are already FDA and/or EMA approved such as recombinant human insulin-like growth factor-I (IGF-I, Increlex®, mecaserim, Ipsen Pharma, 2005 (US), 2007 (EU)) for the treatment of growth failure in children with IGF-I deficiency, recombinant human keratinocyte growth factor (KGF, Kepivance®, palifermin, Swedish Orphan Biovitrum, 2004 (US), 2005 (EU)) for the treatment of severe oral mucositis, recombinant human platelet-derived growth factor BB (PDGF-BB) that was initially developed for the treatment of lower extremity diabetic neuropathic ulcers (Regranex® (becaplermin), Novartis/Johnson & Johnson, 1997 (US), 1999 (EU), withdrawn 2012 (EU)) and later used in a bone matrix of tricalcium phosphate for the treatment of periodontal bone defects and associated gingival recession (GEM 21S®, BioMimetic Pharmaceuticals, 2005 (USA)) as well [2]. In order to restore damaged tissue, the spatiotemporal delivery of such growth factors is essential to avoid local toxicity [70]. Despite many studies going on to investigate such controlled delivery systems, actually just few controlled release systems are on the market. A collagen carrier loaded with bone morphogenetic protein 7 (BMP-7) (OP-1® implant, Stryker Biotech) was approved by the FDA in 2001 for the treatment of bone fractures that do not heal after a normal period of time [71] and a collagen matrix loaded with BMP-2 (INFUSE® bone graft, Medtronic) was approved by the FDA in 2002 for the use in anterior lumbar interbody fusion spine surgical procedures [1]. In 2004 and 2007 INFUSE® bone graft received additional FDA approvals for the use in trauma and oral-maxillofacial (OMF) and the application of INFUSE® bone graft in a several fusion devices was approved by the FDA in 2015 [72].

Growth factors have great therapeutic potential, however, their clinical use is limited because of their poor protein stability, their short serum half-life as well as challenges during production such as low expression yields, high costs and especially the unsatisfying outcome of growth factor delivery out of existing controlled release systems [70]. Hence, there remain a lot of challenges that have to be focused on in the near future in order to develop safe and cost-effective controlled release systems providing an appropriate release rate of a bioactive growth factor.

2 Background and related work

The present work can be structured into three phases.

In **phase I** we focused on instability, stabilization and formulation of liquid protein pharmaceuticals. A new injectable formulation of PR-15 was developed. A short-term storage stability study under accelerated and stressed conditions yielded basic information about pH and stress dependent degradation mechanisms of PR-15. Based on the results from pH screening and forced degradation study excipients were chosen in order to prevent occurred degradation and tested in a DoE.

In **phase II** defined protein modification and coupling reactions as well as the characterization of such modified and coupled proteins were performed. Protein modification is an important tool for the development of biopharmaceuticals with the aim to generate new bioconjugates with maintained structural integrity and bioactivity but with altered features such as prolonged circulating half-life or increased stability.

In **phase III** model surfaces were biofunctionalized for cartilage tissue engineering. Controlled and localized release of required growth factors from matrices is favored for successful cartilage tissue engineering and to reduce potential side effects. Delivered growth factors have short *in vivo* half-lives limiting the successful product outcome. Covalent immobilization of such growth factors on matrices holds promise to maintain their bioactivity. The knowledge in protein modification and bioconjugation reactions as well as in protein characterization gained during phase II was used for covalent immobilization of growth factors and characterization of immobilized growth factors. Finally, cartilage tissue was engineered on biofunctionalized scaffolds using bone marrow-derived mesenchymal stem cells (BMSCs).

2.1 Injectable PR-15 formulation

2.1.1 PR-15

Revacept® is a solution of 40 mg PR-15 per vial for intravenous application. PR-15 is a dimeric fusion protein composed of the extracellular domain of human glycoprotein VI (GP VI, a platelet specific adhesion receptor), a short hinge region and the Fc region of human immunoglobulin G1 (IgG1) (**Figure 17B**) [73]. Two monomers of the fusion protein are covalently linked via intermolecular disulfide bonds in the hinge region. PR-15 is a lesion specific platelet adhesion inhibitor which prevents arterial thrombosis with the same efficacy as known antiplatelet agents but without bleeding risk [74]. PR-15 consists of 483 naturally occurring amino acids (**Figure 17A**). The signal sequence (amino acids 1–20) is cleaved off. Amino acids from 21 to 269 are involved in binding to the GP VI ligand collagen. The polypeptide sequence of the Fc part of the fusion protein covers the residues 275 to 503 [75].

2.1.2 pH screening and forced degradation study

Generally, the scope of pH screening and forced degradation studies is the determination of an adequate pH value for a new protein formulation to ensure the stability and bioactivity of the protein during storage and to obtain information on potential degradation pathways of the protein. Originally, PR-15 is formulated with a concentration of 2.4 mg/mL in PBS buffer, pH 7.4, with 4 % mannitol and 1 % saccharose. This formulation was found to be stable at -80 °C ± 10 °C as well as -25 °C ± 5 °C for at least two years (ongoing stability study at advanceCOR) but at 5 °C ± 3 °C two analyzed parameters were already out of specification after 2 and 6 months. During storage at 4 °C PR-15 mainly degrades to the so-called 90 kDa band [75]. Indeed this fragment is as bioactive as PR-15 itself, but in order to produce a stable protein formulation advanceCOR needs to understand this degradation process to be finally able to circumvent it. Moreover, advanceCOR aimes to develop a formulation that retains bioactivity of PR-15 at 4 °C for a more convenient handling during production, shipping and storage. Therefore, a pH screening and forced degradation study was ordered by advanceCOR.

Not only the pH value of the liquid formulation but also the buffering agent plays a pivotal role in protein stability. Amino acids, for example, are able to stabilize proteins as buffering agents, as antioxidants or by preferential exclusion. Former studies showed that the basic amino acids histidine, lysine and arginine stabilized IgG by binding to IgG side chains and thereby changing the structure of the water solvation shell [76]. These so-called cosolvents ensure that unfolding and aggregation are thermodynamically unfavorable. According to Falconer et al. [76] best results concerning IgG stability were obtained by the usage of the amino acid histidine shown by the highest increase of the unfolding transition temperature (T_m). As PR-15 contains the Fc region of human IgG1 we assumed that the amino acid histidine would be the best choice. Besides, histidine

is commonly used as buffering agent in marketed protein formulations (Herceptin® (Trastuzumab, Roche/Genentech) Xolair® (Omalizumab, Roche/Genentech), Synagis® (Palivizumab, MedImmune)) especially for high concentration monoclonal antibodies [77].
After choosing a 50 mM histidine buffer as formulation buffer for PR-15, four different pH values (pH 5.5, 6.0, 6.5 and 7.0) were chosen for the pH screening study in accordance with the isoelectric point (pI 4.5-5.0) of PR-15 [75]. The isoelectric point is the pH value at which the protein is net neutral charged making protein-protein interactions, and therefore its aggregation is highly probable [78]. Hence, the pH value of protein formulations should be adjusted at least one unit from the protein's isoelectric point [79]. To evaluate the stability of the PR-15 in 50 mM histidine buffer at the different pH values, the samples were incubated at 25 °C as well as 40 °C for 4 and 8 weeks and analyzed afterwards using different analytical methods. Additionally, a forced degradation study was performed to investigate degradation pathways under the different stressing conditions such as heat treatment, freeze-thaw cycles, acidic and basic pH, light exposure, induced oxidation and deamidation.

2.1.3 Design of Experiments

The performance of the pH screening and the forced degradation study provided some useful information narrowing the acceptable pH range and defining suboptimal conditions that had to be avoided or prevented by the addition of additives. In 50 mM histidine buffer, pH 7.0 exposed to be the most favorable pH value during pH screening. However, even at pH 7.0 the degradation of PR-15 reached a high degree. Hence, the formulation had to be further optimized by the usage of Design of Experiments (DoE). DoE and the following statistical analysis allows the evaluation of multiple factors and their interaction simultaneously saving time and money. Thermal stress, acidic conditions as well as light exposure led to a high degree of degradation products as well as aggregates of PR-15 during the forced degradation study. Therefore, thermal stress was chosen to stress the PR-15 solution during Design of Experiments before analyzing. To find the optimal formulation for PR-15 four factors (buffer, pH, Tween® 20 and methionine) were chosen and the responses (PdI, mean size, SEC and bioactivity (determined by collagen ELISA)) were specified. During this Design of Experiment phosphate buffer was tested versus histidine buffer, as well as pH 7.0 was tested versus pH 8.0. In addition, further excipients like Tween® 20 [80, 81] (0.1 %) as stabilizer against protein aggregation and to prevent surface adsorption as well as methionine [82] (20 mM) as reducing agent were chosen to be analyzed for optimization of the formulation.

2.2 Protein modification

Protein chemical modification is an important tool for generating modified proteins and has meanwhile become indispensable in the field of protein therapeutics and tissue engineering. It is of paramount importance to incorporate functional groups – preferably functional groups that naturally do not exist in proteins as for example azido or alkyne groups – in the protein of interest and/or in the used biomaterial in order to immobilize proteins on biomaterials or cells, to modify pharmacokinetic properties and the stability of the protein or to create therapeutic conjugates. During all kind of protein reactions biologically ambient conditions are absolutely essential, meaning < 37 °C, pH 6–8 in aqueous solution to preserve bioactivity of the protein and to prevent denaturation [83]. The combination of genetic and chemical methods as well as site-specific and non-site-specific coupling reactions offer a variety of possibilities adapted to the final application. Recently, biomaterials had successfully been functionalized with growth factors such as bone morphogenetic protein 2 (BMP-2) [84], vascular endothelial growth factor (VEGF) [85], fibroblast growth factor 2 (FGF-2) [86] and transforming growth factor β3 (TGF-β3) [86] through covalent coupling by the usage of 1-Ethyl-3-(3-dimethylaminopropyl)carbodiimide (EDC)/N-hydroxysuccinimide (NHS) chemistry with the aim to engineer bio-instructive scaffolds. A striking limitation of this non-site-specific EDC/NHS chemistry is that most biologic molecules carry both carboxyl and amino groups yielding crosslinking (intra- and/or intermolecular). These covalent aggregates may consequently lead to loss of function and pose an immunological challenge. Site-specific Cu(I) catalyzed azide-alkyne cycloaddition chemistry (CuAAC, click chemistry) promises to overcome this drawback. The suitability of this decoration method for biologics was investigated employing FGF-2 [87].

SF extracted from the cocoons of the silkworm *Bombyx. mori (B. mori)* [88] had found increasing use for tissue engineering application [89] due to its unique mechanical properties, as well as biocompatibility and biodegradability [90, 91]. SF lacks cell adhesion or growth factor binding sites, however, SF features various amino acid residues allowing bioconjugation of functional groups [92].

In this work, we directly compared the decoration of SF in solution by means of click chemistry and EDC/NHS chemistry, respectively. Firstly, we modified the tyrosine groups of the SF primary sequence with azido groups by means of a diazonium coupling reaction with 4-azidoaniline hydrochloride in analogy to what has been described before [93]. Secondly, we PEGylated the FGF-2 in a site-directed pattern by attacking the free thiol groups (4 cysteines residues: two pointing outwards, two pointing into the protein core) with thiol reactive PEGs carrying ethinyl groups as described before with modification [87]. PEGylated FGF-2 was purified using heparin based affinity chromatography on an ÄKTA purifier system and finally characterized by reducing SDS-PAGE, MALDI MS and RP-HPLC. In order to investigate correct folding of FGF-2 after

PEGylation, fluorescence spectrometry was performed. The unfolding temperature of FGF-2 and PEG-FGF-2 was analyzed by differential scanning fluorimetry (DSF). The bioactivity of PEGylated FGF-2 was determined by analysis of the proliferation of NIH 3T3 cells and PEGylated FGF-2 stimulation of MAPK activation was investigated with ERK phosphorylation, an effector kinase of the MAPK pathway. SF-PEG-FGF-2 conjugates were analyzed using western blot analysis.

Furthermore, the covalent immobilization of PEGylated FGF-2 on surfaces of biomaterials by means of click chemistry and EDC/NHS chemistry was investigated and compared during this work. Immobilized FGF-2 was analyzed under the fluorescence microscope or by flow cytometry after incubation with FGF-2 primary and FITC labelled secondary antibody. Additionally, WST-1 proliferation assay as well as ERK1/2 phosphorylation gave information about bioactivity of immobilized FGF-2.

Another approach for the incorporation of functional groups - unnatural amino acids - in growth factors is the genetic engineering. There exist different techniques to integrate unnatural amino acids in proteins during expression. During this work we used the method based on the amber stop codon suppression methodology according to Budisa et al. [94] to integrate alkyne functionality into the sequence of insulin-like growth factor I (IGF-I) with the final aim to covalently couple it to SF scaffolds in a site-directed manner. Therefore, one defined lysine codon (AAG) of IGF-I had to be mutated to the amber stop codon (TAG). The mutated IGF-I gene was then cloned into pET11a vector in order to finally use the *Escherichia coli* (*E. coli*) expression machinery derived from *Methanosarcina barkeri* [95] for plk-IGF-I expression. Additionally, propargyl-L-lysine (plk) bearing an alkyne group had to be synthesized as described before [95] and verified by NMR. The applied modification methods are described below.

2.2.1 Modification of natural amino acids

2.2.1.1 PEGylation

The conjugation of polyethylene glycol to biologics increases their hydrodynamic radius and thereby increases their half-life leading to prolonged therapeutic effects and reduced number of injections. Moreover, antigenic epitopes can be shielded through PEGylation leading to reduced immunogenicity [39]. Herein the binding site of PEG to the protein of interest is essential that pharmacodynamic properties are not affected by the coupling. The number of coupled PEG chains and their molecular weight and structure (linear or branched) are of importance as well and chosen according to the planned application. Many reactive amino acids such as lysine, cysteine, histidine, arginine, aspartic acid, glutamic acid, serine, threonine and tyrosine as well as the N-terminal amino group and the C-terminal carboxylic acid exist for PEGylation in proteins and lots of chemical methods are available for PEGylation [96]. Proteins are labile molecules and require mild reaction conditions. Lysine as the most prevalent amino acid in proteins is readily used for non-

site-specific PEGylation resulting in complex mixtures with different degrees of PEGylation [39]. PEG chains with a carboxylic acid at one end can easily be coupled to lysine residues by EDC/NHS chemistry under mild reaction conditions (see 2.2.1.3). Adagen® (PEGylated adenosine deaminase, Enzon, 1990) and Oncaspar® (PEGylated L-asparaginase, Enzon, 1994) are both complex mixtures of PEGylated therapeutic proteins on the market witnessing that non-site-specific binding can lead to functional proteins [38]. However, non-site-specific binding may reduce bioactivity due to inability of receptor binding [37]. For site-specific PEGylation amino acids that are more rarely in proteins have to be used such as cysteine. PEG maleimide or PEG iodoacetamid are two common reagents that are used for thiol PEGylation easily forming thioether under mild reaction conditions [97]. The usage of transglutaminase is another possibility for site-specific PEGylation resulting in the coupling of glutamine with PEG amine [98]. These PEGylation methods are just examples and several more chemical methods for PEGylation exist. However, the highest selectivity can be obtained with genetically modified proteins by manipulating the amino acid sequence. Amino acids can be deleted or replaced by other amino acids in order to have just one possible reaction partner or unnatural amino acids can be incorporated by site-directed mutagenesis (see 2.2.2.1).

2.2.1.2 Diazonium coupling chemistry

During the so called diazonium coupling reaction aromatic amines react with phenolates. Prior the reaction takes place the aromatic amine has to be activated with nitrous acid or a stronger mineral acid in order to generate diazonium cations. These electrophilic $–N=N^+$ groups then react with strongly activated aromates such as phenols at slight basic pH at ortho or para position [99]. Diazonium coupling offers the possibility to functionalize biomaterials or surfaces with specific functional groups. During this study the tyrosine groups of the SF primary sequence were modified with azido groups by means of a diazonium coupling reaction with 4-Azidoaniline hydrochloride in analogy to what has been described before [93].

2.2.1.3 EDC/NHS chemistry

N-ethyl-N’-(3-(dimethylamino)propyl)carbodiimide/N-hydroxysuccinimide coupling (EDC/NHS) is a standard method for the immobilization of proteins on biomaterials. Thereby primary amines react with carboxylic acids under mild reaction conditions forming peptide bonds. Normally several lysines and even several amino acids carrying carboxylic acid groups such as aspartic acid and glutamic acid are present in proteins resulting in non-site-specific binding with inter- and intramolecular crosslinks [100].

2.2.2 Modification at UAAs

2.2.2.1 Introduction of a non-natural amino acid

Non-natural amino acids carrying functional groups such as alkyne or azide can be incorporated into proteins by genetic engineering. Therefore, different methods are available. The method we used in this work is based on the amber suppression methodology [94, 101]. Actually, protein synthesis is terminated at amber stop codon but with the usage of the translation machinery of archaebacteria that includes the PylRS/tRNA^{Pyl} pair of *Methanosarcina barkeri* a pyrrolysine analogue (Pyl) is inserted into the protein backbone at the position of the amber stop codon (TAG) [95]. Our aim was the incorporation of alkyne functionality into IGF-I to allow site-directed immobilization through click chemistry. The required amber stop codon (TAG) was generated at positon 65 through punctual mutation of the respective lysine (AAG). In order to perform protein expression in *E. coli* cells, the gene for tRNAPyl, the lipoprotein promoter lpp, the rrnC terminator as well as the modified IGF-I gene was cloned into pET11a vector comprising an ampicillin resistance gene and the corresponding pyrrolysyl-transfer-RNA-synthetase (PylRS) was cloned into the pRSF vector containing a kanamycin resistance gene [95].

The pET expression system is widely used for the cloning and *in vivo* expression of recombinant proteins in *E. coli*. The pET11a expression vector carries the T7 promoter with lac operator that promotes high level transcription and translation just in presence of T7 RNA polymerase that is expressed by the host cells after induction with IPTG. Additionally, a lacI gene is located on the pET11a vector coding for a lac repressor protein that binds to the lac operator preventing transcription. The lac repressor protein is removed by IPTG. So protein expression can start after the addition of IPTG.

Both vectors were cotransformed into BL21(DE3) or ArcticExpress(DE3) cells for expression, respectively. A pyrrolysine analogue with an alkyne function, propargyl-protected lysine (plk), was then added to the culture medium. After inducing protein expression with IPTG, plk was recognized by PylRS and incorporated into the protein sequence of IGF-I at position 65 by tRNA^{Pyl} (**Scheme 1**).

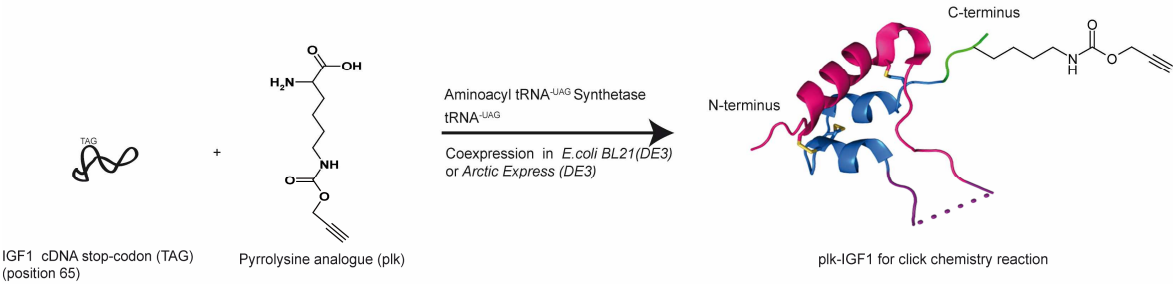

Scheme 1: Schematic illustration of plk-IGF-I expression. PDB code IGF-I = 2GF1.

2.2.2.2 Click chemistry

Kolb et al. firstly used the term “click chemistry” in 2001 and according to them “the reaction must be modular, wide in scope, give very high yields, generate only inoffensive byproducts that can be removed by non-chromatographic methods, and be stereospecific (but not necessarily enantioselective)” [102]. Moreover, the reaction is simple to perform in water or an easily removable benign solvent. Today in particular the copper catalyzed Huisgen 1,3-dipolar cycloaddition of an azide with a terminal alkyne forming a triazole is called “click reaction” and is widely used for bioconjugative applications [103]. After the incorporation of unnatural amino acids containing azide or alkyne functionality into proteins (see 2.2.2.1) site-directed coupling can be performed.

2.3 Biofunctionalized implants for cartilage tissue engineering

Various controlled release systems have already been developed for cartilage tissue engineering but to date none of these systems was able to mimic structure and properties of native cartilage completely [104].

2.3.1 Articluar hyaline cartilage

Articular hyaline cartilage is a highly organized avascular tissue composed of chondrocytes embedded in extracellular matrix (ECM) consisting of collagens and proteoglycans [105]. Unfortunately, damaged articular cartilage caused by traumatic injuries or osteoarthritis has just a limited self-repair capacity leading to the development of therapeutic strategies to repair articular cartilage defects or even slow degenerative processes [106]. Osteoarthritis is a degenerative joint disease affecting the whole joint, its pathogenesis is characterized by loss of cartilage, remodeling of subchondral bone, formation of osteophytes as well as synovial hypertrophy and inflammation (**Figure 3**) [107].

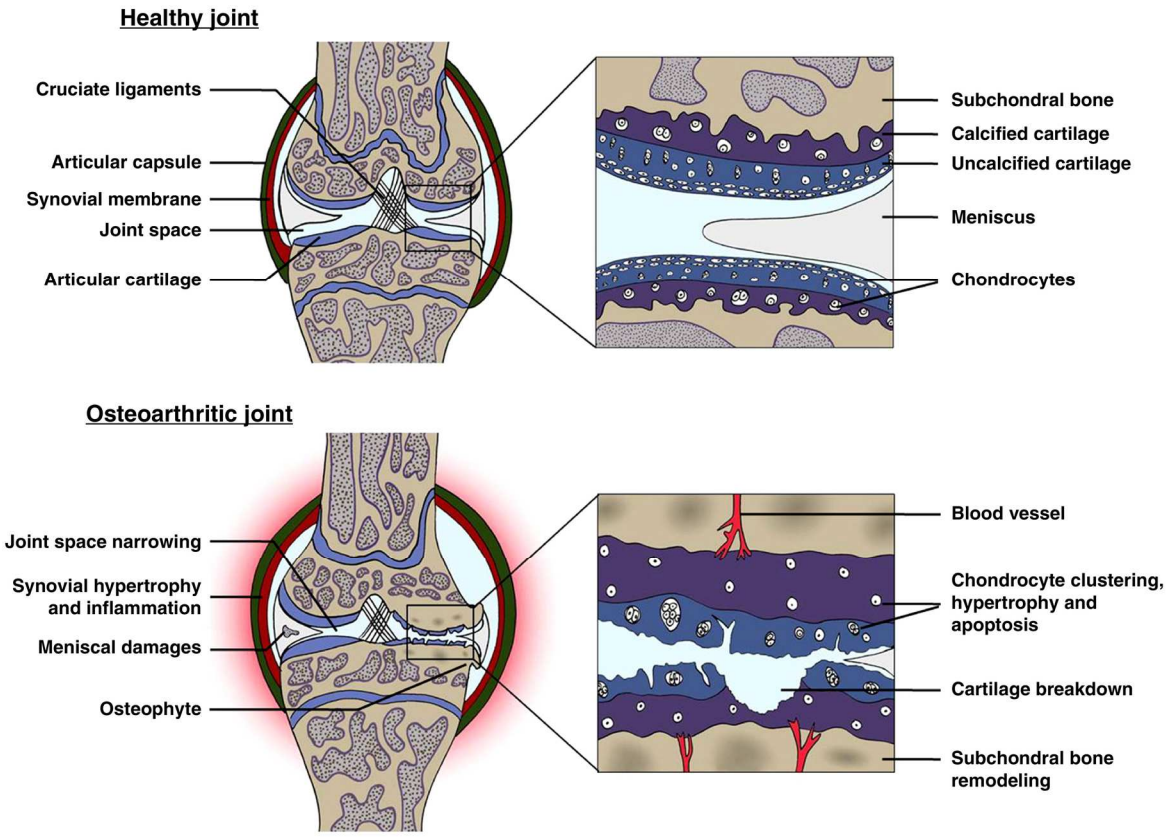

Figure 3: Joint tissue affections in knee osteoarthritis (OA). Reprinted from [107], Copyright (2014), with permission from Elsevier.

2.3.2 Therapeutic strategies to repair articular hyaline cartilage

Widely used cartilage repair techniques include surgical methods such as microfracture, mosaicplasty, autologous chondrocyte implantation and osteochondral allograft implantation [108]. However, none of these techniques mimics satisfactorily the properties and structure of articular hyaline cartilage and is a long term clinical solution. By all these techniques only fibrocartilage and no hyaline cartilage is built, and this fibrocartilage is not as mechanically strong and not as durable as hyaline cartilage leading to abrasion and loss of function [109]. Moreover, none of these techniques leads to a connection of the native cartilage with the newly formed cartilage causing further abrasion of the healthy cartilage in the defect zone [109]. Novel tissue engineering approaches are in development combining cells, biodegradable scaffolds and growth factors that offer further hope for the healing of cartilage defects [110].

2.3.3 Cell sources for cartilage tissue engineering

Chondrocytes are the cells of choice for cartilage engineering but in the last decade research focused on the use of mesenchymal stem cells (MSCs) and recognized their potential therapeutic benefits in cartilage repair. During chondrogenesis MSCs condensate, differentiate into chondroblasts, further differentiate into chondrocytes and finally mature into hypertrophic chondrocytes (**Figure 4**) [111]. However, it is indispensable to keep the chondrocytes in the chondrogenic lineage and to prevent hypertrophic differentiation of chondrocytes during cartilage tissue engineering. To date the required conditions for the formation of stable articular hyaline cartilage is far from being understood.

The differentiation potential of stem cells into both cartilage and bone, and as a consequence, the healing potential of chondral as well as osteochondral defects is one advantage towards chondrocytes [112].

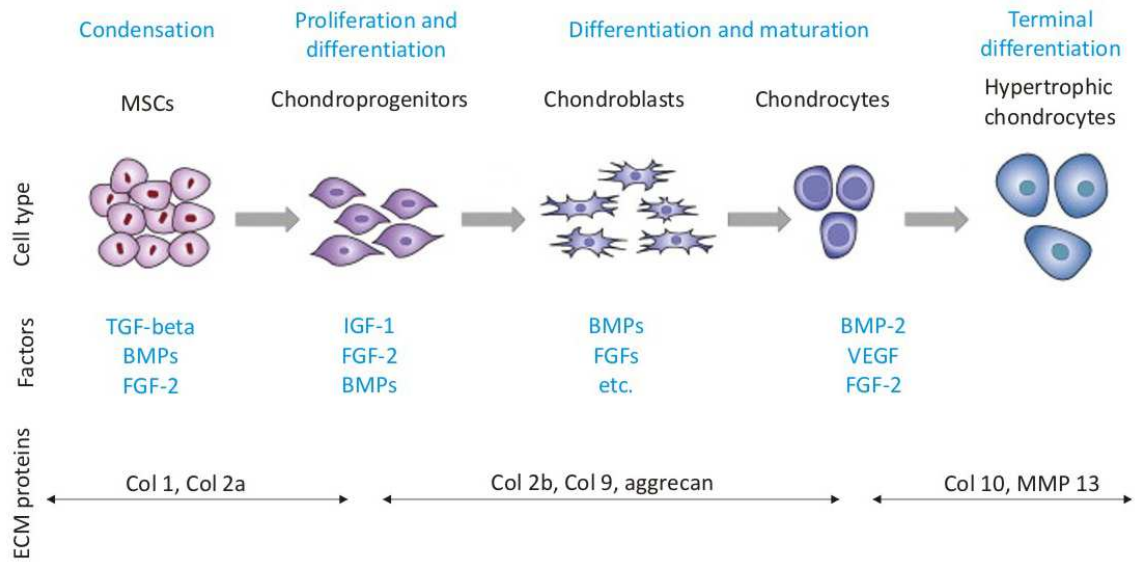

Figure 4: Schematic diagram of different stages of chondrogenesis. Reprinted from [111], Copyright (2013), licensee InTech (http://creativecommons.org/licenses/by/3.0).

2.3.4 Growth factors

MSCs undergo differentiation into chondrocytes by stimulation with several growth factors such as transforming growth factor betas (TGF-βs), bone morphogenetic proteins (BMPs), fibroblast growth factors (FGFs) and insulin-like growth factor I (IGF-I) (**Figure 4**) [106, 111].

2.3.4.1 Insulin-like growth factor I

Insulin-like growth factor I (IGF-I) plays a critical role in skeletal muscle development [113] as well as in cartilage homeostasis through influencing survival and proliferation of chondrocytes, stimulating synthesis of proteoglycans and collagens and inhibiting the rate of matrix degradation. [110, 114]. Furthermore, IGF-I has chondrogenic potential on stem cells concerning proliferation, apoptosis and the expression of chondrogenic markers [115]. By coupling to the insulin-like growth factor I receptor (IGF-IR), a tyrosine kinase membrane receptor, IGF-I activates the mitogen-activated protein kinase/extracellular-signal-regulated kinase-kinase 1/2 (MEK1/2), the extracellular-signal-regulated kinase 1/2 (ERK1/2), the mitogen-activated protein kinase (MAPK) and the phosphoinositid-3-kinase-Akt (PI3K-Akt) pathways, typically leading to matrix expression [116]. In 2005, IGF-I (Increlex® (mecaserim), Ispen Pharma) has been approved by the FDA for the treatment of growth failure in children with IGF-I deficiency or GH gene deletion [117].

2.3.4.2 Bone morphogenetic protein 2

Bone morphogenetic proteins belong to the transforming growth factor β superfamily and play a critical role in heart, neural, cartilage and bone formation [118]. Through binding to a serine/threonine kinase receptor (BMPR-I, BMPR-II) BMPs phosphorylate Smad1/5/8 and thus activate Smad downstream processes [119]. Until now, about 20 different BMPs have been discovered, but just BMP-2, -4, -6, -7 and -9 have been shown to play significant roles in bone formation [120]. BMP-2 has been widely studied in bone formation and regeneration and is one of the most potent growth factor that induces mesenchymal stem cell into osteoblasts [84]. In 2002, BMP-2 has even been approved by the FDA for the promotion of spinal fusion, and in the same year a collagen matrix loaded with BMP-2 (INFUSE® bone graft, Medtronic) came on the market [2]. Except BMP-3 and BMP-15, all other BMPs contain 7 cysteines residues forming 6 intramolecular and 1 intermolecular disulfide bonds, the so-called cystine knot, leading to either homo- or heterodimers [121].

2.3.4.3 Transforming growth factor β3

Transforming growth factor betas (TGF-βs) play a pivotal role in the maintenance of health cartilage. There exist three isotypes of TGF-β, TGF-β1,-2 and -3, which exhibit sequence homologies of about 90 % [122]. These three isoforms are homo dimeric-polypeptides, each monomer consisting of 112 amino acids with a size of about 12.5 kDa [123]. TGF-βs are broadly

expressed in cartilage, stimulate chondrocyte proliferation, inhibit chondrocyte hypertrophy and thereby regulate growth, development and repair of articular cartilage [124].

2.3.4.4 Fibroblast growth factor 2

Acidic and basic fibroblast growth factor (FGF-1 and FGF-2) have been the first two FGFs discovered in the 1970s [125]. To date, 22 FGF family members have been identified in humans and mice [126]. All FGFs, expect FGF-19, -21 and -23, contain a heparin-binding domain leading to the ability to bind heparin and heparin sulfate proteoglycans (HSPGs) [127]. Hence, these FGFs are termed heparin-binding growth factor (HBGF) as well. FGF-2 is a potent stimulator for the proliferation, differentiation and migration of various cell types particularly vascular cells such as endothelial and smooth muscle cells [128]. Furthermore, FGF-2 promotes angiogenesis, wound healing as well as tissue repair [129].

2.3.5 Biomaterial scaffolds for cartilage tissue engineering

For chondrogenic differentiation mechanical robust but still elastic, biodegradable, biocompatible scaffolds in the form of hydrogels, sponges or meshes with a defined porosity for cell migration and diffusion of nutrients are needed [105]. Currently used biomaterials are either natural polymers (agarose, alginate, cellulose, chitosan, collagen, fibrin, gelatin, hyaluronic acid or SF) or artificial polymers (polyethylene glycol (PEG), polylactic acid (PLA), polyglycolic acid (PGA), polylactic-coglycolic acid (PLGA), polycaprolactone (PCL), hydroxyapatite) [130]. SF has been widely used as biomaterial for biomedical applications because of its remarkable mechanical properties as well as its biodegradability and biocompatibility. Moreover, former studies confirm the suitability of SF scaffolds for cartilage tissue engineering with MSCs [131, 132].

Covalent binding of growth factors for spatial control and moderation of release has received continuous attention. N-ethyl-N’-(3-(dimethylamino)propyl)carbodiimide/N-hydroxysuccinimide coupling (EDC/NHS) offers high coupling efficiency, biocompatibility and just little influence on bioactivity of growth factors under mild conditions, and thus EDC/NHS chemistry is widely used for biomedical applications [133]. The EDC/NHS activation approach is applicable for every biomolecule bearing free primary amino groups and immobilizes these biomolecules via formation of stable amide bonds with activated carboxylic acids. Polymethylmethacrylate (PMMA) is one of the most established materials of orthopaedic applications and has been widely used for fixation of joint implants and anchoring total joint replacement over the last 60 years [134]. Due to its mechanical properties, its biocompatibility and its biostability, PMMA beads have been used as carrier for local delivery of antibiotics [135]. In the present study carboxylated PMMA beads served as carrier for immobilized TGF-β3 using EDC/NHS coupling. TGF-β3 loaded beads were embedded in porous SF scaffolds for local sustained delivery of TGF-β3 to induce chondrogenic differentiation of human mesenchymal stem cells. The influence of covalent coupling of TGF-β3

was investigated in comparison to exogenous and adsorbed TGF-β3. Furthermore, the immobilized amount of growth factor was quantified via enzyme-linked immunosorbent assay (ELISA) in order to detect the impact of covalent coupling on its bioactivity, which was assessed by luciferase reporter gene assay.

2.3.6 Osteochondral implants

Articular cartilage defects are typically irreversible and any treatment option available today is not able to fully reconstruct the function and structure of healthy articular hyaline cartilage [109]. One of the major limitations of current implants and grafts is the lack of integration into host tissue [110]. Considering all the studies that have been performed in the field of cartilage restoration, autologous osteochondral grafts are supposed to heal osteochondral defects with the greatest clinical success since a bone-to-bone interface integrates better and faster than a cartilage-to-cartilage interface [136, 137]. However, these autologous osteochondral grafts have several disadvantages such as the creation of new defects, the inability to heal large defects, the poorly connection with adjacent articular cartilage and the formation of mainly fibrocartilage instead of the strong hyaline cartilage [136]. The *in vitro* engineering of cartilage-like and bone-like tissue simultaneously in close proximity with a stratified zone in between on a biodegradable biomaterial has the potential to overcome these drawbacks. *In vitro* engineering of cartilage-like tissue alone has been performed in several studies with different cell types and on different matrices and there even exist several approaches for the engineering of osteochondral grafts but until now it was not possible to fully mimic cartilage ECM environment and create implants with similar characteristics to articular cartilage [109, 138]. Our hypothesis is that BMSCs seeded on SF scaffolds biofunctionalized spatially restricted with growth factors and created with optimized geometry in terms of respective tissue outcome will form osteochondral plugs. Following implantation of such osteochondral plugs better healing success into chondral lesion is expected. The simultaneous engineering of cartilage and bone tissue on one implant promises to translate into better mechanical performances within the implant and better integration into adjacent host cartilage and bone, respectively [139].

There is a need to develop an implant with optimal geometry in order to generate cartilage and bone on one construct. Moreover this implant has to be functionalized with IGF-I and TGF-β3 for chondrogenic differentiation and BMP-2 for osteogenic differentiation of mesenchymal stem cells. For cell growth, cell migration and the flow of nutrients an interconnected pore system is essential [63]. The size of the pores plays an important role as well. Too small pores may inhibit cell migration and the diffusion of nutrients and too large pores may inhibit cell adhesion [140]. According to Klawitter et al. [141] the optimal pore range for bone formation is 100-135 µm. In contrast, larger pore sizes are needed for cartilage tissue engineering. Recent studies show the formation of cartilage with enhanced ECM synthesis in pores with sizes of ~400 µm [142] and

~700 µm [143]. Hence, paraffin spheres with different sizes were prepared according to the method of Uebersax et al. [144] and used as porogen in order to generate SF scaffolds with two porosities. Finally, general suitability of these generated biphasic SF scaffolds were investigated for osteogenic and chondrogenic differentiation of BMSCs.

3 Aims and objectives

This work deals with formulation and delivery strategies of therapeutic proteins.

Aim 1 was the development of a new injectable formulation for the dimeric fusion protein PR-15, a lesion specific platelet adhesion inhibitor. Therefore, a pH screening and a forced degradation study was performed in order to determine an adequate pH value ensuring the stability and bioactivity of PR-15 during storage at 4 °C. The stability of PR-15 in relation to pH was investigated using different analytical methods in a short-term storage stability study. Furthermore, some information on potential degradation pathways of PR-15 were aimed to obtain under stressed conditions (heat/pH/freeze-thaw cycles/light/oxidation/deamidation) during forced degradation study. The results of the pH screening and the forced degradation study aimed at finding the optimal factor settings and the most informative responses to perform a Design of Experiments (DoE) for further optimization of the injectable PR-15 formulation.

Aim 2 was the preparation of multifunctionalized osteochondral implants for the regeneration of cartilage defects (**Figure 5**). Therefore, growth factors were selected and presented for the differentiation of stem cells for tissue engineering of cartilage and bone on implant surfaces. At first ideal geometry and optimal porosity of the SF scaffolds were found, respectively, to generate both tissues on one scaffold. Moreover, these SF scaffolds were biofunctionalized with specific growth factors: BMP-2 as well as TGF-β3 for osteogenic differentiation and IGF-I as well as TGF-β3 for chondrogenic differentiation. Our strategy was to present the required growth factors spatially restricted on the SF scaffolds. Therefore, BMP-2 and IGF-I were modified by the incorporation of unnatural amino acids through genetic engineering in order to incorporate functional groups to perform covalent coupling on two opposite sides of the scaffolds. In contrast, TGF-β3 was used without modification as it was required both for osteogenic and for chondrogenic differentiation.

An alternative approach, the incorporation of functional groups by means of PEGylation was investigated with FGF-2 as model protein.

During this work predominantly two common chemical reactions, site-directed click chemistry and non-site-directed EDC/NHS chemistry, which are often used for bioconjugation, were compared. The focus was on the characterization of the modified as well as the immobilized proteins.

Aim 3 was to evaluate the impact of covalent coupled and adsorbed TGF-β3 for cartilage tissue engineering. Therefore, TGF-β3 was loaded on PMMA beads using non-site-specific EDC/NHS chemistry and a method for the quantification of immobilized protein was originated. Finally, SF-scaffolds were loaded with these beads and chondrogenic differentiation of BMSCs was performed.

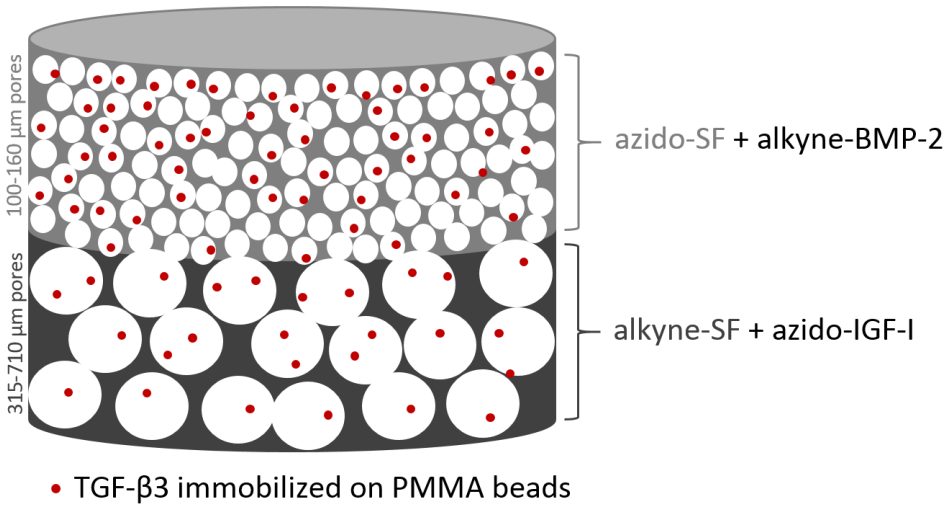

Figure 5: Schematic illustration of multifunctionalized osteochondral implant for the regeneration of cartilage defects.

4 Materials and methods

4.1 Injectable PR-15 formulation

4.1.1 pH screening

To evaluate the stability of the PR-15 at the different pH values, chosen according to the isoelectric point (pI 4.5–5) [75], a pH screening was done. PR-15 was provided in a concentration of 2.4 mg/mL in PBS buffer, pH 7.4, with 4 % mannitol and 1 % saccharose. Ultrafiltration was done for buffer exchange and up-concentration using an Amicon® stirred ultrafiltration cell 8010 (EMD Millipore Corporation, Billerica, MA, USA) and 30 kDa ultrafiltration membrane disk filters (25 mm, PALL® Life Sciences Corporation, Ann Arbor, MI, USA) against a 50 mM histidine buffer with the respective pH value (5.5, 6.0, 6.5 or 7.0), to a concentration of about 2.5 mg/mL according to UV-absorption measurements. Samples were filtered using sterile syringe filter units (Rotilabo® syringe filter, 0.22 µm, CME membrane, 33 mm diameter, Carl Roth, Karlsruhe, Germany) and allocated into clear glass type I vials of 2.0 mL each, closed with 13 mm chlorobutyl rubber stopper and an aluminum crimp (Zscheile & Klinger, Hamburg, Germany). These vials (n = 1, due to limited availability of PR-15) were incubated at 25 °C as well as at 40 °C for 4 and 8 weeks in a heating oven ED 115 and a climate chamber KBF 115 (Binder GmbH, Tuttlingen, Germany) (**Table 4**). After pre-defined time points, samples were aliquoted for each analytical method (510 µL for UV-VIS/120 µL for SEC/110 µL for HIC/130 µLfor DLS/750 µL for collagen ELISA/100 µL for aggregation assay/100 µL for SDS-PAGE), stored at -80 °C and analyzed all together using the below described analytical methods after thawing at room temperature and gentle mixing.

Temperature	*Initial*				*25 °C*				*40 °C*				*25 °C*				*40 °C*			
Time	0 weeks				4 weeks				4 weeks				8 weeks				8 weeks			
pH	5.5	6	6.5	7	5.5	6	6.5	7	5.5	6	6.5	7	5.5	6	6.5	7	5.5	6	6.5	7

Table 4: Overview of the storage periods and conditions.

4.1.2 Forced degradation study

To obtain information on potential degradation pathways, different forms of stress were applied to the protein.

PR-15 was provided in a concentration of 2.4 mg/mL in PBS buffer, pH 7.4, with 4 % mannitol and 1 % saccharose. Ultrafiltration was done for buffer exchange and up-concentration using an Amicon® stirred ultrafiltration cell 8010 (EMD Millipore Corporation, Billerica, MA, USA) and 30 kDa ultrafiltration membrane disk filters (25 mm, PALL® Life Sciences Corporation, Ann

Arbor, MI, USA) against a 50 mM histidine buffer, pH 6.0, to a concentration of about 2.5 mg/mL according to UV-absorption measurements. Samples were filtered using sterile syringe filter units (Rotilabo® syringe filter, 0.22 µm, CME membrane, 33 mm diameter, Carl Roth, Karlsruhe, Germany) and allocated into clear glass type I vials of 2.0 mL each (n = 1, due to limited availability of PR-15), closed with 13 mm chlorobutyl rubber stopper and an aluminum crimp (Zscheile & Klinger, Hamburg, Germany). One sample was aliquoted for each analytical method (510 µL for UV-VIS/120 µL for SEC/110 µL for HIC/130 µL for DLS/750 µL for collagen ELISA/100 µL for aggregation assay/100 µL for SDS-PAGE/15 µL for MALDI-TOF MS/25 µL for LC/ESI-MS after trypsin digest) and stored at -80 °C as initial condition.
Following stress conditions were applied:

- **Thermal [145]**: T_m–10 °C for up to 7 days
- **Freeze-thaw cycles [146]**: -80 °C → room temperature → -80 °C (10 cycles)
- **Acid-base hydrolysis [147]**: pH 3.5 / pH 13, incubation at 37 °C, overnight
- **Light:** not less than 4*200 W*h/m^2 of UV (320–400 nm) exposure and not less than 4*1.2 million lux hours in visible (400–800 nm) exposure with climate chamber TCS-301 Ph (ThermoTec Weilburg GmbH & Co. KG, Germany)
  = Irradiance range (320–400 nm): 17 W/m^2 → 800 W h/m^2 / 17 W/m^2 = 47.06 hours
  = lux range (400–800 nm): 12 klux → 4.8 million lux hours / 12 klux = 400 hours)
  → exposure for 47 hours to UV and 17 days to VIS at 25 °C; reference wrapped with aluminum foil
- **oxidation [146]:** 0.1 % hydrogen peroxide for 20 h at 37 °C; quenching with 12 mg/mL methionine
- **deamidation [147]**: 1 % ammonium carbonate; incubation at 37 °C, removing 200 µL aliquots at 0 h, 24 h and 48 h, addition of 1800 µL ultrapure water

After these degradation treatments the samples were aliquoted for each analytical method (510 µL for UV-VIS/120 µL for SEC/110 µL for HIC/130 µL forDLS/750 µL for collagen ELISA/100 µL for aggregation assay/100 µL for SDS-PAGE/15 µL forMALDI-TOF MS/25 µL for LC/ESI-MS after trypsin digest), stored at -80 °C and analyzed all together using the below described analytical methods after thawing at room temperature and gentle mixing.

4.1.3 Design of Experiments

An experimental worksheet was created by using the Design of Experiments software MODDE 9.0 (Umetrics, Umeå, Sweden). In the MODDE software four controllable process factors were specified and a low (-1) as well as a high level (1) was assigned for each factor (**Table 5**). The center level was denoted by 0.

Factor	*Type*	*Low*	*Center*	*High*
Buffer	qualitative	Phosphate	-	Histidine
pH	quantitative	7 (-1)	7.5 (0)	8 (1)
Tween® 20	quantitative	0 % (-1)	0.05 % (0)	0.1 % (1)
Methionine	quantitative	0 mM (-1)	10 mM (0)	20 mM (1)

Table 5: Specifications of the four chosen factors.

A response surface methodology (RSM) design was chosen to find the optimal formulation for PR-15. Normally, the Central composite design (CCD) is used to create a second-order response surface model with quantitative factors [82]. However, there are also qualitative factors included in our experiment. Therefore, a D-optimal design was generated by the computer (**Table 6**). The D-optimal design is a non-standard design used in screening and optimization considering the effects between the quantitative and qualitative factors [148].

Exp No	*Exp Name*	*Run Order*	*Incl/Excl*	*Buffer*	*pH*	*Tween® 20*	*Methionine*
1	N1	25	Incl	Phosphate	-1	-1	-0,333
2	N2	6	Incl	Phosphate	-1	1	0,333
3	N3	9	Incl	Phosphate	-1	-0,333	-1
4	N4	23	Incl	Phosphate	-1	0,333	1
5	N5	2	Incl	Phosphate	1	-1	0,333
6	N6	3	Incl	Phosphate	1	1	-0,333
7	N7	5	Incl	Phosphate	1	0,333	-1
8	N8	14	Incl	Phosphate	1	-0,333	1
9	N9	20	Incl	Phosphate	0,333	-1	-1
10	N10	17	Incl	Phosphate	-0,333	-1	1
11	N11	18	Incl	Phosphate	-0,333	1	-1
12	N12	21	Incl	Phosphate	0,333	1	1
13	N13	13	Incl	Histidine	-1	-1	-1
14	N14	24	Incl	Histidine	1	-1	-1
15	N15	12	Incl	Histidine	-1	1	-1
16	N16	19	Incl	Histidine	1	1	-1
17	N17	10	Incl	Histidine	-1	-1	1
18	N18	22	Incl	Histidine	1	-1	1
19	N19	16	Incl	Histidine	-1	1	1
20	N20	8	Incl	Histidine	1	1	1
21	N21	7	Incl	Histidine	0	0	0
22	N22	4	Incl	Histidine	0	0	0
23	N23	11	Incl	Histidine	0	0	0
24	N24	15	Incl	Histidine	0	0	0
25	N25	1	Incl	Histidine	0	0	0

Table 6: Experimental plan for PR-15 optimization study.

PR-15 was provided in a concentration of 2.4 mg/mL in PBS buffer, pH 7.4, with 4 % mannitol and 1 % saccharose. Ultrafiltration was done for buffer exchange and up-concentration using an Amicon® stirred ultrafiltration cell 8050 (EMD Millipore Corporation, Billerica, MA, USA) and 30 kDa ultrafiltration membrane disk filters (43 mm, PALL® Life Sciences Corporation, Ann Arbor, MI, USA) against the appropriate buffer (50 mM L-histidine buffer or 50 mM phosphate buffer (NaH_2PO/Na_2HPO_4), with the respective pH value (pH 7.0, 7.333, 7.5, 7.667 or 8.0), to a concentration of about 2.75 mg/mL according to UV-absorption measurements in the appropriate run order (**Table 7**). A solution of 10 % Tween® 20 (1 g Tween® 20 in 10 mL of the appropriate buffer (addition of 1 mL 10x buffer and filling up to 10 mL with ultrapure water; adjusting of pH if necessary)) as well as a solution of 40 mg/mL methionine (0.4 g methionine in 10 mL of the appropriate buffer (addition of 1 mL 10x buffer and filling up to 10 mL with ultrapure water; adjusting of pH if necessary) were prepared.

Run Order	*Buffer*	*pH*	*No.*	*Volume [µL]*			
				PR-15 2.75 mg/mL	*Buffer*	*Tween® 20 10 %*	*Methionine 40 mg/mL*
5	Histidine	7.0	5x	9155	507	40	300
1	Histidine	7.5	5x	9155	423	50	373
4	Histidine	8.0	4x	7324	338	40	300
3	Phosphate	7.0	4x	7324	338.8	39.97	299.2
6	Phosphate	7.333	2x	3662	20	20	300
7	Phosphate	7.667	2x	3662	318	20	0
2	Phosphate	8.0	4x	7324	338	39.97	299.2

Table 7: Run order for ultrafiltration and overview of the needed solutions.

All solutions were filtered using sterile syringe filter units (0.2 µm, PES membrane, 13 mm diameter, Nalge Nunc International Corporation, Rochester, USA) and allocated into clear glass type I vials of 2.0 mL each, closed with 13 mm chlorobutyl rubber stopper and an aluminum crimp (Zscheile & Klinger, Hamburg, Germany) according to the pipetting scheme below (**Table 8**) in the appropriate run order (**supplementary data, Table 18–24**). These 25 vials (n = 1, due to limited availability of PR-15) as well as 1 vial (n = 1) with the old Revacept® formulation (in PBS buffer, pH 7.4, with 4 % mannitol and 1 % saccharose) were incubated at 53 °C for 7 days in a heating oven ED 115 (Binder GmbH, Tuttlingen, Germany).

1 vial with the initial sample (in 50 mM histidine buffer pH 7.0) was aliquoted immediately after preparation and the 25 vials with the samples as well as the old Revacept® formulation were aliquoted after 7 days at 53 °C for each analytical method (510 µL for UV-VIS and pH/120 µL for SEC/110 µL for HIC/130 µL for DLS/750 µL for collagen ELISA/100 µL for aggregation assay/100 µL for SDS-PAGE), stored at -80 °C and analyzed in the appropriate run order (**Table 6**) using the below described analytical methods after thawing at room temperature and gentle mixing.

Exp No	*Buffer*	*pH*	*Tween® 20 [%]*	*Methionine [mM]*	*Volume [µL]*			
					PR-15 2.75 mg/mL	*Buffer*	*Tween® 20 10 %*	*Methionine 40 mg/mL*
1	Phosphate	7.0	0	6.667	1831	119	0	49.7
2	Phosphate	7.0	0.1	13.333	1831	49.9	20	99.5
3	Phosphate	7.0	0.033	0	1831	163	6.67	0
4	Phosphate	7.0	0.067	20	1831	6.9	13.3	150
5	Phosphate	8.0	0	13.333	1831	69.7	0	99.5
6	Phosphate	8.0	0.1	6.667	1831	99	20	49.7
7	Phosphate	8.0	0.067	0	1831	156	13.3	0
8	Phosphate	8.0	0.033	20	1831	13.3	6.67	150
9	Phosphate	7.667	0	0	1831	169	0	0
10	Phosphate	7.333	0	20	1831	20	0	150
11	Phosphate	7.667	0.1	0	1831	149	20	0
12	Phosphate	7.333	0.1	20	1831	0	20	150
13	Histidine	7.0	0	0	1831	169	0	0
14	Histidine	8.0	0	0	1831	169	0	0
15	Histidine	7.0	0.1	0	1831	149	20	0
16	Histidine	8.0	0.1	0	1831	149	20	0
17	Histidine	7.0	0	20	1831	20	0	150
18	Histidine	8.0	0	20	1831	20	0	150
19	Histidine	7.0	0.1	20	1831	0	20	150
20	Histidine	8.0	0.1	20	1831	0	20	150
21	Histidine	7.5	0.05	10	1831	84.6	10	74.6
22	Histidine	7.5	0.05	10	1831	84.6	10	74.6
23	Histidine	7.5	0.05	10	1831	84.6	10	74.6
24	Histidine	7.5	0.05	10	1831	84.6	10	74.6
25	Histidine	7.5	0.05	10	1831	84.6	10	74.6

Table 8: Pipetting scheme.

4.1.4 Analytical methods

4.1.4.1 UV spectroscopy

The concentration of PR-15 was determined spectrophotometrically at a wavelength of 280 nm using a Genesys 10s UV-VIS spectrophotometer (Thermo Fisher Scientific Corporation, Waltham, USA). The absorption measured at a wavelength of 320 nm ($A_{320\ nm}$) was substracted from the absorption measured at 280 nm ($A_{280\ nm}$) for light scattering correction. Precipitates were separated by centrifugation at 13,000 g for 1 min (VWR® Micro2416 centrifuge, VWR, Darmstadt, Germany). 50 µL of the supernatant were diluted to 550 µL to guarantee the measurement in the linear range and analyzed in a disposable UVette® cuvette (VWR International LLC, Radnor, USA) with a pathlength of 1 cm at 25 °C. The molar extinction coefficient ε of 71905 $L \cdot mol^{-1} \cdot cm^{-1}$ as well as the molecular weight M of 53311.09 g/mol was calculated based on the amino acid

sequence of PR-15 monomer using ExPASy [149]. The protein concentration was calculated from $A_{280\ nm} - A_{320\ nm}$ by using the following formula [75]:

$$c\ [g/L] = (A_{280\ nm} - A_{320\ nm}) \cdot (M\ [g/mol]/\varepsilon\ [L \cdot mol^{-1} \cdot cm^{-1}]) \cdot d\ [cm] \cdot \text{dilution factor}$$

$$= (A_{280\ nm} - A_{320\ nm}) \cdot 0.74\ [g/L] \cdot \text{dilution factor}$$

4.1.4.2 pH measurement

The pH meter Lab phenomenal pH 1000 L (VWR International GmbH, Darmstadt, Germany) equipped with the InLab Micro pH electrode (Mettler-Toledo GmbH, Giessen, Germany) was used to measure the pH of the protein samples before and after incubation (n = 1). The glass pH-electrode pHenomenal® 221 (VWR International GmbH, Darmstadt, Germany) was used to adjust the pH value of the different buffers for the protein samples as well as for the analytical methods. Both electrodes were calibrated before usage by a two point calibration with technical buffer pH 4.0 and pH 7.0 (VWR International GmbH, Darmstadt, Germany).

4.1.4.3 Dynamic light scattering (DLS)

Dynamic light scattering (DLS) data of the protein samples were collected with a Delsa™ Nano HC Particle Analyzer (Beckman Coulter®, Inc., Fullerton, CA, USA) at 25 °C to monitor aggregation. For analyzing the size of formed aggregates, the particle size distributions and polydispersity indices, 60 µL of the different samples were loaded into a glass micro-cuvette. Each run consisted of three repetitions and each repetition consisted of 70 (or 200) accumulations. The system was calibrated using particle size standards.

4.1.4.4 Size exclusion chromatography (SEC)

The formation of soluble aggregates as well as degradation products of the protein samples (pH screening and FD: n = 2) were analyzed by size exclusion chromatography (SEC). To remove possible insoluble aggregates, 120 µL samples were centrifuged at 13,000 x g for 5 min (VWR® Micro2416 centrifuge, VWR, Darmstadt, Germany). 100 µL of the supernatants were transferred into 1.5 mL vials with 100 µL glass vial inserts and analyzed using a VWR Hitachi LaChromUltraTM HPLC system equipped with a diode array detector and a 7.5 mm x 60 cm TSKgel G3000SW column as well as a 6.0 mm x 4.0 cm TSKgel SWxl guard column (both Tosoh Bioscience, Stuttgart, Germany). 15 µL of each sample were run at a flow rate of 0.5 mL/min for 60 min with DPBS buffer, pH 7.4 (8 g sodium chloride, 1.15 g disodium hydrogen phosphate, 0.2 g potassium chloride and 0.2 g potassium dihydrogen phosphate per liter ultrapure water, pH was adjusted to 7.4 using sodium hydroxide before vacuum filtration), as mobile phase. Column temperature was kept at room temperature. Data were recorded at 214 nm using a UV-VIS diode array detector and evaluated using the Agilent EZChrom Elite software (Agilent Technologies, Inc., Pleasanton, CA, USA).

4.1.4.5 Hydrophobic interaction chromatography (HIC)

For analyzing degradation products of PR-15 by hydrophobic interaction chromatography (HIC), 110 µL of the protein samples (pH screening and FD: n = 2; DoE: n = 1) were diluted with 65 µL mobile phase B and then subsequently diluted in a 1:2 (v/v) ratio with sample buffer. Diluted samples were centrifuged at 16,000 g for 1 min (VWR® Micro2416 centrifuge, VWR, Darmstadt, Germany) to remove insoluble aggregates. 300 µL of the supernatants were transferred into 1.5 mL vials and analyzed using a VWR Hitachi LaChrom Elite HPLC system equipped with a diode array detector and a 6.4 mm x 30 mm ResourceTM Iso 1 mL column (GE Healthcare, Munich, Germany). 99.5 µL of each sample were run with a flow rate of 1.5 mL/min at room temperature for 28 min. The protein was eluted with a gradient of ammonium sulfate from 2 M to 0 M. The percentage of mobile phase B was increased from 0 % to 30 % in 6.5 min to 55 % in 11 min to 100 % in 6.5 min. The column was regenerated after each run by 100 % mobile phase B for 3.5 CV. Data were recorded at 214 nm using a UV-VIS diode array detector and evaluated using the Agilent EZChrom Elite software (Agilent Technologies, Inc., Pleasanton, CA, USA). For the preparation of the mobile phase A for HIC (25 mM sodium dihydrogen phosphate, 25 mM disodium hydrogen phosphate and 1.5 M ammonium sulfate), 3.0 g sodium dihydrogen phosphate, 3.549 g disodium hydrogen phosphate were dissolved in 800 mL ultrapure water. 198.2 g ammonium sulfate were added and dissolved under stirring. The pH was adjusted to 7.0 using sodium hydroxide and water was added to 1 L before vacuum filtration. The same procedure was done to prepare mobile phase B for HIC (25 mM sodium dihydrogen phosphate, 25 mM disodium hydrogen phosphate) but no ammonium sulfate was added. For the preparation of the sample buffer (2 M ammonium sulfate in mobile phase B), 52.9 g ammonium sulfate were dissolved in 100 mL mobile phase B. The pH was adjusted to pH 7.0 and filled with mobile phase B to 200 mL before vacuum filtration.

4.1.4.6 MALDI-TOF mass spectrometry

Matrix-assisted laser desorption ionization time-of-flight mass spectrometry (MALDI-TOF MS) was performed to analyze degradation products of PR-15 and the formation of aggregates. Following desalting with ZipTip® pipette tips (C18 resin, Millipore, Billerica, MA, USA) according to the manufacturer's instructions, the desalted PR-15 samples were embedded in a matrix consisting of sinapic acid in acetonitrile/0.3 % trifluoroacetic acid in water (60:40 v/v) in a 1:1 ratio. 2 µL of the sample/matrix mixture were spotted onto a 192 well sample plate. MS spectra were recorded in the linear positive mode by employing an Autoflex II LRF instrument from Bruker Daltonics Inc. (Billerica, MA, USA) fitted with a 337 nm wavelength nitrogen laser. External calibration of mass spectra was performed with the protein standard I (Bruker Daltonics Inc. Billerica, MA, USA) containing insulin, ubiquitin, myoglobin and cytochrome C.

4.1.4.7 LC/ESI-MS analysis after trypsin digest

For further investigation of degradation products liquid chromatography coupled with electrospray ionization-mass spectrometry (LC/ESI-MS) was done after trypsin digest.

5 µL NuPAGE LDS Sample Buffer (4x, pH 8.5, containing 106 mM Tris HCl, 141 mM Tris Base, 2 % lithium dodecyl sulfate (LDS), 10 % Glycerol, 0.51 mM EDTA, 0.22 mM SERVA Blue G250, 0.175 mM Phenol Red) were added to 13 µL sample. Samples were reduced with 50 mM DTT at 70 °C for 10 min and alkylated with 107 mM iodoacetamide for 20 min in the dark. For the not reduced samples 50 mM histidine buffer was added instead of DTT solution. The reduced and/or alkylated samples were separated by SDS-PAGE on a 12 % tris-glycine polyacrylamide gel and stained with Coomassie Brilliant Blue. Each sharp band of separated proteins was cut and placed into a PCR-tube for in-gel digestion. The excised gel bands were destained with 30 % acetonitrile, shrunk with 100 % acetonitrile and dried in a vacuum concentrator (Concentrator 5301, Eppendorf, Hamburg, Germany). Subsequently, elastase digests were executed in 0.1 M ammonium hydrogen carbonate (pH 8) at 37 °C overnight. For one gel slice ~0.1 µg protease was applied and peptides were extracted from the gel slices with 5 % formic acid.

Following this, NanoLC-MS/MS analyses were carried out on an LTQ-Orbitrap Velos Pro (Thermo Scientific) equipped with an EASY-Spray Ion Source and coupled to an EASY-nLC 1000 (Thermo Fisher Scientific, Rockford, USA) as described before [150].

Finally, raw data were processed and peak lists were generated using Mascot Distiller 2.5 with standard settings for the Orbitrap Velos (high/high settings). The parameters: peptide mass tolerance: 10 ppm, MS/MS mass tolerance: 0.02 Da, enzyme: “none”; variable modifications: carbamidomethyl (C), Gln → pyroGlu (N-term. Q) and oxidation (M) were adjusted for database searching with Mascot Server 2.5. Database searching was performed against a small custom database including the protein of interest.

4.1.4.8 SDS PAGE

SDS-PAGE analysis was done for evaluating the degree of degradation and the formation of aggregates of PR-15. Samples were diluted with PBS to a final concentration of 1 µg/µL and heat-denatured at 95 °C for 4 minutes after addition of reducing or non-reducing Laemmli sample buffer. A pre-cast gradient polyacrylamide tris-acetate-SDS gel (3–8 %, NuPAGE, Invitrogen, Karlsruhe, Germany) was loaded with Precision Plus Protein™ All Blue Standards (#1610373, Bio-Rad Laboratories GmbH, München, Germany), a PR-15 reference standard as well as the pH-screening samples, the forced degradation samples or the DoE samples and separated using tris-acetate-SDS running buffer. The gel was stained with GelCode™ Blue Safe Protein Stain (Thermo Fisher Scientific, Rockford, USA) and photographed after destaining in water.

4.1.4.9 Collagen ELISA

Binding of PR-15 to its natural ligand collagen was used as parameter for biological activity. Therefore, a collagen ELISA was performed to demonstrate the PR-15-specific collagen binding. 100 µL bovine collagen type I (#354231, BD Biosciences, Heidelberg, Germany) with a final concentration of 10 µg/mL in coating buffer (1.59 g/L Na_2CO_3, 2.93 g/L $NaHCO_3$, pH 9.6) were used for the coating of microtiter plates (Immulon 2HB, Thermo Fisher Scientific, Rockford, USA) for 1 h under gently shaking at room temperature. Samples and standards (n = 2) with concentrations from 0.041 – 900 µg/mL were added into the coated microtiter plates after blocking with 300 µL Roti®-block solution (Carl Roth GmbH + Co. KG, Karlsruhe, Germany) and incubated for 1 h at room temperature under gently shaking. A horse radish peroxidase (HRP)-coupled goat anti-human IgG antibody (#109-035-098, Peroxidase AffinPure Goat Anti-Human IgG, Fcγ fragment specific, Dianova, Hamburg, Germany) was diluted 1:30,000 and 300 µL were subsequently added per well in order to form a sandwich complex with solid phase collagen-PR-15. During all steps each well of the microtiter plate was thoroughly washed with 300 µL PBS containing 0.05 % Tween® 20 for several times. Finally, bound conjugate was detected by addition of 100 µL 1-Step™ Ultra TMB ELISA Substrate Solution (Thermo Fisher Scientific, Rockford, USA). The reaction of HRP-peroxidase with TMB was stopped with 100 µL 1 M sulfuric acid and the amount of hydrolyzed substrate was measured at 450 nm with a microplate reader (Infinite® F200, Tecan, Maennedorf, Switzerland). The amount of hydrolyzed substrate was proportional to the concentration of bound PR-15 on the immobilized collagen. EC_{50} values were determined with four parameter logistics curve fitting function in Sigma Plot after plotting OD_{450nm} values against PR-15 concentrations.

4.1.4.10 Inhibition of platelet aggregation

The inhibition of collagen-induced platelet aggregation as further parameter for biological activity was evaluated by light transmission aggregometry according to Born [151]. Therefore, an optical aggregometer (Apact 4004 aggregometer, Haemochrom Diagnostica, Essen, Germany), a fixed wavelength spectrophotometer with sample chambers heated to 37 °C as well as CRP-XL (collagen-related peptide, cross-linked) were required. CRP-XL (CRP, Anaspec, Seraing, Belgium; cross-linked by advanceCOR) is a chemically defined cross-linked peptide mimicking the triple helical structure of collagen. It is equally suitable for the analysis of collagen-induced aggregation of human platelets even with higher reproducibility because of better standardization compared to collagen. Healthy volunteers, who were at least 14 days untreated with any anti-platelet medication, were taken to draw blood. Citrated blood samples were analyzed within 2.5 hours after blood-sampling. For evaluating the *in vitro* platelet aggregation, a magnetic stirrer with 1,000 rpm was used to simulate shear conditions during blood flow and thereby enable the required platelet to platelet contact. Transmission of infrared light through sample and reference cuvette was measured.

The sample cuvette was filled with 156 µL platelet rich plasma (PRP, obtained by low speed centrifugation, 150 g for 15 min, RT) and 2 µL 2 mg/mL PR-15 to reach a final concentration of 25 µg/mL or 2 µL control buffer (PBS with 4 % mannitol (w/v) and 1 % sucrose (w/v), pH 7.4). The reference cuvette was filled with 160 µL platelet poor plasma (PPP, centrifuged at 13,300 rpm for 5 min, RT) of each donor for calibration. Subsequently, 2 µL 80 µg/µL CRP-XL stock solution were added to the sample cuvette to initiate platelet aggregation followed by measuring the transmission of infrared light over 7 minutes. Aggregation in the sample led to an increase of the light transmission. APACT LPC Software was used for determination of maximal aggregation. Means of maximal aggregation of PR-15 inhibited and non-inhibited CRP-XL induced samples were used for calculating percentage of inhibition.

4.1.4.11 Differential scanning fluorimetry (DSF)

The unfolding temperature of the PR-15 at different pH values was analyzed by differential scanning fluorimetry (DSF). Samples were prepared by diluting PR-15 to a final concentration of 0.2 mg/mL protein in the appropriate buffer. The fluorescent dye Sypro Orange (SYPRO® Orange Protein gel stain, 5,000x concentrated stock solution, Sigma-Aldrich, Steinheim, Germany) was diluted 1:10 in DMSO. 0.5 µL of the diluted dye was added to 99.5 µL sample for a final concentration of 1:2,000. A 96-well RT-PCR plate with a clear bottom (Bio-Rad Laboratories GmbH, Hercules, California, USA) was used with 20 µL of solution per well. The samples were heated from 25 °C which was held stable for 15 seconds to 95 °C by a heating slope of 4 % using a real time PCR ABI Prism® 7900 HT sequence detection system (Applied Biosystems, Foster City, CA, USA). Besides, the samples were excited at 470 nm and the emission was detected at 570 nm all the time. The measured fluorescence intensity of each sample was plotted against the respective temperature. The inflection point of the generated sigmoidal curve (T_m) was calculated by using the first derivation of this function. The first maximum of this derivation can be assigned to the unfolding temperature of the protein [152].

4.1.4.12 Statistical analysis

All measurements were performed in triplicate for each data point, unless otherwise noted, and are reported as means ± standard deviation (SD). Statistical significance was calculated by one-way ANOVA with Tukey's post hoc test or paired student's t-test with a significance level of $p < 0.05$. MODDE 9.0 (Umetrics, Umeå, Sweden) was used to analyze the experimental design.

4.2 Protein modification

4.2.1 Decoration of silk fibroin (SF) for biomedical application

4.2.1.1 Preparation of aqueous SF solution

SF aqueous solution was prepared as described earlier with slight modifications [87, 88, 153]. Cocoons of the silkworm *B. mori* (kind gift of Trudel Silk, Zuerich, Switzerland) were cut, boiled twice for 1 h in a 0.02 M aqueous sodium carbonate solution and rinsed ten times with ultrapure water to remove the sericin. The dried SF fibers were dissolved in an aqueous 9.3 M lithium bromide solution at 60 °C for about 2 h. The generated SF solution was filtered through a 5 µm syringe filter (Versapor, Pall Life Sciences, Washington, NY) dialyzed against borate buffer (300 mM boric acid, 150 mM sodium chloride, pH 9.0) for 24 h and against ultrapure water for another 48 h with five changes of water in SpectraPor dialysis tubes (MWCO 6–8 kDa, Spectrum Labs, Rancho Dominguez, CA), yielding a 2 % (w/v) SF solution. SF solution was stored at 2–8 °C.

4.2.1.2 Diazonium coupling reaction

An aniline bearing azido functional group was chosen for the decoration of SF tyrosine residues as described earlier with slight modification [93]. 0.360 mmol 4-azidoaniline hydrochloride were dissolved in 1 mL of a 1:1 mixture of acetonitrile and water, 1.430 mmol p-toluenesulfonic acid monohydrate were dissolved in 0.5 mL water and 0.715 mmol sodium nitrite were dissolved in 0.5 mL water. After preparation, all solutions were cooled in an ice bath before mixing. For synthesizing the diazonium ion in situ, these three solutions were combined and the mixture was stirred for 15 minutes at room temperature (**Scheme 2A**). The diazonium coupling reaction was then initiated by adding 4 µL diazonium ion in situ and 496 µL 100 mM borate buffer to 2 mL of a 50 mg/mL borate buffered SF solution (**Scheme 2B**). After 30 minutes of stirring on ice the reaction mixture was dialyzed against ultrapure water. In order to reach a modification rate of 1 %, 3 molar equivalents of diazonium ion in situ were added to the SF solution relative to the total number of approximately 280 tyrosine residues per molecule [87].

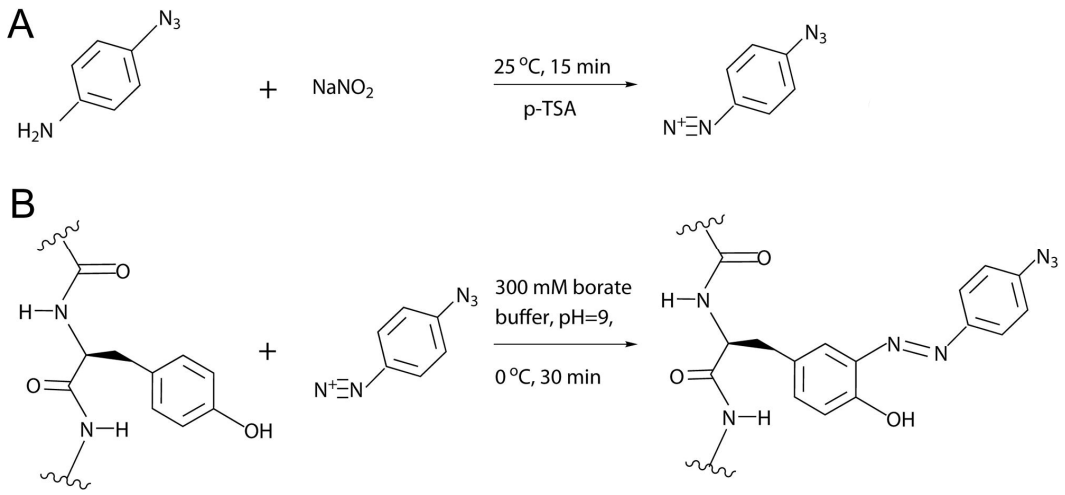

Scheme 2: (A) Synthesis of diazonium ion in situ and (B) diazonium coupling reaction of SF tyrosine residues. Adapted from [87], Copyright (2014), with permission from Elsevier.

4.2.2 Site-directed PEGylation of FGF-2 for biomedical application

4.2.2.1 Expression and purification of FGF-2

Expression and purification of the fusion protein pHisTrx-FGF-2 was performed as previously described [87, 154, 155]. At OD_{600} = 0.6, 0.2 mM IPTG were added to induce protein expression of pHisTrx-FGF-2. After 5 hours incubation at 30 °C and 200 rpm the cells were harvested by centrifugation (Allegra® X-15R, Beckman Coulter, Brea, CA, USA). The obtained pellets were resuspended in lysis buffer (50 mM Tris-HCl, 150 mM sodium chloride, 1 mM phenylmethylsulphonyl fluoride (PMSF), pH 7.5) and solubilized by ultrasonication at 4 °C. After ultracentrifugation at 100,000 g for 1 hour at 4 °C (L8-60M Ultracentrifuge, Beckman Coulter, Brea, CA, USA) pHisTrx tagged FGF-2 remained soluble in the supernatant and was purified by heparin affinity chromatography. For purification pHisTrx tagged FGF-2 was loaded on a HiTrap Heparin HP 1 mL column (GE, Freiburg, Germany) and was eluted via a linear gradient of sodium chloride ranging from 300 mM to 1.5 M using an FPLC system (Aekta Purifier, GE, Freiburg, Germany). The eluted fractions containing pHisTrx tagged FGF-2 were dialyzed against PBS supplemented with 1 mM DTT (SpectraPor, MWCO 6–8 kDa, Spectrum Laboratories, Rancho Dominguez, CA) and, subsequently, the fusion protein pHisTrx-FGF-2 was cleaved by thrombin (GE, Freiburg, Germany) with a final concentration of 1 U thrombin/mg fusion protein at 4 °C overnight. The cleavage was stopped with 1 mM PMSF and murine FGF-2 was purified by heparin affinity chromatography again. After purification, murine FGF-2 was dialyzed against PBS supplemented with 1 mM DTT. Finally, the concentration of murine FGF-2 was determined by UV-absorbance at 280 nm, using an extinction coefficient of 16,766 ± 239 M^{-1} cm^{-1} ($E^{0.1\,\%}$ = 0.964) according to Pantoliano et al. [156]. The determined average yield of murine FGF-2 was 5 mg/L expression culture. Until further use, murine FGF-2 was stored in PBS supplemented with 3 mM DTT at -80 °C.

4.2.2.2 PEGylation of FGF-2

FGF-2 was PEGylated in a site-directed pattern by deploying free thiol groups (four cysteine residues: two pointing outwards, two pointing into the protein core) with thiol reactive 3 kDa PEGs carrying ethinyl- or carboxyl-groups as described before with modification [87, 157]. FGF-2 was dialyzed (Slide-A-Lyzer Mini Dialysis Device, MWCO 10 kDa, Thermo Fisher Scientific, Rockford, USA) against PBS containing 5 mM EDTA (pH 8.0). Subsequently, about 500 µg dialyzed FGF-2 were added to a 20-fold molar excess of iodoacetamido-PEG-alkyne (3,317 g/mol, Rapp Polymere, Tuebingen, Germany) or iodoacetyl-PEG-acid (3,400 g/mol, Nanocs, New York, NY, USA) and incubated for 4 hours at 37 °C with shaking at 300 rpm (Eppendorf Thermomixer Comfort, Hamburg, Germany) (**Scheme 3**). 0.6 mg/mL DTT were added to the reaction mixture to finish PEGylation reaction.

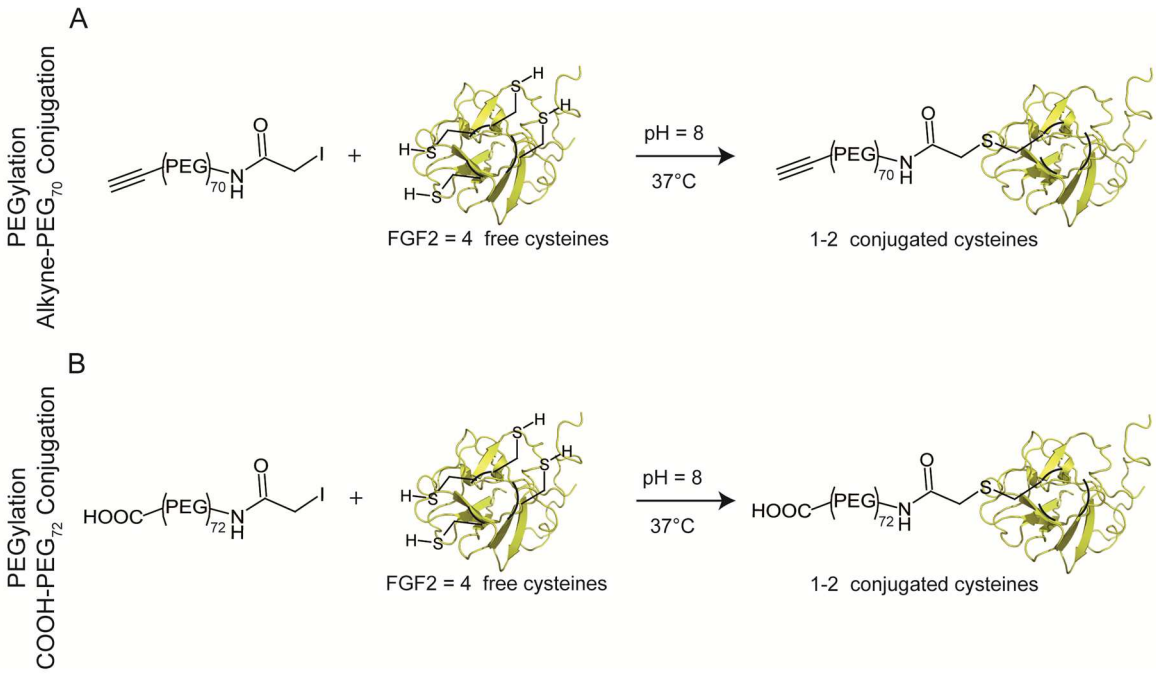

Scheme 3: Regiospecific PEGylation of FGF-2 with 3 kDa PEG bearing (A) alkyne and (B) carboxylic acid functionality. (PEG)Number indicates the number of ethylene glycol monomer units. PDB code FGF-2 = 1BLD. Reprinted from [87], Copyright (2014), with permission from Elsevier.

Heparin based affinity chromatography on an ÄKTA purifier™ system (GE, Munich, Germany) was used to purify PEGylated FGF-2, and via a linear gradient of sodium chloride from 300 mM to 1.5 M the bound PEGylated FGF-2 was eluted from the HiTrap Heparin HP 1 mL column (GE, Munich, Germany). Fractions of the eluted protein were collected and dialyzed (SpectraPor, MWCO 6–8 kDa, Spectrum Laboratories, Rancho Dominguez, CA) overnight against PBS buffer, pH 7.4, containing 0.6 mg/mL DTT. Vivaspin® 6 Centrifugal Concentrators (MWCO 5 kDa, Sartorius Stedim Biotech, Goettingen, Germany) were then used to concentrate protein content by centrifugation at 3,400 rpm and 4 °C (Varifuge, Heraeus, Hanau, Germany). Finally, PEG-FGF-2 was dialyzed (Slide-A-Lyzer Mini Dialysis Device, MWCO 10,000 g/mol, Thermo Fisher

Scientific, Rockford, USA) against PBS buffer (pH 7.4) for 24 h at 4 °C and the yielded PEG-FGF-2 was stored at 2–8 °C until further use.

In order to optimize PEGylation reaction to more protein protecting conditions, different temperatures (4 °C/15 °C/25 °C) and times (1 h/2 h/3 h/4 h) were tested for PEGylation. At all three temperatures PEGylation took place to a comparable degree. Hence, all further reactions were performed at 4 °C to save FGF-2 activity.

Unfortunately, the 3 kDa PEG appeared to be too short for purification via Äkta system as well as quantification via HPLC. As a result, a 10 kDa iodoacetamido-PEG-alkyne (10,267 g/mol, Rapp Polymere, Tuebingen, Germany) and a 10 kDa iodoacetyl-PEG-amine (10,000 g/mol, Nanocs, New York, NY, USA) were used for FGF-2 PEGylation at 4 °C, respectively, as described above (**Scheme 4**).

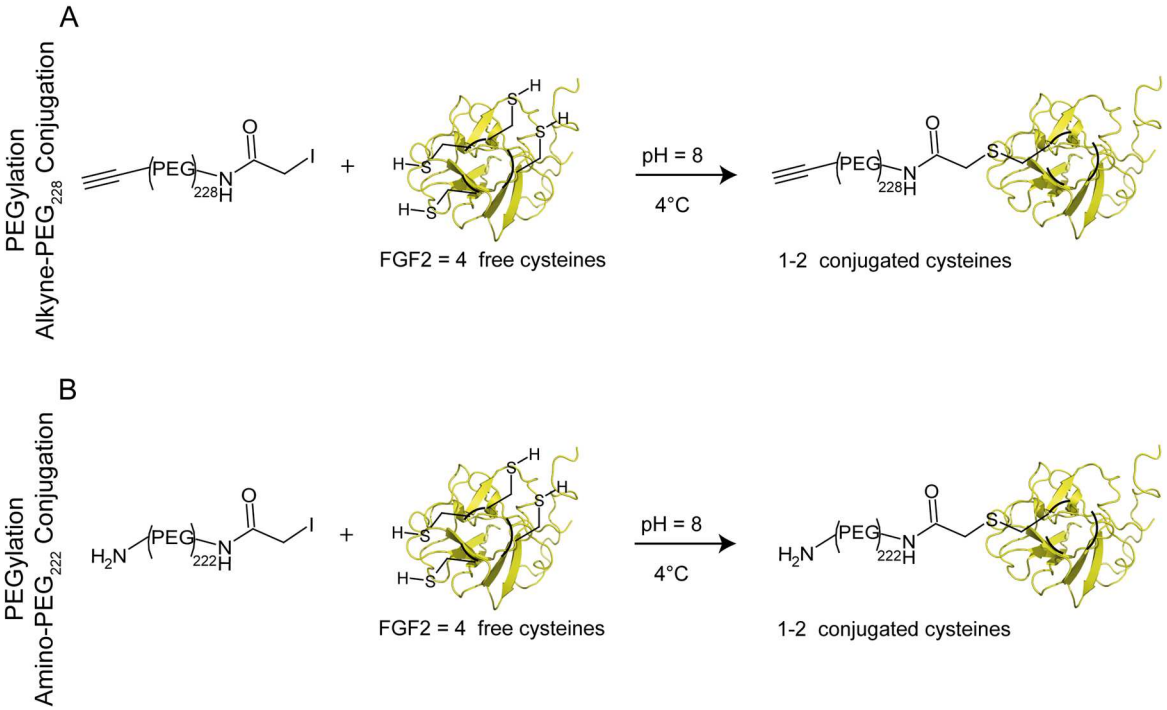

Scheme 4: Regiospecific PEGylation of FGF-2 with 10 kDa PEG bearing (A) alkyne and (B) amine functionality. (PEG)Number indicates the number of ethylene glycol monomer units. PDB code FGF-2 = 1BLD. Adapted from [87], Copyright (2014), with permission from Elsevier.

4.2.2.3 Characterization of PEG-FGF-2

4.2.2.3.1 SDS-PAGE

Purified PEGylated FGF-2 was analyzed by SDS-PAGE analysis under reduced conditions as described before [158] with slight modification. 5 µg sample were loaded per lane. Gels were stained with Coomassie Brilliant Blue and photographed using FluorChem FC2 imaging system (Protein Simple, Santa Clara, CA, USA).

4.2.2.3.2 MALDI-TOF mass spectrometry (MALDI-TOF MS)

MALDI-TOF MS spectra of desalted PEG-FGF-2 as well as FGF-2 samples were obtained according to the procedure described before (4.1.4.6).

4.2.2.3.3 Reversed-phase high performance liquid chromatography (RP-HPLC)

10 kDa PEG-FGF-2 was characterized with RP-HPLC (VWR Hitachi LaChromUltraTM HPLC system equipped with a diode array detector) analysis using Zorbax Eclipse XDB-C18 column (4.6 x 150 mm, particle size = 5 µm, Agilent Technologies, Santa Clara, CA) at 51 °C. Mobile phases comprised two eluents. Eluent A consisted of 0.1 % TFA in ultrapure water and eluent B was 0.1 % TFA in ACN. For separation of FGF-2 and PEG-FGF-2 a gradient of 30–60 % eluent B in 12 minutes was used with a flow rate of 0.5 mL/min. 90 µL sample were injected per run. FGF-2 was detected at 214 nm.

4.2.2.3.4 Fluorescence spectroscopy

In order to investigate correct folding of FGF-2 after PEGylation (10 kDa PEG), a fluorescence spectrum was assessed with a LS-50B luminescence spectrometer (Perkin Elmer, Waltham, MA, USA) using a quartz cuvette (pathlength 10 mm). Excitation was set to 280 nm with 10 nm slit width and a scan speed of 240 nm/min. The emission spectrum was recorded of a 0.2 mg/mL sample solution in PBS buffer. Unfolding of native FGF-2 was evoked by 10 minutes incubation with a guanidinium hydrochloride solution with a final concentration of 6 M at 90 °C. Finally, fluorescence emission was recorded of a 0.02 mg/mL sample solution as described above. Emission spectrum of PBS buffer was used for baseline correction.

4.2.2.3.5 Differential scanning fluorimetry (DSF)

Differential scanning fluorimetry (DSF) was performed according to the procedure described before (4.1.4.11) in order to detect the unfolding temperature of FGF-2 and 10 kDa PEG-FGF-2. Samples were diluted to a final concentration of 0.2 mg/mL protein in PBS buffer.

4.2.2.3.6 WST-1 assay

The murine fibroblast cell line NIH 3T3 (ATCC® CRL-1658™, Rockville, MD, USA) [159] was used to assess bioactivity of PEGylated FGF-2. Cells were cultured in high glucose Dulbecco's Modified Eagle Medium (DMEM) supplemented with 10 % fetal calf serum (FCS), 100 U/mL penicillin and 100 µg/mL streptomycin (growth medium). 1,000 cells per well were plated in 96-well clear tissue culture plates in growth medium and incubated at 37 °C and 5 % CO_2. After 24 h medium was changed to assay medium (high glucose DMEM supplemented with 0.5 % FCS, 0.5 % BSA, 100 U/mL penicillin and 100 µg/mL streptomycin) and incubated at 37 °C and 5 % CO_2 again. Dilution series of FGF-2 references were prepared in assay medium with concentrations from 3.2–0.0016 µg/mL and added to the cells after additional 18 h. For PEG-FGF-2 samples dilution series were started with 12.8 µg/mL. Cell proliferation was stimulated for 48 h at 37 °C

and 5 % CO_2. A water soluble tetrazolium salt reagent (WST-1, 4-[3-(4-Iodophenyl)-2-(4-nitrophenyl)-2H-5-tetrazolio]-1,3-benzene disulfonate , Roche Diagnostics GmbH, Mannheim, Germany) was used to quantify cell proliferation spectrophotometrically. 10 µL WST-1 reagent were added per well and incubated for 4 h at 37 °C and 5 % CO_2. Absorbance was measured at 450 nm using Spectramax 250 microplate reader (Molecular Devices, Sunnyvale, CA, USA).

4.2.2.3.7 Phosphorylated ERK 1/2 (pERK 1/2)

FGF-2 activates mitogen-activated protein kinase (MAPK) pathways [160]. FGF-2 stimulation of MAPK activation after PEGylation was investigated with ERK phosphorylation, an effector kinase of the MAPK pathway. Therefore, NIH 3T3 cells were cultured in high glucose Dulbecco's Modified Eagle Medium (DMEM) supplemented with 10 % fetal calf serum (FCS), 100 U/mL penicillin and 100 µg/mL streptomycin (growth medium). 75,000 cells per well were plated in 6-well clear tissue culture plates in growth medium and incubated at 37 °C and 5 % CO_2. After 18 h medium was changed to assay medium (high glucose DMEM supplemented with 0.5 % FCS, 100 U/mL penicillin and 100 µg/mL streptomycin) and incubated at 37 °C and 5 % CO_2 again. After additional 18 h cells were treated with PEGylated FGF-2 samples as well as FGF-2 as references at final concentrations of 100 ng/mL and 10 ng/mL for 25 minutes at 37 °C and 5 % CO_2. After stimulation, cells were washed thoroughly with ice-cold PBS and lysed using M-PER® Mammalian Protein Extraction Reagent (Thermo Fisher Scientific, Rockford, USA). Total cellular proteins were collected by centrifugation at 12,000 rpm for 20 minutes at 4 °C (Centrifuge Sigma 3K12, Osterode am Harz, Germany) and analyzed by western blot analysis. Therefore, cell lysates were mixed with reducing SDS sample buffer and loaded on a 12 % tris-glycine SDS-polyacrylamide gel after 5 minutes heating at 95 °C as outlined before [158]. After electrophoresis the fixed proteins on the gel were blotted onto a nitrocellulose membrane under wet conditions using an electric field vertical to the surface of the gel (80 V for 2 h). A sterile filtered solution of 5 % BSA in TBST buffer was used for membrane blocking for 90 minutes at room temperature in order to reduce unspecific binding of the antibodies. Phospho p44/42 MAPK rabbit monoclonal antibody (Cell Signaling Technology, Beverly, MA, USA) diluted 1:1,000 in TBST buffer was used as primary antibody and an anti-rabbit IgG HRP-linked secondary antibody (Cell Signaling Technology, Beverly, MA, USA) diluted 1:5,000 in TBST buffer was used for detection. Between all steps the membrane was washed thoroughly with TBST buffer for 5 to 10 minutes. Peroxidase signals were detected with SuperSignal® West Pico Chemiluminescence Substrate (Thermo Fisher Scientific, Rockford, USA) and photographed on the FluorChem FC2 imaging system (Protein Simple, Santa Clara, CA, USA). After finishing detection of phosphorylated ERK 1/2, blots were stripped with Mercapto-Strip-Buffer for 2 h at 50 °C, followed by excessive washing of the blots with distilled water. Subsequently, ERK 1/2 detection was performed using p44/42 MAPK (ERK 1/2) rabbit mAB (Cell Signaling Technology, Beverly, MA, USA) as primary antibody (diluted

1:1,000 in TBST buffer supplemented with 5 % BSA) and an anti-rabbit IgG HRP-linked secondary antibody (Cell Signaling Technology, Beverly, MA, USA) diluted 1:3,000 in TBST buffer for detection according to the same procedure.

4.2.2.4 Synthesis of SF-PEG-FGF-2 conjugates in solution

4.2.2.4.1 Click chemistry

SF-alkyne-PEG-FGF-2 conjugates were synthesized performing copper catalyzed Huisgen 1,3-dipolar cycloaddition of alkyne-PEG-FGF-2 (3 kDa PEG) with azido-SF (**Scheme 5A**). In brief, alkyne-PEG-FGF-2 (2 alkyne groups per molecule) solution and 1 % azido-SF solution (2.8 azido groups per molecule) were mixed in a 1:1.4 molar ratio with 0.2 mM sodium ascorbate, 0.1 mM copper sulfate and 0.02 mM TBTA in aqueous solution at neutral pH and incubated at 4 °C. After 24 h, EDTA was added with a final concentration of 1 mM to stop click reaction by building a complex with copper ions. Subsequently, the solution was dialyzed (Slide-A-Lyzer Mini Dialysis Device, MWCO 10 kDa, Thermo Fisher Scientific, Rockford, USA) against ultrapure water. In addition, negative controls were prepared in the same way, but the copper sulfate solution was replaced by ultrapure water. As further control carboxy-PEG-FGF-2-PEG was used instead of alkyne-PEG-FGF-2 while all other reaction conditions remained unchanged.

4.2.2.4.2 EDC/NHS chemistry

SF-COOH-PEG-FGF-2 conjugates were synthesized performing EDC/NHS chemistry with carboxy-PEG-FGF-2 (3 kDa PEG) and native SF (**Scheme 5B**). Native SF and carboxy-PEG-FGF-2 in MES buffer (0.1 M MES, 0.5 M sodium chloride, pH 6) were mixed in a 1:1.4 molar ratio with 3 mM EDC and 6 mM NHS and incubated at 4 °C. After 4 h, the reaction mixture was dialyzed (Slide-A-Lyzer Mini Dialysis Device, MWCO 10 kDa, Thermo Fisher Scientific, Rockford, USA) against ultrapure water. Additionally, negative controls were prepared in the same way but MES buffer (0.1 M MES, 0.5 M sodium chloride, pH 6) was used instead of EDC as well as NHS solution. As further control alkyne-PEG-FGF-2 was used instead of carboxy-PEG-FGF-2 while all other conditions remained unchanged.

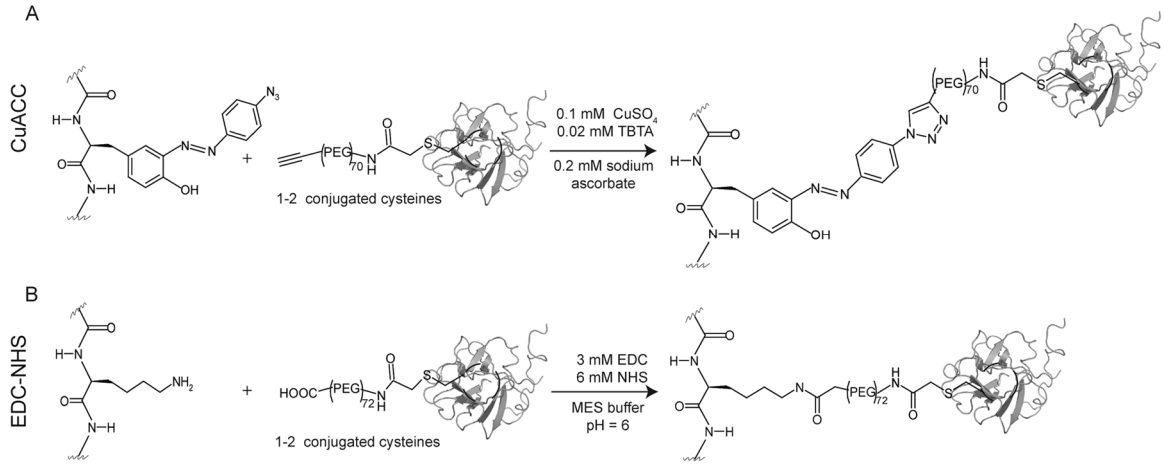

Scheme 5: Reaction scheme detailing the synthesis of SF-FGF-2 conjugates via (A) click and via (B) EDC/NHS chemistry. (PEG)Number indicates the number of ethylene glycol monomer units. PDB code FGF-2 = 1BLD. Reprinted from [87], Copyright (2014), with permission from Elsevier.

4.2.2.5 Characterization of SF-PEG-FGF-2 conjugates

4.2.2.5.1 Western blot

Western blot analysis was performed to visualize SF-PEG-FGF-2 conjugates. Therefore, 200 ng of each SF-PEG-FGF-2 conjugate and native FGF-2 as reference were mixed with reducing SDS sample buffer and loaded per lane on a 12 % tris-glycine SDS-polyacrylamide gel. The proteins fixed on the gel were transferred to a nitrocellulose membrane under wet conditions using an electric field vertical to the surface of the gel (80 V for 3 h). Unspecific binding of the antibody was reduced by blocking the membrane with 3 % (w/v) skin milk powder in PBS buffer for 1 hour at room temperature under gently shaking before incubation with 1 µg/mL anti-FGF-2 primary monoclonal antibody, clone bFM-2 (Merck Millipore, Darmstadt, Germany) in 3 % (w/v) skin milk powder in PBS buffer overnight at 4 °C under shaking. Subsequently, the membrane was washed three times with 0.2 % (w/v) Tween® 20 in PBS and three times with PBS for 15 min each. Then, the membrane was incubated with a secondary peroxidase-conjugated anti-mouse IgG antibody (Sigma Aldrich, St. Louis, MO, USA), diluted 1:2,000, in 3 % (w/v) skin milk powder in PBS buffer. After additional washing steps, peroxidase signals were detected with SuperSignal® West Pico Chemiluminescence Substrate (Thermo Fisher Scientific, Rockford, USA) and pictures were taken on the FluorChem FC2 imaging system (Protein Simple, Santa Clara, CA, USA).

4.2.2.5.2 WST-1 assay

WST-1 proliferation assay was performed according the procedure described above (4.2.2.3.6) with slight modification. 2,000 cells per well were seeded in 96-well clear tissue culture plates in growth medium. Dilution series of 3 kDa PEG-FGF-2, SF-PEG-FGF-2 conjugates and FGF-2 references were prepared in assay medium and added to the cells after additional 24 h with final concentrations from 1,600 – 0.0031 ng/mL. 20 µL WST-1 reagent were added per well for quantification.

4.2.2.6 FGF-2 immobilization on beads

4.2.2.6.1 Decoration of beads with functional groups

SF microspheres decoration with azido groups

100 µL Polystyrene (PS) microspheres (4 µm) were incubated in 1 mL of an aqueous polyethylenimine solution (PEI, 0.5 mg/mL). After 15 minutes the PEI solution was removed by centrifugation with 1,000 g at 4 °C for 2 minutes (Centrifuge Sigma 3K12, Osterode am Harz, Germany), the microspheres were washed twice with ultrapure water and resuspended in 1 mL SF (1 mg/mL) or azido-SF (1.3 mg/mL), respectively. Subsequently, the microspheres were shaken for 10 minutes at 1,000 rpm at 4 °C (Eppendorf Thermomixer Comfort, Hamburg, Germany) and then washed twice with ultrapure water after removing SF solution by centrifugation. In order to induce β-sheet formation, the resulting SF-coated PS microspheres were immersed in 90 % methanol and shaken at 1,000 rpm for 15 minutes at 4 °C. Finally, the SF-coated PS microspheres were dried by a flow of nitrogen gas for about 5 minutes (Zymark Turbovap LV Evaporator, Allschwil, Switzerland). According to this method, four layers of SF and two layers of azido-SF were coated.

NHS-activated sepharose beads decoration with azido groups

NHS-activated sepharose beads (NHS-activated Sepharose™ 4 Fast flow; 20 µmol NHS/mL drained medium; bead structure: highly cross-linked 4 % agarose, spherical; mean particle size: 90 µm, particle size range: 45–165 µm; GE Healthcare, Munich, Germany) were washed with 15 medium volumes of cold 1 mM hydrochloric acid immediately before use. The beads were then modified with 11-azido-3,6,9-trioxaundecan-1-amine (218.25 g/mol, Aldrich, St. Louis, MO, USA) in 1:1 or 1:5 molar ratio in PBS buffer at pH 7.4 for 2 hours at room temperature with gentle shaking on a roll shaker. Non-reacted carboxyl groups on the beads were blocked with a solution containing 0.5 M ethanolamine and 0.5 M sodium chloride (pH 8.3) for 30 minutes at room temperature on a roll shaker. Subsequently, beads were washed thoroughly with PBS buffer.

PMMA beads decoration with azido or carboxyl groups

Carboxylated poly(methyl methacrylate) (PMMA) beads (4.6 µm; 8.3 µmol COOH/g; PolyAn, Berlin, Germany) were resuspended in MES buffer (0.1 M MES, 0.5 M sodium chloride, pH 6). EDC (3 mM), NHS (6 mM) and 11-azido-3,6,9-trioxaundecan-1-amine (218.25 g/mol, Aldrich, St. Louis, MO, USA) for click reaction or carboxy-PEG_4-amine (265.3 g/mol) (Thermo Fisher Scientific, Rockford, USA) for EDC/NHS chemistry were given to 50 µL of the bead suspension. The mixture was briefly vortexed and then mixed by rolling at room temperature for 2 hours. In order to finish the coupling reaction, the beads were thoroughly washed for three times with TBST buffer (20 mM Tris, 150 mM sodium chloride, 0.1 % Tween® 20, pH 7.4) and three times with phosphate buffer with high salt concentration (12 mM phosphate, 1.5 M sodium chloride, pH 7.4).

4.2.2.6.2 Evaluation of presence of azido groups

The presence of azido groups on the bead surface was verified by clicking Acetylene-Fluor 488 (587.62 g/mol) to the modified beads via click chemistry. Therefore, 50 µL copper sulfate solution (final concentration 0.1 mM) in PBS was mixed with 50 µL TBTA solution (final concentration 0.5 mM) in DMSO/tert. butanol (1:4), 50 µL bead suspension and 50 µL Acetylene Fluor 488 solution (final concentration 0.34 mM) were added and mixed. Finally, 50 µL sodium ascorbate solution (final concentration 5 mM) in PBS buffer was added to the reaction and gently mixed for 1.5 hours at room temperature on a roll shaker. Click reaction was stopped by adding EDTA solution to a final concentration of 1 mM to complex copper ions. After 5 minutes gently shaking, beads were washed three times with a high salt buffer (12 mM phosphate, 1.5 M sodium chloride, pH 7.4) and three times with TBST buffer in order to remove unbound Acetylene Fluor 488. Finally, the beads were resuspended in PBS buffer and analyzed using inverted epifluorescence microscope Axio Observer Z1 (Zeiss, Oberkochen, Germany).

4.2.2.6.3 Immobilization of FGF-2 on beads via click or EDC/NHS chemistry

50 µL azide modified beads were coupled with 482 ng PEGylated FGF-2 via click chemistry as described above (4.2.2.6.2.; **Scheme 6A**), and 50 µL carboxylated beads were resuspended in MES buffer (0.1 M MES, 0.5 M sodium chloride, pH 6) before EDC (3 mM) and NHS (6 mM) were added to activate carboxyl groups on the beads. After about 15 minutes of incubation, beads were washed with MES buffer to remove unbound coupling reagents and PEGylated FGF-2 was added (**Scheme 6B**). The EDC/NHS reaction mixture was briefly vortexed and then mixed by rolling at room temperature for 2 hours. Finally, beads were washed three times with TBST buffer to stop reaction and three times with a high salt buffer (12 mM phosphate, 1.5 M sodium chloride, pH 7.4) in order to remove unbound FGF-2.

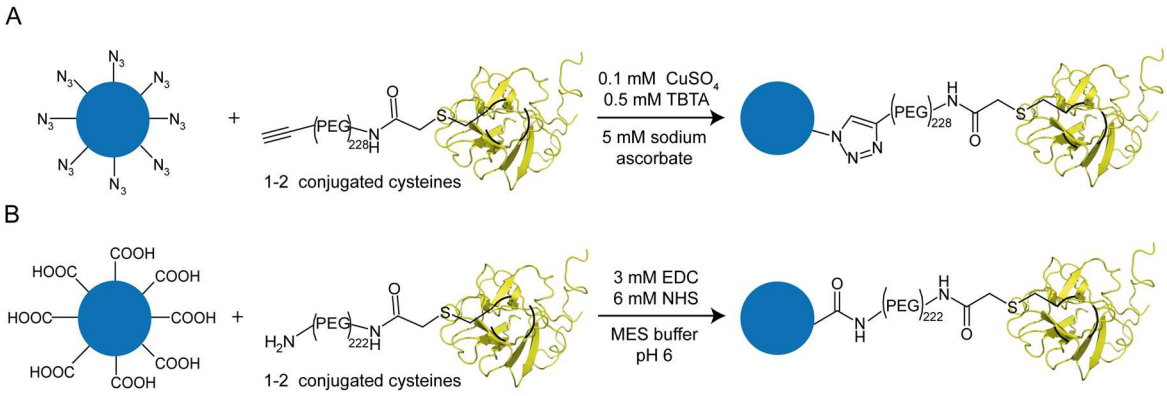

Scheme 6: Reaction schemes detailing the immobilization of FGF-2 on (A) azide modified and (B) carboxylated beads. (PEG)Number indicates the number of ethylene glycol monomer units. PDB code FGF-2 = 1BLD.

Unfortunately, non-specific binding of PEGylated FGF-2 as well as native FGF-2 to the beads was observed for each bead material. Non-specific binding of the primary as well as the secondary FGF-2 antibody was excluded. Several modifications of the procedure were tried to optimize the immobilization reaction and to avoid non-specific binding of FGF-2. On the one hand, the beads were incubated in TBST buffer supplemented with 5 % BSA for 1 hour at room temperature under gently shaking, and on the other hand, the beads were shielded with a 5 kDa amino-PEG-azide (4,790 g/mol; Rapp Polymere, Tuebingen, Germany) instead of the 200 Da PEG. Furthermore, the coupling reactions were performed at different pH values (0.1 M MES, 1 M sodium chloride, pH 4.5/0.1 M MES, 1 M sodium chloride, pH 6 /0.1 M boric acid, 1 M sodium chloride, pH 9.0) or under high salt conditions (12 mM phosphate, 1.5 M sodium chloride, pH 7.4).

4.2.2.7 Characterization of FGF-2 loaded beads

4.2.2.7.1 Fluorescence imaging and flow cytometry

Beads were incubated with a mouse monoclonal anti-FGF-2 primary antibody (clone bFM-2, Merck Millipore, Darmstadt, Germany) and subsequently with a secondary Alexa Fluor® 488 conjugated anti-mouse IgG antibody (Thermo Fisher Scientific, Rockford, USA) prior analysis. Fluorescence imaging was done with an inverted epifluorescence microscope Axio Observer Z1 equipped with a HXP120C lamp, an AxioCam MRm camera and a Plan-Apochromat 40x/0.95 objective (Zeiss, Oberkochen, Germany). Images were recorded using fluorescence excitation at λ = 450–490 nm, dichroic beam splitter at λ = 495 nm and emission at λ = 500–550 nm. Flow cytometry was performed with a FACS Calibur system (Becton Dickinson, Franklin Lakes, NY, USA). A 488 nm argon-ion laser was used for excitation and the emission channel FL2 (530 nm) was used for detection. 5,000 beads were analyzed with BD CellQuestTM Pro and all data were evaluated using Flowing Software (Version 2.5.1; Turku Bioimaging, Turku, Finland).

4.2.2.7.2 Bioactivity of immobilized FGF-2

Bioactivity of coupled FGF-2 was assessed via WST-1 proliferation assay (4.2.2.3.6) as well as the investigation of ERK 1/2 phosphorylation (4.2.2.3.7) according the procedures described above. For WST-1 proliferation assay 5 µL bead suspension were added to each well. In order to asses ERK phosphorylation, NIH 3T3 cells were stimulated with 10 µL bead suspension per well and references FGF-2 and 10 kDa PEGylated FGF-2 were added with a final concentration of 10 ng/mL or 30 ng/mL.

4.2.3 Introduction of a non-natural amino acid into IGF-I

4.2.3.1 Synthesis of propargyl-L-lysine (plk)

Plk was prepared as described before [95]. 13 mmol Boc-Lys-OH ((tert-butyloxycarbonyl)-protected L-lysine; Merck, Darmstadt, Germany) were dissolved in a mixture of 30 mL 1 M sodium hydroxide and 30 mL tetrahydrofuran. The solution was cooled to 0 °C in an ice-bath before 10 mmol propargylcholoroformate were added dropwise over 5 min under stirring. After removing the ice bath, the solution was stirred overnight at room temperature. The next day, the solution was cooled to 0 °C and the aqueous phase was washed with 150 mL ice-cold diethylether in a separating funnel. The organic phase was disposed, and the aqueous phase was acidified with 150 mL ice-cold 1 M hydrochloric acid. The acidified solution was then extracted twice with 150 mL ice-cold ethyl acetate in a separating funnel. Subsequently, the organic layers were combined and dried with magnesium sulfate. After 5 minutes stirring at room temperature, the magnesium sulfate was filtered off and the solvent was removed using a rotary evaporator (Hei-VAP-Precision, Heidolph, Schwabach, Germany). The remaining Boc-protected plk was then dissolved in 26 mL dry dichloromethane, 26 mL trifluoroacetic acid were added dropwise and the solution was stirred for 1 hour at room temperature before evaporating the solvent with a rotary evaporator again. Plk was precipitated by addition of 200 mL diethylether to the residue, filtered off and dried in a vacuum dryer (KVTS 22, SalvisLab, Rotkreuz, Schweiz). NMR analysis was done in order to verify the synthesized product.

4.2.3.2 Nuclear Magnetic Resonance spectroscopy (NMR)

NMR measurements were recorded on a Bruker Avance III 400 MHz spectrometer (Bruker BioSpin, Karlsruhe, Germany) and the data were processed with the TopSpin 3.0 software from Bruker. About 15 mg of the product were weighed in a standard 5 mm NMR tube (ST500; Norell, Landisville, USA) and dissolved in 800 µL deuterated water (D_2O, 99.9 % D; Deutero GmbH, Kastellaun, Germany) and the spectra were referenced to the residual solvent signal of D_2O (4.79 ppm) [161].

4.2.3.3 DNA Sequence of IGF-I

The human cDNA of IGF-I was cloned into pCMV6-XL4 vector using a linker-based strategy, EcoR I on the 5’ and Xho I on the 3’ end of the insert. This human cDNA clone consisted of 5,181 bp and was purchased from Origene (Herford, Germany). The DNA sequence of IGF-I (**supplementary information**) was modified by site-directed mutagenesis in order to incorporate the amber stop codon (TAG) at lysine 65. That means just one point mutation from AAG to TAG was necessary. Additionally, a recognition sequence of the restriction enzyme NdeI (5’CATATG) was inserted at the 5’-terminus and the recognition sequence of BamHI (5’GGATCC) was inserted at the 3’-terminus:

4.2.3.4 Primer design

In order to incorporate point mutation by cyclic mutagenesis, two mutagenic primer without restriction sites and start/stop codons were designed and ordered (forward mutagenic primer: 5‘ GTATTGCGCA CCCCTC**TAG**C CTGCCAAGTC AGCTCG 3‘, reverse mutagenic primer: 5’ CGAGCT GACTTGGCAG G**CTA**GAGGGG TGCGCAATAC 3‘, **amber stop codon**, Invitrogen, Karlsruhe, Germany).

For subsequent insertion of restriction sites (NdeI, BamHI) as well as start/stop codons by PCR of the mutated gene, a universal and an additional mutagenic primer were designed and ordered (forward primer NdeI: 5’ CAAGAACATA TGGGACCGGA GACGCTCTGC 3‘, reverse primer BamHI: 5’ CAAGAAGGAT CCTTAAGCTG ACTTGGCAGG **CTA**G 3‘, **amber stop codon**, restriction site, *start/stop codon*, Invitrogen, Karlsruhe, Germany).

4.2.3.5 Mutagenesis

Site-directed mutagenesis by polymerase chain reaction (PCR) was performed according the procedure of the Stratagene’s QuikChange® Site-Directed Mutagenesis Kit (La Jolla, CA, USA) in order to insert point mutation. PCR was carried out using supercoiled double-stranded DNA (pCMV6-XL4 vector containing IGF-I cDNA) as template with a pair of mutagenic primers, each complementary to opposite strands of the vector (**Table 9**).

1. *PCR*

Reactants	*Volume [µL]*
ddH_2O	37
10x buffer (Promega)	5
dNTP Mix 10 mM	1
fw. mut. Primer 5 µM	2.5
rev. mut. Primer 5 µM	2.5
IGF-I cDNA 5 ng/µL	1
Pfu Polymerase	1

Temperature	*Time*	*Cycles*
95 °C	30 sec	
95 °C	30 sec	
55 °C	1 min	16
68 °C	10 min 22 sec	
4 °C		

Table 9: Reaction mixture and cycling conditions of the 1st PCR.

Digestion with DpnI

Parental supercoiled dsDNA was digested with 1 µL DpnI restriction enzyme (10 U/µL). Reaction was thoroughly mixed, spun down in a microcentrifuge and incubated for 1 hour at 37 °C followed by 20 minutes at 80 °C.

Purification of DpnI digested PCR products

DpnI digested PCR products were purified with QIAquick PCR purification Kit (Qiagen, Hilden, Germany). 200 µL buffer PB were added to 40 µL PCR sample and mixed thoroughly. A QIAquick spin column was placed in a 2 mL collection tube. The PCR sample was applied on the

column in order to bind DNA and incubated for 1 minute. Subsequently, the column and the collection tube were centrifuged at 13,000 rpm for 1 minute and the flow-through was discarded. The column was washed with 750 µL buffer PE and centrifuged twice at 13,000 rpm for 1 minute, discarding the flow-through in between. QIAquick column was placed in a clean 1.5 mL microcentrifuge tube and DNA was eluted by addition of 30 µL nuclease-free water to the center of the membrane. After 1 minute incubation at room temperature, DNA was eluted by centrifugation for 1 minute at 13,000 rpm. DNA was quantified with an Infinite® 200 NanoQuant (Tecan, Maennedorf, Switzerland) at 260 nm, analyzed on an agarose gel as described below and stored at -20 °C.

2. *PCR*

A second PCR was performed to incorporate restriction sites NdeI and BamHI as well as a start codon. The two primers flanked the mutated IGF-I sequence in order to finally cut the insert of interest. The forward primer contained the NdeI sequence and the ATG start codon which serves as ATG codon for the N-terminal methionine residue as well. The reverse primer contained the BamHI sequence as well as the amber stop codon (**Table 10**).

Reactants	*Volume [µL]*
ddH_2O	32
10x buffer (Promega)	5
dNTP Mix 10 mM	1
fw. Primer NdeI 5 µM	5
rev. Primer BamHI 5 µM	5
1. *PCR product 8.4 ng/µL*	1
or IGF-I cDNA 5 ng/µL	
Pfu Polymerase	1

Temperature	*Time*	*Cycles*
95 °C	1 min	
95 °C	30 sec	
59 °C	1 min	35
72 °C	2 min	
72 °C	5 min	
4 °C		

Table 10: Reaction mixture and cycling conditions of the 2nd PCR.

PCR products were purified with QIAquick PCR purification Kit as described above, quantified at 260 nm using Infinite® 200 NanoQuant (Tecan, Maennedorf, Switzerland), analyzed on an agarose gel as described below and stored at -20 °C.

Agarose gel electrophoresis

DNA fragments were separated by length using agarose gel electrophoresis. Therefore, 0.35 g agarose powder were dispersed in 50 mL TAE buffer and dissolved under heating to get a 0.7 % agarose gel. 4 µL ethidium bromide were added before the agarose solution was poured into the gel cast. Finally, a gel comb was placed in the cast to form wells for sample loading. Samples were mixed with 6x Gel Loading Buffer (Orange; Jena Bioscience, Jena, Germany) and subsequently loaded into the wells of the agarose gel. A GeneRuler 1 kb DNA Ladder (250–10,000 bp), a

GeneRuler™ Ladder Mix (100–10,000 bp) and a GeneRuler™ 100 bp Plus DNA Ladder (100–3,000 bp) (Thermo Fisher Scientific, Braunschweig, Germany) were used. The gel was run at 300 mA, 80 V, 50 W until sufficient separation of the DNA ladder.

4.2.3.6 Subcloning

The modified IGF-I insert obtained by site-directed mutagenesis of pCMV6-XL4 vector and the pET11a vector (kind gift of M.Rubini, Konstanz, Germany) were digested simultaneously with the restriction enzymes BamHI as well as NdeI for 4 hours at 37 °C (**Table 11**).

Reactants	*Volume [µL]*
ddH_2O	4
NEBuffer 3	2
BSA	0.2
pET11a vector (4 µg)	11.8
BamHI	1
NdeI	1

Reactants	*Volume [µL]*
ddH_2O	3.1
NEBuffer 3	2
BSA	0.2
2. PCR product (3 µg)	12.7
BamHI	1
NdeI	1

Table 11: Reaction mixtures of pET11a vector and IGF-I insert digestion with BamHI and NdeI.

In order to prevent self-ligation, the digested pET11a vector was dephosphorylated with antarctic phosphatase. Therefore, 1.5 µL ddH_2O, 2.5 µL antarctic phosphatase buffer and 1 µL antarctic phosphatase (New England BioLabs GmbH, Frankfurt, Germany) were added and the reaction was incubated for 15 minutes at 37 °C and 5 minutes at 65 °C.
The obtained fragments were analyzed using agarose gel electrophoresis. Therefore, a 0.7 % agarose gel was prepared as described above. A GeneRuler™ 1 kp Plus DNA Ladder (75–20,000 bp) (Thermo Fisher Scientific, Braunschweig, Germany) was used. The gel was run at 300 mA, 80 V and 50 W until sufficient separation of the DNA ladder. The yielded fragments were cut out and purified using GeneJET Gel Extraction Kit (Thermo Fisher Scientific, Rockford, USA) according to manufacturer's instruction. After quantifying DNA of the purified fragments, ligation between the modified IGF-I insert and the pET11a vector was performed with different molar ratios by the use of DNA ligase.

Calculation of required insert and vector volumes for ligation

Molar ratio insert/vector 3:1:

8.5 µL / ((40.5 ng/µL vector · 0.25 kb insert · 3)/ (20.25 ng/µL insert · 5.637 kb vector) + 1)
= 6.7 µL vector
8.5 µL – 6.7 µL = 1.8 µL insert

Molar ratio insert/vector 5:1:

8.5 µL / ((35 ng/µL vector · 0.25 kb insert · 3) /(26 ng/µL insert · 5.637 kb vector) + 1)
= 6.5 µL vector
8.5 µL – 6.5 µL = 2 µL insert

Molar ratio insert/vector 3:1:

Reactants	*Volume [µL]*
IGF-I 20.25 ng/µL	1.8
pET11a vector 40.5 ng/µL	6.7
10x T4 DNA Ligase buffer	1
T4 DNA Ligase	0.5

Molar ratio insert/vector 5:1:

Reactants	*Volume [µL]*
IGF-I 26 ng/µL	2
pET11a vector 35 ng/µL	6.5
10x T4 DNA Ligase buffer	1
T4 DNA Ligase	0.5

Table 12: Reaction mixtures for pET11a vector and IGF-I insert DNA ligation with different molar ratios of insert/vector (3:1; 5:1).

Vector and insert DNA were transferred to a plastic reaction tube and heated to 45 °C for 5 minutes to melt any reannealed cohesive termini. After 30 seconds incubation on ice, T4 DNA Ligase buffer and T4 DNA Ligase were added (**Table 12**). The reaction was mixed thoroughly and incubated at 22 °C for 5 hours. Subsequently, the ligation products were transformed into competent *E. coli* cells (DH5α) to amplify the plasmid DNA. Therefore, 50 µL of DH5α cells were thawed on ice for 5 minutes before adding 5 µL of the ligation reaction. The vial was mixed gently by tapping and incubated on ice for 30 minutes. The cells were heat shocked in a water bath at 42 °C for 60 seconds and then placed on ice for 5 minutes. Afterwards, 250 µL SOC medium were warmed to 37 °C, added and the vial was incubated at 37 °C for 1 hour at 300 rpm. 200 µL of the transformation reaction were spread on agar plates containing ampicillin (100 µg/mL) and the plates were incubated at 37 °C overnight. On the next day, three single colonies were selected from the agar plate and each colony was transferred into 5 mL liquid Lysogeny Broth (LB) medium with 100 µg/mL ampicillin. The bacterial cultures were incubated at 37 °C in a shaking incubator overnight. Plasmid DNA was purified by the use of NucleoSpin® Plasmid DNA Purification System (Macherey-Nagel, Dueren, Germany) according to manufacturer's instruction. After performing minipreparation, DNA was quantified by measuring absorbance at 260 nm using NanoDrop and sent to Eurofin Genomics (Ebersberg, Germany) for sequencing.

4.2.3.7 Cotransformation

Cotransformation of the verified pET11a/TAG-IGF-I plasmid containing ampicillin resistance gene and the pRSFduet plasmid (kind gift of M. Rubini, Konstanz, Germany) containing kanamycin resistance gene into *E. coli* BL21(DE3) as well as ArcticExpress(DE3) cells was performed. Therefore, 50 µL of competent BL21(DE3) cells were thawed on ice for 10 minutes before adding 250 ng DNA of each plasmid. The vial was mixed gently by tapping and incubated on ice for

30 minutes. The cells were heat shocked in a water bath at 42 °C for 50 seconds and then placed on ice for 5 minutes. Afterwards, 300 µL SOC medium were warmed to 37 °C, added and the vial was incubated at 37 °C for 1 hour at 300 rpm. 200 µL of the transformation reaction were spread on agar plates containing carbenicillin and kanamycin and the plates were incubated at 37 °C overnight. On the next day, one single colony was selected from the agar plate, transferred into LB medium with 100 µg/mL ampicillin and 34 µg/mL kanamycin and cultured overnight at 37 °C in a shaking incubator (Sanyo-Gallenkamp, Loughborough, United Kingdom) at 180 rpm. After 16 hours the bacterial culture was centrifuged at 4 °C with 2,000 rpm for 5 minutes (Allegra® X-15R, Beckman Coulter, Brea, CA, USA). The yielded pellet was resuspended in 1.5 mL LB glycerol medium and frozen in a cryovial at -80 °C (glycerol stock).

The cotransformation of the verified pET11a/TAG-IGF-I plasmid containing ampicillin resistance gene and the pRSFduet plasmid containing kanamycin resistance gene into *E. coli* ArcticExpress(DE3) cells was performed as described for BL21(DE3) cells with slight modification. 0.85 µL 1.42 M β-mercaptoethanol were added to the cells before the addition of the vectors to increase transformation efficiency. The heat pulse at 42 °C was decreased to 25 seconds to increase efficiency as well and SOC medium was preheated to 42 °C. In order to select for the cpn10/cpn60 chaperonin expression plasmid before induction, 20 µg/mL gentamycin were added to the overnight culture supplementary to carbenicillin and kanamycin.

4.2.3.8 Protein expression

Protein expression in BL21(DE3) cells was performed in TB medium (Terrific Broth) containing 100 µg/mL carbenicillin and 34 µg/mL kanamycin. 4 mM plk were added at an OD_{600} of 0.3–0.4 and expression media was inoculated with overnight culture (1:100 dilution) and the cells were grown at 37 °C at 190 rpm. At OD_{600} = 0.6–0.8 IPTG was added with a final concentration of 1 mM to induce protein expression. After 24 hours expression, cells were harvested by centrifugation for 20 minutes at 4,750 rpm (Allegra® X-15R, Beckman Coulter, Brea, CA, USA) and stored at -80 °C until further usage.

The protein expression method was modified by varying the temperature (20 °C / 30 °C / 37 °C), the medium (LB or TB) and the duration of expression until a maximum of 24 hours as well as the plk concentration (1–30 mM). Finally, even another cell line, ArcticExpress(DE3), was used. Protein expression in ArcticExpress(DE3) cells was done in TB medium without selection antibiotics. Expression medium was inoculated with overnight culture (1:100 dilution) and the cells were grown at 30 °C at 225 rpm. At OD_{600} = 0.3–0.4 15 mM plk were added and at OD_{600} = 0.6–0.8 the culture was equilibrated to 12 °C before IPTG was added to a final concentration of 1 mM to induce protein expression. After 24 hours expression at 180 rpm, cells were harvested by centrifugation for 20 minutes at 4,750 rpm (Allegra® X-15R, Beckman Coulter, Brea, CA, USA) and stored at -80 °C until further usage.

4.2.3.9 Inclusion body purification

Inclusion body purification was done for protein isolation using different methods [162],[163]. According to van Kimmenade et al. [162], the cell pellet was resuspended in 30 mL Tris/HCl buffer, pH 8 (50 mM Tris/HCl, 50 mM sodium chloride, 1 mM EDTA and 0.1 mM PMSF). The suspended cells were disintegrated by ultrasonication (6x 1 min: 1 sec pulse, 0.8 sec pause, 75 W with 2 min pause between cycles) and the resulting lysate was centrifuged at 25,000 g for 15 minutes (Beckman L8-70M Ultrazentrifuge, Beckman Coulter, Krefeld, Germany) at 4 °C. The yielded pellet containing plk-IGF-I was resuspended in Tris/HCl buffer pH 8 supplemented with 5 M guanidine hydrochloride, 2 mM reduced and 0.2 mM oxidized glutathione (9 mL buffer per gram pellet). The suspension was incubated for 1 hour at room temperature and subsequently filled up to the 10 fold volume with Tris/HCl buffer pH 8 supplemented with 2 mM reduced and 0.2 mM oxidized glutathione but without PMSF. After 2.5 hours incubation at room temperature, centrifugation was performed at 2,500 g for 15 minutes at 4 °C to remove formed precipitates. Finally, the supernatant was dialyzed against PBS buffer, pH 7.4, at 4 °C with three buffer changes in 24 hours. Formed precipitates were removed by centrifugation at 2,500 g for 15 minutes at 4 °C and supernatant was concentrated using Vivaspin® 6 Centrifugal Concentrators (MWCO 5 kDa, Sartorius Stedim Biotech, Goettingen, Germany) at 3,400 rpm and 4 °C (Varifuge, Heraeus, Hanau, Germany).

According to Wangsa-Wirawan et al. [163], the cell pellet was resuspended in 50 mL 20 mM Tris buffer, pH 8.5, with 50 mM sodium chloride and sonicated (6x 1 min: 1 sec pulse, 0.8 sec pause, 75 W with 2 min pause between cycles) [163]. The yielded cell lysate was centrifuged at 10,000 rpm for 15 minutes at 4 °C, the resulting pellet was resuspended in 50 mL 20 mM Tris buffer, pH 8, supplemented with 5 mM EDTA and 0.02 % (w/v) lysozyme were added. After 3 hours incubation at room temperature, the suspension was centrifuged at 10,000 rpm for 15 minutes at 4 °C and resuspended in 50 mL 20 mM Tris buffer, pH 8, with 5 mM EDTA and 2 % Triton X. Inclusion bodies were precipitated by centrifugation at 10,000 rpm for 15 minutes at 4 °C and washed twice with 50 mL 20 mM Tris buffer pH 7.5.

4.2.3.10 SDS-PAGE

SDS-PAGE was performed to analyze cell samples after expression as well as inclusion body purification according to the method of Laemmli [164]. The stacking gel consisted of a 3.9 % polyacrylamide gel pH 6.8 and the separating gel consisted of a 15 % polyacrylamide gel pH 8.8, both adjusted by the use of Tris-HCl buffer. The samples were mixed with 6x reducing SDS sample buffer before heating at 95 °C for 10 minutes. The denatured samples as well as a protein ladder were loaded onto the gel (Bio-Rad Laboratories GmbH, München, Germany) and electrophoresis was run at 120 V.

4.2.3.11 Western blot

Following SDS-PAGE, western blot was performed to identify IGF-I from the extracted protein mixture. The proteins fixed on the polyacrylamide gel were transferred to a nitrocellulose membrane under wet conditions using an electric field vertical to the surface of the gel (80 V for 2 h). Unspecific binding of the antibody was reduced by blocking the membrane with 5 % (w/v) skin milk powder in PBS buffer for 1 hour at room temperature under gently shaking before incubation with 0.2 µg/mL polyclonal anti-IGF-I antibody (produced in goat; Sigma Aldrich, St. Louis, MO, USA) in 5 % (w/v) skin milk powder in PBS buffer overnight at 4 °C under shaking. Subsequently, the membrane was washed three times with 0.2 % (w/v) Tween® 20 in PBS and three times with PBS for 15 minutes each. Then, the membrane was incubated with a secondary peroxidase-conjugated anti-mouse IgG antibody (Sigma Aldrich, St. Louis, MO, USA), diluted 1:2,000, in 5 % (w/v) skin milk powder in PBS buffer. After additional washing steps, peroxidase signals were detected with SuperSignal® West Pico Chemiluminescence Substrate (Thermo Fisher Scientific, Rockford, USA) and pictures were taken on the FluorChem FC2 imaging system (Protein Simple, Santa Clara, CA, USA).

4.2.3.12 In gel tryptic cleavage and mass spectrometry

For in-gel tryptic digestion protein samples were separated by SDS-PAGE again and visualized by Coomassie Blue G250 (Thermo Fisher Scientific, Rockford, USA) staining [165]. The appropriate bands were cut and in-gel reduction with DTT and alkylation with iodoacetamide were performed prior tryptic cleavage as described previously [166, 167]. The peptides eluted from polyacrylamide matrix were desalted using ZipTip® pipette tips (C18 resin, Millipore, Billerica, MA, USA) according to the manufacturer's instructions. Subsequently, Electrospray Ionization Mass Spectrometry Analysis (ESI-MS) was performed on an APEX-II FT-ICR mass spectrometer (Bruker Daltonic GmbH, Bremen, Germany) equipped with a 7.4 T magnet and an Apollo ESI ion source in positive mode. Therefore, the samples were injected with a speed of 2 µL/min directly into the ESI ion source with a capillary voltage of 160 V. The detection range of the mass spectrometer was adjusted to 300–2100 m/z. Each spectrum was acquired by accumulation of 256 scans with a resolution of 256 K. Bruker Xmas software was utilized for evaluation in order to deconvolute mass spectra to the single protonated ion form and to select the monoisotopic signal for mass determination.

4.2.4 Statistical analysis

All measurements were performed in triplicate for each data point, unless otherwise noted, and are reported as means ± standard deviation (SD). Statistical significance was calculated by paired student´s t-test with a significance level of $p < 0.05$.

4.3 Biofunctionalized implants for cartilage tissue engineering

4.3.1 Preparation of aqueous SF solution

SF aqueous solution was prepared as described earlier with slight modifications [88, 153]. Cocoons of the silkworm *B. mori* were cut, boiled twice for 1 hour in a 0.02 M aqueous sodium carbonate solution and rinsed ten times with ultrapure water to remove the sericin. The dried SF fibers were dissolved in an aqueous 9.3 M lithium bromide solution at 60 °C for about 2 hours. The generated SF solution was filtered through a 5 µm syringe filter (Versapor, Pall Life Sciences, Washington, NY) dialyzed against borate buffer (300 mM boric acid, 150 mM sodium chloride, pH 9.0) for 24 hours and against ultrapure water for another 48 hours with five changes of water in SpectraPor dialysis tubes (MWCO 6–8 kDa, Spectrum Labs, Rancho Dominguez, CA), yielding a 2 % (w/v) SF solution. SF solution was stored at 2–8 °C.

4.3.2 Preparation of paraffin spheres

Paraffin spheres, which were prepared in an emulsion process using water, gelatin and solid paraffin, were used as porogen for the preparation of SF scaffolds as previously described with modifications [144]. 4 g/L gelatin were dissolved in hot ultrapure water and mixed with melted paraffin to obtain a final concentration of 200 g/L. The emulsion was stirred at 1,400 rpm for 10 minutes. Paraffin spheres were obtained by casting emulsion into stirred ice cold water. After 5 more minutes stirring the spheres were harvested with a 100 µm sieve and washed several times with cold ultrapure water. Fractions of 100–160 µm, 160–315 µm and 315–710 µm were collected by sifting the dried paraffin spheres through sieves with different mesh sizes (100 µm, 160 µm, 315 µm and 710 µm).

4.3.3 Preparation of SF scaffolds

4.3.3.1 Scaffolds with one porosity

2 % (w/v) SF solution was up-concentrated using an Amicon® stirred ultrafiltration cell 8010 (EMD Millipore Corporation, Billerica, MA, USA) and 30 kDa ultrafiltration membrane disk filters (25 mm, PALL® Life Sciences Corporation, Ann Arbor, MI, USA) until a 20 % (w/v) SF solution was obtained. SF scaffolds were prepared according to the literature [144, 153] with some modifications (**Figure 6**). 60 mg of 315–710 µm paraffin spheres were weighed into 1 mL syringes. For reaching interconnectivity of the pores, the syringes were incubated at 37 °C for 1 hour in a heating oven (Binder GmbH, Tuttlingen, Germany). After cooling to room temperature, 55 µL 20 % (w/v) SF solution was pressed over the paraffin mold until all pores between the paraffin spheres were filled with SF solution. The constructs were flash frozen in liquid nitrogen for a minimum of 5 minutes and lyophilized at -30 °C for 36 hours in a laboratory freeze-dryer alpha 1–4 (Martin Christ GmbH, Osterode, Germany). Lyophilized scaffolds were treated with

90 % (v/v) methanol for 30 minutes to reach water insolubility and allowed to air dry in a fume hood before leaching paraffin two times with n-hexane for 12 hours. The resulting porous SF scaffolds were dried under vacuum for a minimum of 12 hours. Finally, the dried SF scaffolds were cut into ~2 mm thick slices using a racer blade.

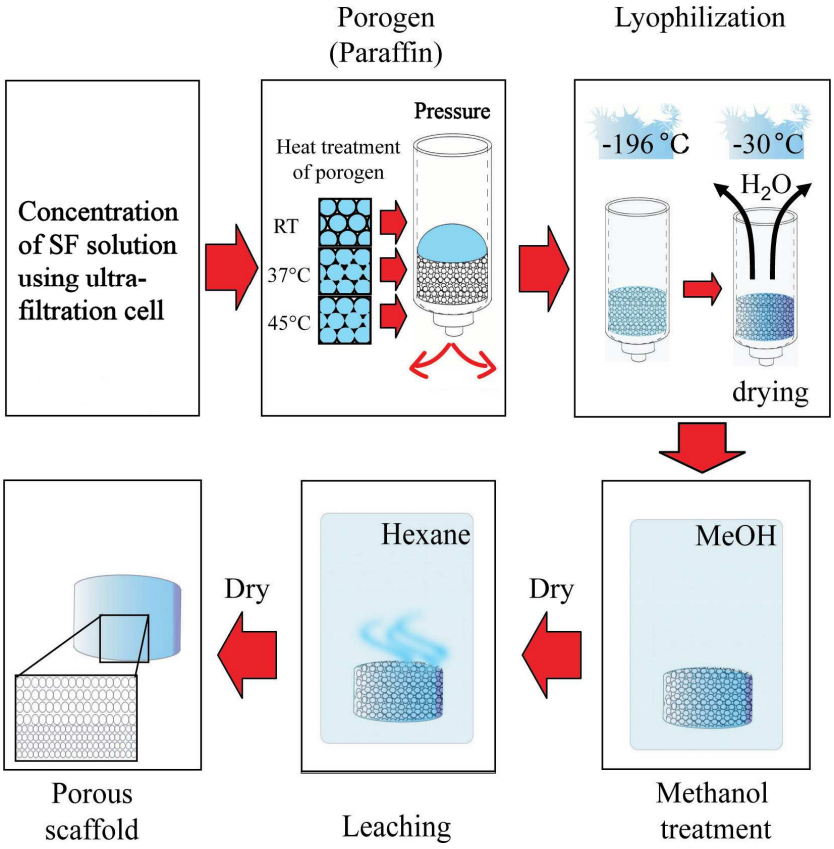

Figure 6: Schematic illustration of SF scaffold preparation. Adapted from [144], Copyright 2006, with permission from Mary Ann Liebert, Inc.

4.3.3.2 Scaffolds with two porosities

20 % (w/v) SF solution was prepared as described above (4.3.1 and 4.3.3.1.) and SF scaffolds were prepared according to the literature [144, 153] with some modifications. 30 mg of 100–180 µm paraffin spheres were weighed into 1 mL syringes. For reaching interconnectivity of the pores, the syringes were incubated at 45 °C for 45 minutes in a heating oven (Binder GmbH, Tuttlingen, Germany). After cooling to room temperature 30 mg of 315–710 µm paraffin spheres were weighed into 1 mL syringes on the melted 100–180 µm paraffin spheres. For reaching interconnectivity of the pores the syringes were incubated at 37 °C for 1 hour in a heating oven (Binder GmbH, Tuttlingen, Germany). When the paraffin mold reached room temperature again 55 µL 20 % (w/v) SF solution was pressed over the paraffin mold until all pores between the paraffin spheres were filled with SF solution. The constructs were flash frozen in liquid nitrogen for a minimum of 5 minutes and lyophilized at -30 °C for 36 hours in a laboratory freeze-dryer alpha 1-4 (Martin Christ GmbH, Osterode, Germany). Lyophilized scaffolds were treated with

90 % (v/v) methanol for 30 minutes to reach water insolubility and allowed to air dry in a fume hood before leaching paraffin two times with n-hexane for 12 hours. The resulting porous biphasic SF scaffolds were dried under vacuum for a minimum of 12 hours. Finally, the dried biphasic SF scaffolds were cut into ~2 mm thick slices using a racer blade.

4.3.4 Scanning electron microscopy (SEM)

Slices of dried SF scaffolds were sputter coated with gold/palladium (SSCD, Bal-Tec AG, Liechtenstein) and scanning electron microscopy (SEM) images were recorded with a JSM-7500F field emission scanning electron microscope (Joel, Tokyo, Japan) at an accelerating voltage of 5 kV in secondary electron imaging (SEI) mode.

4.3.5 Immobilization of TGF-β3 on PMMA beads

Poly(methyl methacrylate) (PMMA) beads (4.6 µm; 8.3 µmol COOH/g; PolyAn, Berlin, Germany) were chosen as carrier for immobilization of TGF-β3. In order to covalently immobilize the growth factor on the beads, EDC/NHS chemistry was used (**Scheme 7**). Supplied TGF-β3 (a kind gift from Novartis Pharma AG, Basel, Switzerland) was dialyzed (Slide-A-Lyzer Mini Dialysis Device, MWCO 10 kDa, Thermo Fisher Scientific, Rockford, USA) against 5 mM citrate buffer, pH 3.8. PMMA beads were sterilized by washing with 70 % (v/v) ethanol, subsequently washed with ultrapure water and resuspended in MES buffer (0.1 M MES, 0.5 M sodium chloride, pH 6). EDC (3 mM) and NHS (6 mM) were given to 50 µL of the bead suspension and incubated for at least 15 minutes in order to activate carboxyl groups. Following activation, beads were washed with MES buffer and TGF-β3 (9.64 ng/µL) was added to the bead suspension. The reaction mixture was briefly vortexed and then mixed by rolling at room temperature for 2 hours. In order to finish the coupling reaction, the beads were thoroughly washed for three times with TBST buffer (20 mM Tris, 150 mM sodium chloride, 0.1 % Tween® 20, pH 7.4) and three times with phosphate buffer with high salt concentration (12 mM phosphate, 1.5 M sodium chloride, pH 7.4) to remove unbound TGF-β3. Finally, the beads were washed with PBS, resuspended in PBS and counted with a Neubauer hemocytometer (Brand GmbH, Wertheim, Germany) to determine the number of beads per µL bead suspension. In addition, a negative control was prepared the same way but without the coupling reagents. Each solution was sterilized by filtration (0.2 µm, PES membrane, 13 mm diameter, Nalge Nunc International Corporation, Rochester, USA).

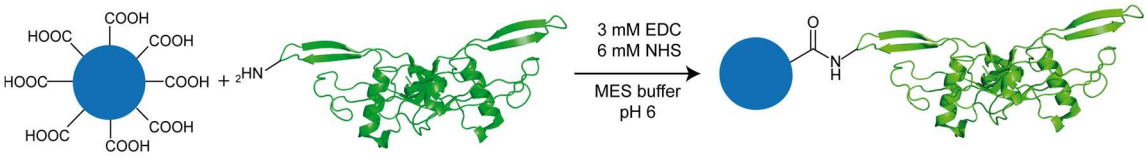

Scheme 7: Reaction scheme detailing the immobilization of TGF-β3 on carboxylated beads. PDB code TGF-β3 = 1TGK.

4.3.6 Determination of coupling efficiency of TGF-β3 on PMMA beads

4.3.6.1 Fluorescence imaging and flow cytometry

Coupling efficiency of TGF-β3 was investigated using fluorescence imaging as well as flow cytometry. Therefore, beads were incubated with a mouse monoclonal anti-TGF-β3 primary antibody (R&D Systems, Minneapolis, MN, USA) and subsequently with a secondary Alexa Fluor® 488 conjugated anti-mouse IgG antibody (Thermo Fisher Scientific, Rockford, USA) prior analysis. Fluorescence imaging was done with an inverted epifluorescence microscope Axio Observer Z1 equipped with a HXP120C lamp, an AxioCam MRm camera and a Plan-Apochromat 40x/0.95 objective (Zeiss, Oberkochen, Germany). Images were recorded using fluorescence excitation at λ = 450–490 nm, dichroic beam splitter at λ = 495 nm and emission at λ = 500–550 nm. Flow cytometry was performed with a FACS Calibur system (Becton Dickinson, Franklin Lakes, NY). A 488 nm argon-ion laser was used for excitation and the emission channel FL2 (530 nm) was used for detection. 5,000 beads were analyzed with BD CellQuestTM Pro and all data were evaluated using Flowing Software (Version 2.5.1; Turku Bioimaging, Turku, Finland).

4.3.6.2 Enzyme-linked immunosorbent assay (ELISA)

TGF-β3 loading on the beads was determined by indirect Enzyme-linked immunosorbent assay (ELISA). A dilution series of TGF-β3 stock solution was prepared from 780 ng/mL to 1.52 ng/mL for calibration. 100 µL of these dilutions were used to coat the wells of a 96-well ELISA microplate overnight at 4 °C. After washing, the remaining protein-binding sites in the coated wells were blocked by addition of 200 µL 1 % BSA in PBS and incubation for 2 hours at room temperature. Accordingly, the wells were washed again and 100 µL of mouse monoclonal anti-TGF-β3 primary antibody (R&D Systems, Minneapolis, MN, USA) with a concentration of 0.5 µg/mL were added to each well and incubated for another 2 hours at room temperature. After washing the wells thoroughly, 100 µL of secondary horseradish peroxidase (HRP) conjugated anti-mouse IgG antibody (Sigma Aldrich, St. Louis, MO, USA), diluted 1:5,000, was added and incubation was performed at room temperature for 2 hours. Following the last washing procedure, the detection with the Thermo Scientific TMB Substrate Kit (Thermo Fisher Scientific, Rockford, USA) was performed. The detection of HRP was carried out by the addition of 100 µL of mixed TMB substrate solution to each microplate well. After 25 minutes incubation at room temperature, 100 µL of 2 M sulfuric acid were added in order to stop reaction. Absorbance was measured of each well at a wavelength of 450 nm using a Spectramax 250 microplate reader (Molecular Devices, Sunnyvale, CA, USA). Beads were incubated with a mouse monoclonal anti-TGF-β3 primary antibody overnight at 4 °C and subsequently incubated with a secondary HRP-conjugated anti-mouse IgG antibody for 2 hours at room temperature prior analysis. Beads were thoroughly washed, resuspended in PBS and counted with a Neubauer hemocytometer (Brand GmbH, Wertheim, Germany) to determine the number of beads per µL bead suspension. 10 µL bead

suspension were added to 100 µL mixed TMB substrate solution and detection was performed as described above. All samples and standards were assayed in triplicate.

4.3.7 Bioactivity of immobilized TGF-β3

Bioactivity of immobilized TGF-β3 was assessed using luciferase reporter gene assay. Human mesenchymal stem cells (hMSCs) transduced with a lentivirus containing the human telomerase reverse transcriptase (TERT) gene [168], and stably transfected with a pGl3ti vector containing a SMAD binding element (SBE) at the promotor of the firefly luciferase gene as well as a hygromycin resistance to select for transfected cells, were used. SBE consists of a CAGACA motif, which is a direct binding site for SMAD proteins [169, 170]. It responds to all R-SMAD and co-SMAD proteins and therefore covers TGF-β, activin, myostatin and BMP signaling. hMSC-TERT cells were plated in 96-well clear tissue culture plates at a density of 30,000 cells per well in high glucose DMEM with L-glutamine supplemented with 10 % FCS, 100 U/mL penicillin, 100 µg/mL streptomycin and 50 µg/mL hygromycin and incubated for 24 hours to reach a confluence of 50–60 %. hMSC-TERT cells were washed two times with PBS and treated with TGF-β3 reference solutions with different concentrations, ranging from 0.122 to 15.625 ng/mL for calibration as well as a dilution series of a defined amount of TGF-β3 coupled beads on the same plate in high glucose DMEM with L-glutamine supplemented with 0.5 % FCS, 100 U/mL penicillin, 100 µg/mL streptomycin and 50 µg/mL hygromycin. The number of beads per well was determined by counting 10 µL of the bead suspension with the use of a Neubauer hemocytometer (Brand GmbH, Wertheim, Germany). After 48 hours, cells were washed once with PBS and lysed using 80 µL of luciferase assay buffer (Pierce® Luciferase Cell lysis buffer (2x), no 16189, Thermo Fisher Scientific, Rockford, USA) and 50 µL of the lysates were transferred to a white bottom 96-well plate and frozen at -80 °C. Luminescence was measured by addition of 100 µL luciferase assay reagent (D-Luciferine (PJK GmbH, Germany) in luciferase flash buffer) to each well directly in the Orion II luminometer (Berthold Detection Systems GmbH, Pforzheim, Germany) and luminescence was read after 1 second. For normalization to cell number, a Bradford Assay with the cell lysates was conducted using Quick Start™ 1x dye reagent (Biorad, Germany). Therefore, 5 µL of the lysates were mixed with 200 µL Bradford reagent (Biorad, Germany) and absorbance was measured at 595 nm with a Spectramax 250 microplate reader (Molecular Devices, Sunnyvale, CA, USA). Protein content was determined by a BSA calibration (50-1,000 µg/mL BSA standard curve) and luciferase activity was specified as relative light units (RLU) per µg protein.

4.3.8 Isolation and culture of BMSCs

Human BMSCs were isolated of trabecular bone obtained from patients during total hip arthroplasty by extensive washing with PBS. The ethics committee of the University of Würzburg approved the study and all patients signed a written informed consent. After centrifugation of the

isolated cells at 300 g for 10 minutes, the cells were resuspended in expansion medium (Dulbecco's Modified Medium/Ham's F-12 (DMEM/F12, Thermo Fisher Scientific, MA, USA) supplemented with 10 % fetal bovine serum (FBS) and 1 % penicillin-streptomycin (PS; 100 U/mL penicillin, 0.1 mg/mL streptomycin)) and seeded in T175 cm^2 culture flasks (Greiner Bio-One, Frickenhausen, Germany). After 48 hours non-adherent cells were removed by washing with PBS. Then expansion medium was supplemented with 5 ng/mL basic fibroblast growth factor (bFGF; BioLegend, London, UK) and changed every 3–4 days until cells reached ~80 % confluence. The cells were trypsinized with 0.25 % trypsin-EDTA (Invitrogen, Karlsruhe, Germany) and expanded for 2 passages (P2) until seeding on the scaffolds.

4.3.9 Culture of MSC-SF scaffold constructs and chondrogenic and osteogenic differentiation of BMSCs

Each biphasic scaffold was pre-wetted overnight in expansion medium (DMEM/F12 (Thermo Fisher Scientific, MA, USA) supplemented with 10 % FBS, 1 % PS (100 U/mL penicillin, 0.1 mg/mL streptomycin, Thermo Fisher Scientific, MA, USA)) and subsequently put in a syringe (Omnican 40, B. Braun, Melsungen, Germany) for cell seeding. 8 x 10^5 MSCs (P2) were resuspended in 20 µL expansion medium and soaked into one scaffold. A homogeneous cell distribution was achieved by moving the plunger of the syringe. The resulting constructs were incubated at 37 °C, 5 % CO_2 and 21 % O_2 for 4 hours to allow cell attachment.

To test the suitability of the biphasic scaffolds for chondrogenesis the seeded scaffolds were then cultured in chondrogenic medium (DMEM high glucose 4.5 g/L supplemented with 1 % PS, 10 nM dexamethasone, 50 µg/mL ascorbic acid-2-phosphate, 1 mM sodium pyruvate, 40 µg/mL proline, 1 % ITS-Mix and 10 ng/mL TGF-β1; Biolegend, London, UK) for 21 days at 37 °C, 5 % CO_2 and 21 % O_2. Media exchange was performed every 2–3 days.

In order to investigate the suitability of the biphasic scaffolds for osteogenesis, the seeded scaffolds were cultured in osteogenic medium (DMEM/F12 supplemented with 10 % FBS, 1 % PS, 0.5 µg/mL Amphotericin B, 10 nM dexamethasone, 50 µg/mL ascorbic acid-2-phosphate, 7 mM β-glycerolphosphate and 1 µg/mL BMP-2) for 28 days at 37 °C, 5 % CO_2 and 21 % O_2. Media exchange was performed every 2–3 days.

For evaluating chondrogenesis induced by TGF-β3 coupled PMMA beads chondrogenic differentiation was performed as described above with slight modification. 8 x 10^5 MSCs (P2) were suspended in 20 µL expansion medium and merged with 10 µL bead suspension (with coupled TGF-β3, adsorbed TGF-β3 or without TGF-β3) before soaking into one scaffold with 315–710 µm pore size. Chondrogenic medium was supplemented with 10 ng/mL recombinant human TGF-β3 or without TGF-β3 instead of TGF-β1.

4.3.10 Histology and immunohistochemistry

Chondrogenesis and osteogenesis were histologically and immunohistochemically investigated by staining of the constructs after fixation using 3.7 % buffered formalin, dehydration by increasing sucrose concentrations from 10–60 % and embedding in Tissue-Tek® O.C.T. compound (Sakura, Torrance, CA, USA). Scaffolds were cut into 7 µm thick sections before staining.

To stain for glycosaminoglycan (GAG), sections were treated with aqueous 0.2 % safranin-O solution, counter-stained with 0.02 % fast green and mounted with Glycergel® Mounting Medium (Dako, Hamburg, Germany).

To immunostain for collagen I and II, the EnVision™ G|2 Doublestain System (Dako, Hamburg, Germany) was used according to the manufacturer's instruction with slight modifications. Sections were incubated in proteinase K for 7 minutes and subsequently blocked with 10 % goat serum (Dako, Hamburg, Germany) in PBS for 30 minutes to prevent non-specific binding of the antibody. Collagen type I alpha 1 chain antibody (1:800, Abcam, Cambridge, UK) and collagen type II alpha 1 chain antibody (clone II-4C11, 1:100, Acris, Herford, Germany) were used for immunostaining.

Additionally, cell nuclei were counterstained with haematoxylin. Species-matched immunoglobulins in equivalent concentrations on identically treated sections served as negative controls.

For calcium staining slides were stained with 2 % aqueous alizarin red solution (pH 4.2) for 5 minutes and mounted in glycerol (Sigma Aldrich, Steinheim, Germany).

Immunohistochemical staining for osteopontin was performed by a 7 minutes proteinase K digestion, followed by a 30 minutes block with 1 % BSA before incubation with a rabbit osteopontin antibody (1:200, Abcam, Cambridge, UK) overnight. Slides were thoroughly washed with PBS, and a Cy3-conjugated AffiniPure goat anti-rabbit secondary antibody (Jackson Immuno Research, West Grove, PA, USA) was added for 2 hours in the dark.

Nuclei were counterstained with IS Mounting Medium DAPI (Dako, Hamburg, Germany). Equivalent concentrations of species-matched immunoglobulins on identically treated sections were used as negative controls.

All sections were analyzed by light microscopy using an Olympus BX51 fluorescent and bright-field microscope and the cellSens™ imaging software from Olympus (Olympus, Hamburg, Germany).

4.3.11 Biochemical analysis

After 10, 21 or 28 days of cultivation, constructs were harvested and prepared for biochemical analysis and histology according to Eyrich et al. [171]. The disintegration of the scaffolds (n = 3) was performed with the TissueLyser (Qiagen, Hilden, Germany) and subsequently the disintegrated

constructs were digested with 1 mL of a papainase solution (3 U/mL papainase, 100 mmol disodium hydrogen phosphate, 10 mmol disodium EDTA, pH 6.5) for 16 hours at 60 °C.
For DNA content determination, Hoechst 33258 dye (Polysciences, Warrington, USA) was added and samples were measured fluorometrically at an excitation wavelength of 365 nm and an emission wavelength of 458 nm.
Sulfated GAG content of the samples was determined using dimethylmethylene blue (DMMB) dye assay with chondroitin sulfate as standard and the reaction was observed on a spectrophotometer at 525 nm [172].
Hydroxyproline content of the samples was accessed spectrophotometrically at 550 nm after acid hydrolysis and reaction with chloramine-T and p-dimethylaminobenzaldehyde [173]. For the calculation of the total collagen amount a hydroxyproline to collagen ratio of 1:10 was assumed [174].
Calcium content was determined using the LiquiColor® test (Stanbio Laboratory, Boerne, TX, USA) according to the protocol of the manufacturer. In brief, calcium content was measured at 550 nm using ortho-cresolphthalein complexone (oCPC) for color reaction.
Alkaline phosphatase activity was measured using the Alkaline Phosphatase Assay Kit (Abcam, Cambridge, England) according to the protocol of the manufacturer. In brief, the alkaline phosphatase activity was measured at 405 nm using p-nitrophenyl phosphate as phosphatase substrate which turns yellow when dephosphorylated by alkaline phosphatase.

4.3.12 RNA isolation and quantitative real-time PCR

For quantitative real-time polymerase chain reaction (qRT-PCR) constructs (n = 3) were lysed using a TissueLyser (Quiagen, Hilden, Germany). Subsequently, TRIzol® reagent (Invitrogen, Karlsruhe, Germany) was used according to the manufacturer's instruction for RNA isolation. The synthesis of first strand cDNA from total RNA was performed with the ImProm™-II Reverse Transcription System (Promega, Madison, USA). qRT-PCR analysis was then carried out with an MJ Research Opticon 2 Cycler (BioRad, Hercules, CA, USA) using the MESA GREEN qPCRMasterMix Plus with MeteorTaq polymerase (Eurogentec, Seraing, Belgium) and QuantiTec® Primer Assays (Qiagen, Hilden, Germany) for Sox9, ACAN, COL2A1, COL1A1, COL10A1, SPP1, IBSP, RPL13a with cycling parameters according to Wittmann et al. [175] with slight modifications: 50 °C for 2 minutes → 95 °C for 10 minutes → 40 cycles at 95 °C for 15 seconds, 55 °C for 30 seconds and 72 °C for 30 seconds → 72 °C for 10 minutes. mRNA expression levels were normalized to the housekeeping gene GAPDH or RPL13a, respectively. The $2^{-\Delta\Delta CT}$ method was used to assign fold increase in expression levels for each gene. For easier comparison, the resulting values were further normalized to the expression at day 0.

4.3.13 Statistical analysis

All measurements were performed in triplicate for each data point, unless otherwise noted, and are reported as means ± standard deviation (SD). Statistical significance was calculated by one-way ANOVA with Dunnett's post hoc test, two-way ANOVA with Sidak's post-hoc test or unpaired/paired student´s t-test with a significance level of $p < 0.05$.

5 Results

5.1 Injectable PR-15 formulation

5.1.1 Evaluation of PR-15 stability at different pH values

5.1.1.1 Determination of the concentration after incubation by UV-spectroscopy

The concentrations of the PR-15 samples before and after incubation at 25 °C or 40 °C for 4 or 8 weeks, respectively, were determined by measuring UV absorption at 280 nm to observe loss of protein concentration during incubation. At pH 6.5 and pH 7.0 the protein concentration stayed constant at about 2.5 mg/mL under accelerated as well as stressed conditions. As opposed to this a significant loss of protein concentration was observed at pH 5.5 and pH 6.0 under stressed conditions whereas the concentrations remained constant under accelerated conditions. PR-15 concentration decreased to 1.60 ± 0.03 mg/mL (64.3 % of the start concentration) after 4 weeks and 1.69 ± 0.03 mg/mL (67.5 %) after 8 weeks at pH 5.5, to 1.85 ± 0.04 mg/mL (79.0 %) after 4 weeks and 1.83 ± 0.03 mg/mL (78.0 %) after 8 weeks at pH 6.0 incubated at 40 °C (**Figure 7**).

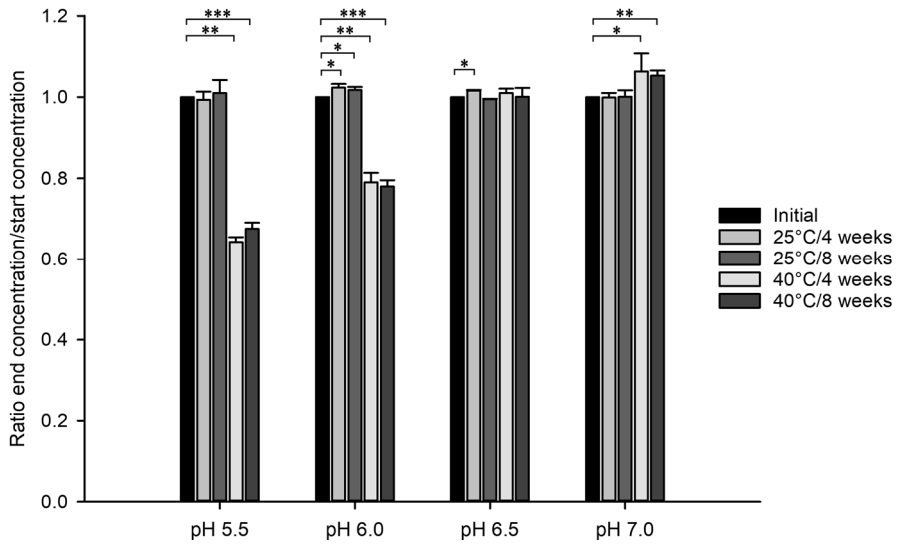

Figure 7: Concentration change of PR-15 samples at different pH values (5.5/6.0/6.5/7.0) after incubation at 25 °C and 40 °C for 4 and 8 weeks depicted as ratios of end and start concentration. Asterisks denote statistically significant differences between the groups referring to the initial sample (*** $p < 0.001$, ** $p < 0.01$, * $p < 0.05$).

5.1.1.2 Determination of the pH value after incubation

The pH values of the PR-15 samples were measured after incubation at 25 °C or 40 °C for 4 or 8 weeks, respectively, to see if the pH had changed during storage. All pH values remained constant under accelerated as well as stressed conditions over the entire 8 weeks (**Figure 8**).

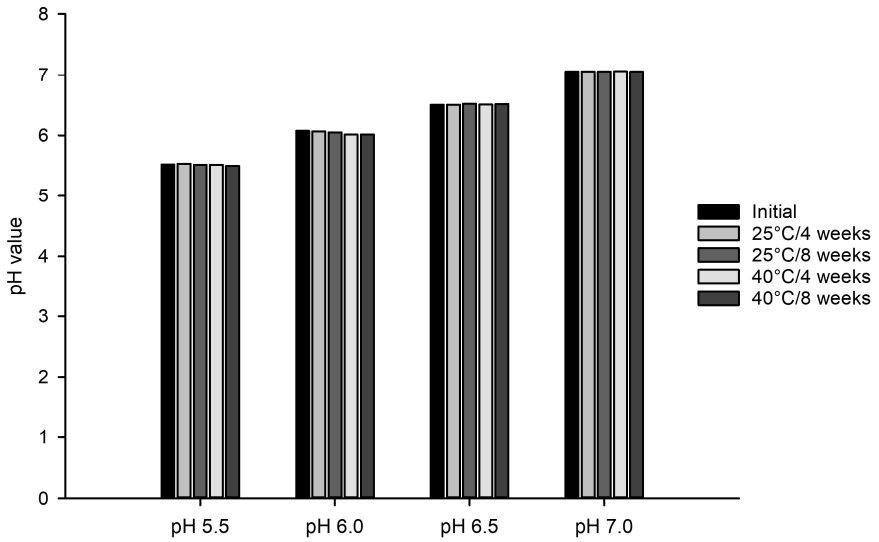

Figure 8: pH values of PR-15 samples after incubation at 25 °C and 40 °C for 4 and 8 weeks in comparison to the initial sample.

5.1.1.3 Analysis of aggregates by DLS

One major aspect of protein instability is the formation of aggregates. Aggregates can reduce the efficacy of protein formulations, resulting into immunological reactions and toxicity [176]. DLS was performed as a tool to assess protein aggregates, particle size distributions and polydispersity indices of PR-15 after incubation at different pH values (**Figure 9A** and **B**). The polydispersity index (PdI) characterizes the dimensionless width of the particle size distribution [176]. All samples incubated at 25 °C as well as the pH 7.0 sample incubated at 40 °C showed a PdI below 0.2, indicating a monodisperse distribution of PR-15 and a lack of aggregates [176]. For the samples incubated at 40 °C, except the pH 7.0 samples, the PdIs were significantly higher than the initial sample and even higher than 0.2 indicating the presence of aggregates (**Figure 9A**). The highest PdI (0.753 ± 0.126) was reached at pH 5.5 after 8 weeks incubation at 40 °C. These data were consistent with the increase of mean sizes of the protein for the 40 °C samples, except the pH 7.0 samples (**Figure 9B**). The largest mean size was detected for the pH 5.5 sample after 8 weeks incubation at 40 °C with 5771.3 ± 503.0 nm.

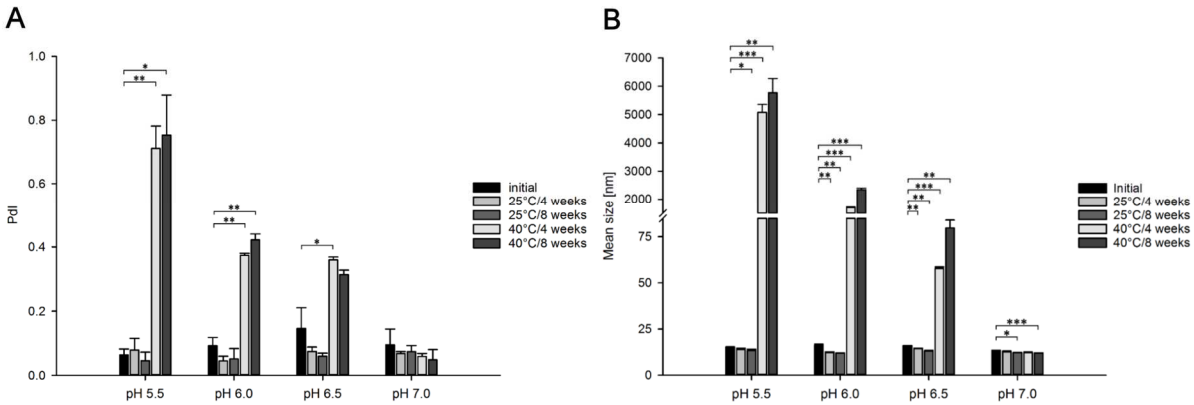

Figure 9: Analysis of aggregates of PR-15 samples by DLS. (A) Polydispersity indices (PdI) and (B) mean sizes of PR-15 at the different pH values (5.5/6.0/6.5/7.0) after incubation for 4 and 8 weeks at 25 °C and 40 °C in comparison to the initial sample. Asterisks denote statistically significant differences between the groups referring to the initial sample (*** $p < 0.001$, ** $p < 0.01$, * $p < 0.05$).

5.1.1.4 Analysis of aggregates and degradation products by SEC

The formation of soluble aggregates and degradation products during storage of PR-15 samples at different pH values (5.5/6.0/6.5/7.0) at 25 °C and 40 °C was assessed using SEC. During SEC molecules are separated according to their size, and therefore this method is ideal for evaluating oligomerization. Aggregates of PR-15 with a larger size eluted before the PR-15 monomer because they have passed the column without entering the pores of the stationary phase of the SEC column. In contrast, degradation products with a smaller size than PR-15 itself eluted at higher retention times because they were trapped in the pores of the stationary phase (**Figure 10**). Insoluble aggregates were removed before analysis by centrifugation. During incubation at pH 6.5 and pH 7.0 as well as under accelerated conditions at pH 5.5 and pH 6.0 the total peak areas and therefore the concentration of PR-15 remained constant indicating no formation of insoluble aggregates (**Figure 11**). In contrast, the major loss of PR-15 under stressed conditions at pH 5.5 and pH 6.0, shown by the decrease of total peak areas, was due to the formation of insoluble aggregates. Merely under stressed conditions at pH 6.5 (**Figures 10C** and **12C**) and pH 7.0 (**Figures 10D** and **12D**) a small amount of soluble aggregates was observed. However, the amount of degradation products increased at all pH values during incubation at 25 °C as well as 40 °C (**Figures 10** and **12**).

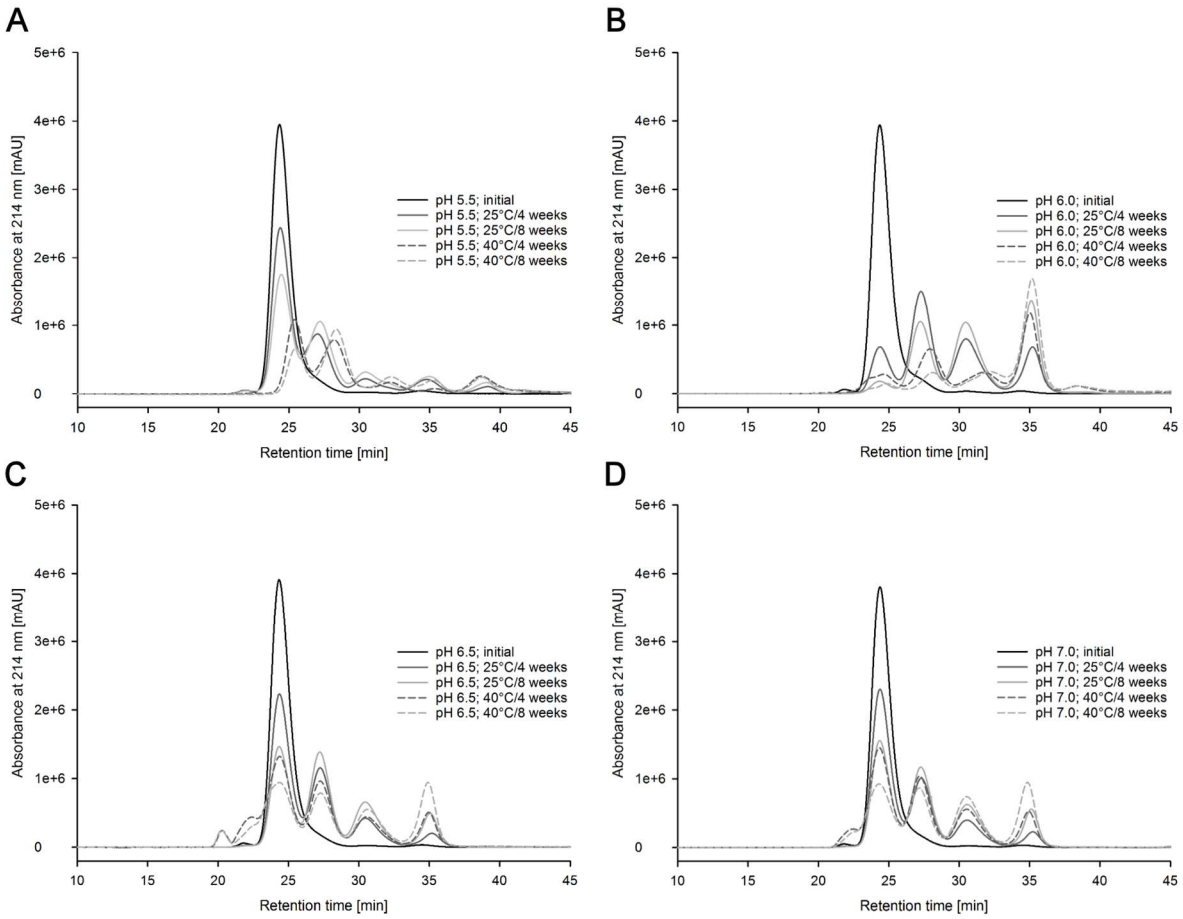

Figure 10: SEC chromatograms of PR-15 after incubation at 25 °C and 40 °C for 0 (initial), 4 and 8 weeks at (A) pH 5.5, (B) pH 6.0, (C) pH 6.5 and (D) pH 7.0.

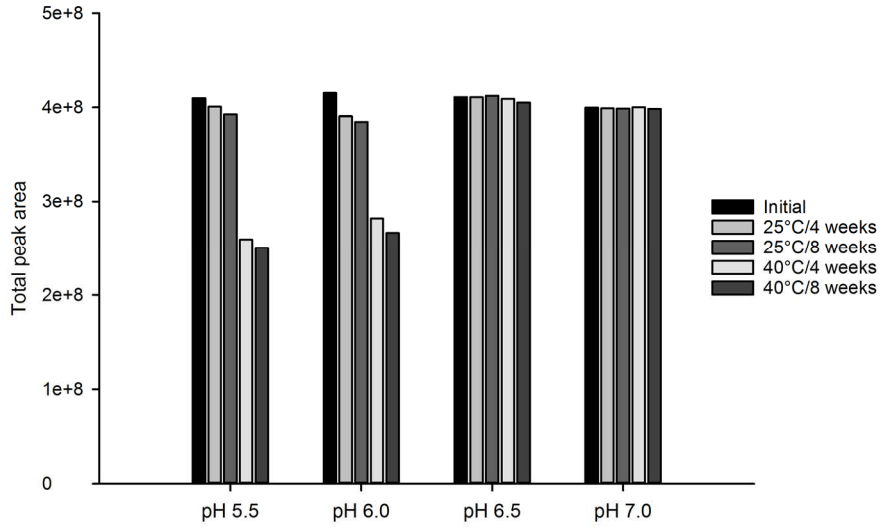

Figure 11: SEC of PR-15. Total peak areas of PR-15 at the different pH values (5.5/6.0/6.5/7.0) after incubation at 25 °C and 40 °C for 4 and 8 weeks in comparison to the initial amount of PR-15.

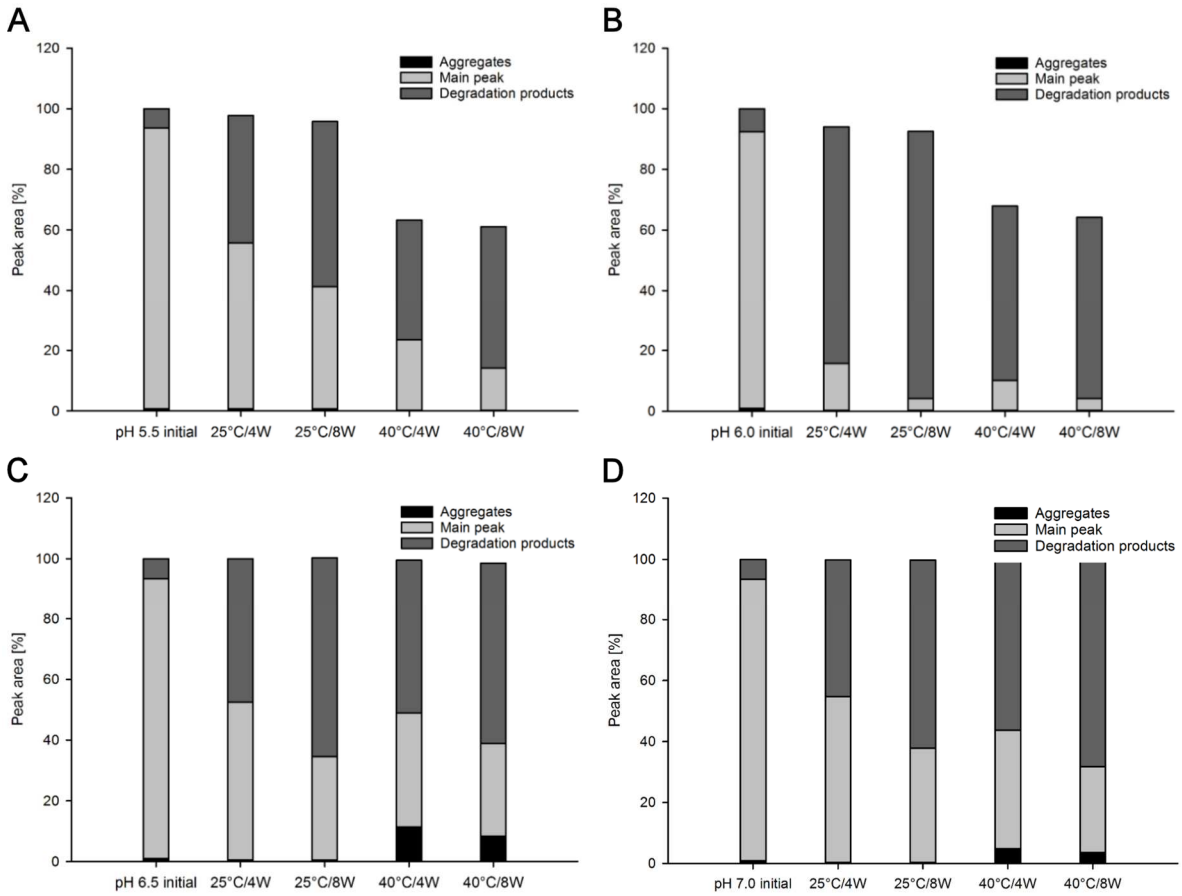

Figure 12: SEC of PR-15. Percentages of the fusion protein (main peak), aggregates and degradation products of PR-15 at the different pH values: (A) pH 5.5, (B) pH 6.0, (C) pH 6.5 and (D) pH 7.0 after 0 (initial), 4 and 8 weeks incubation at 25 °C and 40 °C.

5.1.1.5 Analysis of aggregates and degradation products by HIC

The stability of PR-15 at the different pH values was observed by HIC. HIC separates proteins based on their hydrophobicity. As a consequence, less hydrophobic proteins are eluted before more hydrophobic ones. Soluble aggregates of PR-15 are more hydrophobic than the fusion protein itself, as manifested by longer retention times, whereas degradation products are less hydrophobic resulting into a faster elution compared to the fusion protein. Besides, unfolded proteins have an increased hydrophobicity because the hydrophobic side chains of the protein, which are normally packed into the interior of the protein, are exposed to the surface resulting into a longer retention time compared to the proper folded monomer. The major loss of PR-15 shown by the decrease of total peak areas of pH 5.5 and pH 6.0 samples at 40 °C was assigned to the formation of insoluble aggregates which were removed by centrifugation before analysis (**Figure 14**). In contrast, no loss due to the formation of insoluble aggregates was observed at pH 5.5 and pH 6.0 under accelerated conditions as well as at pH 6.5 and pH 7.0 depicted by constant total peak areas indicating no variation of the concentration of PR-15 (**Figure 14**). A small amount of more hydrophobic oligomers or unfolded PR-15 was just observed at pH 6.5 after incubation at 40 °C (**Figures 13C** and **15C**). The low amount of aggregates at pH 7.0 under stressed conditions detected during SEC (**Figures 10D** and **12D**) was not found during HIC (**Figures 13D** and **15D**) indicating the

formation of reversible aggregates that were removed by dilution during sample preparation. The amount of less hydrophobic degradation products increased at all pH values during incubation at 25 °C as well as 40 °C (**Figures 13** and **15**).

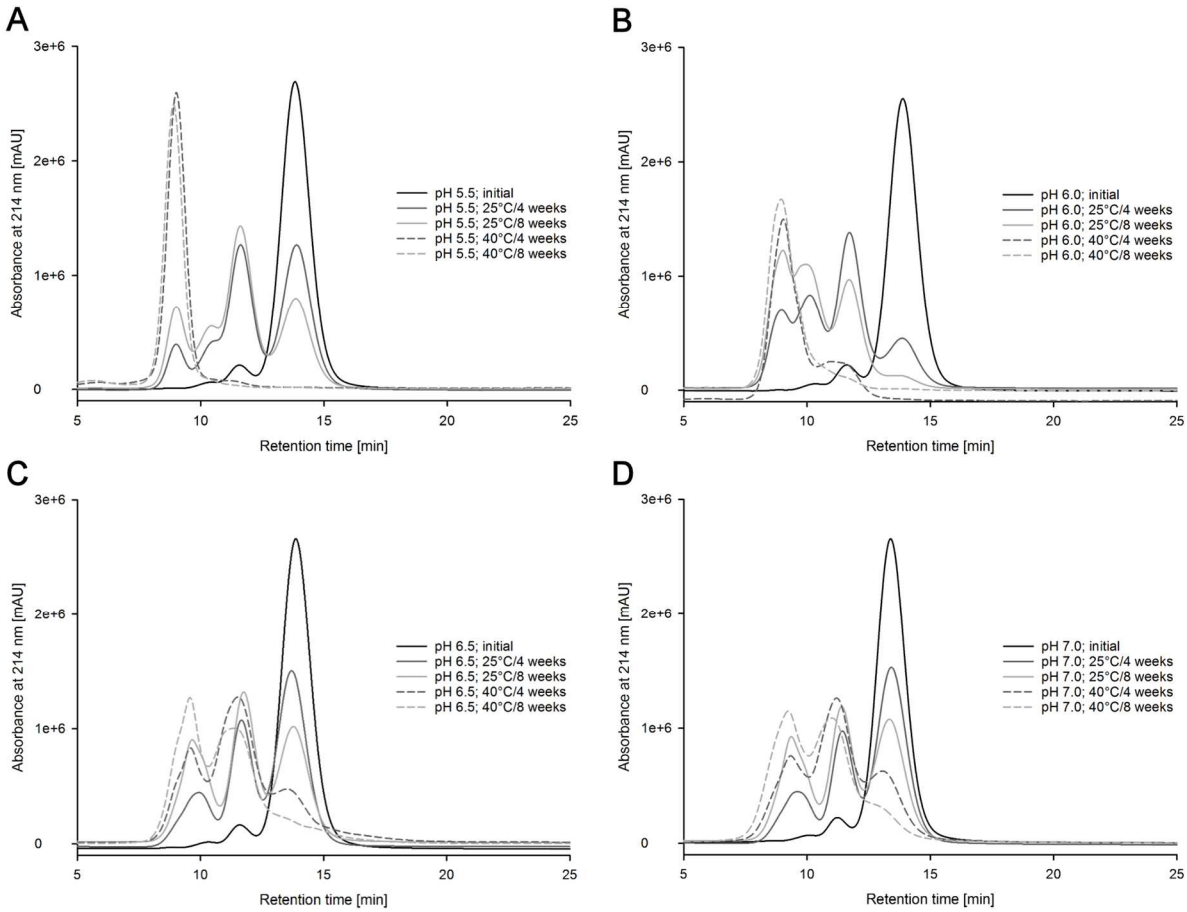

Figure 13: HIC chromatograms of PR-15 at the different pH values: (A) pH 5.5, (B) pH 6.0, (C) pH 6.5 and (D) pH 7.0 after 0 (initial), 4 and 8 weeks incubation at 25 °C and 40 °C.

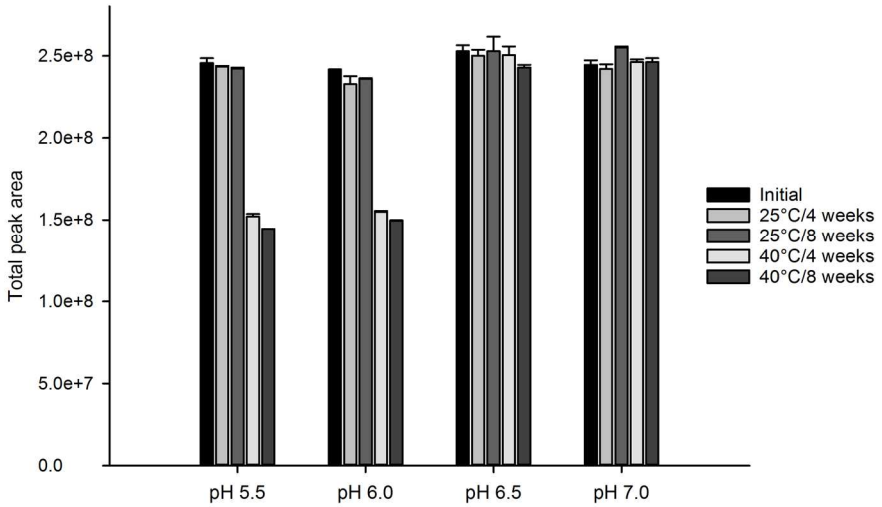

Figure 14: HIC of PR-15. Total peak areas of PR-15 at the different pH values (5.5/6.0/6.5/7.0) after incubation at 25 °C and 40 °C for 4 and 8 weeks in comparison to the initial amount of PR-15.

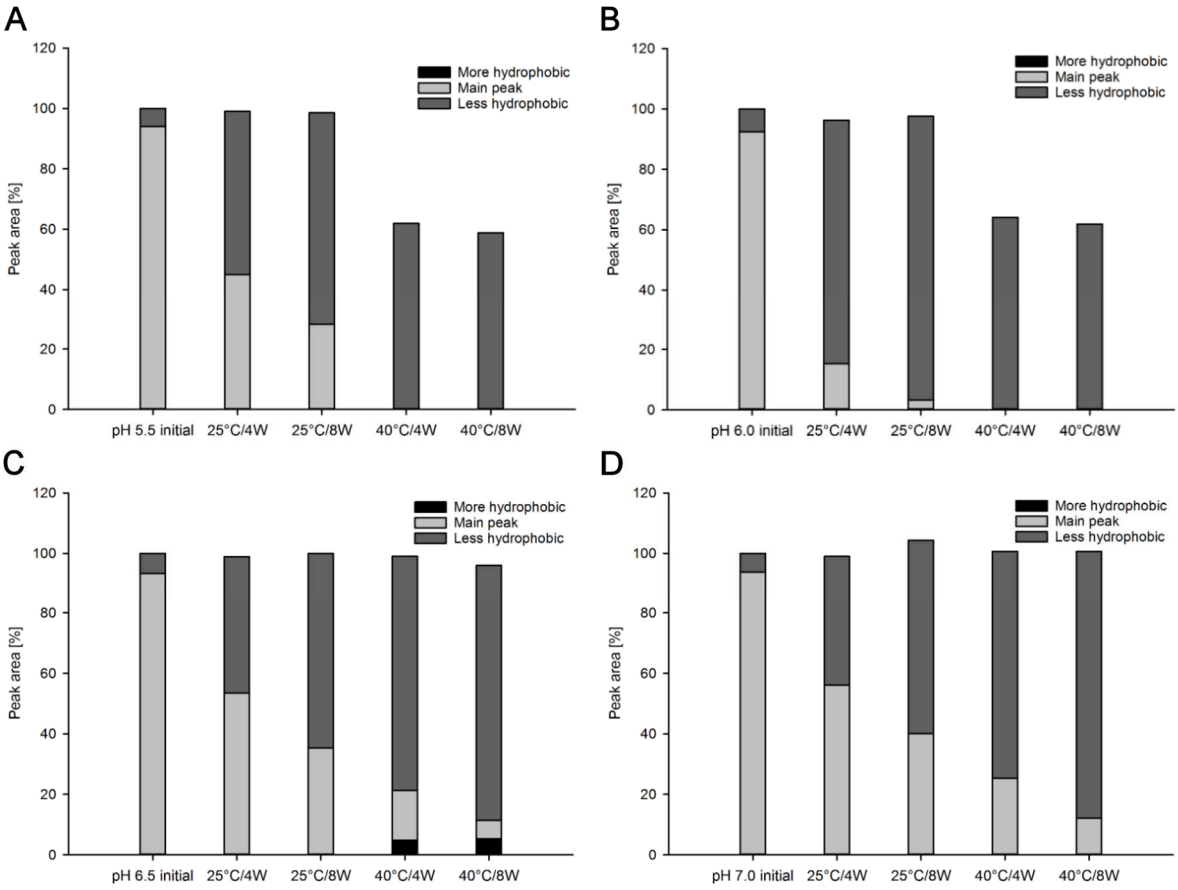

Figure 15: HIC of PR-15. Percentages of the fusion protein (main peak), more hydrophobic aggregates or degradation products and less hydrophobic degradation products of PR-15 at the different pH values: (A) pH 5.5, (B) pH 6.0, (C) pH 6.5 and (D) pH 7.0 after 0 (initial), 4 and 8 weeks incubation at 25 °C and 40 °C.

5.1.1.6 Analysis of aggregates and degradation products by MALDI-TOF MS

MALDI-TOF MS was performed to analyze degradation products of PR-15 and the formation of oligomers. The spectra of all initial samples (**Figure 16**) showed the PR-15 fusion protein (126 kDa), the monomer of the fusion protein (63 kDa), the dimer of the fusion protein (252 kDa) and the 90 kDa degradation fragment. At pH 5.5 and pH 6.0 nearly none of these peaks was observed at 25 °C (**Supplementary Figures 1A, 1B, 2A** and **2B**) as well as 40 °C (**Supplementary Figures 3A, 3B, 4A** and **4B**) whereas most of the peaks still existed even after incubation at 40 °C for the pH 6.5 and pH 7.0 samples (**Supplementary Figures 3C, 3D, 4C** and **4D**).

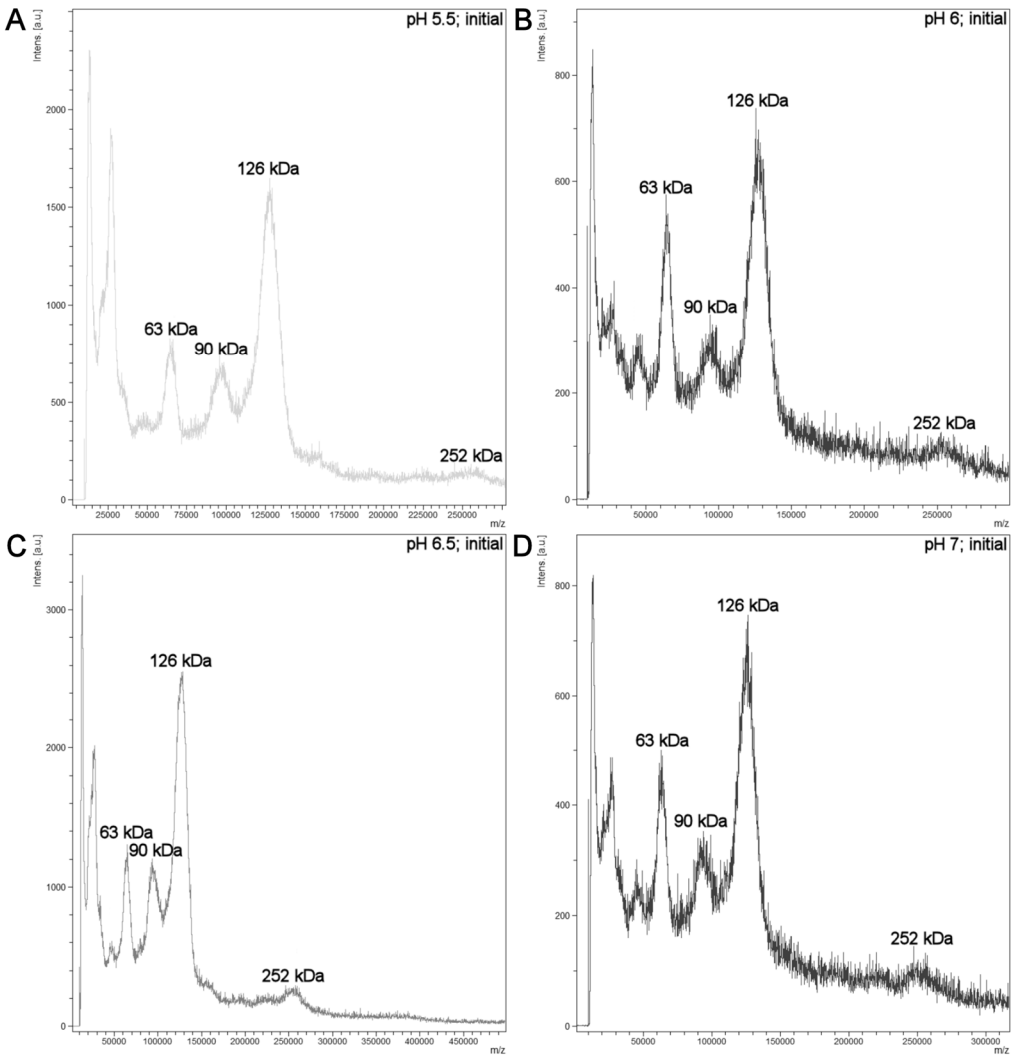

Figure 16: MALDI-TOF MS spectra of PR-15 initial samples at (A) pH 5.5, (B) pH 6.0, (C) pH 6.5 and (D) pH 7.0.

5.1.1.7 Analysis of degradation products by LC/ESI-MS

Mostly, the site-specific serine protease trypsin, that cleaves peptide bonds specifically between arginine and lysine, is used for proteomic studies [177]. But not for all proteins trypsin is the best choice for digestion. For example, hydrophobic and aggregated proteins are not sufficiently cleaved by the usage of trypsin [178]. Hence, the non-specific enzyme elastase with a preference for hydrophobic residues like alanine, valine, leucine, isoleucine, serine and threonine was used for PR-15 digestion [177]. Many overlapping peptides were the result of this non-specific cleavage with elastase leading to a better coverage of the protein sequence. Indeed, the number of isobaric peptides was increased but the determination of the smaller peptides was much easier [179].

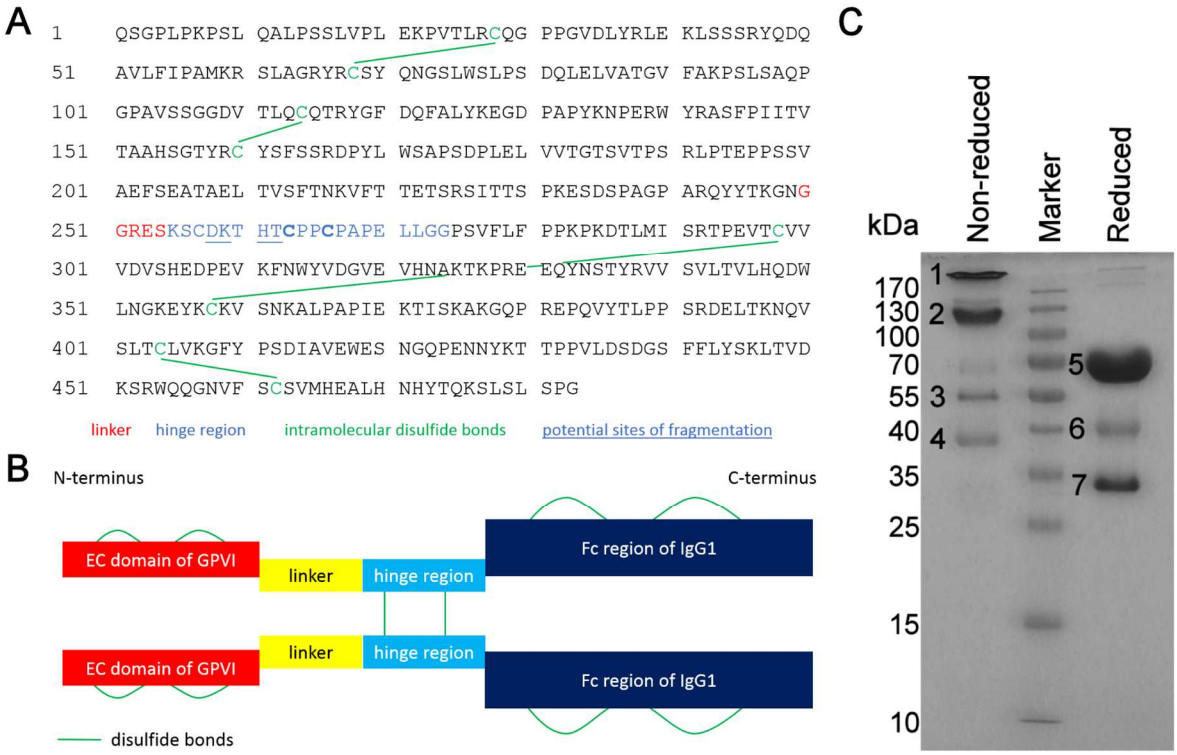

Figure 17: (A) Amino acid sequence of PR-15 (cysteines for 2 intermolecular disulfide bonds are depicted in bold). Adapted from [75] with permission from advanceCOR GmbH. (B) Schematic representation of PR-15. Adapted from [75] with permission from advanceCOR GmbH. (C) SDS-PAGE analysis of a reduced and alkylated PR-15 sample and a non-reduced but alkylated PR-15 sample (pH 7.0; 25 °C / 4 weeks) for elastase digest.

Comparing the gained peptide intensities of each band of the reduced PR-15 sample separated by SDS-PAGE, the 70 kDa band (63 kDa; **Figure 17C #5**) was identified as the monomer of PR-15 fusion protein (**Figure 18A** and **B (red), Table 13 #5**), the 35 kDa band (~27 kDa; **Figure 17C #7**) covered the C-terminus (**Figure 18A (blue), Table 13 #7**) and the 40 kDa band (~ 26 kDa + O-glycan; **Figure 17C #6**) covered the N-terminus of the fusion protein (**Figure 18B (blue), Table 13 #6**). Considering the non-reduced PR-15 sample separated by SDS-PAGE as well, the 55 kDa band (2x ~27 kDa; **Figure 17C #3**) covered the C-terminus (**Figure 18C (red), Table 13 #3**) and the 40 kDa band (~26 kDa + O-glycan; **Figure 17C #4**) covered the N-terminus of PR-15 (**Figure 18C (red), Table 13 #4**). Both the > 170 kDa band (**Figure 17C #1)** and the 130 kDa band (**Figure 17C #2)** covered the whole protein sequence indicating the fusion protein itself (126 kDa, **Figure 18D (red), Table 13 #1**) as well as a monomer of the fusion protein connected with the C-terminus (63 kDa + 27 kDa, **Figure 18D (blue), Table 13 #2**).

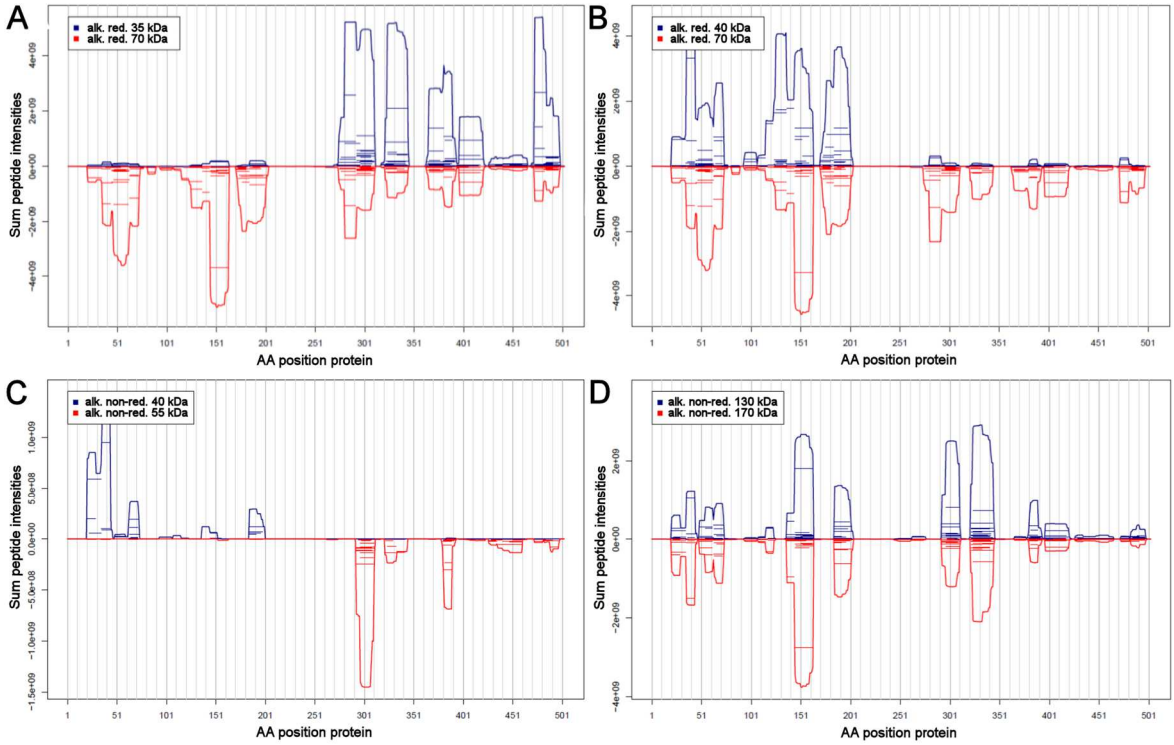

Figure 18: ESI-MS intensities after LC of elastase digested PR-15 sample (pH 7; 25 °C / 4 weeks).

No.	*Non-red.*	*Red.*	*Part of PR-15*	*M_W*	*Schematic representation*
1	> 170 kDa		fusion protein	126 kDa	
2	130 kDa		monomer + C-terminus	63 kDa+27 kDa	
3	55 kDa		2x C-terminus	2x 27 kDa	
4	40 kDa		N-terminus	26 kDa + O-glycan	
5		70 kDa	monomer	63 kDa	
6		40 kDa	N-terminus	26 kDa + O-glycan	
7		35 kDa	C-terminus	27 kDa	

Table 13: For elastase digest cut bands after SDS-PAGE analysis and their meaning.

During former SDS-PAGE analysis by advanceCOR under reduced conditions, the presence of O-glycans was investigated. The molecular weight of the glycosylated monomer was determined to be approximately 69 kDa and was 63 kDa after depletion of N-glycans by PNGase and 54 kDa after additional depletion of sialic acids and O-glycans by O-glycosidase [75]. According to these results, we assume that the calculated size [180] differs from the size in the SDS-PAGE because of the presence of O-glycans in the N-terminus of PR-15, leading to a band at approximately 40 kDa instead of the calculated 26 kDa.

Considering the results gained by LC/ESI-MS analysis combined with SDS-PAGE analysis it is obvious that PR-15 has an instability in the upper hinge region or in the linker because all fragments are assigned to the whole C- or N-terminus of the fusion protein. Typically, peptide bonds are remarkable stable with respect to non-enzymatic hydrolysis. In absence of a catalyst the lifetime of a peptide bond approaches several hundreds of years in aqueous solution [181]. Nevertheless, cleavage of peptide bonds occurs via specific degradation mechanism during storage of proteins. Possible reason for such spontaneous fragmentation is the amino acid sequence itself if there exist specific side-chains that trigger cleavage as well as the characteristics of the local structure, its flexibility or its accessibility to water [182]. Moreover, solvent conditions like pH and temperature play an important role for the fragmentation pattern of the protein. PR-15 is a homodimeric Fc-based fusion protein composed of the Fc domain of IgG1 and the extracellular domain of Glycoprotein VI (**Figure 17B**) [73]. The Fc fragment consists of two heavy chains connected via two disulfide bridges in the hinge region (Cys^{263} and Cys^{266}) and the EC domain of GP VI is connected with a short linker (^{250}GGRES) directly to the flexible hinge region (^{255}KSCDKTHTCPPCPAPELLGG) (**Figure 17A** and **B**). According to Cordoba et al. [183] recombinant antibodies tend to degrade by building a Fab and a Fab + Fc fragment in liquid formulations. In the pH range from 5 to 7 this cleavage mostly occurs across the upper hinge sequence ^{256}SCDKTHT between Asp-Lys (^{256}SCDKTHT) and His-Thr (^{256}SCDKTHT) presumably because of the high flexibility of the hinge region making hydrolytic cleavage easier by lowered activating energy for the cleavage [182, 183]. This predication fits to the results gained through this pH screening study by LC/ESI-MS analysis. So we conclude with some certainty that PR-15 degrades by cleavage in the upper hinge region. The exact site of fragmentation is mere speculation and cannot be assessed through this kind of analysis.

5.1.1.8 Analysis of aggregates and degradation products by SDS-PAGE (red./non-red.)

To monitor the degree of PR-15 degradation and the formation of covalent aggregates reducing and non-reducing SDS-PAGE analysis was done. Considering the main band of PR-15 under non-reduced (170 kDa or 126 kDa) as well as reduced conditions (70 kDa or 63 kDa) a decrease of the bands strength was observed by time and temperature (**Figures 19** and **20**). Moreover, the amount of degradation products increased by time and temperature, shown by the appearance of more bands of smaller sizes in the gel. The highest degree of degradation was observed at pH 5.5 and pH 6.0 where nearly no main band existed after 4 and 8 weeks incubation at 40 °C (**Figures 19A** and **B, 20A** and **B**). Furthermore, no formation of covalent aggregates was observed during non-reducing SDS-PAGE analysis (**Figure 20**).

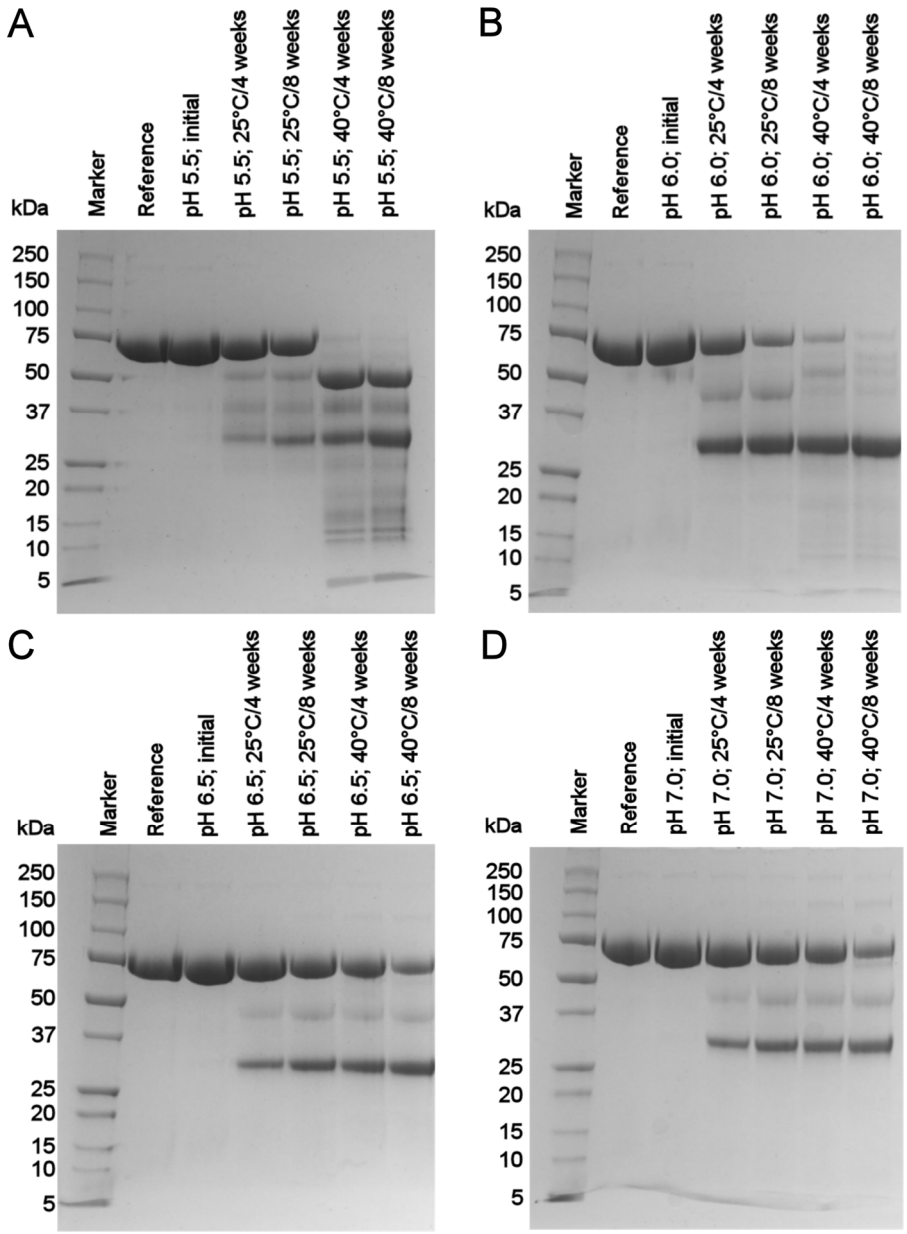

Figure 19: Reducing SDS-PAGE analysis of PR-15 samples after incubation at 25 °C and 40 °C for 0 (initial), 4 and 8 weeks at (A) pH 5.5, (B) pH 6.0, (C) pH 6.5 and (D) pH 7.0.

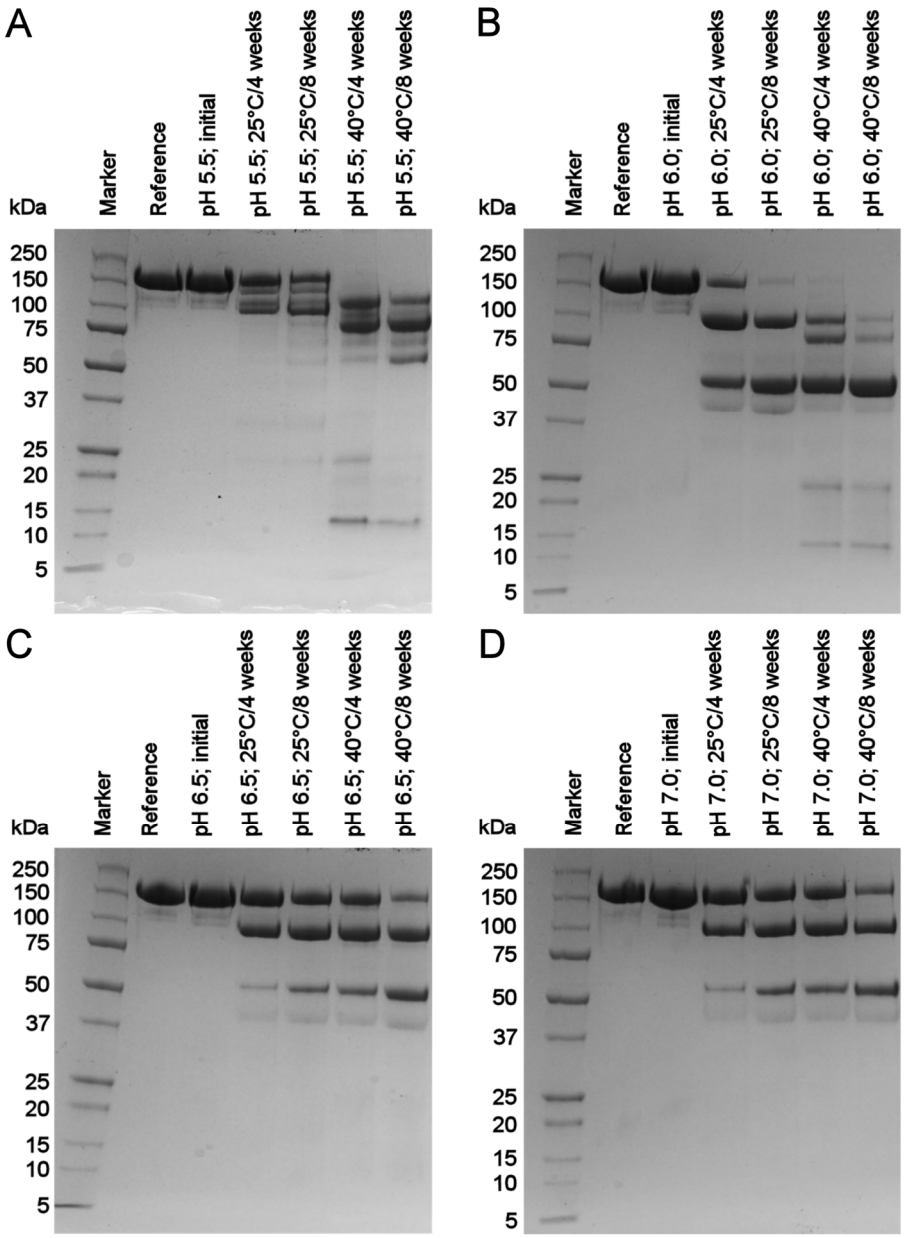

Figure 20: Non-reducing SDS-PAGE analysis of PR-15 samples after incubation at 25 °C and 40 °C for 0 (initial), 4 and 8 weeks at (A) pH 5.5, (B) pH 6.0, (C) pH 6.5 and (D) pH 7.0.

5.1.1.9 Determination of bioactivity by collagen ELISA

Collagen-induced aggregation of human platelets in the human body is inhibited by binding of PR-15 to collagen I, III and IV [74, 75]. So the biological activity of PR-15 was determined by evaluating its binding to bovine collagen type I with a specific ELISA method, leading to the concentration of half maximal binding (EC_{50}). An EC_{50} of about 100 nM (10–400 nM; 1.5–60 µg/mL) was determined by different laboratories confirming published affinity data of native GPVI to collagen with a value of 576 ± 64 nm [184]. All samples except pH 5.5 / 40 °C/ 4 and 8 weeks (**Figure 21A**), pH 6.0 / 25 °C / 4 and 8 weeks and 40 °C / 8 weeks (**Figure 21B**) showed good results with low EC_{50} values in the range of 2.9–84.4 µg/mL indicating maintained

bioactivity. Excluded samples reached EC_{50} values between 161.4–76225.6 µg/mL demonstrating loss of bioactivity due to storage conditions (**Figure 21; Table 14)**.

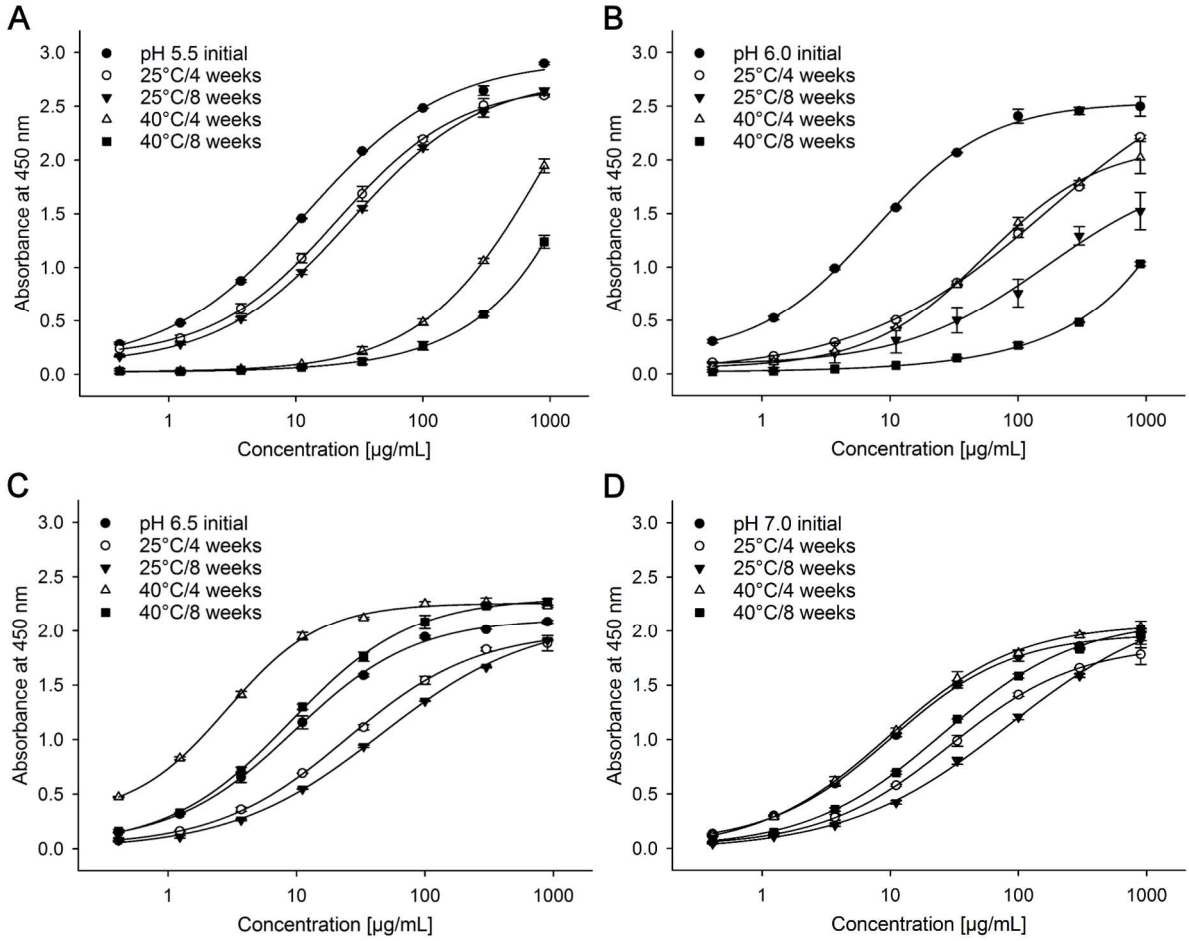

Figure 21: Determination of EC_{50} values of PR-15 samples via collagen ELISA to test potency of PR-15 after incubation at 25 °C and 40 °C for 0 (initial), 4 and 8 weeks at (A) pH 5.5, (B) pH 6.0, (C) pH 6.5 and (D) pH 7.0.

5.1.1.10 Determination of bioactivity by inhibition of aggregation of human platelets

Light transmission aggregation was used to evaluate collagen induced inhibition of human platelets aggregation by PR-15. Cross-linked collagen-related peptide (CRP-XL) which mimics collagen triple helix was used instead of collagen because of a higher reproducibility. Recent trials showed that a concentration of 25 µg/mL of PR-15 is sufficient to reach up to 100 % inhibition of collagen or CRP induced aggregation [75]. Unfortunately, all pH 5.5 and pH 6.0 samples failed to inhibit aggregation except initial samples (**Table 14**). Moreover, both samples stored at 25 °C for 8 weeks at pH 6.5 and pH 7.0 did not inhibit platelet aggregation. To some extent, these results are inconsistent to the results obtained during collagen ELISA, indicating different binding affinities of PR-15 to collagen and to CRP [184]. There are five samples which showed good bioactivity regarding EC_{50} values, however, they were not able to inhibit platelet aggregation (**Table 14**).

	pH 5.5		*pH 6.0*		*pH 6.5*		*pH 7.0*	
	Inh. of agg.	*EC_{50}*	*Inh. of agg.*	*EC_{50}*	*Inh. of agg.*	*EC_{50}*	*Inh. of agg.*	*EC_{50}*
Initial	yes	12.1	yes	7.5	yes	9.6	yes	10
25 °C/4 weeks	no	20.8	no	161.4	yes	24.8	yes	29.2
25 °C/8 weeks	no	26.5	no	166.7	no	45.4	no	84.4
40 °C/4 weeks	no	986.2	no	55.3	yes	2.9	yes	9.7
40 °C/8 weeks	no	76226.2	no	3149.6	yes	9	yes	25.6

Table 14: Bioactivity of PR-15 samples at the different pH values (5.5/6.0/6.5/7.0) after incubation at 25 °C and 40 °C for 0 (initial), 4 and 8 weeks. Inhibition of platelet aggregation of human platelets and EC_{50} values [µg/mL].

5.1.1.11 Determination of the unfolding temperature of PR-15 at different pH values

To confirm that pH 7.0 is the best formulation pH for PR-15, a thermal shift assay, also called differential scanning fluorimetry (DSF), was performed to detect the unfolding temperature of PR-15 at the different pH values. Non-covalent extrinsic fluorescent dyes such as SYPRO® orange dye interact with a protein undergoing thermal unfolding [185]. The dye's fluorescence signal is quenched in the aqueous environment of a properly folded protein in solution, but becomes unquenched when exposed to the protein's hydrophobic core upon unfolding [152]. As the fluorescence emission of the dye sample mixtures were analyzed over a temperature range from 25 °C to 95 °C, the unfolding temperature was determined as maximum of the first derivation of the emission intensity-temperature-curve [152]. PR-15 showed the highest unfolding temperature at pH 7.0 with 66.3 ± 0.1 °C (**Figure 22**) which is significantly different from the unfolding temperature of the pH 5.5 (59.5 ± 0.5 °C) as well as the pH 6.0 (63.9 ± 0.2 °C) sample. The pH with the highest unfolding temperature indicates the pH at which the protein is most stable. These data confirm the results of the pH screening study and consequently determine pH 7.0 as best formulation pH.

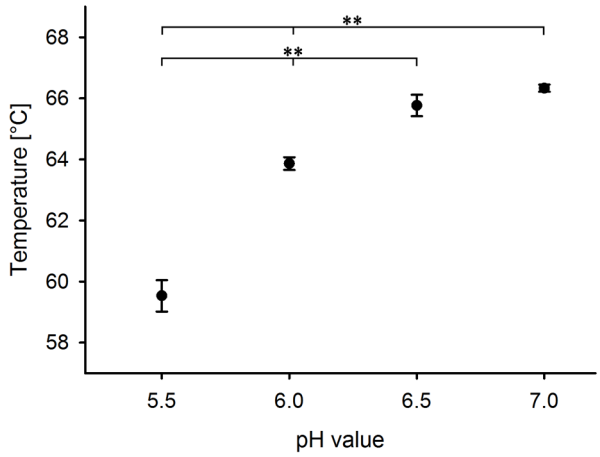

Figure 22: Unfolding temperature of PR-15 at the different pH values (5.5/6.0/6.5/7.0) of the initial samples determined by DSF. Asterisks denote statistically significant differences between the groups (** $p < 0.01$).

5.1.2 Evaluation of potential degradation pathways of PR-15

5.1.2.1 Determination of the concentration after stressing by UV-spectroscopy

To determine the loss of protein during stressing, UV absorptions at 280 nm were measured to calculate the concentrations of the samples. All protein concentrations, except the concentrations of the oxidation sample and the light sample, remained constant at about 2.5 mg/mL under stressing conditions (**Figure 23**). Forced oxidation with hydrogen peroxide led to a significant decrease of the PR-15 concentration to 2.22 ± 0.04 mg/mL (87.8 %) and, in contrast, the exposure to light increased the protein concentration significantly to 2.83 ± 0.05 mg/mL (112.0 %). Mostly the amino acid tryptophan (14 (quantity in PR-15)), tyrosine (44), phenylalanine (32) and cysteine (22) are the targets of photodegradation by UV-light. It is reported that tyrosine radicals are built during UV exposure. These radicals lead to the formation of di-tyrosine by intra- and/or intermolecular crosslinkage. The deprotonated and protonated forms of di-tyrosine have absorption maxima at 283 nm and 315 nm explaining the significant increase of protein concentration of the light sample [186]. The significant decrease of the 0 h and the 48 h deamidation sample was probably caused by dilution mistakes. Otherwise, a significant loss of protein would have been observed after 24 h of the deamidation reaction as well.

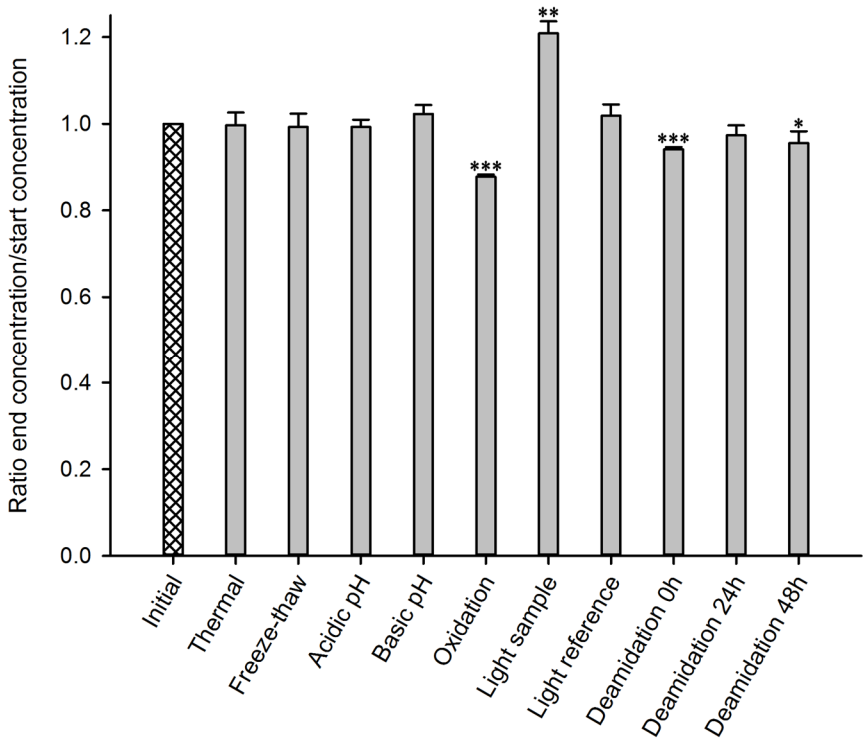

Figure 23: Concentration change of PR-15 samples after the different stress conditions in comparison to the initial PR-15 sample depicted as ratios of end and start concentration. Asterisks denote statistically significant differences between the groups referring to the initial sample (*** $p < 0.001$, ** $p < 0.01$, * $p < 0.05$).

5.1.2.2 Determination of the pH value after stressing

The pH values of the PR-15 samples were measured after each stressing procedure. All pH values stayed constant at the starting pH for all stressing conditions (**Figure 24**).

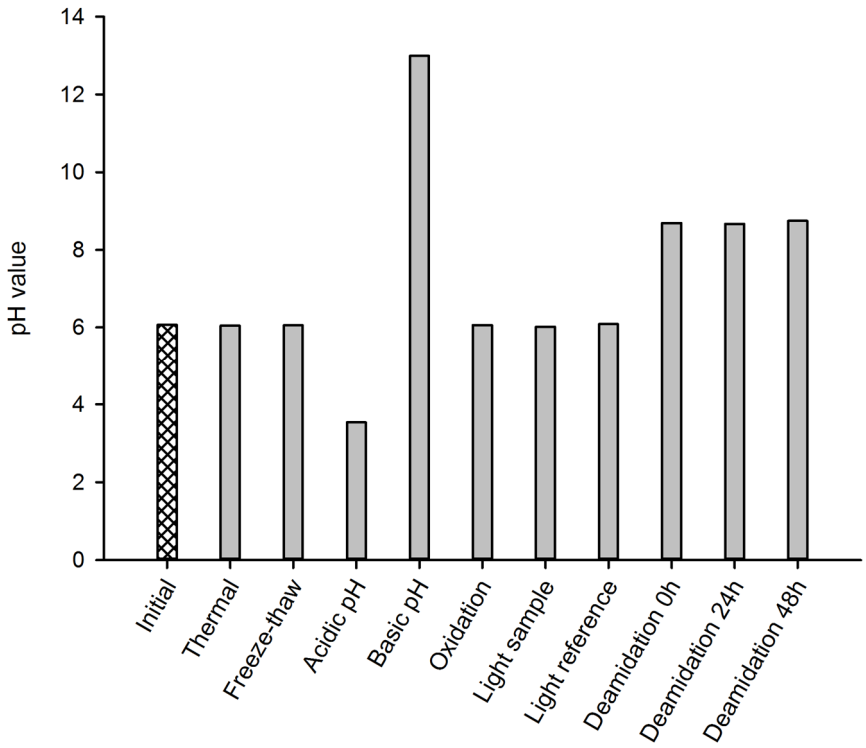

Figure 24: pH values of PR-15 samples after stress tests in comparison to the initial sample.

5.1.2.3 Analysis of aggregates by DLS

DLS was performed to investigate particle size distributions and polydispersity indices (PdI) of PR-15 after forced degradation procedures. The highest PdI values were observed for the acidic pH sample (PdI 0.254 ± 0.015) as well as the basic pH sample (PdI 0.195 ± 0.010) with a statistically significant difference to the initial PR-15 sample. All other stressed samples showed a PdI below 0.2 indicating a monodisperse distribution of PR-15 and the lack of aggregates [176] (**Figure 25A**). The mean sizes of the protein lay around 15 nm, except the thermal sample (39.5 nm ± 0.7), the acidic pH sample (25.5 nm ± 0.3), the basic pH sample (233.9 nm ± 72.7) and the light sample (18.2 nm ± 0.473), indicating the formation of aggregates (**Figure 25B**).

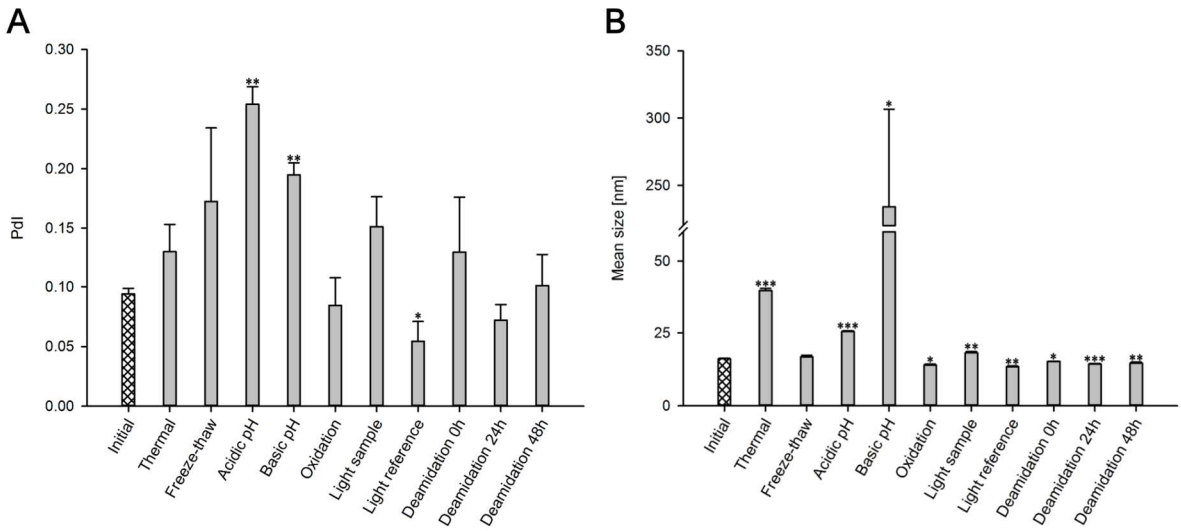

Figure 25: Analysis of aggregates of PR-15 samples by DLS. (A) Polydispersity indices (PdI) and (B) mean sizes of stressed PR-15 samples in comparison to the initial PR-15 sample. Asterisks denote statistically significant differences between the groups referring to the initial sample (*** $p < 0.001$, ** $p < 0.01$, * $p < 0.05$).

5.1.2.4 Analysis of aggregates and degradation products by SEC

SEC was performed to evaluate the formation of soluble aggregates and degradation products after stress tests. Insoluble aggregates were removed before analysis by centrifugation. Therefore, the major loss of protein that occurred at acidic and basic pH, during thermal and oxidative stress, shown by the decrease of total peak areas, was assigned to formed insoluble aggregates (**Figure 27A**). These four samples, except the basic pH sample, as well as the light sample, also showed a high degree of soluble aggregates indicating the sensitivity of PR-15 to pH, heat, light and oxidative stress (**Figures 26** and **27B**). The amount of degradation products increased for all stressed samples except for the freeze-thaw sample (**Figure 27B**). The high basic pH nearly completely destroyed PR-15, just degradation products were detected and not even a small amount of the fusion protein was left. The peak with a retention time of about 48 minutes was found in all chromatograms and was assigned to histidine in the sample buffer. For the basic pH sample probably many other amino acids formed during alkaline hydrolysis of PR-15 were located under this ‘histidine’ peak.

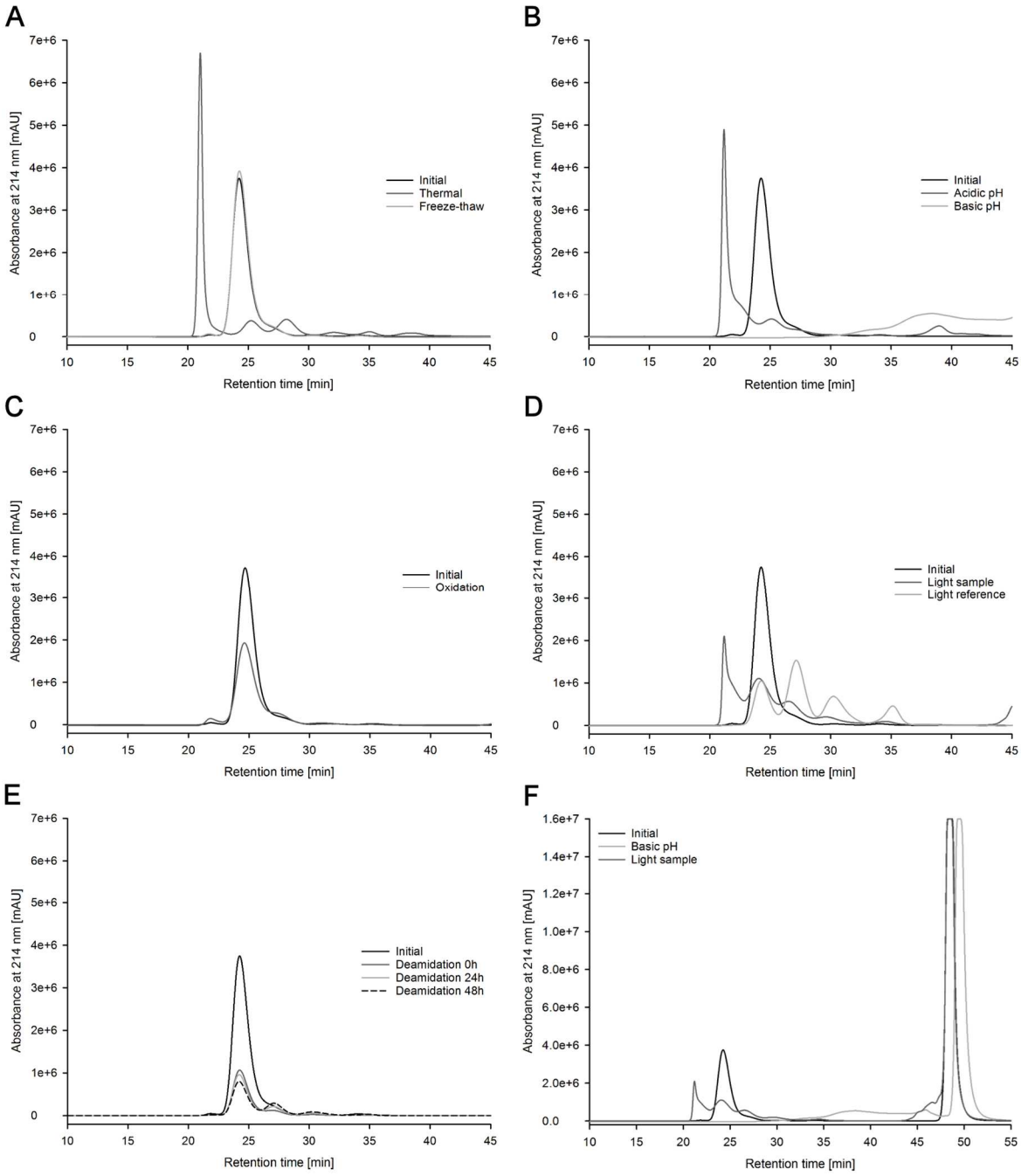

Figure 26: SEC chromatograms of PR-15 after forced degradation studies in comparison to initial PR-15 sample.

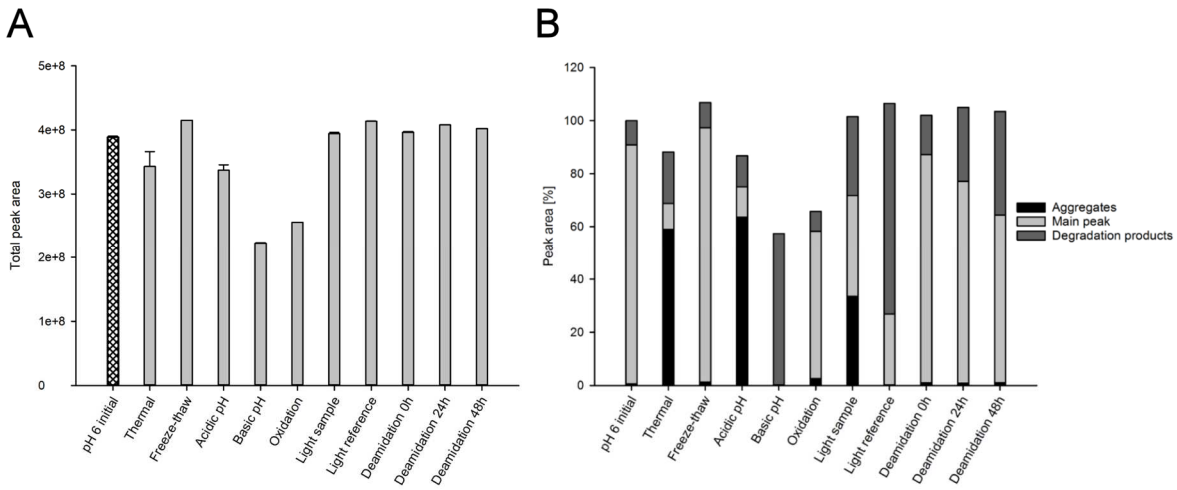

Figure 27: SEC of PR-15. (A) Total peak areas, (B) percentages of the fusion protein (main peak), aggregates and degradation products of stressed PR-15 in comparison to the initial PR-15 sample.

5.1.2.5 Analysis of aggregates and degradation products by HIC

The aggregation and degradation of PR-15 by different forced degradation procedures was evaluated using HIC. The major loss of PR-15, shown by the decrease of total peak area of acidic and basic pH, oxidation as well as light sample, was assigned to the formation of insoluble aggregates which were removed by centrifugation before analysis. After the residual stress tests the total peak area and therefore the concentration of PR-15 stayed constant and no loss due to the formation of insoluble aggregates was observed (**Figure 29A**). A small amount of more hydrophobic aggregates or degradation products was just observed after thermal and oxidative stress (**Figures 28A, 28C** and **29B**). The peak shift to a longer retention time of the oxidation sample was probably not solely caused by the formation of aggregates as there was just a little amount of oligomers detected during SEC (**Figures 26C** and **27B**) and no covalent aggregates were found during non-reducing SDS-PAGE analysis (**Figure 31B**). Presumably, oxidation provoked unfolding of PR-15 leading to an increase of protein's hydrophobicity. The amount of less hydrophobic degradation products increased after all forced degradation procedures except for the freeze-thaw sample (**Figures 28** and **29B**).

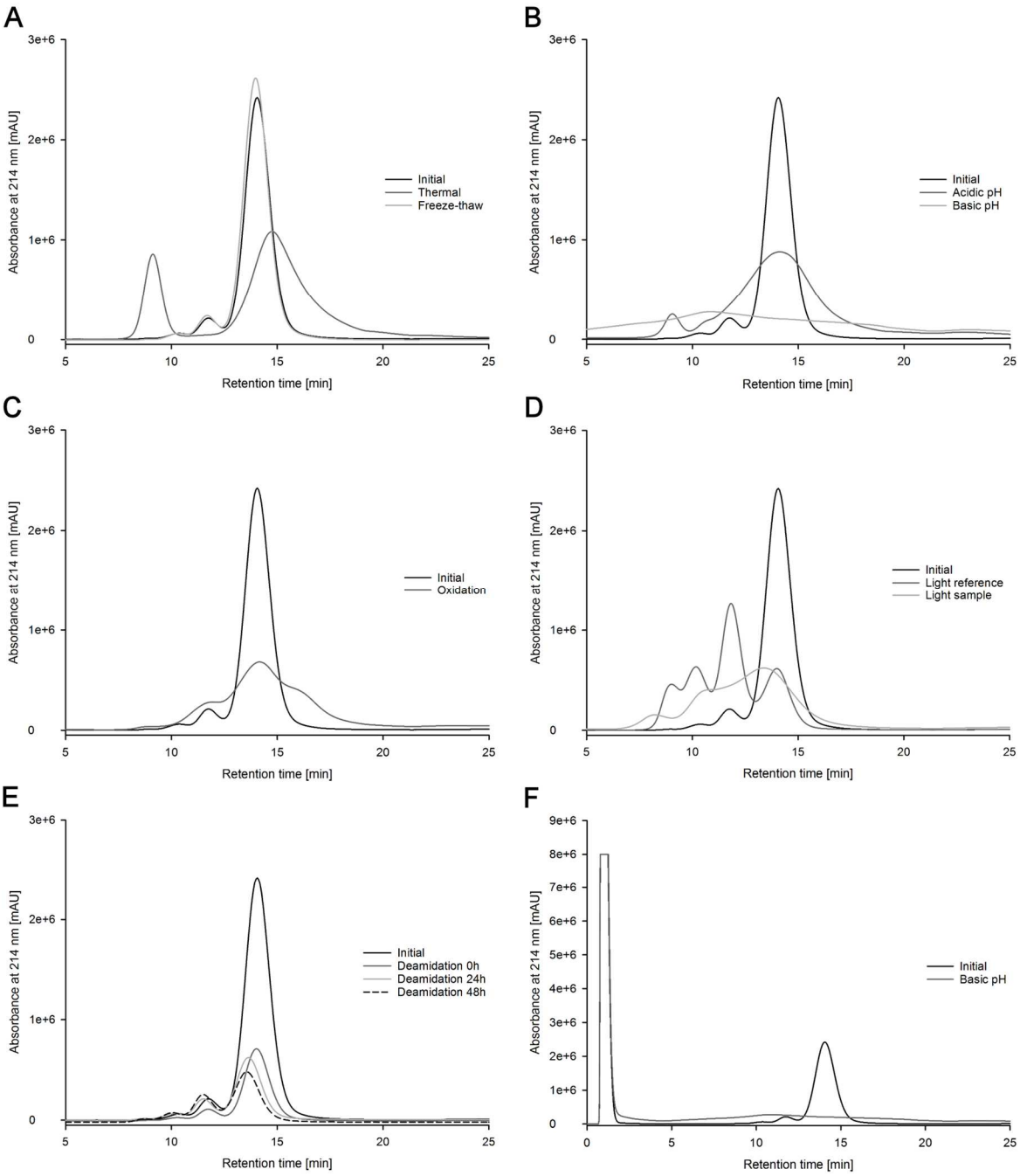

Figure 28: HIC chromatograms of PR-15 after forced degradation studies in comparison to the initial PR-15 sample.

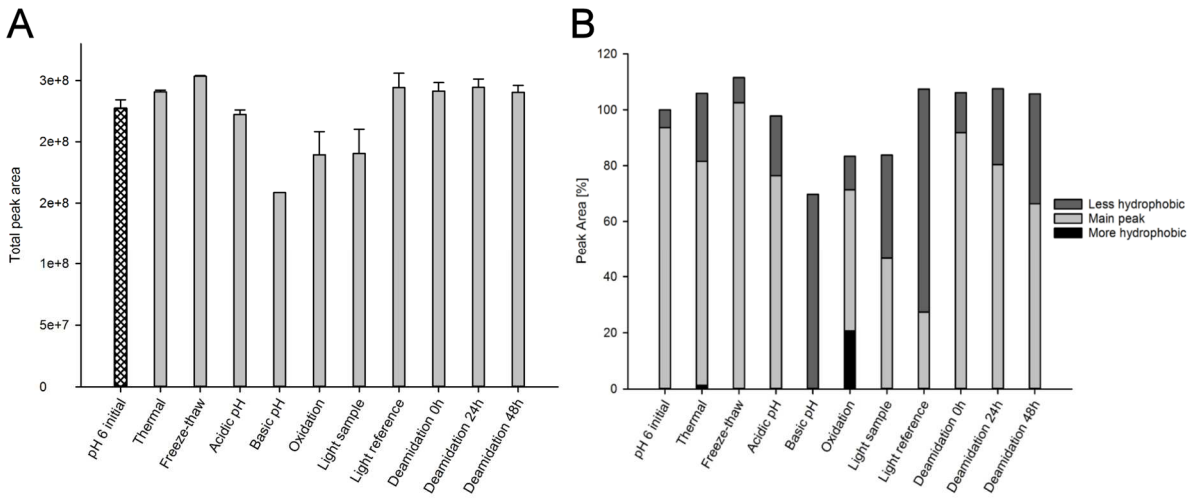

Figure 29: HIC of PR-15. (A) Total peak areas, (B) percentages of the fusion protein (main peak), more hydrophobic aggregates or degradation products and less hydrophobic degradation products of stressed PR-15 in comparison to the initial PR-15 sample.

5.1.2.6 Analysis of aggregates and degradation products by MALDI-TOF MS

MALDI-TOF MS was implemented to monitor the formation of aggregates as well as the development of degradation products of PR-15 (**Figure 30**). The spectrum of the initial sample showed the PR-15 fusion protein (126 kDa), the monomer of the fusion protein (63 kDa), the dimer of the fusion protein (252 kDa) and the 90 kDa degradation fragment (**Figure 30A**). After stressing at acidic (**Figure 30D**) as well as basic pH (**Figure 30E**), with heat (**Figure 30B**) and light (**Figure 30J**) nearly none of these peaks were observed whereas most of the peaks still existed after all the other stressing procedures.

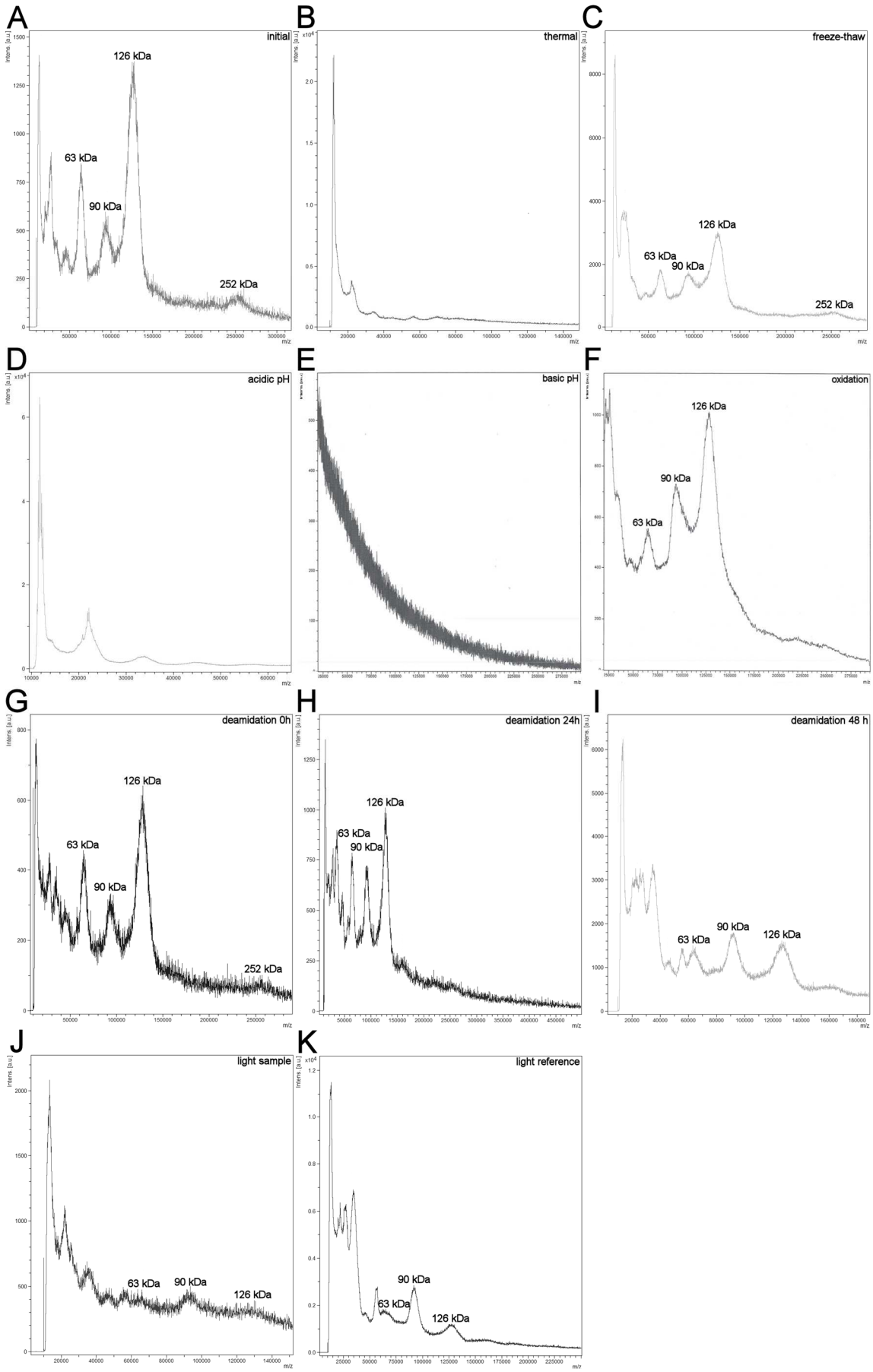

Figure 30: MALDI-TOF-MS spectra of PR-15 after forced degradation studies in comparison to the initial PR-15 sample.

5.1.2.7 Analysis of aggregates and degradation products by SDS-PAGE (red./non-red.)

Reducing and non-reducing SDS-PAGE analysis was performed to investigate the degree of PR-15 aggregation and degradation under stressed conditions. Considering the main band of PR-15 under non-reduced conditions (170 kDa or 126 kDa), a decrease of the main band combined with an increase of degradation products for thermal, acidic pH and light samples was observed (**Figure 31)**. Furthermore, the light as well as the thermal sample even showed a band with a size of about 250 kDa indicating the formation of covalent aggregates caused by light and heat (**Figure 31)**. The basic pH treatment caused a complete destruction of PR-15 in small fragments shown by faintly viewable smear between 5 and 15 kDa. However, even all other samples, except the freeze-thaw sample, showed an increase of the so-called 90 kDa lane (130 kDa) under non-reduced conditions. Under reduced conditions the main band (70 kDa or 63 kDa) became weaker and the amount of smaller bands increased for thermal, acidic pH and light samples indicating degradation of PR-15 under these conditions (**Figure 32**).

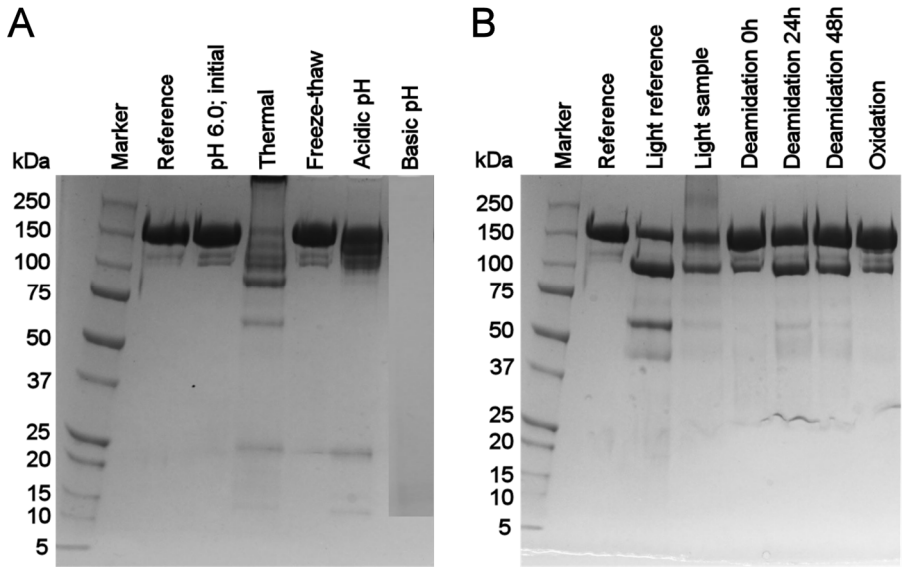

Figure 31: Non-reduced SDS-PAGE analysis of PR-15 after forced degradation studies in comparison to the initial PR-15 sample.

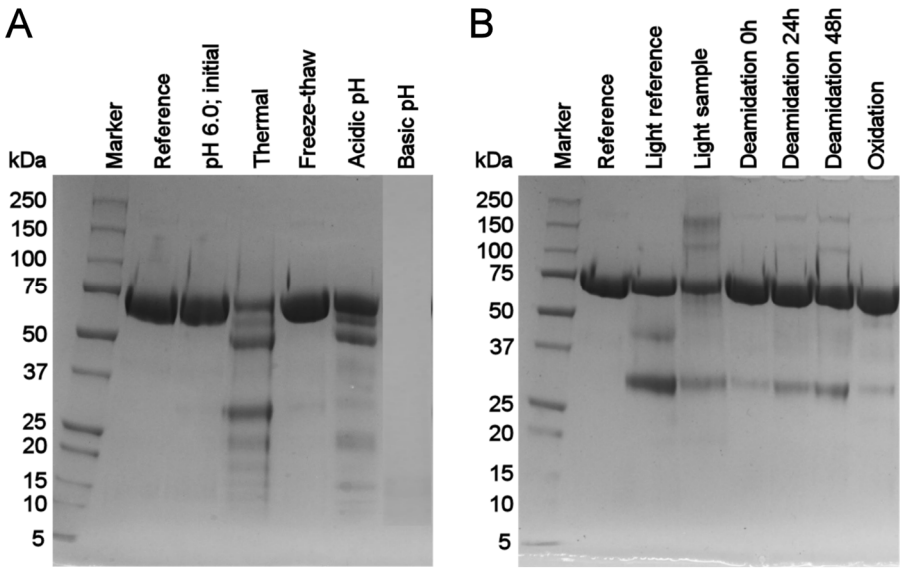

Figure 32: Reduced SDS-PAGE analysis of PR-15 after forced degradation studies in comparison to the initial PR-15 sample.

5.1.2.8 Determination of bioactivity by collagen ELISA

Bioactivity of stressed PR-15 samples was evaluated via collagen ELISA. The shape of the obtained curve looked similar to the initial sample for all samples, except the once stressed with acid, base, heat and light, indicating a loss of bioactivity due to these stress conditions (**Figure 33**).

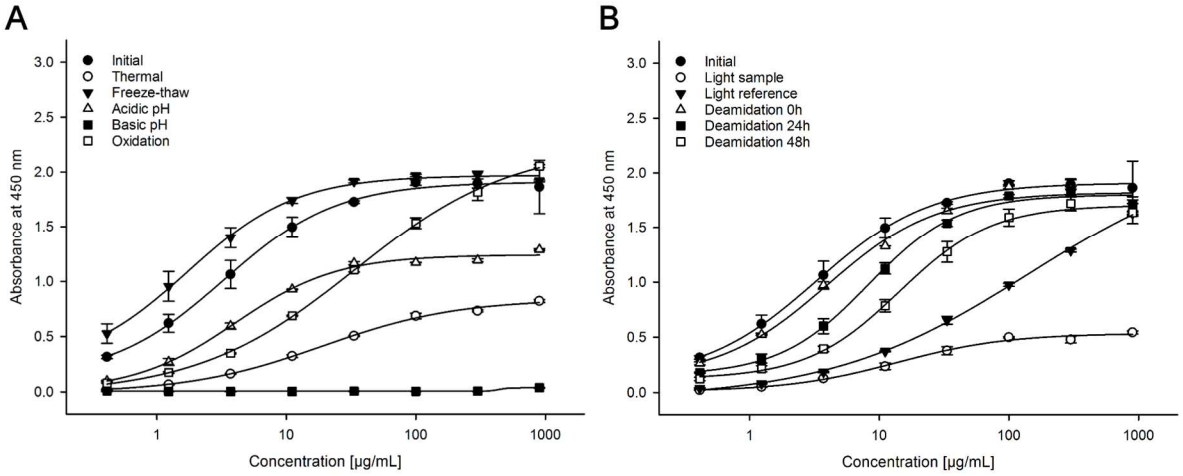

Figure 33: Determination of EC_{50} via collagen ELISA to test potency of stressed PR-15 samples in comparison to the initial PR-15 sample.

5.1.2.9 Determination of bioactivity by inhibition of aggregation of human platelets

The biological activity of PR-15 was additionally analyzed through light transmission aggregation. Thereby, collagen induced inhibition of human platelets aggregation by PR-15 was tested using cross-linked collagen peptide (CRP) instead of collagen because of a higher reproducibility [75]. The most stressed samples failed to inhibit aggregation except initial, freeze-thaw, basic pH and oxidation sample. Unfortunately, these results are inconsistent to the results obtained with collagen ELISA indicating different binding affinities of PR-15 to collagen and to CRP [184]. Deamidation

samples, for example, showed good bioactivity regarding EC_{50} values, however, they were not able to inhibit platelet aggregation (**Table 15**). As opposed to this, the basic pH sample inhibited platelet aggregation of CRP but EC_{50} value obtained by collagen ELISA was very high indicating low bioactivity.

	Inh. of aggregation	*EC_{50} [µg/mL]*
Initial	ja	3.3
Thermal	nein	19.1
Freeze-thaw	ja	1.7
Acidic pH	nein	4.0
Basic pH	ja	436.1
Oxidation	ja	34.1
Light sample	nein	13.8
Light reference	nein	142.3
Deamidation 0 h	nein	4.0
Deamidation 24 h	nein	8.3
Deamidation 48 h	nein	14.3

Table 15: Bioactivity of stressed PR-15 samples and the initial PR-15 sample determined by the inhibition of platelet aggregation of human platelets and collagen ELISA (EC_{50} values).

5.1.3 Optimization of Revacept® formulation

5.1.3.1 Determination of the concentration after incubation by UV-spectroscopy

The protein concentrations of the samples were determined before and after incubation at 53 °C for 1 week by measuring UV absorptions at 280 nm to observe loss of protein during thermal stressing. For all samples, the protein concentration stayed nearly constant under stressed conditions (**Figure 34**).

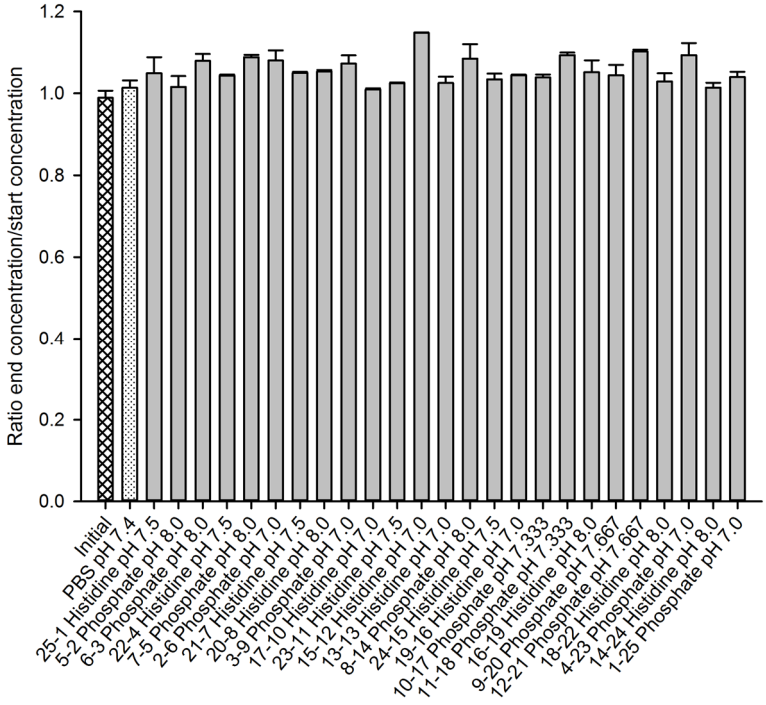

Figure 34: Concentration change of PR-15 DoE samples after thermal stressing depicted as ratios of end and start concentration in comparison the initial PR-15 sample and the former Revacept® formulation sample (PBS, pH 7.4).

5.1.3.2 Determination of the pH value after incubation

The pH values of the PR-15 samples were measured after incubation at 53 °C for 1 week, to see if the pH had changed during stressing. All pH values stayed constant after 1 week heating (**Figure 35**).

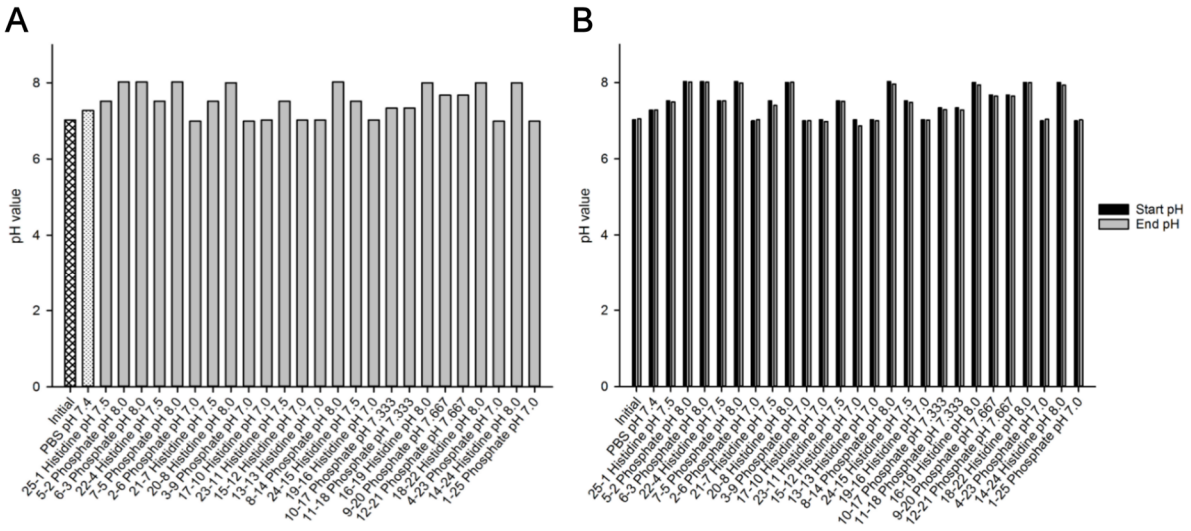

Figure 35: pH values of PR-15 DoE samples after thermal stressing in comparison to the initial PR-15 sample and the former Revacept® formulation sample (PBS, pH 7.4).

5.1.3.3 Analysis of aggregates by DLS

The formation of aggregates after incubation at 53 °C for 1 week was assessed by DLS. Particle size distributions as well as polydispersity indices (PdI) of PR-15 were determined (**Figure 36**). All samples except 5-2, 6-3, 7-5, 2-6, 3-9, 13-13 and 4-23 showed a PdI below 0.2, indicating monodispersity [176]. However, the excluded samples showed a PdI below 0.4 considering a reproducible measurement according to the manufacturer and a rather monodisperse than polydisperse size distribution (**Figure 36A**).

Mean sizes were determined with DLS as well. For the initial sample and the histidine buffered samples the determined mean sizes (11–15 nm) correlated with the calculated mean size (~11 nm) [187]. In contrast, the mean sizes of the former Revacept® formulation (PBS, pH 7.4) and the phosphate buffered samples indicated the formation of aggregates (26–33 nm) (**Figure 36B**). These data correlate with the data obtained from SEC (**Figure 37B**).

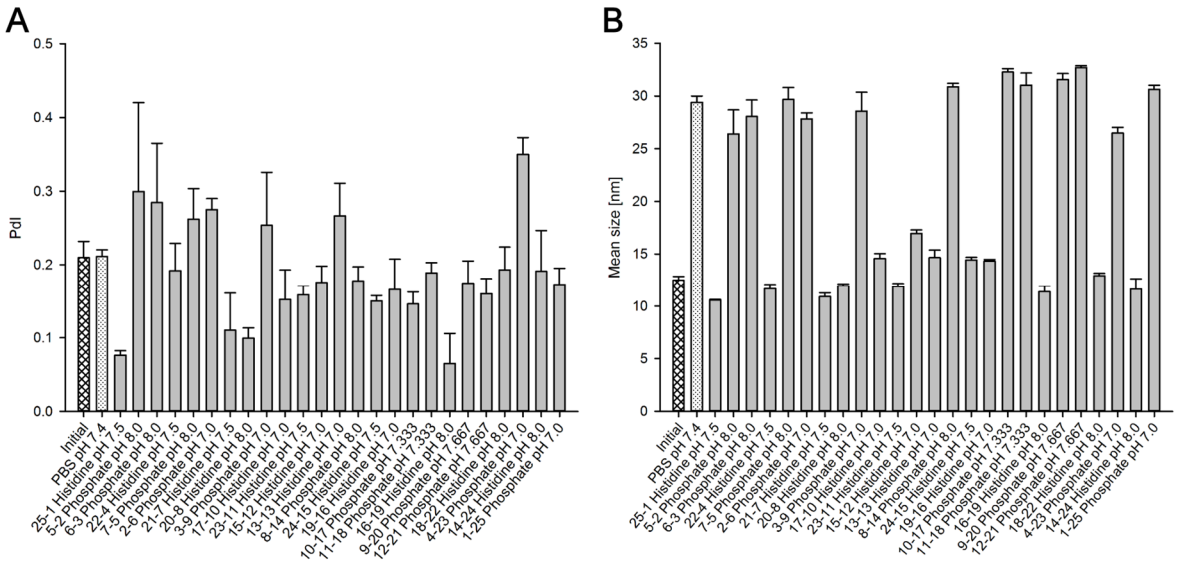

Figure 36: Analysis of aggregates of PR-15 DoE samples by DLS. (A) Polydispersity indices (PdI) and (B) mean sizes of PR-15 after thermal stressing in comparison to the initial PR-15 sample and the former Revacept® formulation sample (PBS, pH 7.4).

5.1.3.4 Analysis of aggregates and degradation products by SEC

The formation of soluble aggregates and degradation products of PR-15 after incubation at 53 °C for 1 week was evaluated with SEC. Insoluble aggregates were removed before analysis by centrifugation. During thermal stressing the total peak areas and therefore the concentration of PR-15 remained constant indicating no loss due to the formation of insoluble aggregates (**Figure 37A**). The initial sample showed a percentage of 1 % aggregates and a percentage of 7 % degradation products. After incubation at 53 °C for 1 week merely phosphate buffered samples tended to build soluble aggregates and reached values between 59 % and 74 %, whereas histidine buffered samples just reached values between 8 % and 31 %. In contrast, the former Revacept® formulation even reached a percentage of 32 % aggregates after incubation. However, the amount of degradation products was higher for histidine buffered samples (23–39 %) than for phosphate buffered samples (16–22 %) similar to the former Revacept® formulation (23 %) (**Figure 37B–D**).

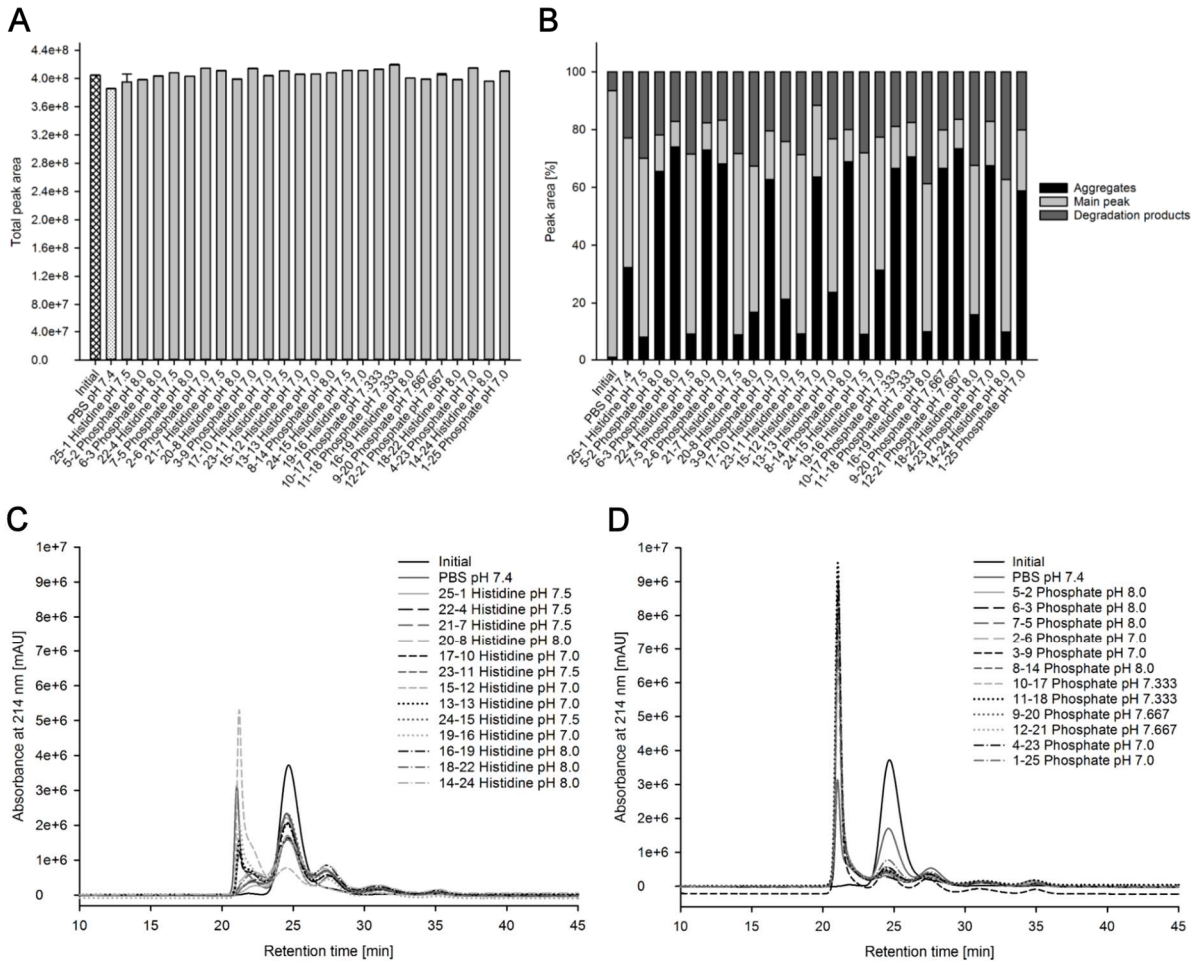

Figure 37: SEC of PR-15. (A) Total peak areas, (B) percentages of fusion protein (main peak), aggregates and degradation products and (C+D) SEC chromatograms of PR-15 DoE samples after thermal stressing in comparison to the initial amount of PR-15 and the amount of the former Revacept® formulation sample (PBS, pH 7.4).

5.1.3.5 Analysis of aggregates and degradation products by HIC

Thermal stability of PR-15 was analyzed by HIC. No loss due to the formation of insoluble aggregates was observed after thermal stressing depicted by constant total peak areas indicating no variation of PR-15 concentration (**Figure 38A**). The amount of less hydrophobic degradation products increased for histidine buffered samples to percentages of 27–34 % and for phosphate buffered samples to percentages of 16–27 % compared to 7 % for the initial sample and 36 % for the former Revacept® formulation sample (**Figure 38B–D**). More hydrophobic aggregates or degradation products were just observed for the former Revacept® formulation sample as well as all histidine buffered samples, except the initial sample, shown by a shoulder of the main peak to different extent (**Figure 38C**). All phosphate buffered samples showed a shift of the main peak, but without a shoulder (**Figure 38D**). Hence, no more hydrophobic aggregates or degradation products were depicted in **Figure 38B**. However, even the phosphate buffered samples became more hydrophobic during thermal stressing. During SDS-PAGE analysis we observed the formation of reducible as well as non-reducible covalent aggregates in phosphate buffered PR-15 samples

(**Figure 39**). The formation of such disulfide bridges and the resulting conformational change is a conceivable reason for increased hydrophobicity of PR-15 explaining the peak shift in HIC chromatograms (**Figure 38C**). As opposed to this, in histidine buffered samples the fusion protein remained stable to a large extent and just non-reducible covalent aggregates were generated (see SDS-PAGE analysis **Figure 39**) depicted by the main peak with a shoulder to longer retention times in the HIC chromatograms of histidine buffered PR-15 samples (**Figure 38C**).

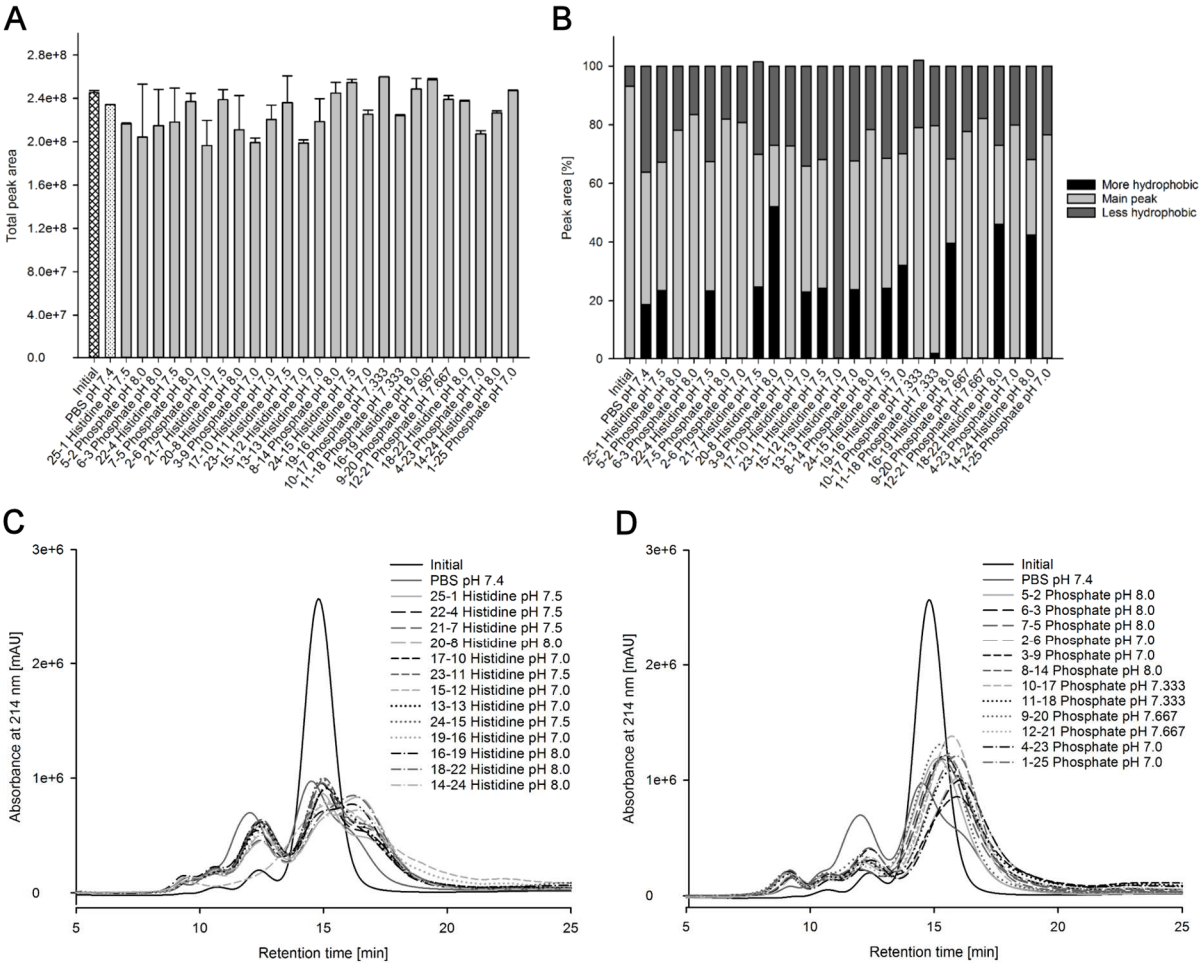

Figure 38: HIC of PR-15. (A) Total peak areas, (B) percentages of the fusion protein (main peak), more hydrophobic aggregates or degradation products and less hydrophobic degradation products and (C+D) HIC chromatograms of PR-15 DoE samples after thermal stressing in comparison to the initial PR-15 sample and the former Revacept® formulation sample (PBS, pH 7.4).

5.1.3.6 Analysis of aggregates and degradation products by SDS-PAGE (red./non-red.)

Non-reducing as well as reducing SDS-PAGE analysis was done to visualize the formation of PR-15 aggregates and degradation products. Regarding the gels under reduced conditions, histidine and phosphate buffered samples differed in intensity of the main band of the PR-15 monomer (70 kDa or 63 kDa) with a weaker intensity for the phosphate buffered samples (**Figure 39A-C**). Despite reduced conditions, bands on the level of the fusion protein (170 kDa or 126 kDa) as well as on the level of the so-called 90 kDa band (130 kDa; monomer (63 kDa) + C-terminus (27 kDa)) were observed for all samples with similar intensities indicating non-reducible covalent aggregates.

In addition, degradation products with a size of 40 kDa (26 kDa + O-glycan; N-terminus) and 35 kDa (27 kDa; C-terminus) appeared for all samples. Moreover, phosphate buffered samples showed an additional band with a size of 55 kDa (2x 27 kDa; C-terminus), maybe non-reducible covalent aggregates of the C-terminus (**Figure 39A–C**). Under non-reduced conditions the main band of PR-15 fusion protein (170 kDa or 126 kDa) as well as the so-called 90 kDa band (130 kDa; monomer (63 kDa) + C-terminus (27 kDa)) were more intense for histidine buffered samples (**Figure 39D–F**). Moreover, all phosphate buffered samples showed reducible covalent aggregates of the fusion protein (> 250 kDa) and all samples showed slight bands with a size of 55 kDa (2x 27 kDa; C-terminus) and 40 kDa (26 kDa + O-glycan; N-terminus) (**Figure 39D–F**).

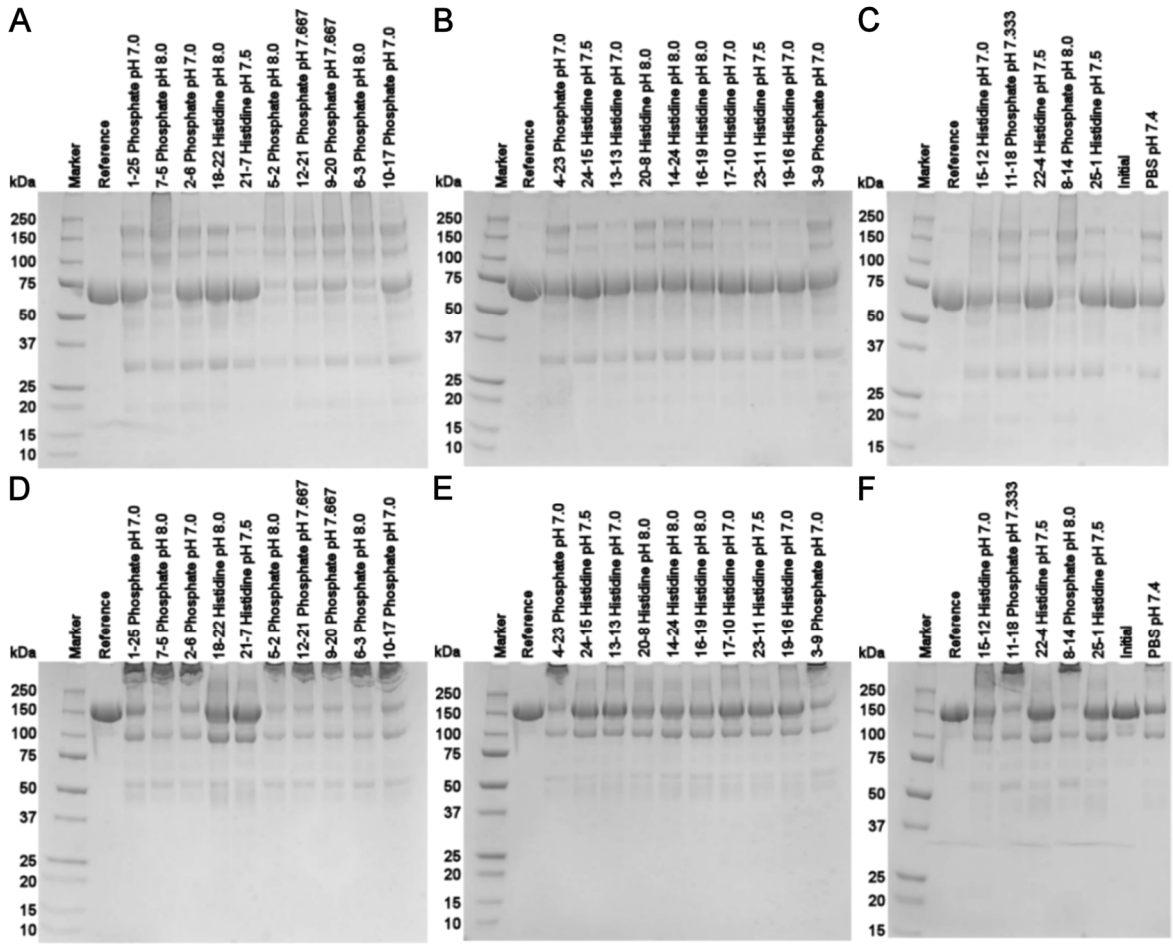

Figure 39: SDS-PAGE analysis. (A-C) Reduced and (D-F) non-reduced PR-15 DoE samples after thermal stressing in comparison to the initial PR-15 sample and the former Revacept® formulation sample (PBS, pH 7.4).

5.1.3.7 Determination of bioactivity by collagen ELISA

The biological activity of PR-15 was determined using a specific ELISA method. Through the binding of PR-15 to bovine collagen type I the concentration of half maximal binding (EC_{50}) was assessed. All histidine buffered samples showed good results with low EC_{50} values in the range of 3.2–8.1 µg/mL indicating maintained bioactivity compared to the initial sample with 16.1 µg/mL

and the former Revacept® formulation sample with 4.5 µg/mL (**Figure 40A; Table 16**). In contrast, phosphate buffered samples reached higher but still good EC_{50} values between 6.5–24.3 µg/mL (**Figure 40B; Table 16**).

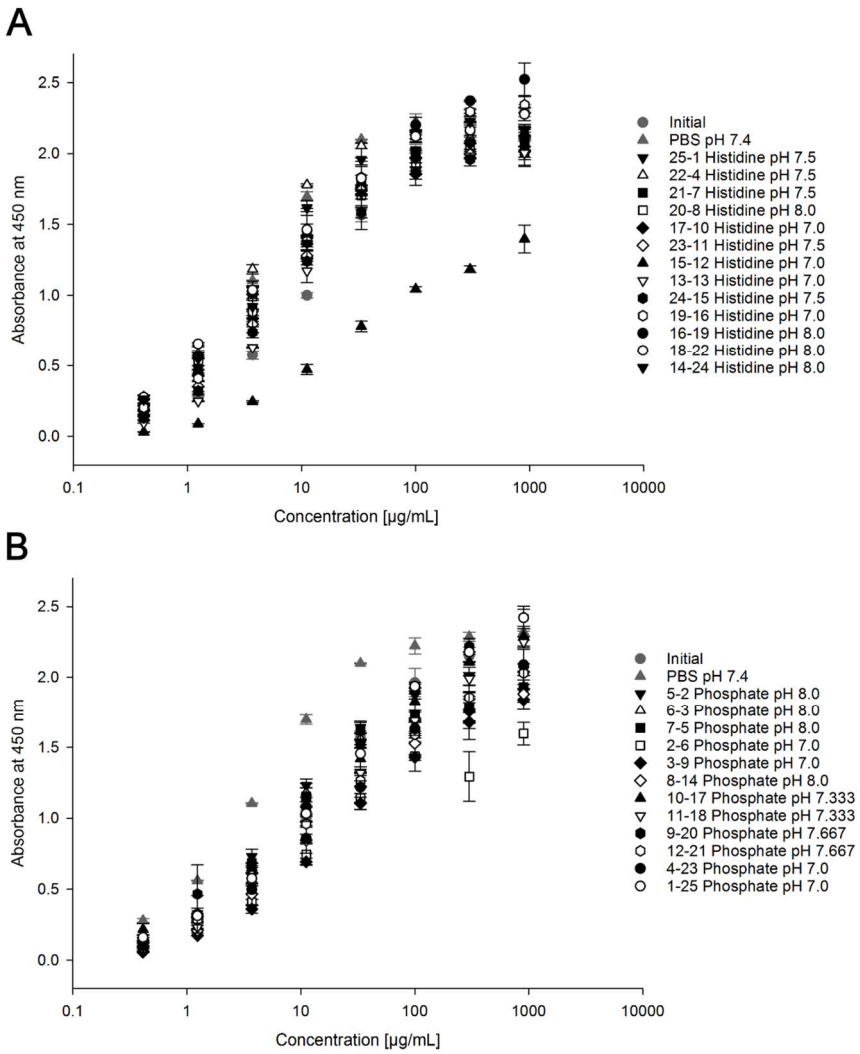

Figure 40: Determination of EC_{50} values via collagen ELISA to test potency of PR-15 DoE samples after thermal stressing in comparison to the initial PR-15 sample and the former Revacept® formulation sample (PBS, pH 7.4).

5.1.3.8 Determination of bioactivity by inhibition of aggregation of human platelets

Next to collagen ELISA, bioactivity of PR-15 was assessed through evaluating the inhibition of aggregation of human platelets, induced by cross-linked collagen peptide (CRP) as well. Unfortunately, nearly all phosphate buffered samples failed to inhibit aggregation except samples 3-9, 10-17 and 1-25. These results are inconsistent to the results obtained with collagen ELISA, indicating different binding affinities of PR-15 to collagen and to CRP [184]. There were nine phosphate buffered samples which showed good bioactivity regarding EC_{50} values, however, they were not able to inhibit platelet aggregation (**Table 16**). In contrast, all histidine buffered samples, the initial as well as the former Revacept® formulation sample inhibited platelet aggregation.

	Inh. of agg.	*EC_{50} [µg/mL]*
Initial	ja	16.1
PBS pH 7.4	ja	4.5
25-1 Histidine pH 7.5	ja	3.9
5-2 Phosphate pH 8.0	nein	7.1
6-3 Phosphate pH 8.0	nein	6.5
22-4 Histidine pH 7.5	ja	3.2
7-5 Phosphate pH 8.0	nein	6.8
2-6 Phosphate pH 7.0	nein	*11.4*
21-7 Histidine pH 7.5	ja	5.0
20-8 Histidine pH 8.0	ja	3.0
3-9 Phosphate pH 7.0	ja	23.5
17-10 Histidine pH 7.0	ja	5.7
23-11 Histidine pH 7.5	ja	6.0
15-12 Histidine pH 7.0	nein	28.6
13-13 Histidine pH 7.0	ja	8.1
8-14 Phosphate pH 8.0	nein	15.9
24-15 Histidine pH 7.5	ja	6.6
19-16 Histidine pH 7.0	ja	7.3
10-17 Phosphate pH 7.333	ja	19.5
11-18 Phosphate pH 7.333	nein	22.7
16-19 Histidine pH 8.0	ja	6.0
9-20 Phosphate pH 7.667	nein	19.2
12-21 Phosphate pH 7.667	nein	15.2
18-22 Histidine pH 8.0	ja	4.0
4-23 Phosphate pH 7.0	nein	24.3
14-24 Histidine pH 8.0	ja	6.3
1-25 Phosphate pH 7.0	ja	21.7

Table 16: Bioactivity of PR-15 DoE samples, the initial PR-15 sample and the former Revacept® formulation sample (PBS, pH 7.4) determined by the inhibition of platelet aggregation of human platelets and collagen ELISA (EC_{50} values).

5.1.3.9 Design of Experiments (DoE) analysis with MODDE

The analysis of the DoE comprised three steps, the evaluation of the obtained raw data, the regression analysis as well as the model interpretation and was done with the software MODDE 9.0 (Umetrics, Umeå, Sweden) as used before for the creation of the experimental worksheet [148]. For raw data evaluation the replicate plot (**Figure 41**) as well as the normal probability plot of residuals (**Figure 42**) are useful tools to detect outliers. Systematic errors arise by plotting the residuals versus run order (**Figure 43**), but during this DoE no systematic errors occurred. In the replicate plot, each measured value of the response is plotted against the number of the experiment depicted as single bars (**Figure 41**). The last bar of each plot consists of five arrows representing the five so-called center points with identical factor settings. These center points provide information about the experimental error. In the residual N-Plot the normal probability of the distribution of the residuals is plotted against standardized residuals, the raw residuals divided by the residual standard deviations (RSD) (**Figure 42**). The results are normally distributed if the regression line goes through most of the data points and the standard deviations are smaller than ± 2. Considering the raw data gained by DLS, SEC and collagen ELISA, sample 15-12 appeared to be an outlier as

shown in the replicate plot of SEC and bioactivity (**Figure 41**) as well as in the residual N-plot of SEC showing a standard deviation > 2 (**Figure 42**). The yellow color developed after 1 week incubation at 53 °C emphasized the experimental results and led to the conclusion to exclude this outlier.

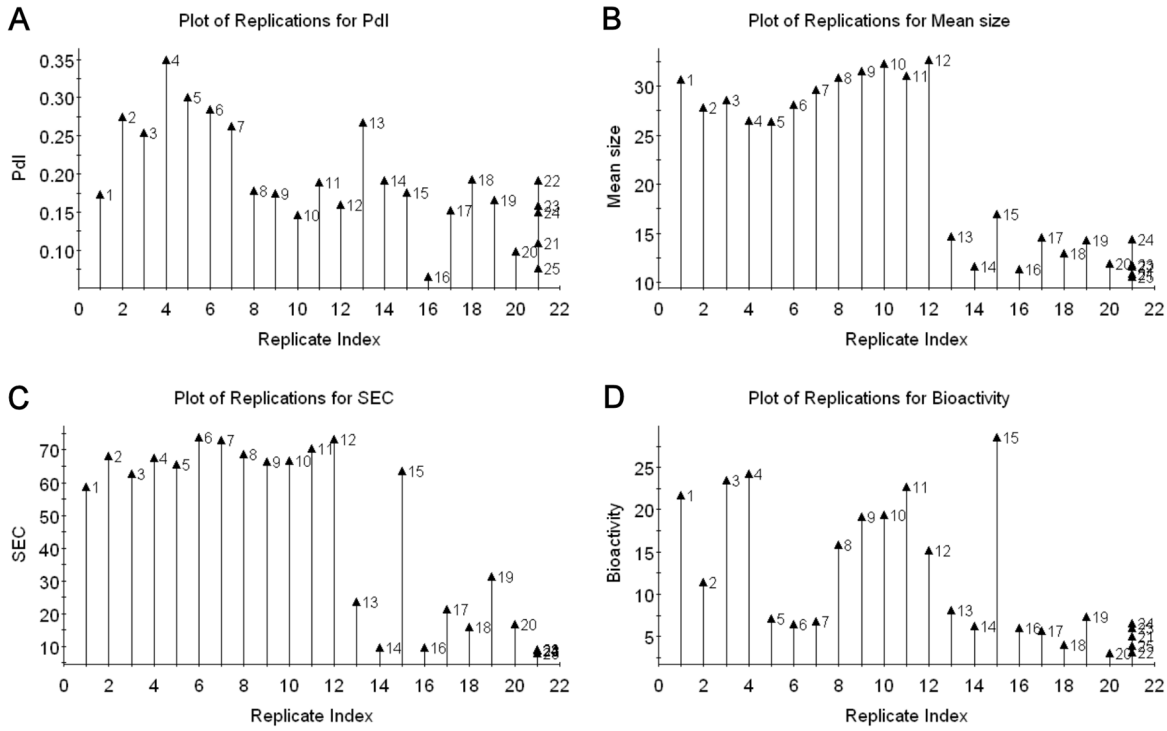

Figure 41: Replicate plots for the responses (A) PdI, (B) mean size, (C) SEC and (D) bioactivity.

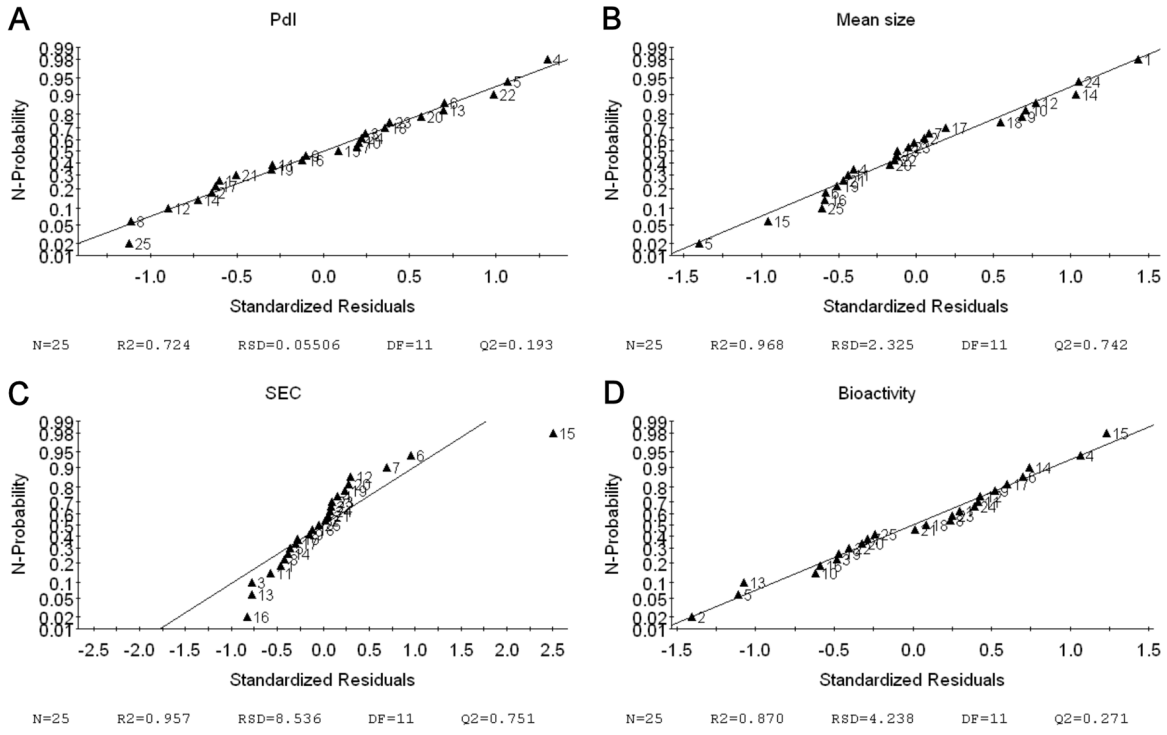

Figure 42: N-plots of residuals (standardized residuals) for the responses (A) PdI, (B) mean size, (C) SEC and (D) bioactivity.

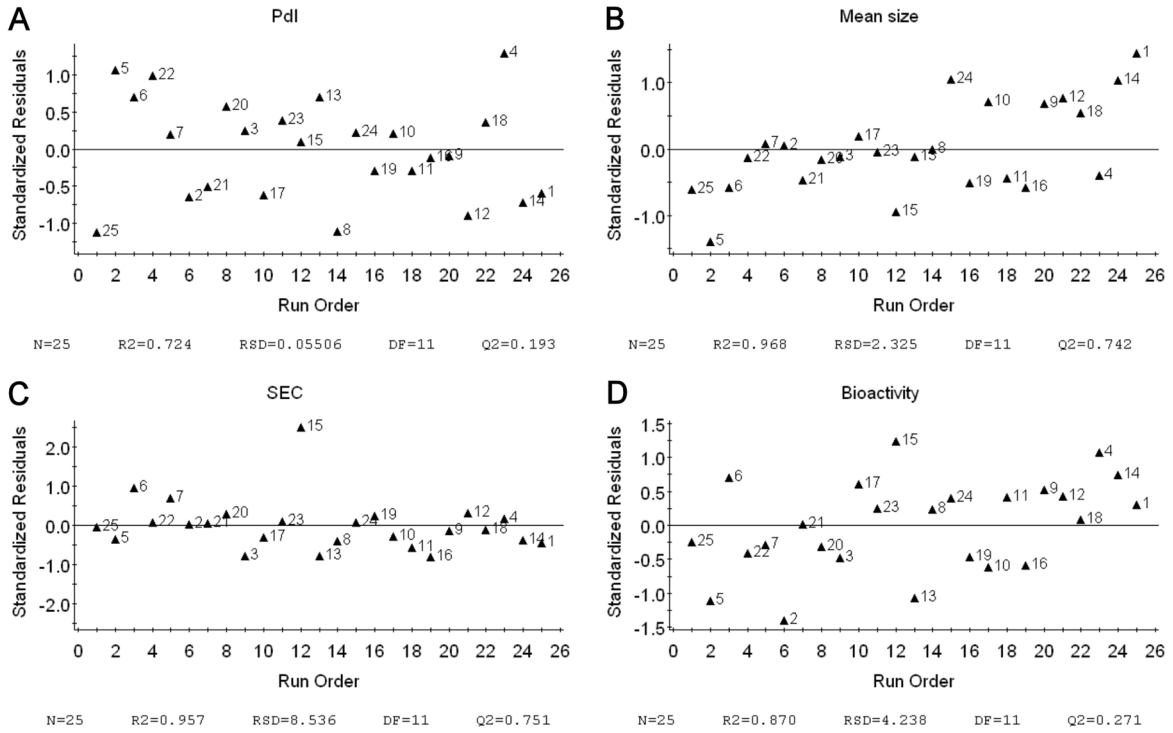

Figure 43: Residuals versus run order plots for the responses (A) PdI, (B) mean size, (C) SEC and (D) bioactivity.

In order to link the factors (i) buffer, (ii) pH, (iii) Tween® 20 and (iv) methionine with the responses (i) PdI, (ii) mean size, (iii) SEC and (iv) bioactivity, regression analysis was done. The two most important parameters of regression analysis are R^2 and Q^2. R^2 can reach values between 0 and 1 and describes the goodness of fit and Q^2 is the goodness of prediction and should be > 0.5. Preferably, both values should reach 1 and the difference should be < 0.2–0.3. The model validity is another parameter deciding if the right type of model was chosen. Values > 0.25 reflect a valid model with no lack of fit. The last parameter of the regression analysis is the reproducibility summarizing the variabilities plotted in the replicate plot. Values > 0.5 guarantee small pure errors [148].

In order to improve model validity and the efficiency of data analysis, the data of all responses should be normally distributed. The histogram of response (**Figure 44**) as well as the descriptive statistics plot also called Box-Whisker plot (**Figure 45**), are useful tools to investigate normal distribution of the data. The histograms of the responses and the Box-Whisker plots showed that the responses mean size, SEC and bioactivity were not normally distributed (**Figures 44A** and **45A**). Positively skewed responses were identified by a tail to the right in the histogram and non-symmetrical whiskers with a longer upper horizontal line in the Box-Whisker plot and had to be logarithmically transformed to become more normally distributed. In contrast, negatively skewed responses tailed to the left in the histogram and had a longer lower horizontal line in the Box-Whisker plot. In order to reach nearly normally distributed data, a negative logarithmic transformation had to be performed (**Figures 44B** and **45B**) [148].

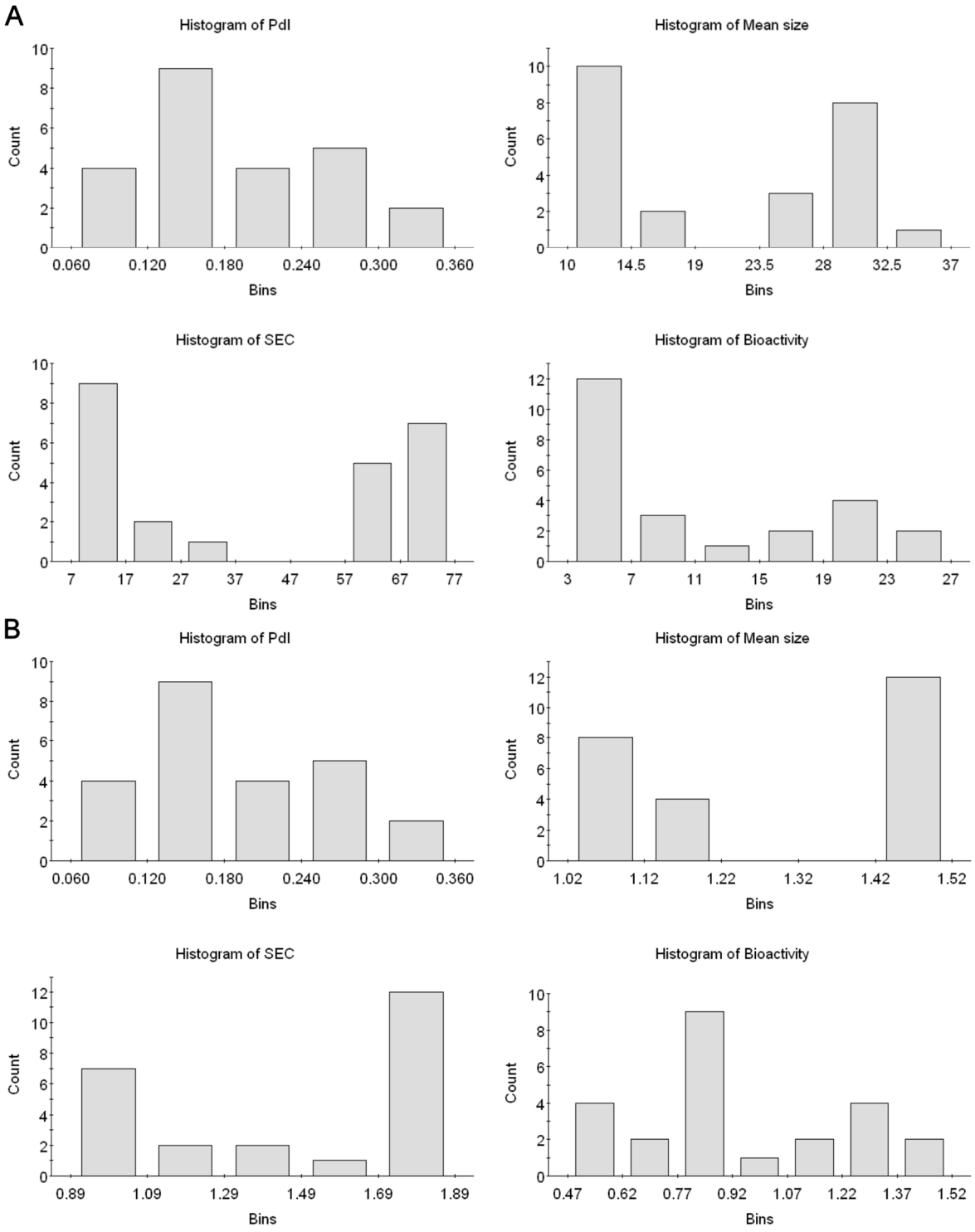

Figure 44: Histograms of responses (A) before and (B) after transformation.

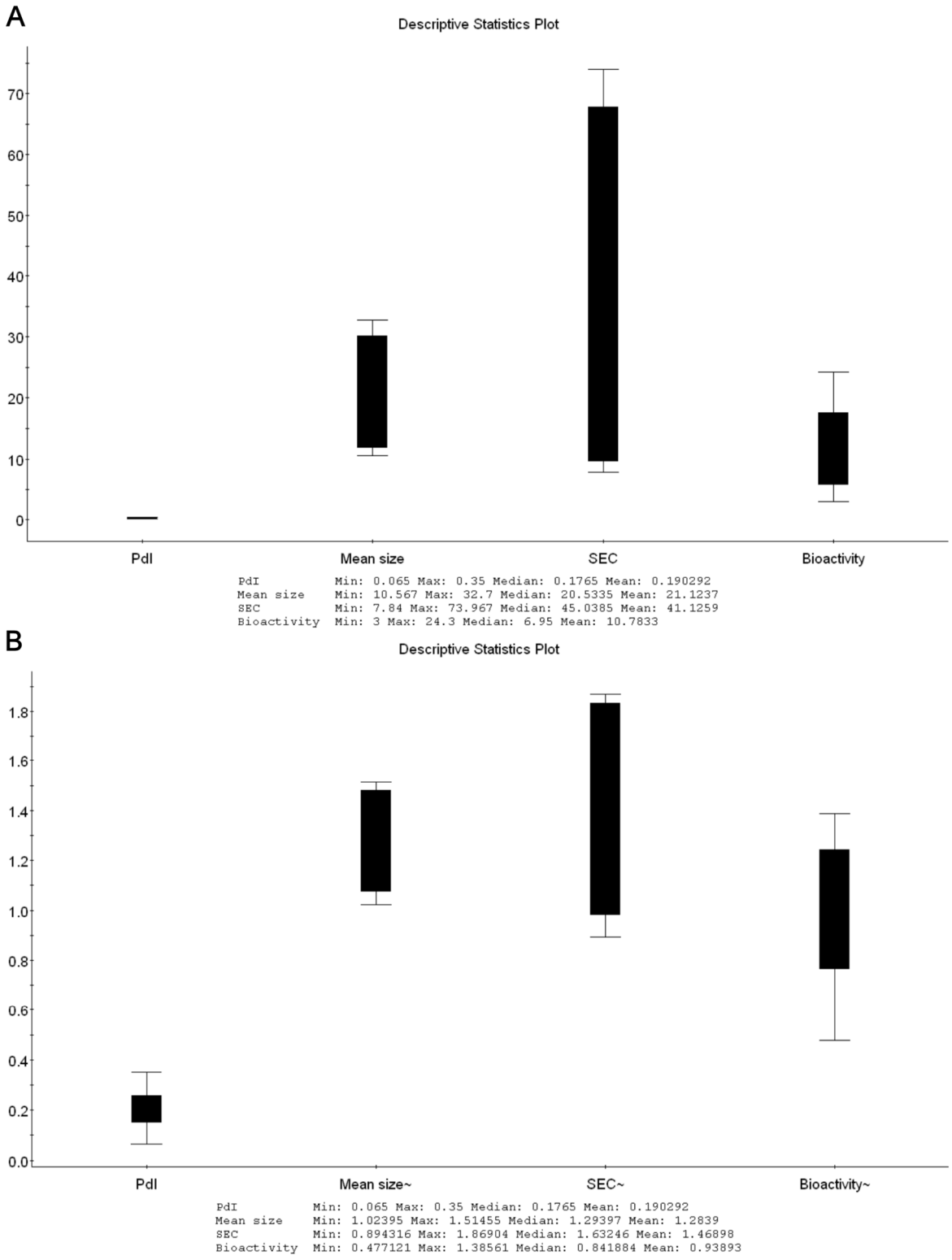

Figure 45: Descriptive statistics plots (A) before and (B) after transformation.

In the regression coefficient plot the mean values and their 95 % confidence intervals (uncertainty, noise) of the factors (linear terms, real effects) and factor interactions (interaction term, interactions among the factors) are depicted and present the significance of the model terms graphically (**Figure 46A**).

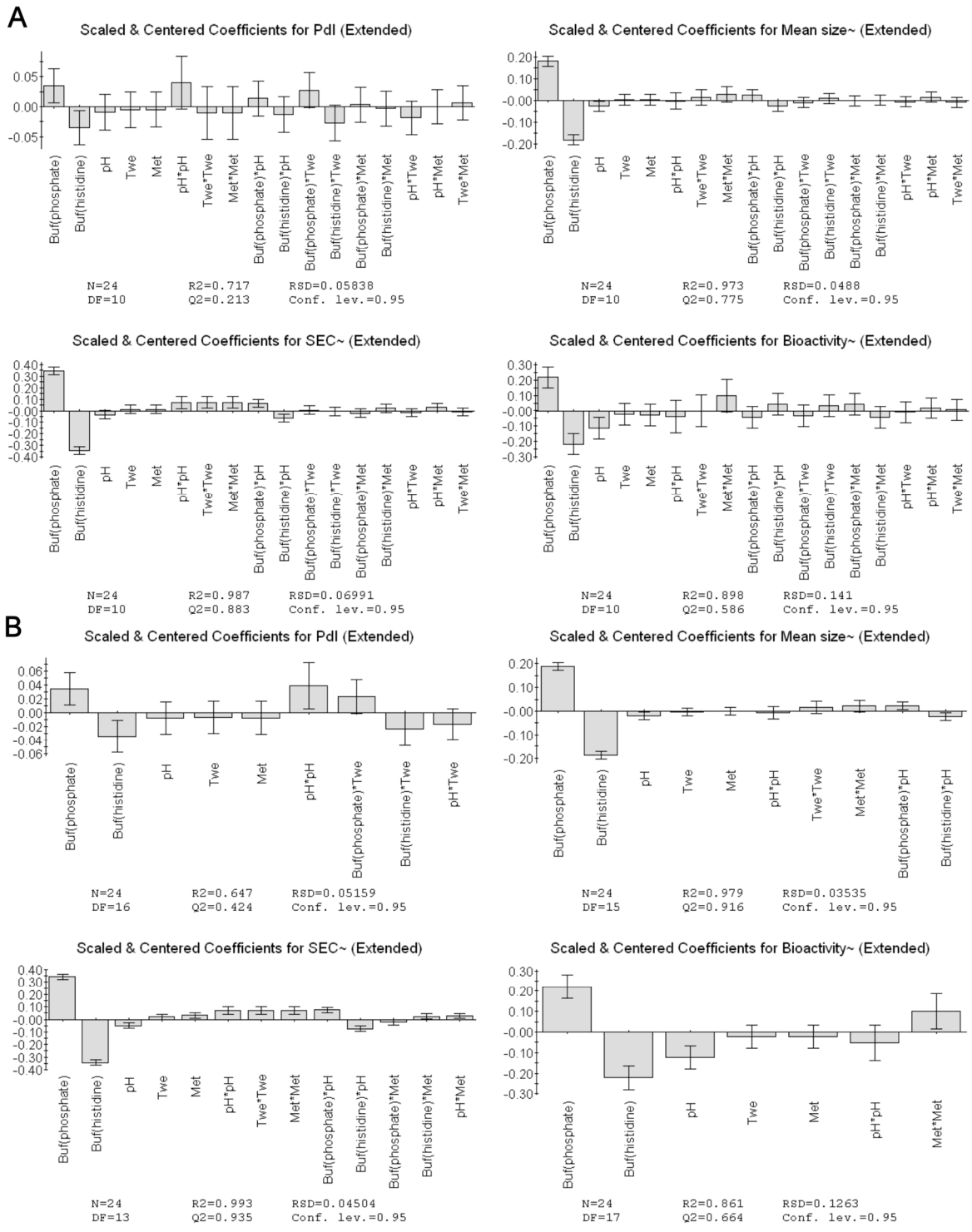

Figure 46: Coefficient plots (A) before and (B) after deletion of non-significant factors and factor interactions.

It is used as a tool for tuning the model in order to reach a simpler model with better predictive ability. Therefore, non-significant model terms that included the value of zero were deleted and the model was refitted until the model was not improved anymore (**Figure 46B**) [148]. After deletion of the outlier, the transformation of the not normally distributed responses and the removal of non-significant factors and factor interactions nearly all the requirements for a good model were met

after regression analysis (**Table 17**). Solely, Q^2 of PdI not slightly reached a value > 0.5 (0.424) but a value > 0.1 indicates a significant model [148]. Looking at the results of the analysis of variance (ANOVA) and its lack of fit test, which compares the model error with the replicate error, the results were satisfied. All p values of the regression model were < 0.05 and the p values of the lack of fit test were > 0.05 as postulated. The variations among the replicates (pure error: 0.0002 (PdI), 0.0528 (mean size), 0.0247 (SEC) and 0.1303 (bioactivity)) were smaller than the variations in the experimental design (model error: 0.0006 (PdI), 0.1923 (mean size), 0.3973 (SEC) and 0.3035 (bioactivity)) for all responses indicating a good model [148].

	R^2	Q^2	$R^2–Q^2$	*Model validity*	*Reproducibility*	*p Regression*	*p Lack of fit*
PdI	0.647	0.424	0.223	0.769	0.612	0.008	0.398
Mean size	0.979	0.916	0.063	0.993	0.927	0.000	0.971
SEC	0.993	0.935	0.058	0.382	0.996	0.000	0.085
Bioactivity	0.861	0.664	0.197	0.871	0.800	0.000	0.597

Table 17: Values of the summary of fit and ANOVA.

Considering the observed versus predicted plot, where the observed values are plotted against the fitted response values, we come to the conclusion that after detecting and eliminating inhomogeneities in the raw data with the tools described above, the response-factor relationship was finally linear for all responses making the interpretation of the model as well as the prediction much easier (**Figure 47**).

Data evaluation and regression analysis led to the conclusion that the model was correct and valid and was used for model interpretation. First, the coefficient plot was examined carefully because herein it is depicted how the factors affect all responses (**Figure 46B**). The value of the coefficient displays the real effect of a factor on the response while all other factors stay at their average. During this study just the factors phosphate buffer and histidine buffer were significant for all responses and the factor pH was significant for all responses except PdI. The factor methionine was just significant for the response SEC. In addition, the factor interactions phosphate buffer/pH as well as histidine buffer/pH were significant for the responses mean size and SEC, and furthermore, the factor interactions histidine buffer/methionine as well as pH/methionine were significant for the response SEC (**Figure 46B**). The main effect plots of the responses confirmed the data of the coefficient plots concerning the factor buffer (**Figure 48**). According to theses main effect plots phosphate buffer was significant different from histidine buffer for all responses expect the response PdI leading to a more stable formulation for histidine buffer (**Figure 48**). The factor pH was just significant for the response SEC whereby pH 7.0 was significant different from higher pH values (**Figure 49**). All other factors had no significant influence on the stability of the PR-15 formulation (**Figures 50** and **51**).

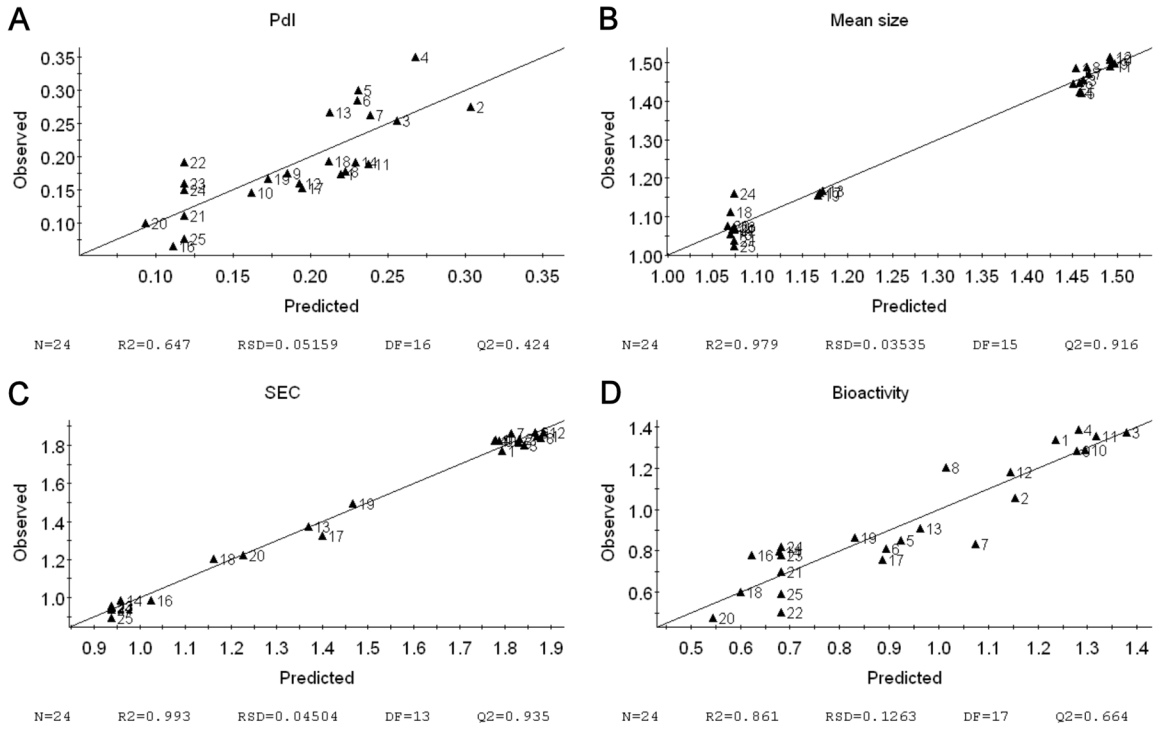

Figure 47: Observed versus predicted plots for the responses (A) PdI, (B) mean size, (C) SEC and (D) bioactivity.

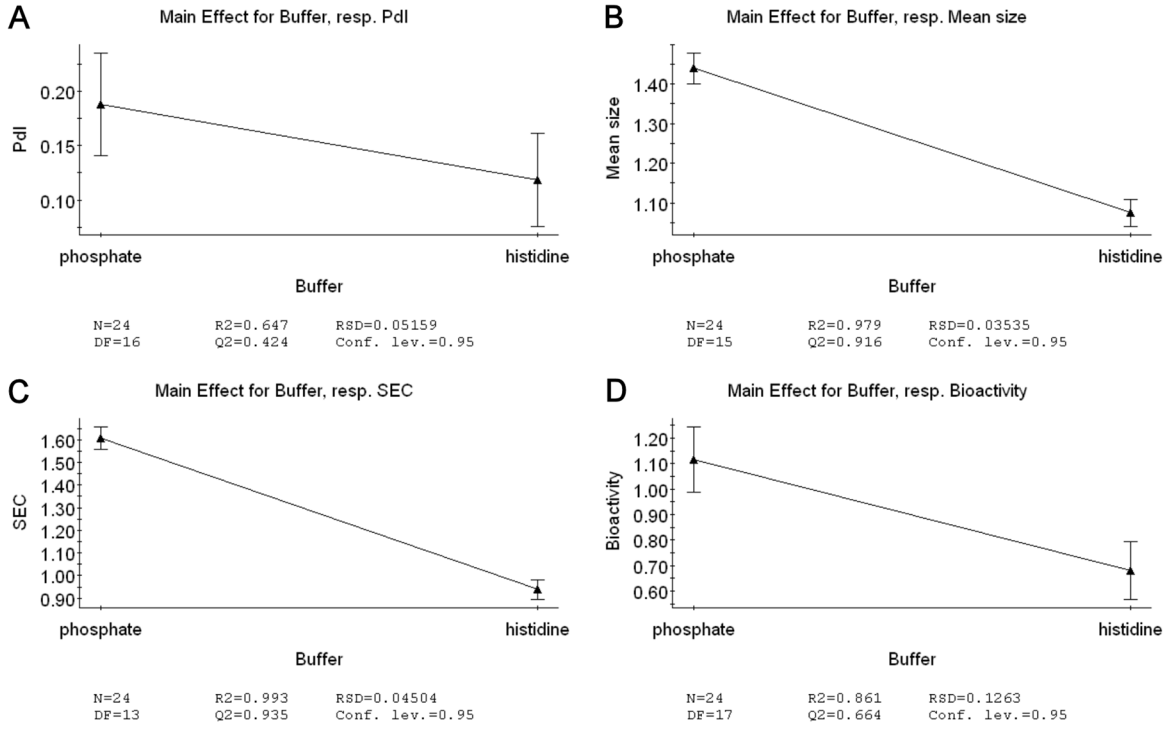

Figure 48: Main effect plots of the responses (A) PdI, (B) mean size, (C) SEC and (D) bioactivity for the factor buffer.

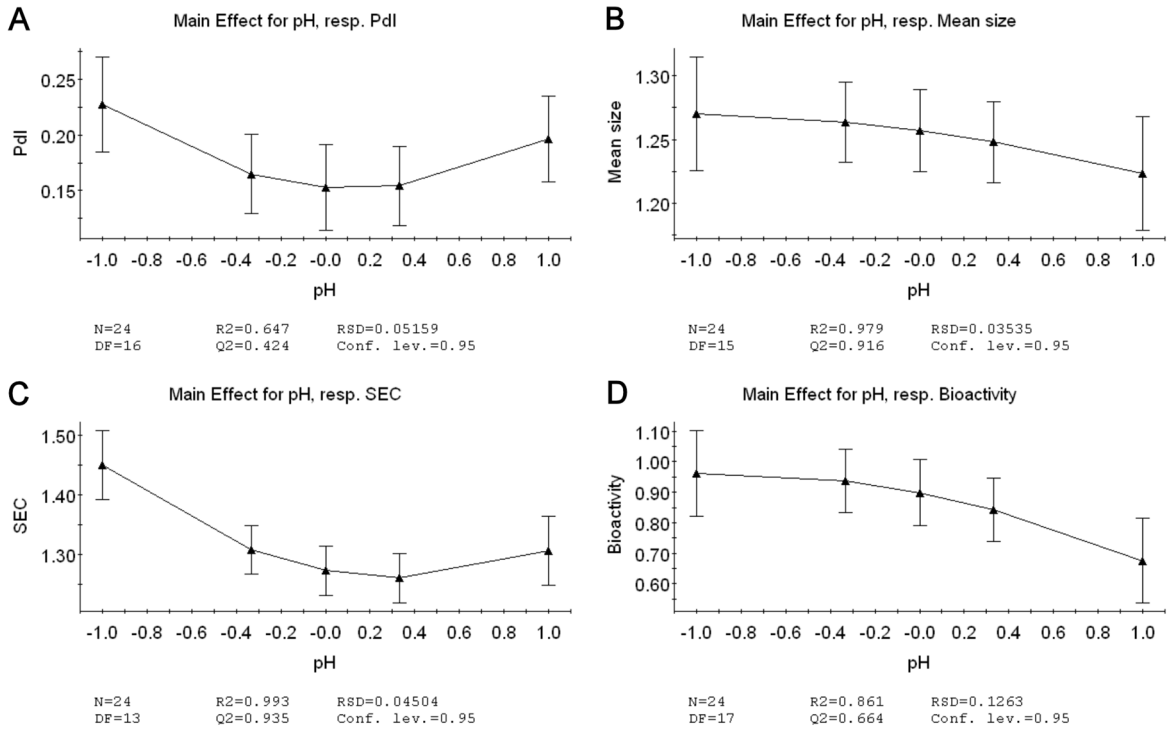

Figure 49: Main effect plots of the responses (A) PdI, (B) mean size, (C) SEC and (D) bioactivity for the factor pH.

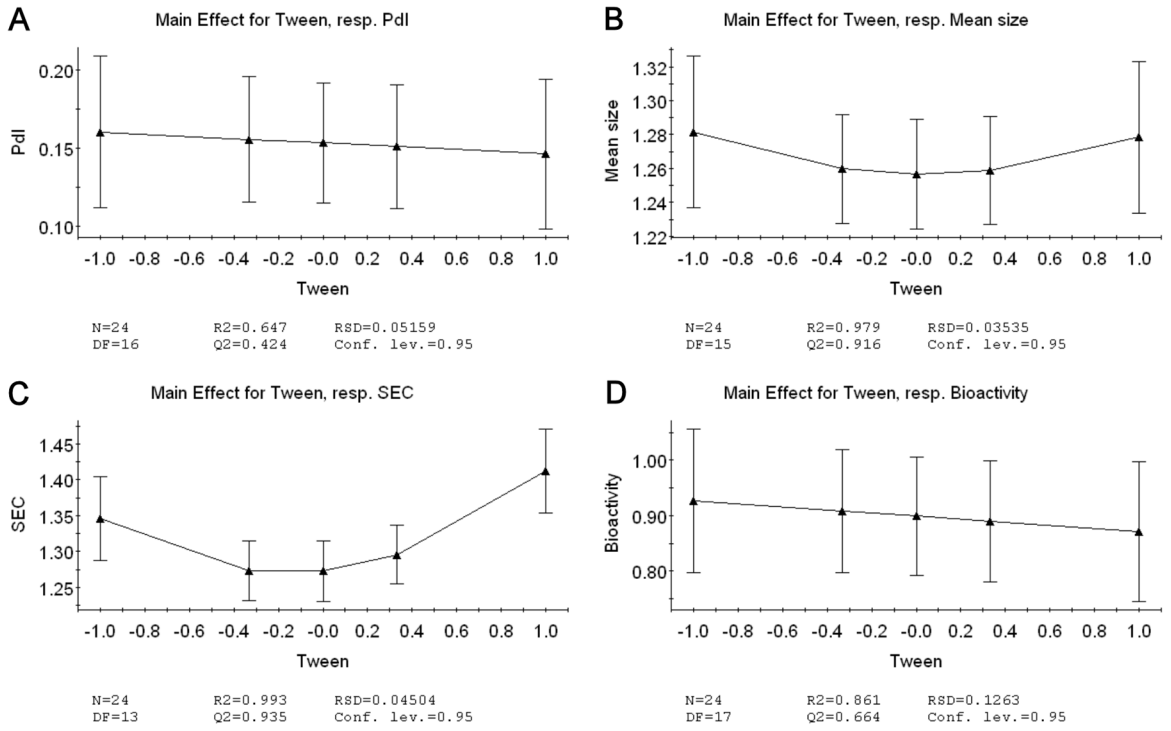

Figure 50: Main effect plots of the responses (A) PdI, (B) mean size, (C) SEC and (D) bioactivity for the factor Tween® 20.

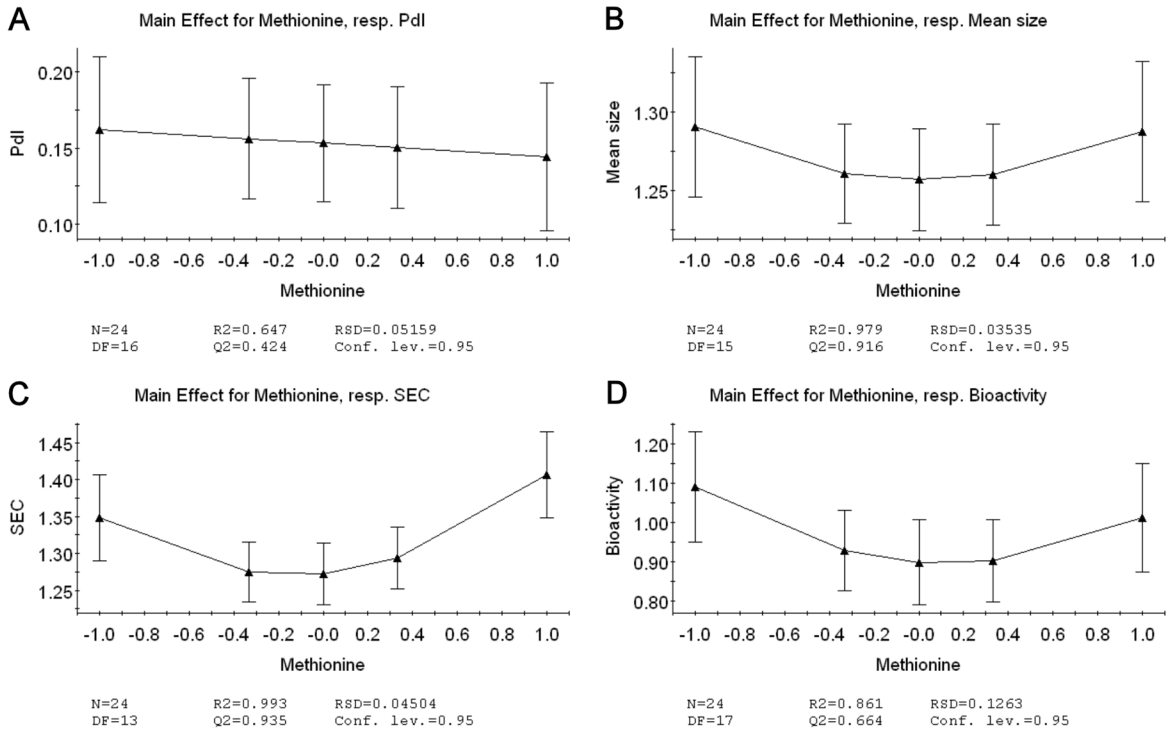

Figure 51: Main effect plots of the responses (A) PdI, (B) mean size, (C) SEC and (D) bioactivity for the factor methionine.

After model interpretation the model was used to make predictions and to find the optimal factor combination for a stable PR-15 formulation. The response prediction plot shows the predictions of the responses for one factor at all levels listed in the worksheet for the appropriate factor and its 95 % confidence intervals while the other factors are kept at their center level. According to the prediction plot of the first factor buffer, histidine buffer obviously has to be chosen over phosphate buffer as all responses were predicted to be smaller and therefore lead to a more stable protein formulation (**Figure 52**). For all other factors the predictions were not that definite. For the responses PdI and SEC, pH values around the center are preferred but for the responses mean size and bioactivity high pH values at the high level are privileged (**Figure 53**). The addition of Tween® 20 at its center level leads to the best results for the responses mean size and SEC by avoiding the formation of aggregates but bioactivity is not influenced by the addition of Tween® 20 (**Figure 54**). Methionine at its center level gives the best results for mean size, SEC and bioactivity but PdI is not influenced through methionine concentration (**Figure 55**).

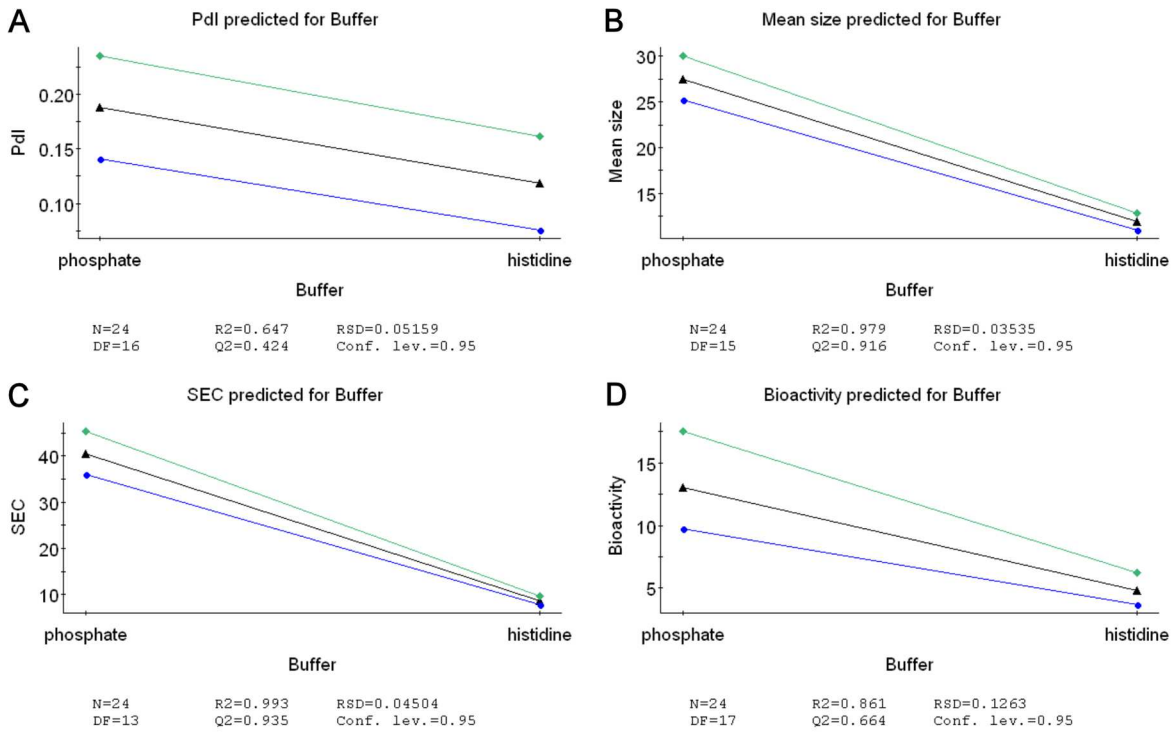

Figure 52: Response prediction plots of the responses (A) PdI, (B) mean size, (C) SEC and (D) bioactivity for the factor buffer.

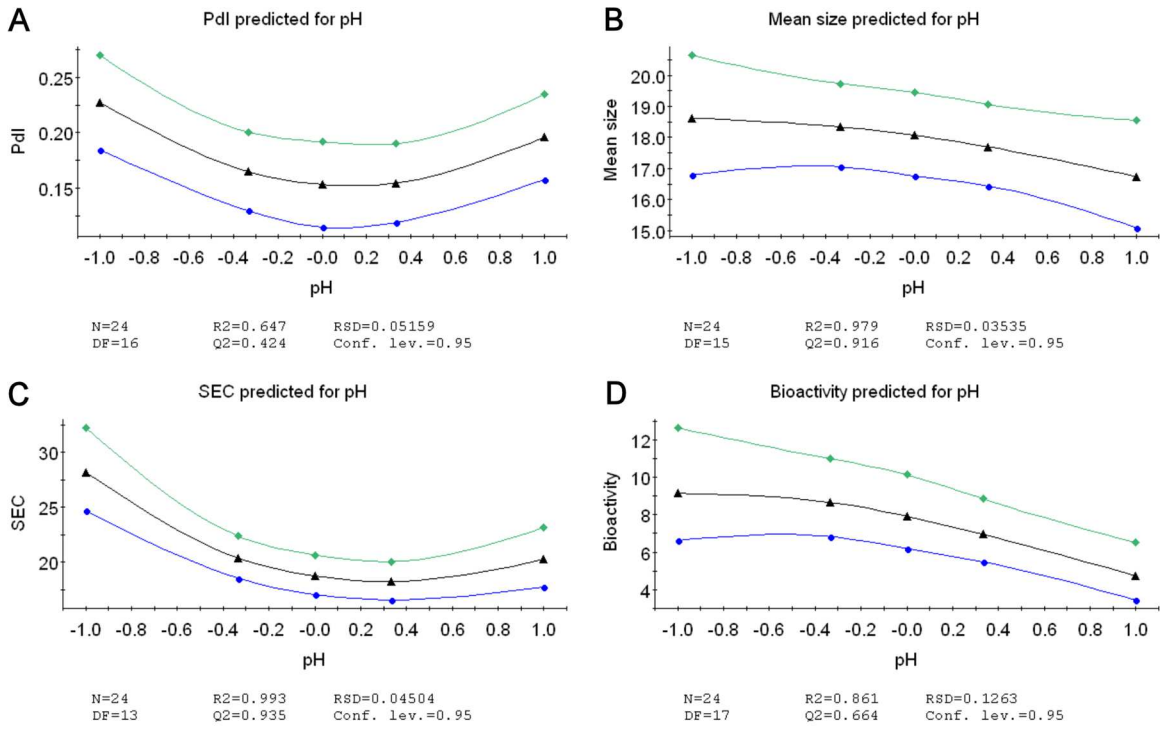

Figure 53: Response prediction plots of the responses (A) PdI, (B) mean size, (C) SEC and (D) bioactivity for the factor pH.

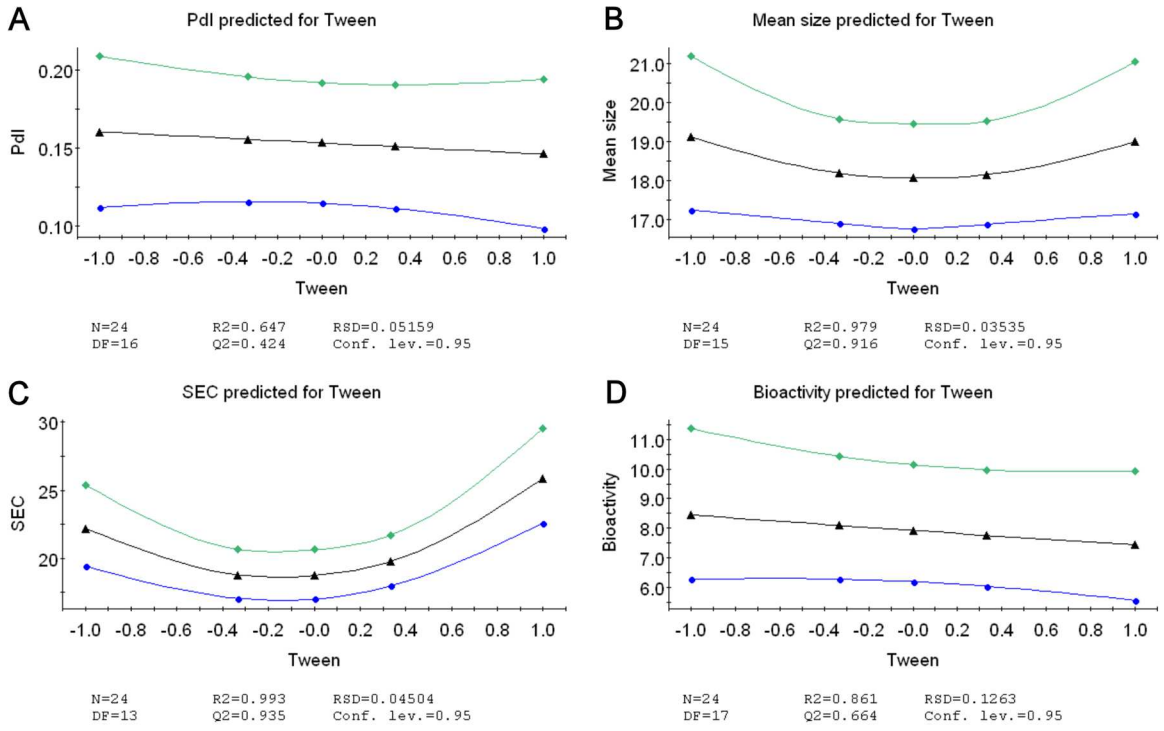

Figure 54: Response prediction plots of the responses (A) PdI, (B) mean size, (C) SEC and (D) bioactivity for the factor Tween® 20.

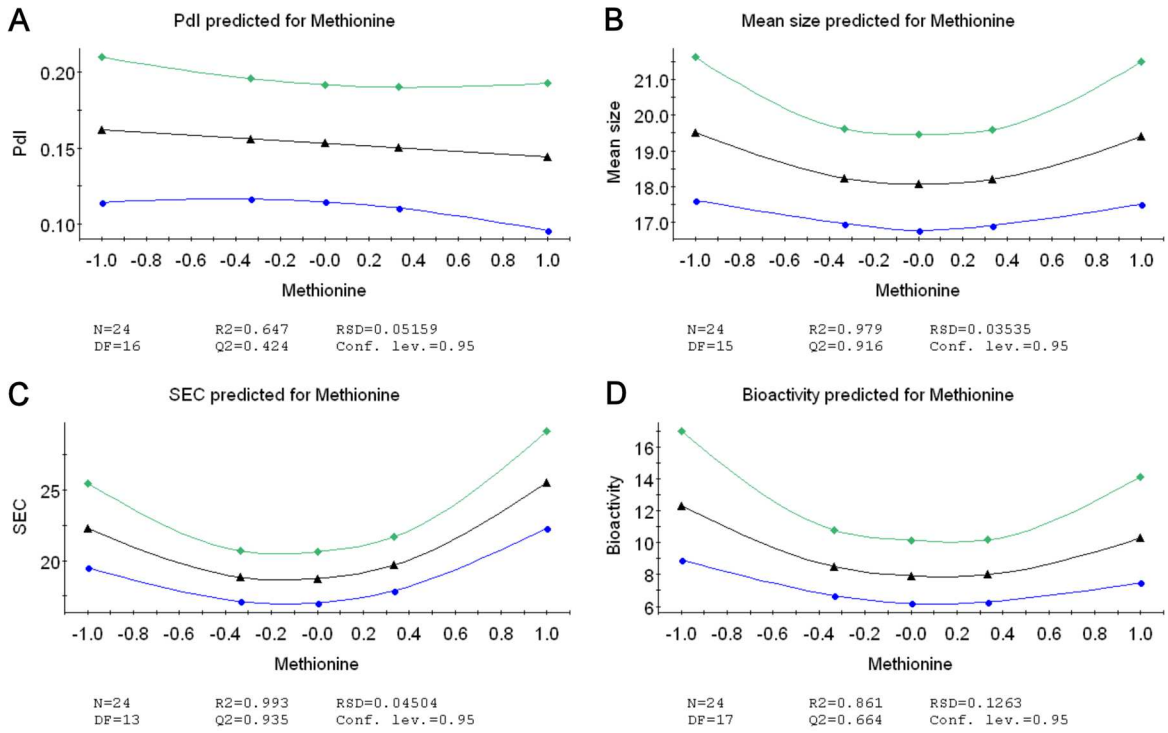

Figure 55: Response prediction plots of the responses (A) PdI, (B) mean size, (C) SEC and (D) bioactivity for the factor methionine.

Within the optimizer software of MODDE the maximal accepted values for all responses were defined (PdI: max. 0.10407, mean size: max. 12.657 nm, SEC: max. 12.0761 %, bioactivity: max. 4.52696 µg/mL). Additionally, the qualitative factor buffer was set to histidine buffer on the basis of the results shown in the main effect plots (**Figure 48**). After running the optimizer, PR-15 was found to be optimal in histidine buffer, pH 7.813, with 0.0904 % Tween® 20 and 8.121 mM methionine. Contour plots as well as sweet spot plots were created in order to evaluate the result obtained from the optimizer. The shaded parts in the contour plots lie outside the defined factor settings and the point where the arrows coincide the optimal factor setting is located (**Figures 56–58**) [148].

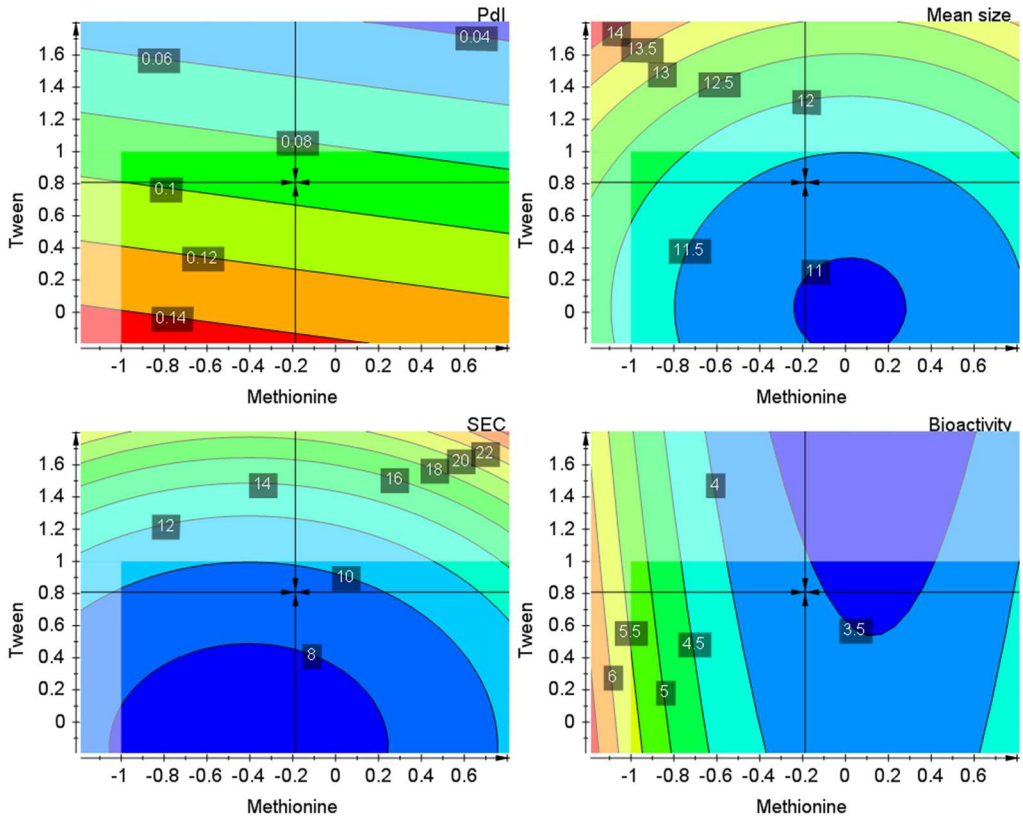

Figure 56: Contour plots with maximized responses (PdI: max. 0.10407, mean size: max. 12.657 nm, SEC: max. 12.0761 %, bioactivity: max. 4.52696 µg/mL) in histidine buffer for optimal pH value (0.6259 ≙ pH 7.8130).

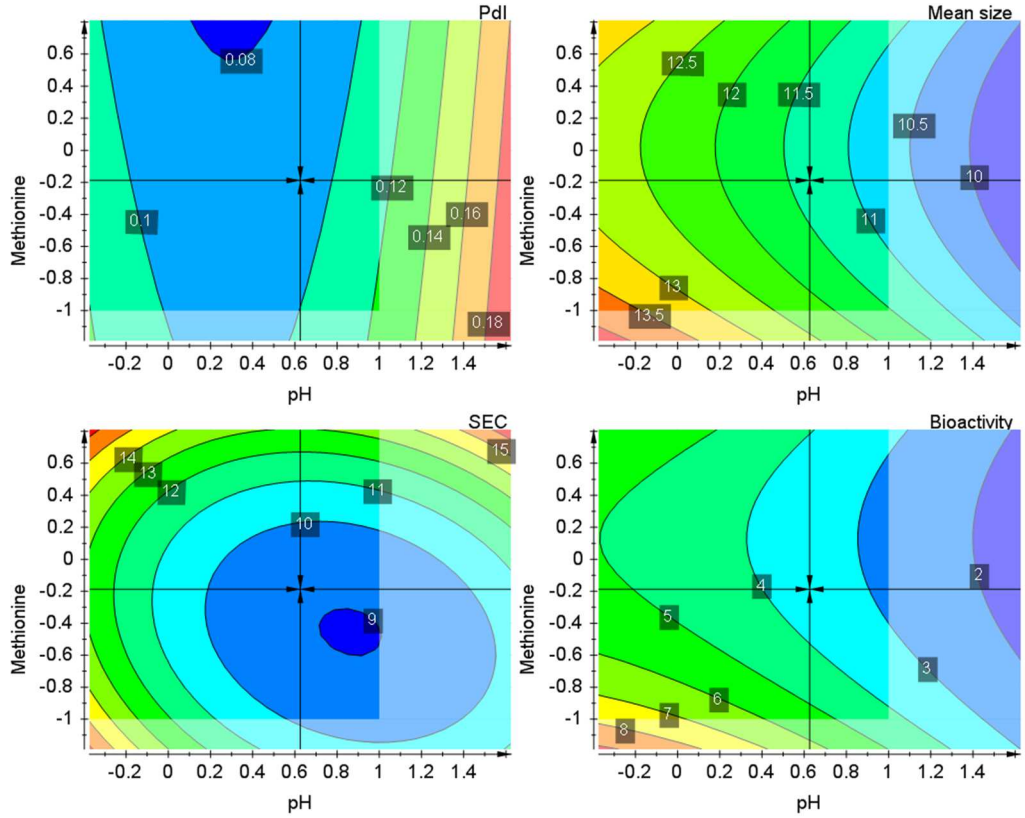

Figure 57: Contour plots with maximized responses (PdI: max. 0.10407, mean size: max. 12.657 nm, SEC: max. 12.0761 %, bioactivity: max. 4.52696 µg/mL) in histidine buffer for optimal Tween® 20 concentration (0.808 ≙ 0.0904 %).

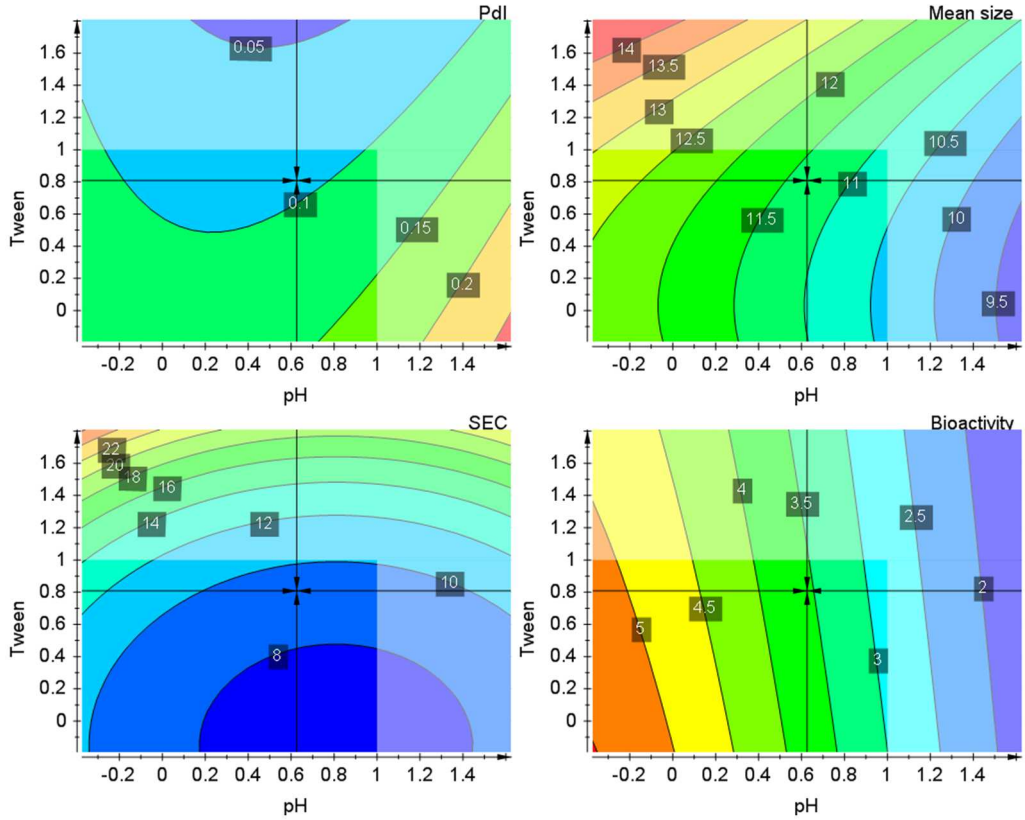

Figure 58: Contour plots with maximized responses (PdI: max. 0.10407, mean size: max. 12.657 nm, SEC: max. 12.0761 %, bioactivity: max. 4.52696 µg/mL) in histidine buffer for optimal methionine concentration (-0.1879 ≙ 8.121 mM).

In the sweet spot plots the areas where all responses lie in the defined ranges (PdI: max. 0.10407, mean size: max. 12.657 nm, SEC: max. 12.0761 %, bioactivity: max. 4.52696 µg/mL) are highlighted in green. Considering these plots, methionine concentration can be varied from about 3 mM to 15 mM with Tween® 20 concentration from about 0.09 % to 0.1 % if pH is about 7.8 and pH can be varied from about 7.55 to 7.9 with Tween® 20 concentration from about 0.09 % to 0.1 % if methionine concentration is about 8 mM without exceeding specified maxima of the responses (**Figures 59–61**). Here, too, the point where the arrows coincide the optimal factor setting is located in each plot [148].

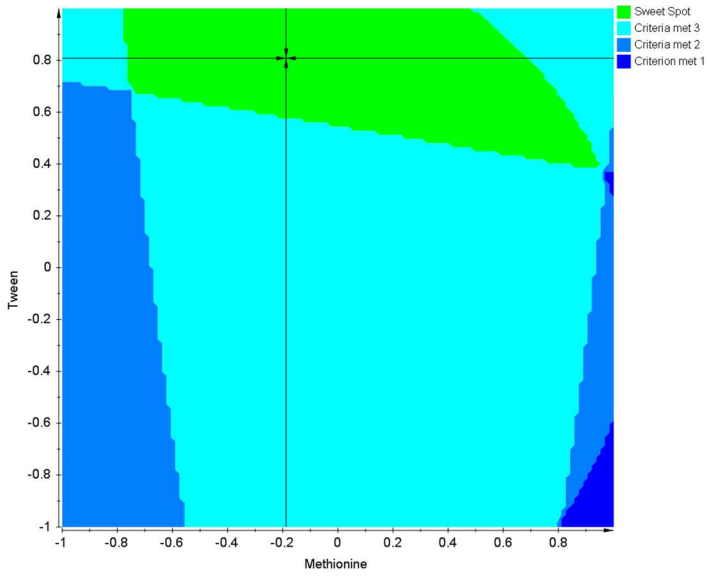

Figure 59: Sweet spot plot with maximized responses (PdI: max. 0.10407, mean size: max. 12.657 nm, SEC: max. 12.0761 %, bioactivity: max. 4.52696 µg/mL) in histidine buffer for optimal pH value (0.6259 ≙ pH 7.8130).

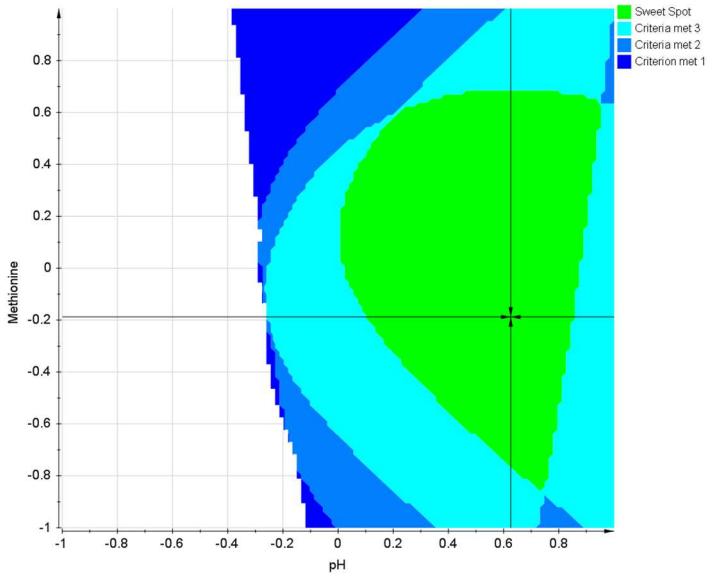

Figure 60: Sweet spot plot with maximized responses (PdI: max. 0.10407, mean size: max. 12.657 nm, SEC: max. 12.0761 %, bioactivity: max. 4.52696 µg/mL) in histidine buffer for optimal Tween® 20 concentration (0.808 ≙ 0.0904 %).

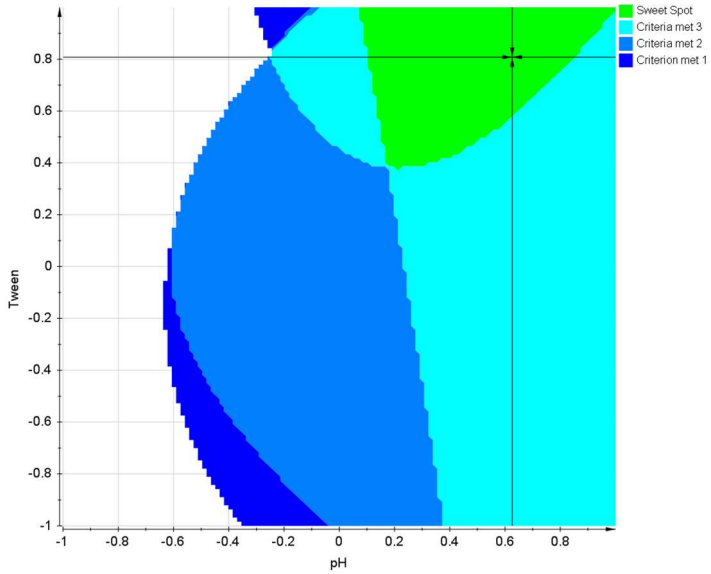

Figure 61: Sweet spot plot with maximized responses (PdI: max. 0.10407, mean size: max. 12.657 nm, SEC: max. 12.0761 %, bioactivity: max. 4.52696 µg/mL) in histidine buffer for optimal methionine concentration (-0.1879 ≙ 8.121 mM).

The prediction plots were created by varying one factor from low, center to high level while all other factors were kept at their optimum found by the optimizer software. The predicted responses displayed with their 95 % confidence intervals showed that the variation of the three factors pH, Tween® 20 and methionine concentration did not really change the responses PdI, mean size, SEC as well as bioactivity and therefore did not play a pivotal role if histidine buffer was chosen (**Figure 62**). So the conclusion is drawn that in fact the most and only statistically significant factor for a stable PR-15 formulation with satisfying bioactivity is the choice of histidine buffer instead of phosphate buffer. Nevertheless, the most stable PR-15 formulation can be prepared in histidine buffer, pH 7.8130, with 0.0904 % Tween® 20 and 8.121 mM methionine. But according to the results shown in the sweet spot plots formulations with pH values between 7.55 and 7.9, Tween® 20 concentration between 0.09 % and 0.1 % and methionine concentration between 8 mM and 14 mM can be prepared without exceeding all set criteria.

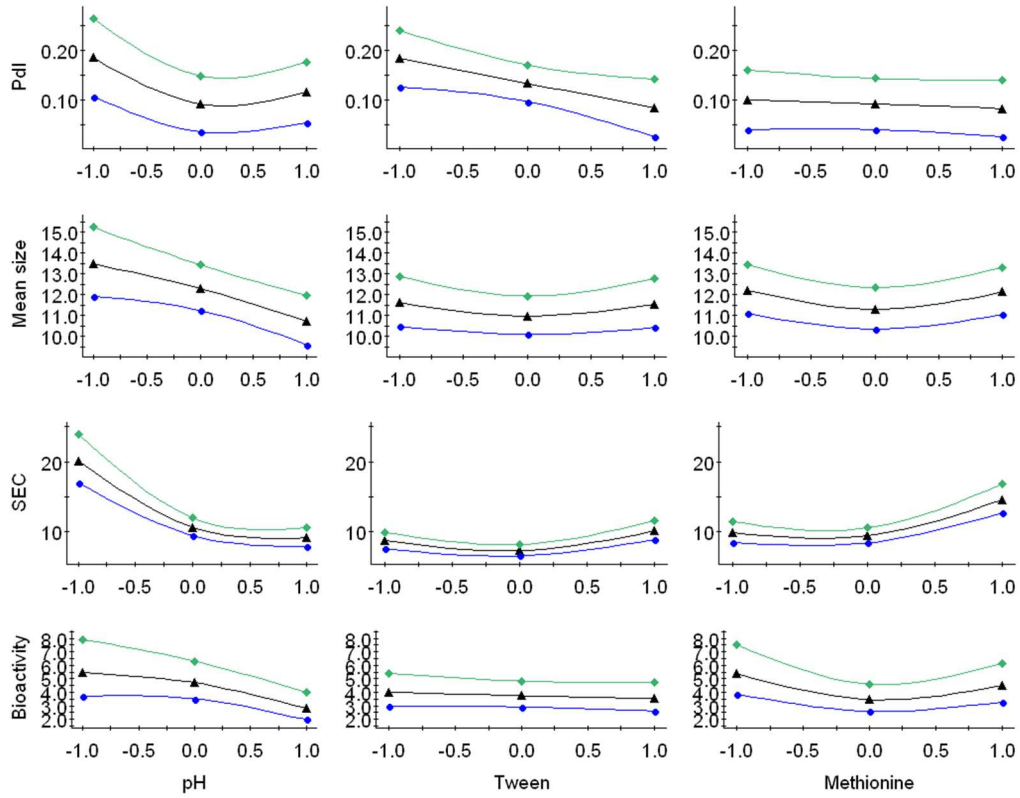

Figure 62: Prediction plots with one factor varying from low, center to high level and the other factors adjusted to their optimum (buffer: histidine, pH: 0.6259, Tween® 20: 0.808, methionine: -0.1879).

5.2 Protein modification

5.2.1 Site-directed PEGylation of FGF-2 for biomedical application

5.2.1.1 Characterization of PEG-FGF-2

FGF-2 was used as model protein in order to investigate the suitability of click and EDC/NHS chemistry for biologics. The successful incorporation of the required functional groups – alkyne or carboxyl functional group – for the performance of such reactions in FGF-2 through PEGylation was visualized after purification via heparin affinity chromatography (**Supplementary Figure 5**) by reducing SDS-PAGE (**Figure 63**). After PEGylation with iodoacetamido-PEG-alkyne two bands were observed, one intensive band at approximately 31 kDa, and another less intensive band at approximately 25 kDa (**Figure 63**, lane #2) and after PEGylation of FGF-2 with iodoacetyl-PEG-acid two bands were visualized as well, one intensive band at approximately 25 kDa and another less intensive band at approximately 31 kDa (**Figure 63**, lane #3). Unfortunately, both PEGylation reactions were incomplete, as indicated by small bands at approximately 17 kDa running at the same position as unmodified FGF-2 (**Figure 63**, lane #4). Furthermore, PEGylated FGF-2 samples were analyzed by MALDI-TOF MS (**Supplementary Figure 6**). The PEGylation of FGF-2 with iodoacetamido-PEG-alkyne resulted in two main broad peaks of 20,999.64 Da and 24,073.64 Da apart from unmodified FGF-2 (calc. mass 17,667.03 Da) indicating that either one or two cysteine residues were modified (**Supplementary Figure 6A**). For the COOH-PEG-FGF-2 one intensive peak of 21,368.37 Da and one less intensive peak of 24,810.73 Da (**Supplementary Figure 6B**) were detected besides unmodified FGF-2, indicating that either one or two FGF-2 cysteine residues were PEGylated.

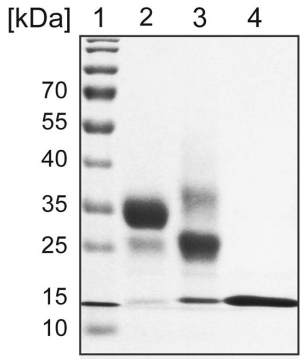

Figure 63: The PEGylation of FGF-2 with iodoacetamido-PEG-alkyne or iodoacetyl-PEG-acid was analyzed by SDS-PAGE analysis. Lane #1 was loaded with a molecular weight ladder, lane #2 is alkyne-PEG-FGF-2, lane #3 is COOH-PEG-FGF2, lane #4 is unmodified FGF-2 for reference. Reprinted from [87], Copyright (2014), with permission from Elsevier.

NIH3T3 cell proliferation assay was performed in order to determine bioactivity of alkyne-PEG-FGF-2, COOH-PEG-FGF-2 (**Figure 64A**) as well as the SF-FGF-2 constructs obtained by click (**Figure 64B**) or EDC/NHS chemistry (**Figure 64C**). All samples showed an increase of proliferation with increasing concentration – even the samples without coupling reagents – so it cannot be excluded that the remaining FGF-2 was responsible for the climb of proliferation. But even through extensive dialyzing the unbound FGF-2 could not be removed because at physiological pH, FGF-2 bears a net positive charge and as opposed to this SF bears a net negative charge rendering them to form a complex.

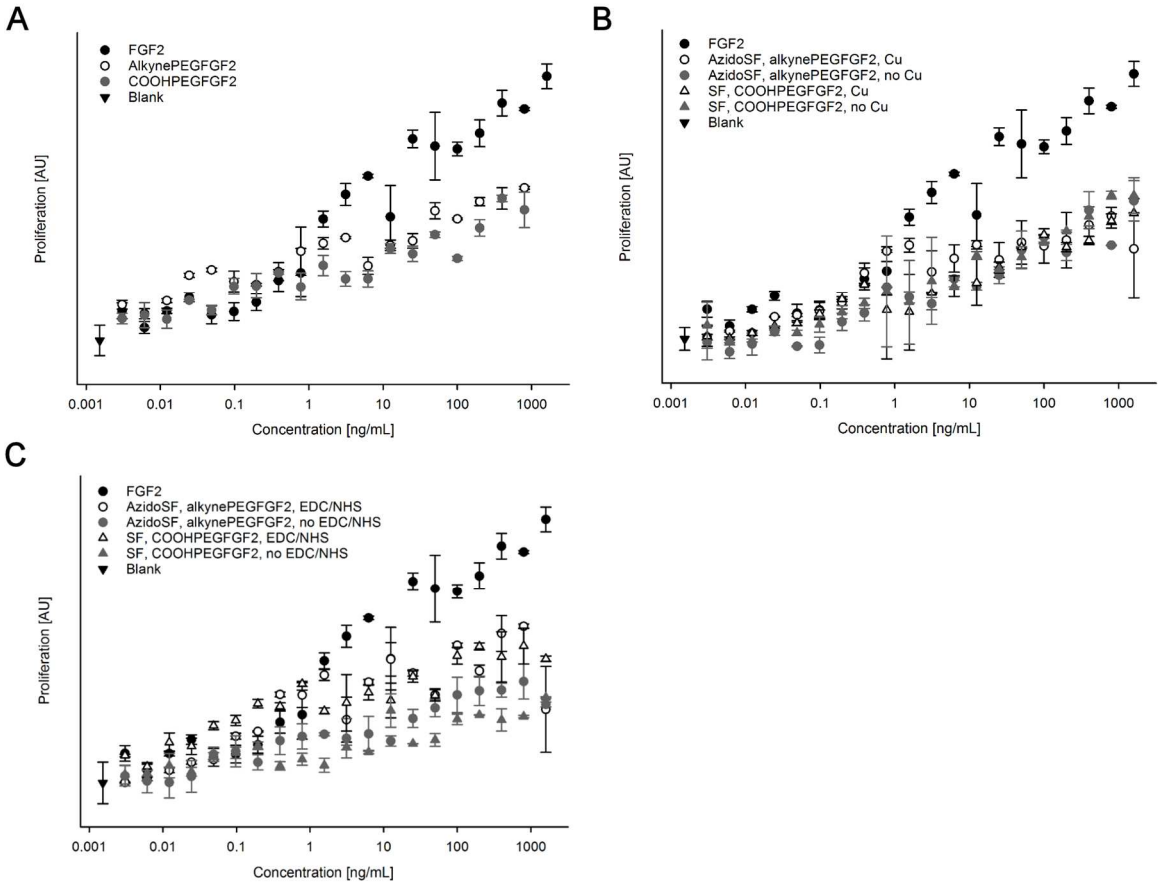

Figure 64: WST-1 proliferation assay of 3 kDa PEGylated FGF-2 and SF-PEG-FGF-2 conjugates.

In order to achieve homogeneity and no heterogeneity of PEGylated FGF, the PEGylation reaction was performed at three different temperatures (4 °C, 15 °C and 25 °C) for 1 h, 2 h, 3 h and 4 h. The residual reaction conditions were not changed. Unfortunately, under all conditions heterogeneous PEGylated FGF-2 was obtained but to various extent (**Figure 65**). The smallest amount of twofold PEGylated FGF-2 was built at 4 °C for alkyne-PEG-FGF-2 as well as COOH-PEG-FGF-2 compared to higher temperatures. Moreover, FGF-2 is a thermosensitive protein and the performance of the PEGylation reaction at 4 °C, consequently, will maintain its bioactivity. Hence, subsequent PEGylation reactions were performed at 4 °C.

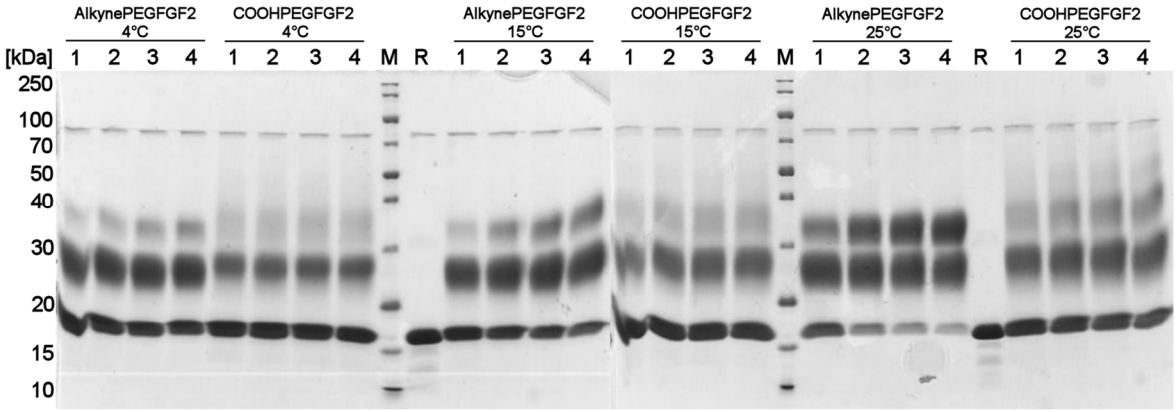

Figure 65: SDS-PAGE analysis of optimization of PEGylation reaction with 3 kDa PEG.

Additionally, we were interested in the coupling efficiency of PEGylation reaction, and thus we wanted to quantify the PEGylated FGF-2. Therefore, the PEGylated FGF-2 was purified using a heparin column on an Aekta purifier system. However, the 3 kDa PEG-FGF-2 did not differ enough from native FGF-2 and though heparin binding affinity of FGF-2 did not change substantially through PEGylation (**Supplementary Figure 5**). Hence, we chose 10 kDa PEGs for FGF-2 PEGylation and performed PEGylation under the same conditions as before (4 °C, 4 h). The 10 kDa PEG chain reduced the heparin binding affinity of FGF-2, and thus PEG-FGF-2 was eluted at a lower salt concentration than native FGF-2 from the heparin column leading to the desired separation (S**upplementary Figure 7**). Indeed, the single peaks were not completely separated and as a consequence three fractions were collected: the 1st peak (alkyne-PEG-FGF-2: fractions 1–10; amino-PEG-FGF-2: fractions 1–9), the fractions between the 1st and the 2nd peak (alkyne-PEG-FGF-2: fractions 11–13; amino-PEG-FGF-2: fractions 10–12) and the 2nd peak (alkyne-PEG-FGF-2: fractions 14–21; amino-PEG-FGF-2: fractions 13–25). The collected fractions of the PEGylation samples were characterized by reducing SDS-PAGE analysis (**Figure 66**). The PEGylation with 10 kDa iodoacetamido-PEG-alkyne resulted in two bands, one intensive band at approximately 35 kDa, and another less intensive band at approximately 55 kDa (**Figure 66A,** lane #2, 1st peak). The PEGylation of FGF-2 with 10 kDa iodoacetyl-PEG-amid resulted in one intensive band at approximately 40 kDa and another less intensive band at approximately 70 kDa (**Figure 66B,** lane #1, 1st peak). Both PEGylation approaches were incomplete, as indicated by the intensive bands at approximately 17 kDa running at the same position as unmodified FGF-2 (**Figure 66A,** lane #4, 2nd peak and **Figure 66B**, lane #3, 2nd peak).

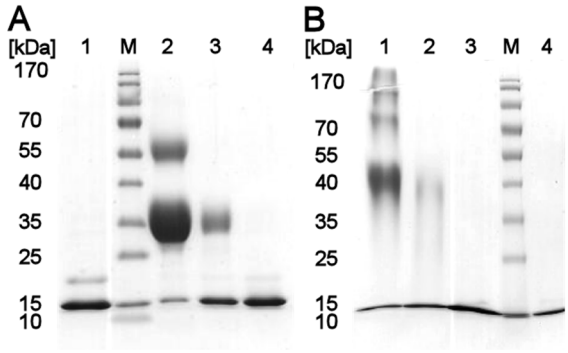

Figure 66: SDS-PAGE analysis. The PEGylation of FGF-2 with 10 kDa (A) iodoacetamido-PEG-alkyne; lane #1: FGF-2 reference, lane #2: 1st peak; lane #3: between 1st and 2nd peak; lane #4: 2nd peak. (B) iodoacetyl-PEG-amid; lane #1: 1st peak; lane #2: between 1st and 2nd peak; lane #3: 2nd peak; lane #4: FGF-2 reference.

Further analysis of FGF-2 conjugates after PEGylation with either iodoacetamido-PEG-alkyne or iodoacetamido-PEG-amid was performed by MALDI-TOF MS (**Supplementary Figure 8**). Besides, unmodified FGF-2 (17,651.0 Da; calc. mass 17,667.03 Da), two main broad peaks of 26,262.6 Da and of 35,037.9 Da were observed for alkyne-PEGylated FGF-2, indicating that either one or two cysteine residues were modified (**Supplementary Figure 8B**). All other existing peaks were supposed to be dimers of FGF-2 and alkyne-PEG-FGF-2 (44,161.5 Da), alkyne-PEG-FGF-2 and alkyne-PEG-FGF-2 (52,385.4 Da), alkyne-PEG-FGF-2 and alkyne-PEG-FGF-2-PEG-alkyne (60,797.1 Da). Another PEGylation of FGF-2 with iodoacetyl-PEG-amid resulted in one intensive peak of 28,665.2 Da (**Supplementary Figure 8C**), indicating that just one FGF-2 cysteine residue was PEGylated. All other existing peaks were supposed to be dimers of FGF-2 and amino-PEG-FGF-2 (46,467.7 Da) or amino-PEG-FGF-2 and amino-PEG-FGF-2 (56,279.6 Da).
RP-HPLC analysis was used for the separation of PEGylated FGF-2 from native FGF-2 in order to quantify the remaining non-PEGylated FGF-2 (**Figure 67**). Unfortunately, the 10 kDa PEG itself did not change hydrophobicity of the protein adequately resulting in a double peak of FGF-2 and PEGylated FGF-2. Though several things had to be changed and modified such as the RP media, the gradient, run time, flow rate as well as the column temperature. Finally, the column temperature was the crucial point that led to an improved peak shape and resolution, maybe by influencing the diffusion coefficient. The elevated temperature probably achieved that the samples were going in and out of the pores more rapidly and the difference in hydrophobicity became larger. In the end, native FGF-2 was eluted first after 11.5 minutes, followed by onefold alkyne-PEGylated FGF-2 after 14.3 minutes and the twofold alkyne-PEGylated FGF-2 eluted at a retention time of 15.8 minutes (**Figure 67A**). For the amino-PEGylated FGF-2 it was exactly the same elution order with a slight shift of the retention times backwards (**Figure 67B**, amino-PEG-FGF: 14.8 minutes). According to the created RP-HPLC calibration curve 2–8 % native FGF-2 remained in the alkyne-PEGylated FGF-2 sample compared to 3–11 % for the amino-PEGylated FGF-2 sample.

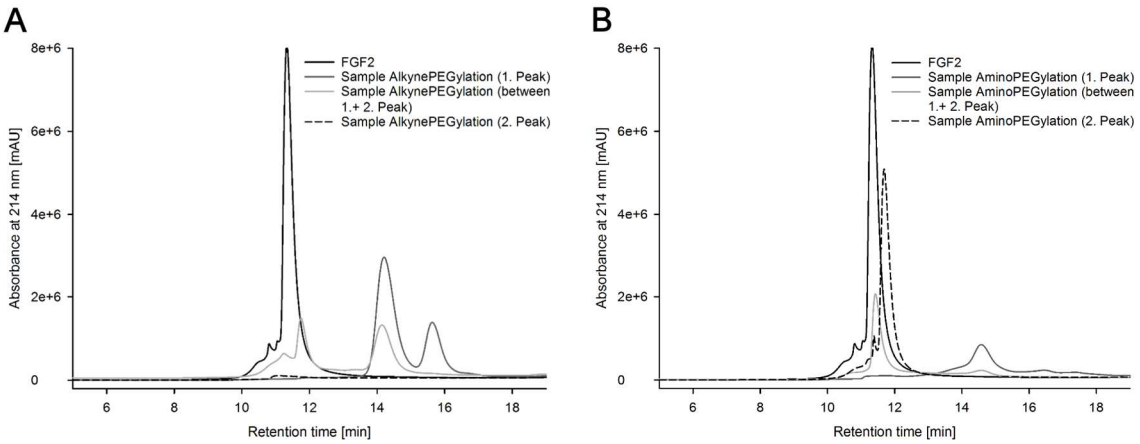

Figure 67: RP-HPLC analysis of PEGylated FGF-2. (A) Alkyne-PEGylated samples and (B) amino-PEGylated samples.

Fluorescence emission spectroscopy was performed to study structural integrity of FGF-2 after PEGylation. Thereby excitations of tryptophan and tyrosine residues were detected at 280 nm [188]. Murine FGF-2 bears one single tryptophan residue at position 114, that is inside the protein core, and seven tyrosine residues, distributed on the surface as well as inside the protein core, in the folded state [189]. Emission spectra of FGF-2 as well as PEGylated FGF-2 just showed the tyrosine peak with a maximum at ~306 nm and the tryptophan signal was quenched in the protein core indicating correct folding after PEGylation reaction (**Figure 68A**). As reference the denatured FGF-2 was shown with a shift of the maximum to ~360 nm as the tryptophan residues became fully exposed to the solvent after forced unfolding with a 6 M guanidinium hydrochloride solution at 90 °C for 10 minutes. Tryptophan absorbs at a longer wavelength and has a larger extinction coefficient than tyrosine [190], hence, the emission was dominated by tryptophan and the tyrosine residues were just shown by a shoulder at ~306 nm.

A thermal shift assay, also called differential scanning fluorimetry (DSF), was performed to detect the unfolding temperature of FGF-2 before and after PEGylation. Hereby, the fluorescence emission of SYPRO® orange dye, a fluorescent dye that binds non-specifically to hydrophobic surfaces, was investigated over a temperature range from 25–95 °C. In the aqueous environment of properly folded FGF-2 the fluorescence of SYPRO® orange dye is quenched, but during unfolding of FGF-2 the fluorescence of the dye becomes unquenched when the dye binds to the exposed hydrophobic core of FGF-2 [152]. The maximum of the first derivation of the emission intensity-temperature-curve is defined as the proteins unfolding temperature [152]. FGF-2 itself showed the lowest unfolding temperature with 54.1 ± 0.7 °C which was significantly different from the unfolding temperature of amino-PEGylated (57.6 ± 1.0 °C) and alkyne-PEGylated (56.9 ± 0.0 °C) FGF-2 (**Figure 68B**). These results indicate that PEGylation induced an increase of conformational stability of FGF-2.

Finally, the potency of PEGylated FGF-2 was demonstrated by NIH 3T3 cell proliferation assay. A reagent of the tetrazolium salt WST-1 was used for quantification of viable cells. Both PEGylated

FGF-2 variants stimulated the growth of NIH 3T3 cells but PEGylation enlarged EC_{50} values compared to native FGF-2 (for alkyne-PEGFGF-2 about 4-fold; FGF-2 EC_{50} ~50 ng/mL; alkyne-PEG-FGF-2 EC_{50} ~200 ng/mL) (**Figure 68C**). These results are consistent with other reports on the mitogenic activity of site-specific PEGylated FGF-2 [191]. Further, ERK phosphorylation in comparison to total ERK expression was examined using NIH 3T3 cells to study signaling effects of FGF-2 after PEGylation. Native FGF-2 references as well as PEGylated FGF-2 samples induced ERK phosphorylation at both tested concentrations whereas no ERK phosphorylation was observed for the non-stimulated cells (**Figure 68D**).

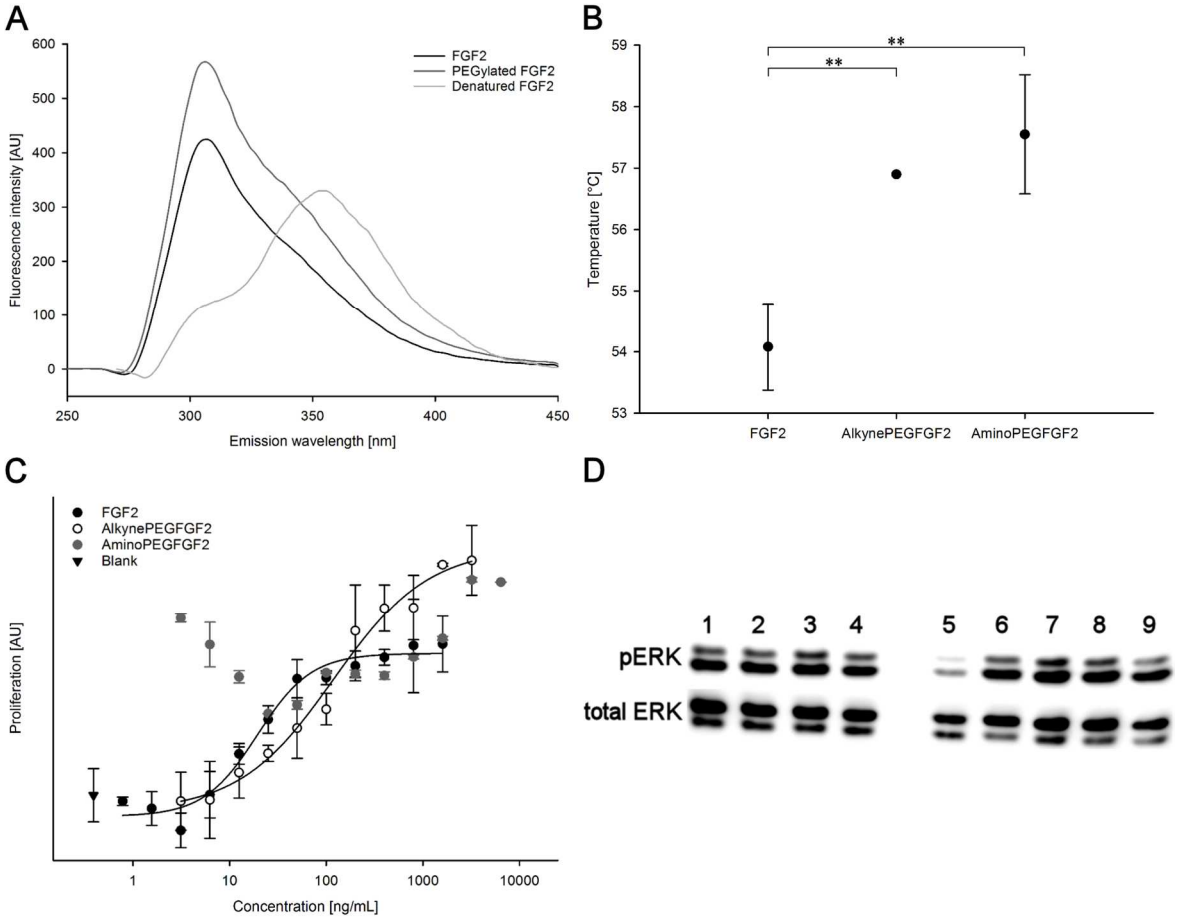

Figure 68: (A) Analysis of FGF-2 folding after PEGylation. (B) Unfolding temperatures of PEGylated FGF-2 detected by DSF. (C) WST-1 proliferation assay and (D) ERK phosphorylation of PEGylated FGF-2: FGF-2 (amino): 10 ng/mL (lane #1), 100 ng/mL (lane #2); FGF-2 (alkyne): 10 ng/mL (lane #3), 100 ng/mL (lane #4); non-stimulated cells (lane #5); alkyne-PEG-FGF-2: 100 ng/mL (lane #6), 10 ng/mL (lane #7); amino-PEG-FGF-2: 100 ng/mL (lane #8), 10 ng/mL (lane #9)) Asterisks denote statistically significant differences between the groups (** $p < 0.01$).

5.2.1.2 Characterization of SF-PEG-FGF-2

SF-PEG-FGF-2 conjugates were visualized by western blot analysis (**Figure 69**).
Alkyne-PEGylated FGF-2 (**Figure 63**, lane #2) was coupled to azido-SF in presence of copper (**Figure 69**, lane #5) whereas carboxyl-PEGylated FGF-2 (**Figure 63**, lane #3) was not conjugated (**Figure 69**, lane #3) to azido-SF. In contrast, no bioconjugation of azido-SF with alkyne-PEGylated FGF-2 was observed (**Figure 69**, lane #2, #4) in absence of copper.
The reaction between SF and PEGylated FGF-2 using EDC/NHS chemistry was successful for both, alkyne-PEG-FGF-2 (**Figure 69**, lane #6) and carboxyl-PEGylated FGF-2 (**Figure 69**, lane #8) and no bioconjugation occurred in absence of the coupling reagents EDC and NHS (**Figure 69**, lane #7, #9). However, all reactions were incomplete as substantial amounts of PEGylated and free FGF-2 remained uncoupled to SF (**Figure 69**).

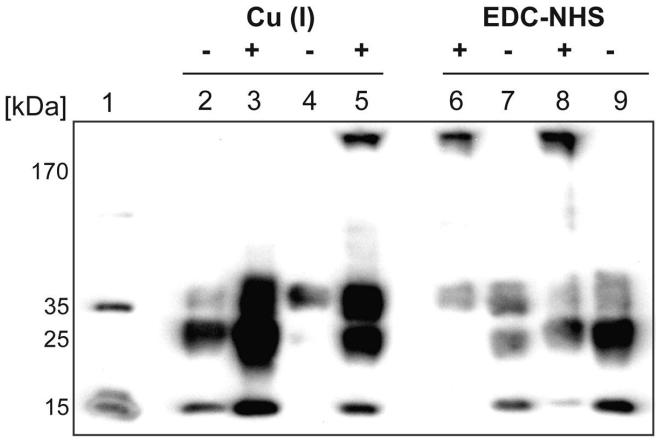

Figure 69: Western blot analysis of the conjugation efficiency of PEGylated FGF-2 to SF via either click (lanes # 2–5) or EDC/NHS chemistry (lanes # 6–9). Lane #1 was loaded with native FGF-2 for reference. Lanes #2 and #3 were loaded with a control to check for unexpected binding to SF (#2 without copper using COOH-PEG-FGF-2; #3 with copper using COOH-PEG-FGF-2). Lane #4 was loaded with another control, within which the reaction of alkyne-PEG-FGF-2 was performed in presence of SF but in absence of copper and lane #5 in presence of copper. Lanes #6 and #7 were loaded with alkyne-PEG-FGF-2 and SF in presence (#6) and in absence (#7) of EDC/NHS. Lanes #8 and #9 were loaded with the product of the synthesis of COOH-PEG-FGF-2 and SF in presence (#8) and in absence (#9) of EDC/NHS. Reprinted from [87], Copyright (2014), with permission from Elsevier.

5.2.1.3 Characterization of immobilized FGF-2 on microspheres

The results observed after coupling of PEGylated FGF-2 to SF by EDC/NHS as well as click chemistry in solution were not very satisfactory. Especially coupling efficiency of FGF-2 to SF had to be optimized and side products as well as unbound FGF-2 had to be removed after coupling. Covalent immobilization of FGF-2 on microspheres via click and EDC/NHS chemistry was supposed to solve addressed problems. Moreover, covalent immobilization of proteins on microspheres or any other biomaterial matrices bears solutions for the challenges associated with localized and sustained protein delivery [192].

First SF microspheres were decorated with FGF-2 using click chemistry. The coupling of alkyne-PEGylated FGF-2 to the azido-SF-microspheres was confirmed by flow cytometry after incubation with FGF-2 primary and FITC labelled secondary antibody. But not only azido-SF coated microspheres exposed to alkyne-PEGylated FGF-2 in presence of copper showed fluorescence, unfortunately, all controls meaning the absence of copper and/or the usage of native SF without the required azido group or the usage of native FGF-2 without the required alkyne group for click reaction showed fluorescence, respectively (**Figure 70B**). Unspecific binding of the used antibodies was excluded as negative controls without alkyne-PEG-FGF-2 or FGF-2 showed no fluorescence. Hence, non-specific adsorption of FGF-2 was the only logical implication as observed before in solution. Here, too, opposed charges of SF and FGF-2 under reaction conditions (pH 7.4) lead to electrostatic interactions. Blocking with BSA, washing with 1.5 M salt and clicking under high salt conditions to weaken electrostatic interactions were vainly and did not remove the adsorbed alkyne-PEG-FGF-2.

Consequently, sepharose microspheres were used in hopes that electrostatic interaction would be less. Actually, NHS activated sepharose beads were used and modified with 11-Azido-3,6,9-trioxaundecan-1-amine for the incorporation of azido groups. The coupling efficiency of azido groups was tested by coupling of acetylene fluor to the modified spheres via click chemistry. Fluorescence images of samples with and without copper verified the presence of azido groups on the microsphere surface (data not shown). Subsequently, click chemistry was performed and alkyne-PEGylated FGF-2 was clicked to the azide modified sepharose beads. The coupling efficiency of alkyne-PEGylated FGF-2 to the azide modified microspheres was verified with fluorescence microscopy after incubation with FGF-2 primary and FITC labelled secondary antibody. Flow cytometry could not be performed because the sepharose microspheres were too large for the FACS Calibur System. Azide modified microspheres exposed to alkyne-PEGylated FGF-2 in presence of copper showed fluorescence (**Figure 70A**) but even in the absence of copper fluorescence was observed (**Figure 70B**). Sepharose (Separation-Pharmacia-Agarose) is a crosslinked, beaded-form of agarose. NHS activated sepharose was synthesized by the addition of EDC that couples NHS to carboxyl groups through the o-acylisourea intermediate forming an NHS ester. Under physiological conditions carboxyl groups are preferentially deprotonated leading to a net negative charge of the beads and thereby to the same limitations as with SF.

To overcome this drawback NHS activated sepharose beads were modified with long PEG chains in order to shield the microspheres and thereby avoid unspecific binding of FGF-2. PEG chains with two different sizes (11-Azido-3,6,9-trioxaundecan-1-amine (PEG200), azido-PEG(5,000)-amine) were coupled to the beads in various ratios (1/1, 1/5). The coupling efficiency of azido groups was tested by coupling of acetylene fluor to the modified spheres via click chemistry. Fluorescence images of samples with and without copper verified the presence of azido groups on

the microsphere surface (data not shown). Additionally, BSA was used again as blocking reagent before performing click reaction. Unfortunately, neither the shielding with PEG chains nor the blocking with BSA prevented non-specific adsorption of FGF-2. All samples including FGF-2 showed fluorescence under the fluorescence microscope regardless of whether copper was included or not, BSA was used or not, PEG200 or PEG500 was used and regardless which PEG ratio was used (**Supplementary Figure 9**).

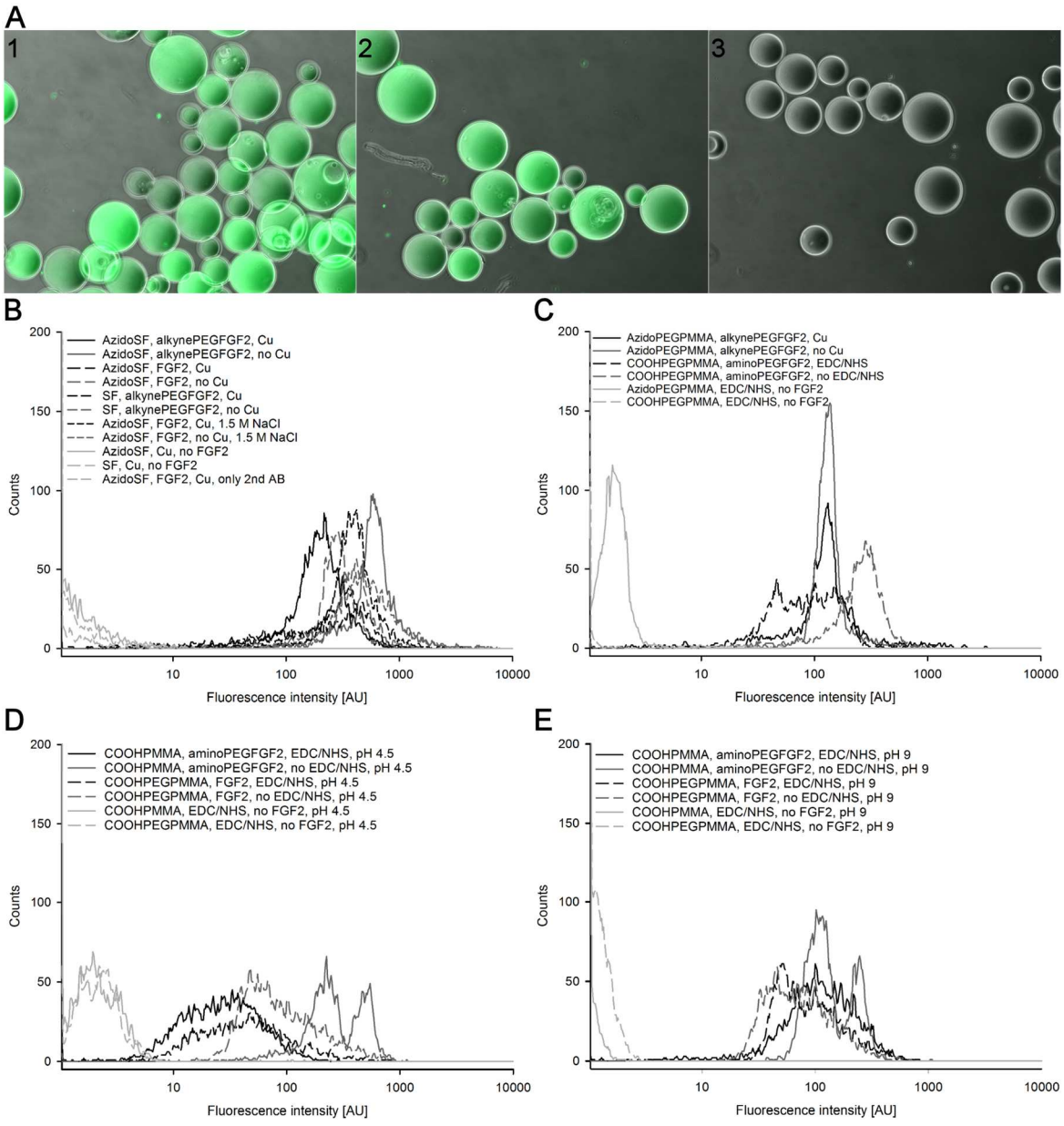

Figure 70: Fluorescence imaging and flow cytometry of immobilized FGF-2 on beads. (A) Merged images of fluorescence and bright field of azide modified sepharose beads after click reaction with alkyne-PEG-FGF-2 (1) in presence of copper, (2) in absence of copper and (3) in absence of alkyne-PEG-FGF-2 but in presence of copper. (B) Analysis of fluorescence intensities of immobilized FGF-2 on SF-beads and (C–E) immobilized FGF-2 on PMMA beads using flow cytometry.

As a last trial the coupling reaction was performed at different pH values: pH 4.5, pH 7.4 and pH 9. With the pH shift the negative bead charge or the positive charge of FGF-2 should be neutralized and thereby electrostatic interactions minimized. In addition, carboxylated PMMA beads were used and modified with 11-Azido-3,6,9-trioxaundecan-1-amine (PEG200) or carboxy-PEG_4-amine. The coupling efficiency of PEGylated FGF-2 to the azido or carboxyl modified microspheres was verified with flow cytometry after incubation with FGF-2 primary and FITC labelled secondary antibody. First, click reaction and EDC/NHS coupling were performed under physiological conditions with the same results as before. All samples with and without coupling reagents showed nearly the same fluorescence. Just the negative controls without FGF-2 but with coupling reagents showed no fluorescence (**Figure 70C**). Afterwards, EDC/NHS coupling was performed at pH 4.5 and pH 9.0 with disillusioning results: all samples including FGF-2 showed fluorescence at both pH values (**Figure 70D** and **E**). In the end, we were not able to prevent non-specific binding of FGF-2 to the different kind of beads.

Nevertheless, mitogenic activity of immobilized FGF-2 was analyzed using NIH 3T3 cells and WST-1 reagent. Anticipated was a difference concerning bioactivity of adsorbed and coupled FGF-2, but the results showed no statistically significant difference in mitogenic activity of EDC/NHS coupled and clicked FGF-2 in the absence or presence of the appropriate coupling reagents (**Figure 71A**). There was just a statistically significant difference between the bead samples containing FGF-2 and the control samples without FGF-2.

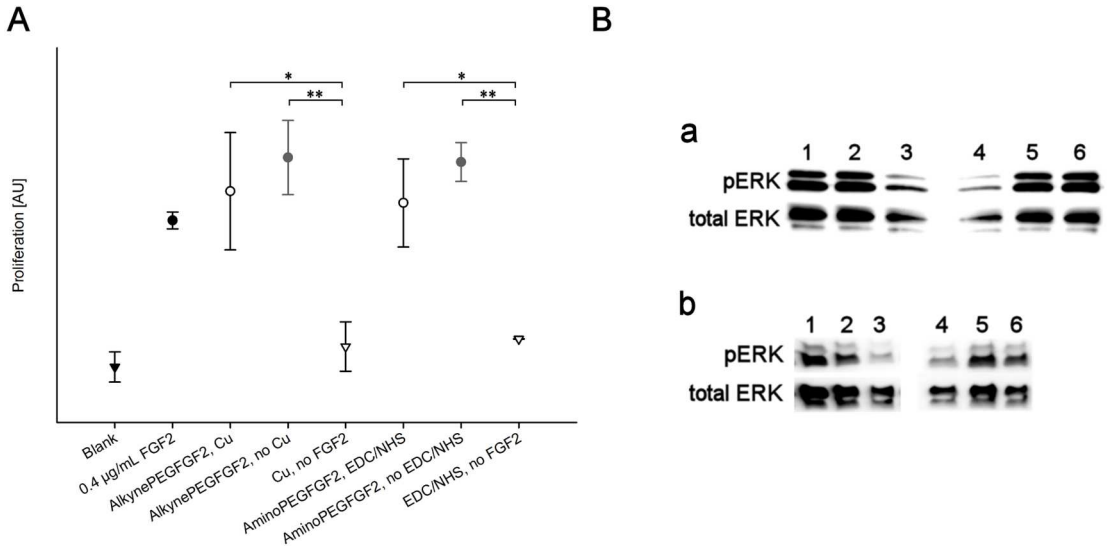

Figure 71: (A) WST-1 proliferation assay and (B) ERK phosphorylation of PEGylated FGF-2 and immobilized FGF-2 on PMMA beads: (a) alkyne-PEG-FGF-2: 30 ng/mL (lane #1); FGF-2 (alkyne): 10 ng/mL (lane #2); control I: no beads, no FGF-2 (lane #3); control II: 10 µL bead suspension, with copper but no FGF-2 (lane #4); click reaction: 10 µL bead suspension with copper and alkyne-PEG-FGF-2 (lane #5); 10 µL bead suspension with alkyne-PEG-FGF-2, no copper (lane #6); (b) amino-PEG-FGF-2: 30 ng/mL (lane #5); FGF-2 (amino): 30 ng/mL (lane #6); control I: no beads, no FGF-2 (lane #4); control II: 10 µL bead suspension, with EDC/NHS but no FGF-2 (lane #3); EDC/NHS coupling: 10 µL bead suspension with EDC/NHS and amino-PEG-FGF-2 (lane #1); 10 µL bead suspension with amino-PEG-FGF-2 but no EDC/NHS (lane #2). Asterisks denote statistically significant difference between the samples (** $p < 0.01$, * $p < 0.05$).

Furthermore, the ability of ERK phosphorylation was tested in comparison to total ERK expression with NIH 3T3 cells. Native FGF-2 references as well as PEGylated FGF-2 samples induced ERK phosphorylation (**Figure 71B**: (a) alkyne-PEG-FGF-2 (lane #1), FGF-2 (alkyne) (lane #2); (b) amino-PEG-FGF-2 (lane #5), FGF-2 (amino) (lane #6)) whereas no ERK phosphorylation was observed for the non-stimulated cells (**Figure 71B**: (a) control I: no beads, no FGF-2 (lane #3); control II: 10 µL bead suspension, with copper but no FGF-2 (lane #4); (b) control I: no beads, no FGF-2 (lane #4); control II: 10 µL bead suspension, with EDC/NHS but no FGF-2 (lane #3)). Here, too, all bead samples containing FGF-2, adsorbed or coupled, induced ERK phosphorylation and did not differ (**Figure 71B**: (a) click reaction: 10 µL bead suspension with copper and alkyne-PEG-FGF-2 (lane #5); 10 µL bead suspension with alkyne-PEG-FGF-2, no copper (lane #6); (b) EDC/NHS coupling: 10 µL bead suspension with EDC/NHS and amino-PEG-FGF-2 (lane #1); 10 µL bead suspension with amino-PEG-FGF-2 but no EDC/NHS (lane #2)). Presumably, longer cell culture trials under circumstances in which diffusion processes play a pivotal role would be necessary to verify a difference.

5.2.2 Introduction of non-natural amino acids into IGF-I

^{1}H and ^{13}C NMR spectra confirmed the formation of propargyl-L-lysine. 3.83 g plk were synthesized out of 6.2 g boc-L-lysine (62 %) with high purity (approximately 94 %). The first signal in the ^{1}H spectrum reflected the residual solvent D_2O (4.79 ppm) [161]. All the other peaks were allocated to the hydrogens of propargyl-L-lysine (**Figure 72A** and **B, supplementary information**). Additionally, the ^{13}C spectrum showed all C atoms of propargyl-L-lysine (**Figure 72B** and **C; supplementary information**) [193]. The missing signals at 164.2 ppm and 116.6 ppm of trifluoroacetic acid in the ^{13}C spectrum indicated that the free acid of propargyl-L-lysine and no TFA salt was built [193]. Besides, signal 9 would have been shifted to the left in the ^{1}H spectrum if the salt form would have been present.

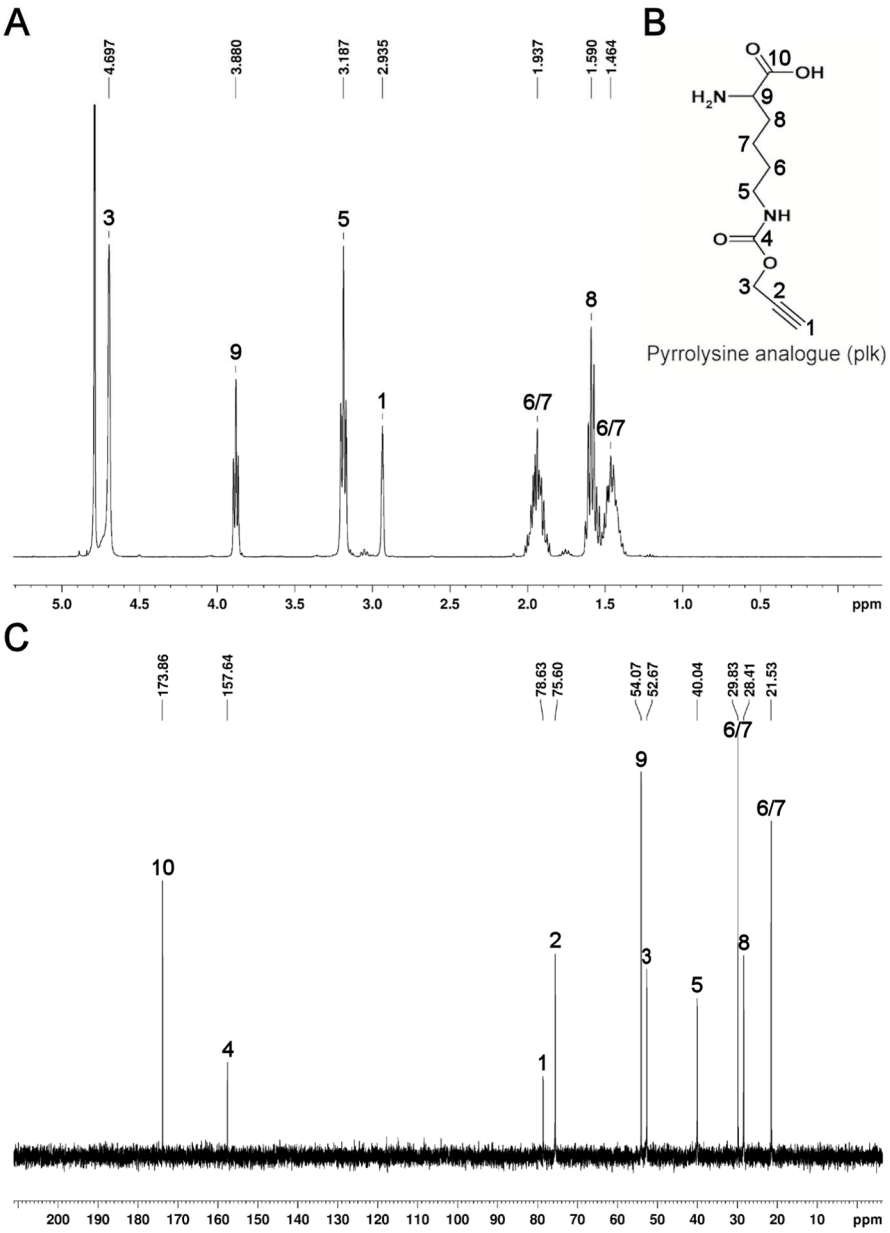

Figure 72: NMR spectra of propargyl-L-lysine. (A) ^{1}H spectrum, (B) plk structure and (C) ^{13}C spectrum.

The native cDNA of IGF-I and the product after mutagenesis were analyzed by agarose gel electrophoresis (**Figure 73A**). The pCMV6-XL4 vector containing cDNA of IGF-I (5181 bp; **Figure 73A**, lane #1) was visible in the range of 5,000 and 6,000 bp after the first PCR. After the second PCR the DNA fragment of TAG-IGF-I with restriction sites and start codon (225 bp; **Figure 73A**, lane #2 and 3) was detected between 200 and 300 bp.

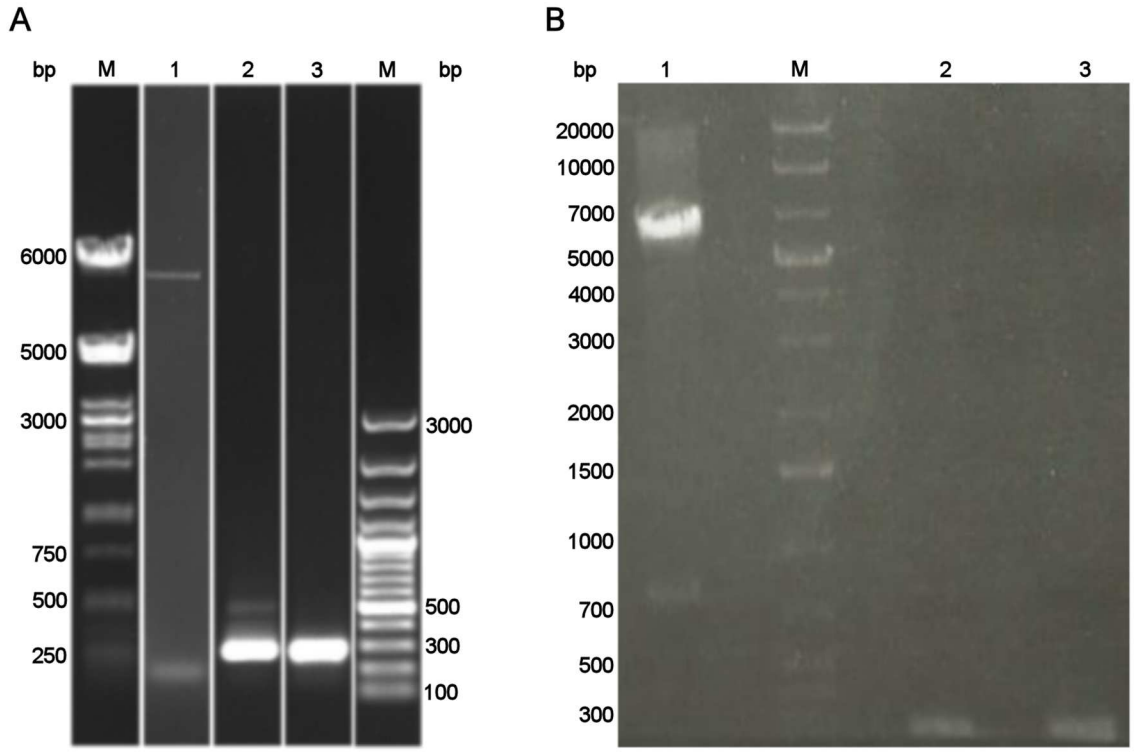

Figure 73: Agarose gel electrophoresis. (A) M (= marker): DNA ladder in the range from 250–10,000 bp; #1: Product of the 1st PCR, cDNA from IGF-I as template; #2: product of the 2nd PCR, 1st PCR product as template; #3: Product of the 2nd PCR, cDNA from IGF-I as template; M: DNA ladder in the range from 100–3,000 bp. (B) #1: Digested pET11a vector; M: DNA ladder in the range from 75–20,000 bp; #2: digested 2nd PCR product; #3: digested 2nd PCR product (cDNA from IGF-I as template).

Agarose gel electrophoresis was performed after restriction digestion of the PCR product (DNA of TAG-IGF-I) and the pET11a vector with BamHI and NdeI as well. The digested pET11a vector (5,637 bp) was detected in the range of 5,000 and 7,000 bp and the digested insert was detected between 700 and 1,000 bp on the agarose gel (**Figure 73B,** lane #1). Additionally, the digested TAG-IGF-I insert (218 bp) was visible between 200 and 300 bp (**Figure 73B,** lane #2 and 3). Subsequently, the digested pET11a vector (5,637 bp) and the digested TAG-IGF-I insert (218 bp) were cut and the DNA was extracted from the agarose gel. The purified fragments were then ligated by the usage of DNA ligase and finally the correct insertion of punctual mutation and the correct composition of the designed purified pET11a/TAG-IGF-I plasmid was confirmed by DNA sequencing (**Figure 74**). The synthesized IGF-I mutant contained the stop codon TAG coding for the unnatural amino acid, propargyl-L-lysine (plk), at position 65 (K (AAG (lysine) → TAG (plk)).

AGCTTCCTTTCGGGCTTTGTTAGCAGCCGGATCCTTAAGCTGACTTGGCAGGCTAGAGGG
GTGCGCAATACATCTCCAGCCTCCTTAGATCACAGCTCCGGAAGCAGCACTCATCCACGA
TGCCTGTCTGAGGCGCCCTCCGACTGCTGGAGCCATACCCTGTGGGCTTGTTGAAATAAA
AGCCCCTGTCTCCACACACGAACTGAAGAGCATCCACCAGCTCAGCCCCGCAGAGCGTCT
CCGGTCCCATATGTATATCTCCTTCTTAAAGTTAAACAAAATTATTTCTAGAGGGGAATT
GTTATCCGCTCACAATTCCCCTATAGTGAGTCGTATTAATTTCGCGGGATCGAGATCTCG
ATCCTCTACGCCGGACGCATCGTGGCCGGCATCACCGGCGCCACAGGTGCGGTTGCTGGC
GCCTATATCGCCGACATCACCGATGGGGAAGATCGGGCTCGCCACTTCGGGCTCATGAGC
GCTTGTTTCGGCGTGGGTATGGTGGCAGGCCCCGTGGCCGGGGGACTGTTGGGC

Figure 74: Complementary DNA sequence of pET11a/TAG-IGF-I plasmid. pET11a vector in orange, IGF-I sequence in blue, amber stop codon in red, BamHI restriction site in grey and start codon in purple, NdeI restriction site and stop codon in black and green.

After successful cotransformation of pET11a/TAG-IGF-I and pRSFduet plasmid into the appropriate *E. coli* cells protein expression was started.

In order to find optimal expression conditions, media, temperatures and plk concentrations were varied. Western blot analysis after expression of plk-IGF-I showed the obtained results (**Figure 75**). The expression in TB medium at 37 °C with 6.8 mM plk resulted in a strong band between 10 and 15 kDa after 1 hour (**Figure 75A,** lane #2). IGF-I reference with a size of 7.7 kDa was detected at about 10 kDa (**Figure 75A**, lane #8). So there was a chance that the existing band is the plk-IGF-I. Unfortunately, this band faded by time and even shifted to smaller sizes after 12 and 20 hours (**Figure 75A**, lane #2–7). Additionally, several bands were observed between 25 and 55 kDa for all plotted samples. These bands changed appearance by time, the 25 kDa band became weaker and as opposed to this the 55 kDa band became sharper. Conceivably, these bands were plk-IGF-I aggregates. Results of plk-IGF-I expression at 20 °C looked similar to the once at 37 °C but the bands were paler, just barely visible and there was no shift to smaller sizes (**Figure 75A**, lane #9-14). Plk-IGF-I expression in LB medium at 37 °C and with 6.8 mM plk resulted in one intensive band between 10 and 15 kDa after 3 hours (**Figure 75B**, lane #3). Here too, this band faded by time and even disappeared after 12 hours (**Figure 75B**, lane #3–7). Under these conditions the bands between 25 and 55 kDa became weaker as well. It seemed as if the expressed plk-IGF-I was degraded, for instance, by built proteases. The results obtained by expression in LB medium at 20 °C corresponded with the results at 37 °C in TB medium. The same shift of the plk-IGF-I band to smaller sizes occurred after 6 hours (**Figure 75B**, lane #9–14). The bands between 25 and 55 kDa became more intense by time, but on the whole the bands were not as intense as in the TB medium, 37 °C plot. Consequently, TB medium was considered as preferred medium and was used for the next trials. The following expression of plk-IGF-I at 30 °C with 23.7 mM plk did not show the expected band between 10 and 15 kDa, there were just bands between 25 and 55 kDa

visible (**Figure 75C**). The samples taken between 10 and 18 hours after induction with IPTG (**Figure 75C**, lane #4 and 6–9) looked similar to the sample taken before the addition of plk (**Figure 75C**, lane #2) and the sample taken before the addition of IPTG (**Figure 75C**, lane #3). The assumption that plk-IGF-I degraded by time remained as there were no samples taken at earlier time points. The next plk-IGF-I expression at 37 °C with 30 mM plk confirmed this assumption. The plk-IGF-I sample taken 1 hour after induced by IPTG showed a sharp band between 10 and 15 kDa (**Figure 75D**, lane#3) which was not visible before the addition of IPTG (**Figure 75D**, lane #2). Unfortunately, here too, this sharp band paled by time. After 2.5 hours the band was hardly visible (**Figure 75D**, lane #4) and after 16 hours the band disappeared completely (**Figure 75D**, lane #5). So the assumption of a successful expression of plk-IGF-I that degraded by time was confirmed. Temperatures between 20 and 37 °C were chosen, medium was changed and plk concentration was varied without expressing plk-IGF-I in a sufficient amount.

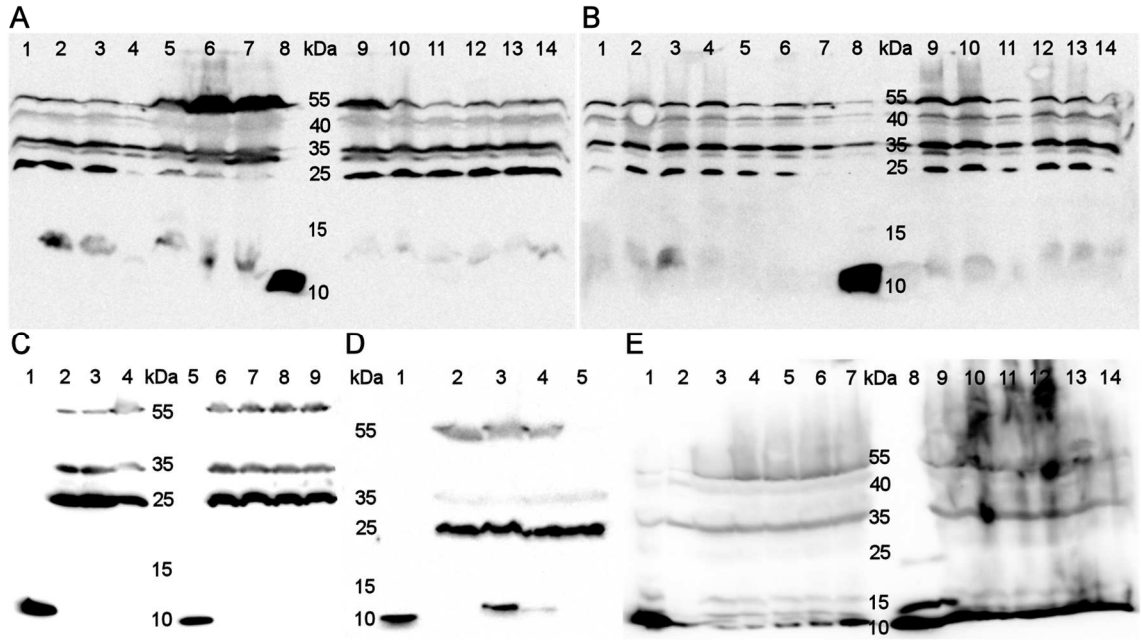

Figure 75: Western blot analysis after expression. (A) TB medium, 6.8 mM plk: lane #1 before adding IPTG; lane #2–7 37 °C samples (lane #2 1h, lane #3 3h, lane #4 6h, lane #5 12h, lane #6 20h, lane #7 24h); lane # 8 IGF-I reference, lane #9–14 20 °C samples (lane #9 24h, lane #10 20h, lane #11 12h, lane #12 6h, lane #13 3h, lane #14 1h); (B) LB medium, 6.8 mM plk : lane #1 before adding IPTG; lane #2–7 37 °C samples (lane #2 1h, lane #3 3h, lane #4 6h, lane #5 12h, lane #6 20h, lane #7 24h); lane # 8 IGF-I reference, lane #9–14 20 °C samples (lane #9 24h, lane #10 20h, lane #11 12h, lane #12 6h, lane #13 3h, lane #14 1h); (C) TB medium, 30 °C, 23.7 mM plk: lane #1+5 IGF-I reference, lane #2 before adding plk, lane #3 before adding IPTG, lane #4 10h, lane #6 12h, lane #7 14h, lane #8 16h, lane #9 18h; (D) TB medium 37 °C, 30 mM plk: lane #1 IGF-I reference, lane #2 before adding IPTG, lane #3 1h, lane #4 2.5 h, lane #5 16h; (E) ArcticExpress(DE3) cells; 12 °C, 15.9 mM plk: lane #1 OVC, lane #2 before adding plk, lane #3 before adding IPTG, lane #4 1h, lane #5 2h, lane #6 3h, lane #7 4h, lane #8 IGF-I reference, lane #9 14.5h, lane #10 16h, lane #11 18h, lane #12 20.5h, lane #13 22h, lane #14 24 h..

As collected from published literature, IGF-I is expressed in inclusion bodies in *E. coli* cytoplasm, meaning denatured protein in the form of particles [194]. Hence, some inclusion body purification procedures were tested. Inclusion body purification according to van Kimmenade et al. [162]

resulted in one band between 25 and 35 kDa (**Figure 76A**, lane #1–3). The band between 10 and 15 kDa disappeared and was even not found in the supernatant (**Figure 76A**, lane #4). During performing method B from Wangsa-Wirawan et al. [163], the plk-IGF-I band between 10 and 15 kDa got lost as well (**Figure 76B**, lane #7). In contrast, the wanted plk-IGF-I band was still detected after inclusion body purification according to method C [163] (**Figure 76C**, lane #6). Curiously, procedures for inclusion purification that included lysozyme for cell debris digestion showed a band between 10 and 15 kDa and the once without lysozyme showed no band at this height. Hence, this sharp band was analyzed by ESI/MS after tryptic in-gel digestion and, unfortunately, this band between 10 and 15 kDa was verified as lysozyme (**Supplementary Figure 10**). But the peptide fragment from amino acid 22 to 36 (m/z = 1667.783), one of the peptide fragments obtained after tryptic in-gel digestion of IGF-I reference, was detected as well, indicating the presence of plk-IGF-I (**Supplementary Figure 10**). Presumably, plk-IGF-I had the same size as lysozyme in the western blot analysis and both proteins lay on top of each other. In order to provide evidence that plk-IGF-I was really expressed, the yield of plk-IGF-I had to be increased and as a consequence expression had to be further optimized.

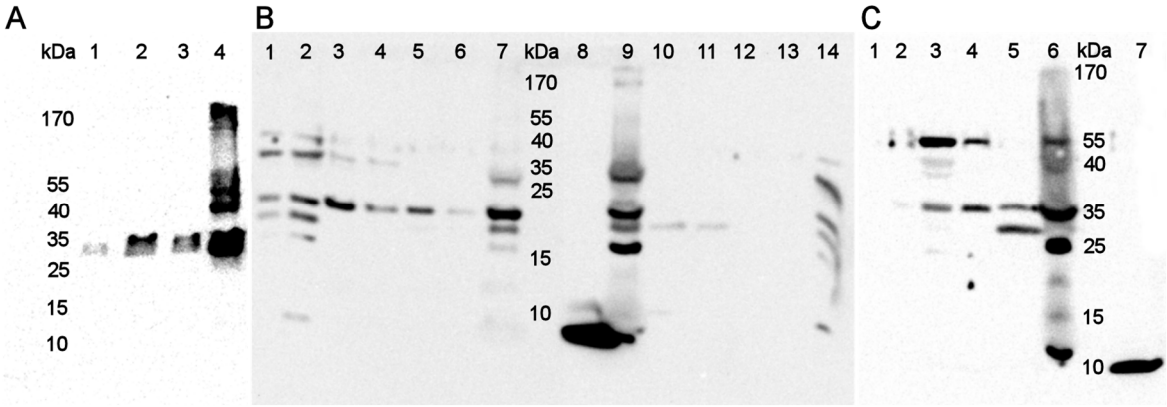

Figure 76: Western blot analysis after inclusion body purification (A) according to van Kimmenade et al. [162]: lane #1–3 plk-IGF-I, lane #4 supernatant plk-IGF-I; (B) according to Wangsa-Wirawan et al. [163], method B: lane #1–6 steps of plk-IGF-I inclusion body purification, lane #7 purified pellet of plk-IGF-I, lane #8 IGF-I reference, lane #9 pellet of plk-IGF-I before inclusion body purification, lane #10–14 steps of plk-IGF-I inclusion body purification; (C) according to Wangsa-Wirawan et al. [163], method C: lane #1–5 steps of plk-IGF-I inclusion body purification, lane #6 purified pellet of plk-IGF-I, lane #7: IGF-I reference.

Therefore, another cell line was used to perform plk-IGF-I expression at lower temperatures. ArcticExpress(DE3) cells co-express cold-adapted chaperonins (Cpn10 and Cpn60) that allow protein expression at lower temperatures and increase the yield of soluble protein [195]. The expression of plk-IGF-I in ArcticExpress(DE3) cells at 12 °C with 15.9 mM plk resulted in a band between 10 and 15 kDa that became darker and larger by time (**Figure 75E**, lane #4–7 and 9–14). These results indicated the expression of plk-IGF-I. However, even the sample of the overnight culture (**Figure 75E**, lane #1) and the sample before adding plk (**Figure 75E**, lane #2) as well as the sample before adding IPTG (**Figure 75E**, lane #3) showed a band with the same molecular

weight meaning the expression of IGF-I without induction with IPTG. Basal expression is not uncommon but pET vectors are the gold standard for protein expression in *E. coli* and promise the lowest basal expression level of the *E. coli* expression systems [196]. Even so the intense band between 10 and 15 kDa of the overnight culture implied basal expression to a large extent. Or perhaps the IGF-I antibody was bound non-specifically to other proteins. The expressed chaperonin 10 has a molecular weight of 10 kDa as well.

In order to test antibody specificity, the plot was not incubated with the primary polyclonal IGF-I antibody but with the secondary detection antibody. No proteins were detected and non-specific binding of the secondary detection antibody was excluded (data not shown). Moreover, a sample of protein expression with BL21(DE3) cells using the same vector system but without IGF-I epitope was plotted and incubated with polyclonal IGF-I antibody. Unfortunately, this sample showed protein bands in the range between 25 and 55 kDa comparable to the samples before adding plk and IPTG, indicating non-specific binding of polyclonal IGF-I antibody (data not shown). However, no bands were visible in the range between 10 and 15 kDa. Hence, it was obvious that the detected band between 10 and 15 kDa was plk-IGF-I.

After in-gel tryptic digestion ESI/MS spectra of IGF-I reference and plk-IGF-I sample of the expression with ArcticExpress(DE3) cells were recorded. The spectrum of IGF-I showed six peptide fragments (amino acid (aa) 22–36: m/z = 1,667.783, aa 22–37: m/z = 1,823.885, aa 37–50 (Cys 47 and 48 alkylated: m/z = 1,708.795, aa 38–50: m/z = 1,436.633, aa 38–50 (cys 47 and 48 alkylated): m/z = 1,552.695, aa 56–68 (Cys 61 alkylated: m/z = 1,592.736; [197]) (**Figure 77A**). The peptide fragment from amino acid 22 to 36 (m/z =1667.783) was the only fragment that was found in the plk-IGF-I spectrum as well (**Figure 77B**). This result is no evidence that plk-IGF-I was really expressed but it is quite likely as the matching peak is the one with the highest intensity. Certainly the protein amount was not sufficient to detect the residual fragments. As a consequence another approach has to be found in order to overcome the low expression yield of plk-IGF-I.

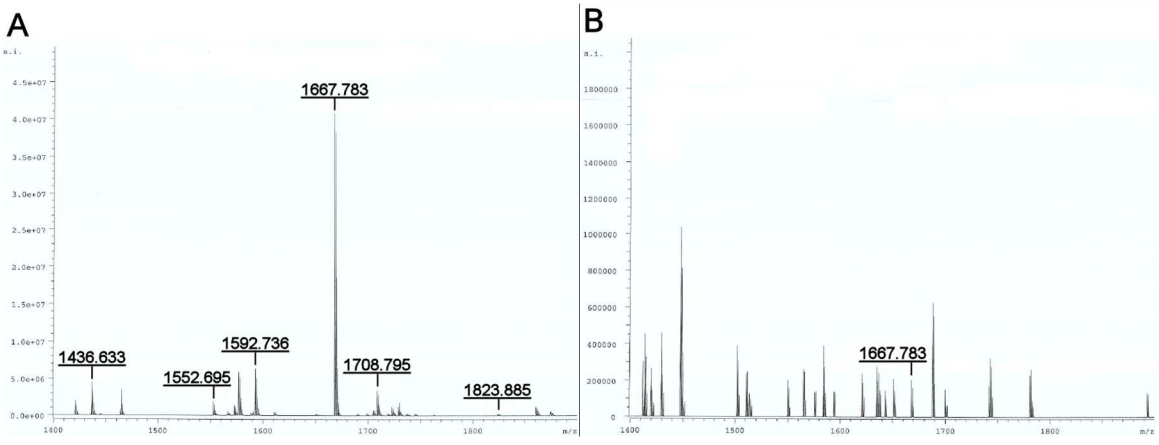

Figure 77: ESI/MS spectra of (A) IGF-I reference and (B) plk-IGF-I after in-gel tryptic digestion.

5.3 Biofunctionalized implants for cartilage tissue engineering

5.3.1 Scanning electron microscopy (SEM)

SF-Scaffold morphology was recorded by SEM (**Figure 78**). A highly interconnected and porous microstructure with pore sizes in the range of the used paraffin spheres was formed. On the one hand SF scaffolds with one porosity were prepared (**Figure 78A**; pores in the range from 315 to 710 µm) and on the other hand biphasic SF scaffolds with two porosities on one scaffold were produced (**Figure 78B**: pores in the range from 315 to 710 µm and pores in the range from 100 to 180 µm).

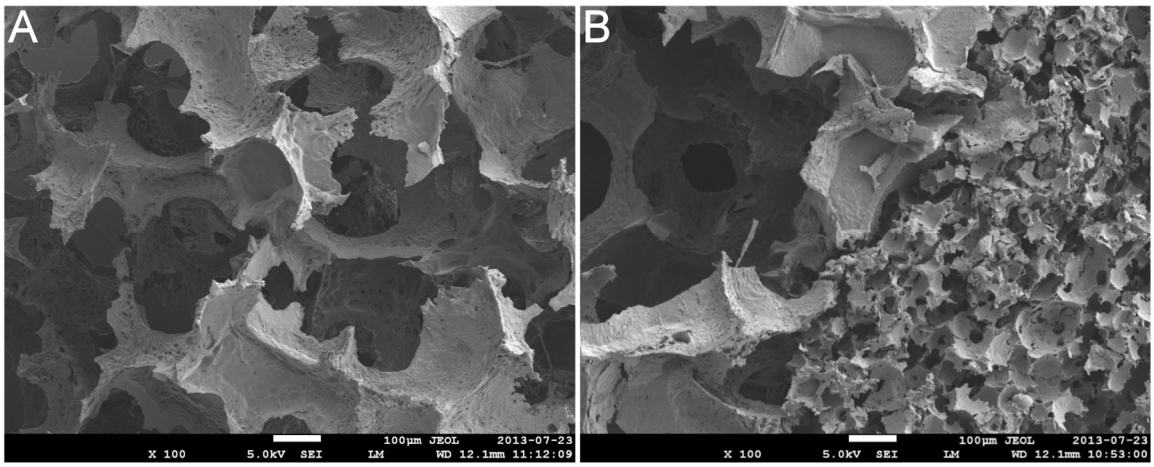

Figure 78: SEM images of porous SF scaffolds using paraffin spheres with a diameter of (A) 315–710 µm or (B) 315–710 µm and 100–180 µm as porogen.

5.3.2 Determination of coupling efficiency of TGF-β3 on PMMA beads

The covalent coupling of TGF-β3 to PMMA beads was confirmed by fluorescence microscopy and flow cytometry. The beads which reacted with TGF-β3 in presence of the coupling reagents EDC and NHS showed fluorescence (**Figure 79A-1** and **B**) demonstrating covalent immobilized TGF-β3 on the PMMA beads. However, no fluorescence occurred in absence of the coupling reagents showing that no TGF-β3 was coupled without EDC and NHS (**Figure 79A-2** and **B**). The negative control with coupling reagents but without TGF-β3 served to check unspecific binding of the antibodies to the beads and showed no fluorescence as well **(Figure 79A-3** and **B)**.

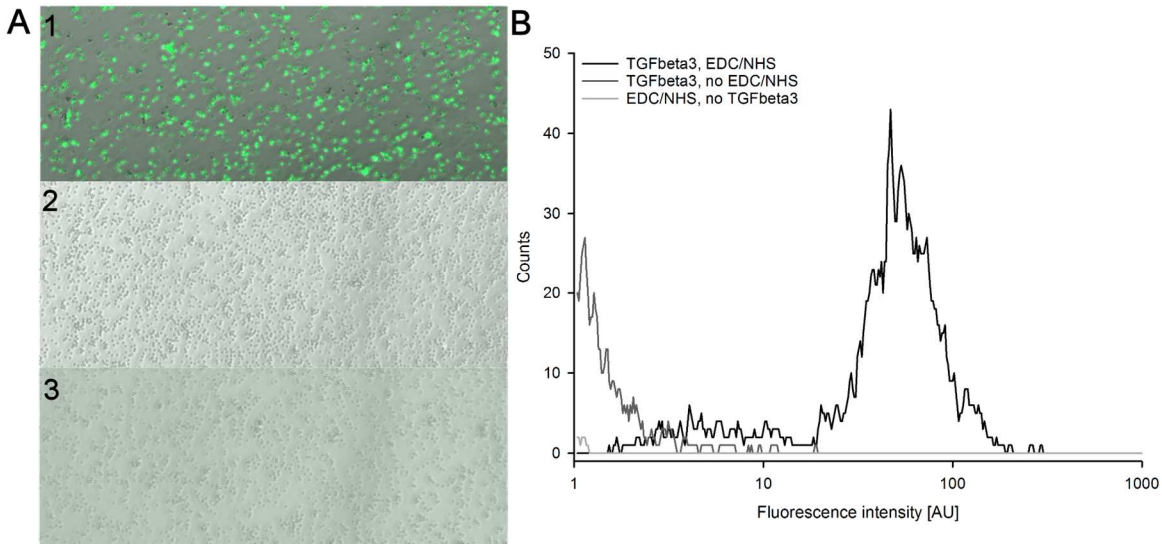

Figure 79: Fluorescence imaging and flow cytometry after EDC/NHS coupling of TGF-β3 to carboxylated 5 µm PMMA beads and incubation with a primary mouse anti-TGF-β3 antibody and subsequently with a secondary Alexa Fluor® 488 conjugated anti-mouse IgG antibody. (A) Merged images of fluorescence and bright field of (1) the reaction with TGF-β3 and coupling reagents, (2) the reaction with TGF-β3 but without coupling reagents and (3) the reaction without TGF-β3 but with coupling reagents. (B) Analysis of fluorescence intensities with flow cytometry.

Quantification of TGF-β3 on the PMMA beads was performed with an indirect ELISA. The TGF-β3 coupled beads were counted and the coupling efficiency was obtained by comparing the coupled TGF-β3 amount with the amount of TGF-β3 (9.64 ng/µL bead suspension) given to the coupling reaction. The coupling of TGF-β3 to the PMMA beads was determined to 7.77 ng/µL bead suspension for the reaction with EDC/NHS and 1.25 ng/µL bead suspension for the reaction without coupling reagents, corresponding to 81 % and 13 % coupling efficiency with statistically significant difference (**Figure 80**).

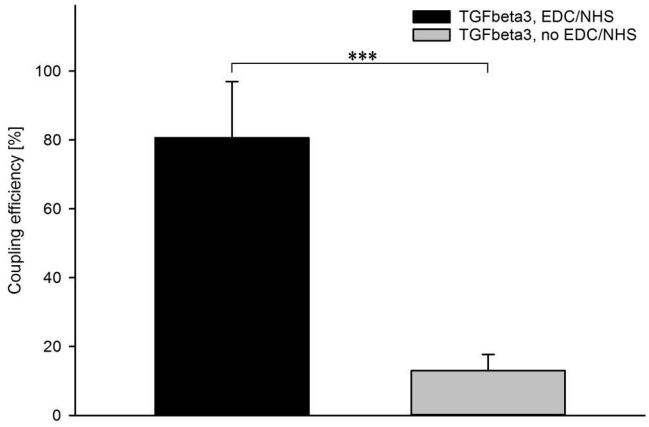

Figure 80: Coupling efficiencies of TGF-β3 to PMMA beads in presence or absence of EDC and NHS presented as percentage of applied TGF-β3. Asterisks denote statistically significant difference between the groups (*** $p < 0.001$).

5.3.3 Bioactivity of TGF-β3 after coupling on PMMA beads

In order to test biological activity of TGF-β3 after coupling reaction, a luciferase reporter gene assay was performed with transfected hMSC-TERT cells containing SBE. The bead suspensions used for luciferase assay as well as for ELISA were counted using a Neubauer hemocytometer (Brand GmbH, Wertheim, Germany) and the number of beads per µL bead suspension was determined for each assay. In this way, the active amount of TGF-β3 per well was determined, and by means of the results obtained by ELISA even the total amount of TGF-β3 on the beads was calculated. Both the beads with covalent coupled TGF-β3 and the beads with a little amount of adsorbed TGF-β3 were able to activate SMAD2/3 as evidenced by luciferase assay, and even nearly the same luciferase signals were achieved by covalent coupled and adsorbed TGF-β3 beads.

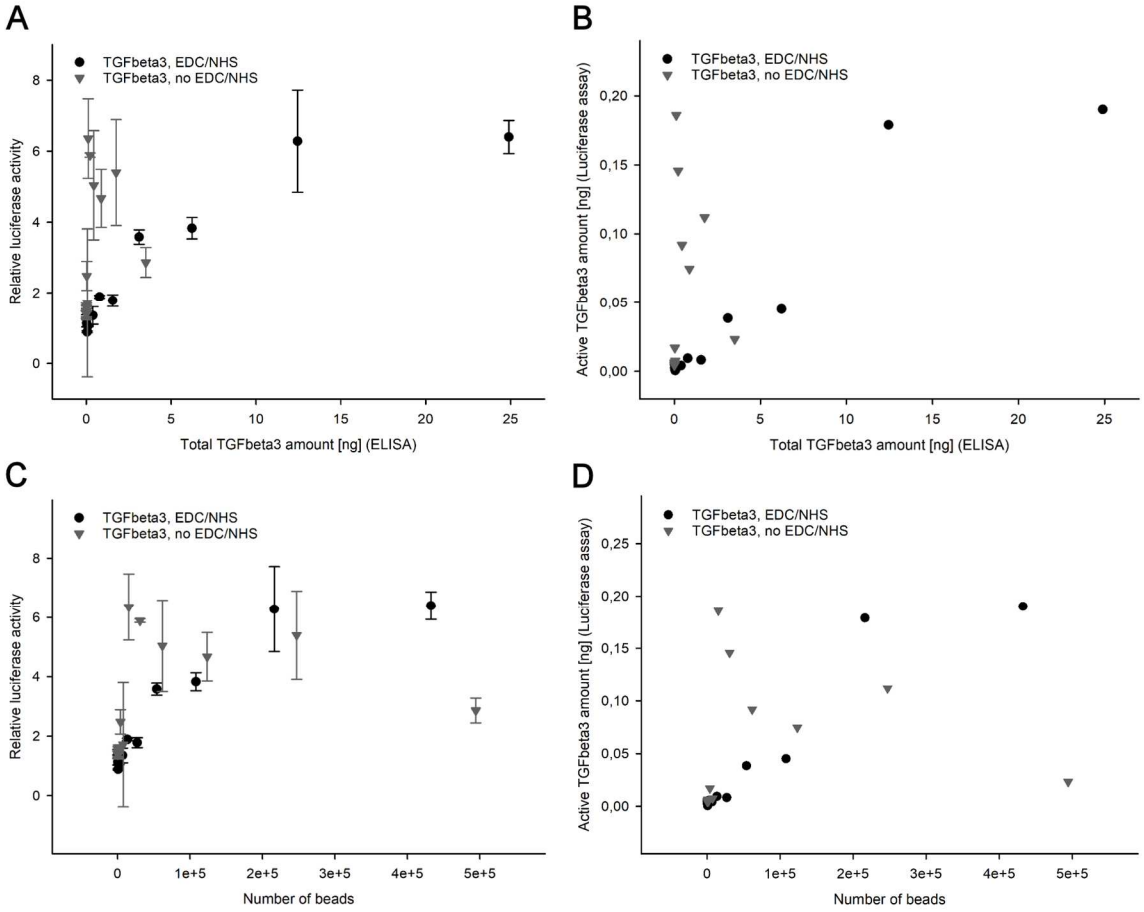

Figure 81: Relative luciferase activity of TGF-β3 immobilized beads with and without EDC/NHS is shown (A) against the total TGF-β3 amount [ng] determined by ELISA and (C) against the number of beads. Active TGF-β3 amount [ng] of TGF-β3 immobilized beads with and without EDC/NHS determined by luciferase assay is shown (B) versus total TGF-β3 amount [ng] determined by ELISA and (D) versus the number of beads.

Comparing the active TGF-β3 amount on the beads in presence or absence of EDC/NHS resulting from luciferase assay, similar results were obtained regardless of whether coupling reagents were used for covalent coupling or not (**Figure 81A**). On the other hand, the results differed considerably regarding the total TGF-β3 amount on the beads of the reaction with or without

coupling reagents obtained from ELISA (**Figure 81B**). ELISA results showed that much more TGF-β3 was immobilized on the beads by implementation of EDC/NHS chemistry. However, the effect during luciferase assay was nearly the same indicating a loss of bioactivity by covalent coupling with EDC/NHS chemistry and the concomitant crosslinks.

5.3.4 Histological and biochemical investigation of chondrogenesis/osteogenesis

First of all biocompatibility of generated biphasic SF scaffolds was verified in a Live/Dead assay (data not shown). Subsequently, general suitability of these biphasic SF scaffolds for chondrogenesis as well as osteogenesis was investigated. Therefore, osteogenic marker such as calcium and osteopontin (**Figure 82A–D**) as well as chondrogenic marker such as GAG and collagen II (**Figure 82E–H**) were visualized by the appropriate staining procedures as described above (see 4.3.10). All sections of SF scaffolds cultured in growth medium showed neither calcium or osteopontin (**Figure 82A** and **C**) nor GAG or collagen II deposition (**Figure 82E** and **G**). In contrast, the SF scaffolds cultured in osteogenic medium showed the deposition of calcium (**Figure 82B**) and osteopontin (**Figure 82D**) and the scaffolds cultured in chondrogenic medium showed the deposition of GAG (**Figure 82F**) and collagen II (**Figure 82H**). The presence of cells was verified by counterstaining of cell nuclei with DAPI in blue (**Figure 82C, D, G** and **H**).

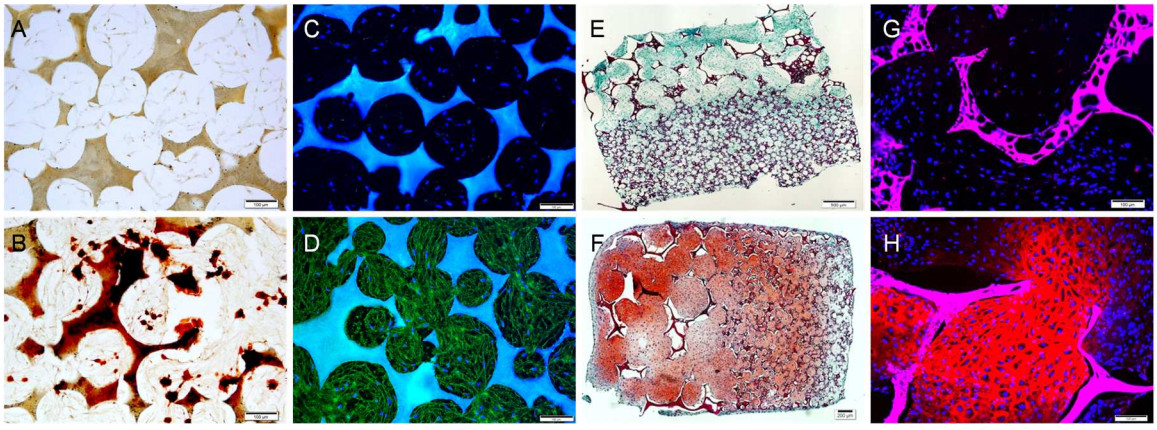

Figure 82: Sections of SF scaffolds seeded with BMSCs. Detection of ECM components, osteogenic and chondrogenic markers by immunohistochemical staining. (A-D) osteogenic marker (calcium and osteopontin), (E-H) chondrogenic marker (GAG and collagen II). (A+C+E+G) BMSCs cultured in (B+D) osteogenic medium or (F+H) chondrogenic medium. (A+B) Calcium staining in red, (C+D+G+H) counterstaining of cell nuclei with DAPI in blue, (C+D) staining of osteopontin in green, (G+H) staining of collagen II in red and (E+F) Safranin O staining in red.

Additionally, quantitative biochemical analysis maintained these observations, an increase of the osteogenic markers calcium (**Figure 83A**) and alkaline phosphatase (**Figure 83B**) as well as the chondrogenic markers collagen II (**Figure 83C**) and GAG (**Figure 83D**) was shown after 28 or 21 days in culture compared to non-induced samples. According to these results and the results from quantitative RT-PCR, depicted under 5.3.5. (**Figure 86**), the generated biphasic SF scaffolds were suitable for osteogenesis as well as chondrogenesis.

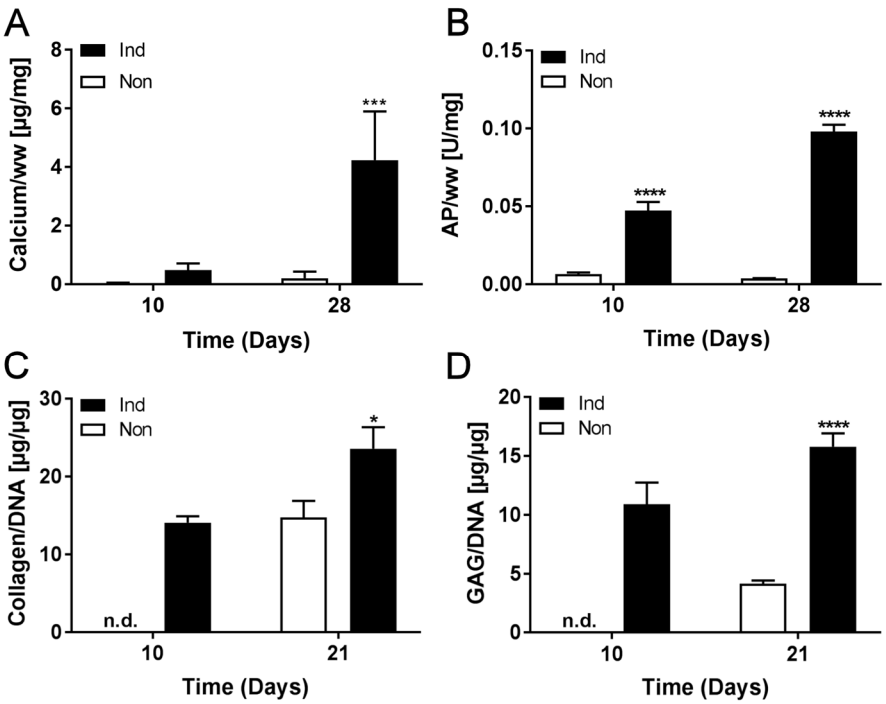

Figure 83: Biochemical analysis of SF scaffolds seeded with BMSCs. Quantification of osteogenic markers: (A) calcium and (B) alkaline phosphatase after 28 days. Quantification of chondrogenic markers: (C) collagen and (D) GAG after 21 days. Asterisks denote statistically significant differences between the induced and non-induced groups (****$p < 0.0001$, *** $p < 0.001$, * $p < 0.05$). n.d. = not determined.

Subsequently, the influence of immobilized TGF-β3 on chondrogenesis of BMSCs seeded on SF scaffolds was investigated after 21 days in chondrogenic medium. Chondrogenic differentiation of BMSCs was assessed by histology and immunohistochemistry. Extracellular glycosaminoglycan (GAG) deposition was visualized with Safranin-O. All TGF-β3 including samples (Saf-O, exogenous, coupled, adsorbed, **Figure 84**) increased the accumulation of GAGs to a variable extent. Exogenous supplemented TGF-β3, as single dose at the beginning (burst, data not shown) or over culture time (Saf-O, exogenous, **Figure 84**), generated homogenous distribution of GAG in comparison to immobilized TGF-β3, adsorbed or covalently coupled, that caused punctual GAG deposition (Saf-O, adsorbed, coupled **Figure 84**). Both controls, beads with coupling reagents but without TGF-β3 (data not shown) as well as non-treated beads, showed no GAG deposition (Saf-O, blank, **Figure 84**). Moreover, extracellular deposition of collagenous matrix, collagen I and II, was visualized. Collagen I as well as collagen II were built to a large extent for all samples including TGF-β3 (Col I, Col II, exogenous, coupled, adsorbed, **Figure 84**). In contrast, no collagen I and collagen II were generated without the addition of TGF-β3 (Col I, Col II, blank, **Figure 84**). Comparing the effect of adsorbed and covalently coupled TGF-β3 on GAG, collagen I and collagen II deposition, covalently coupled TGF-β3 generated more GAG as well as collagen II than the adsorbed TGF-β3, but less collagen I. But exogenous TGF-β3 reached the strongest staining for all three deposited substances.

Similar results were obtained by biochemical analysis. After 21 days of cultivation GAG as well as collagen deposition increased significantly for all samples compared to blank beads (**Figure 85**).

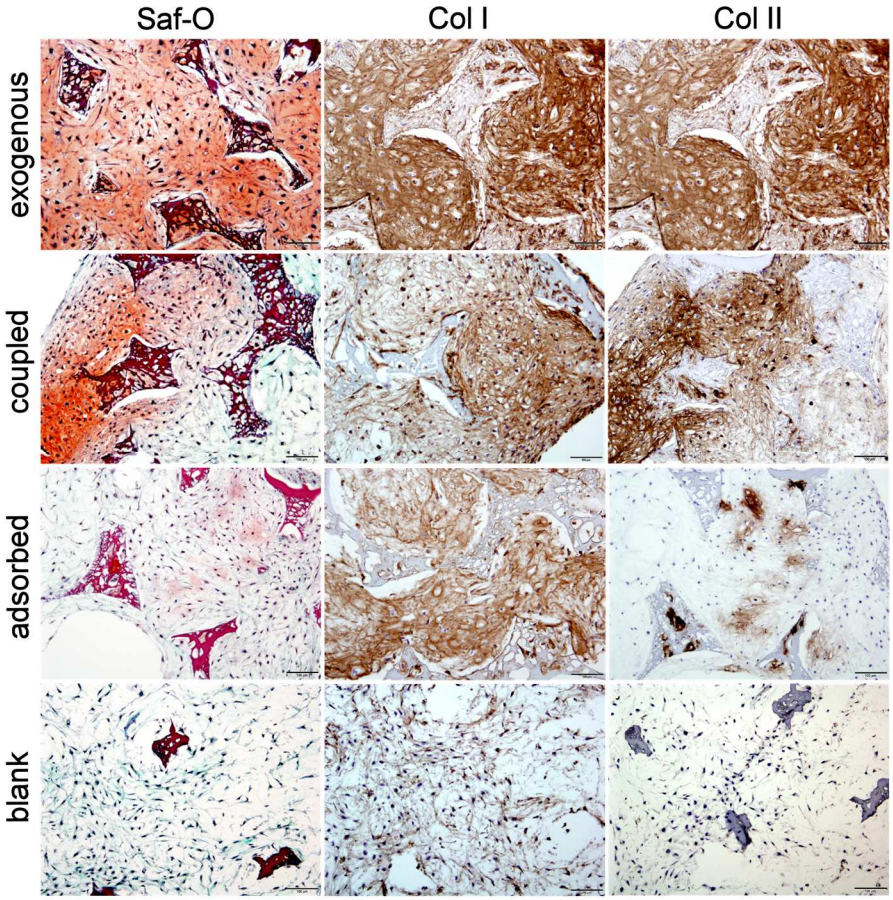

Figure 84: Sections of SF scaffolds seeded with BMSCs and loaded with PMMA beads. Detection of ECM components and chondrogenic markers by immunohistochemical staining. Safranin O staining, GAG in red, collagen I staining in brown, collagen II staining in brown. Exogenous = medium supplemented with TGF-β3 (10 ng/mL, 1 mL each, 9 medium changes → 90 ng TGF-β3); coupled = 78 ng TGF-β3 coupled covalently to PMMA beads; adsorbed = 13 ng TGF-β3 adsorbed to PMMA beads; blank = non-treated PMMA beads.

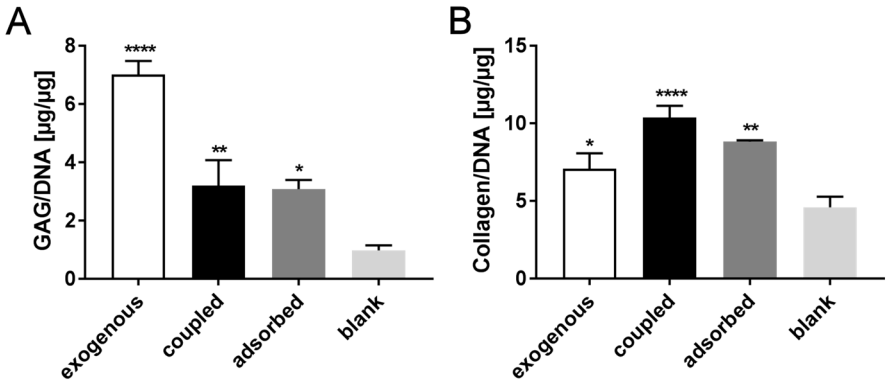

Figure 85: SF scaffolds were seeded with BMSCs and loaded with PMMA beads. Biochemical analysis of GAG and collagen II content after 21 days in culture. Exogenous = medium supplemented with TGF-β3 (10 ng/mL, 1 mL each, 9 medium changes → 90 ng TGF-β3); coupled = 78 ng TGF-β3 coupled covalently to PMMA beads; adsorbed = 13 ng TGF-β3 adsorbed to PMMA beads (n = 2); blank = non-treated PMMA-beads. Asterisks denote statistically significant differences between the groups referring to the blank (****$p < 0.0001$, ** $p < 0.01$, * $p < 0.05$).

5.3.5 Molecular investigation of chondrogenesis/osteogenesis by real time RT-PCR

Biphasic SF scaffolds were further analyzed by qRT-PCR to investigate the expression of osteogenic and chondrogenic marker genes. An upregulation of bone sialoprotein and osteopontin (**Figure 86A** and **B**, osteogenic marker genes) as well as Sox9 and Collagen II (**Figure 86C** and **D**, chondrogenic marker genes) was detected verifying osteogenesis as well as chondrogenesis.

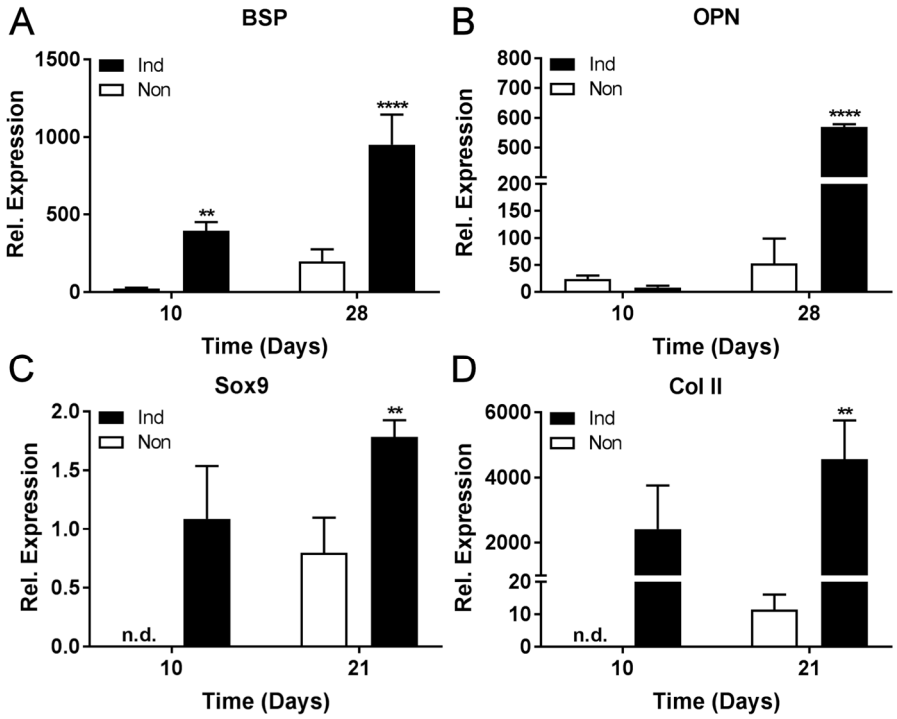

Figure 86: Analysis of osteogenic and chondrogenic marker genes with qRT-PCR. Normalization of gene expression levels of (A) bone sialoprotein (BSP), (B) osteopontin (OPN), (C) Sox9 and (D) collagen II on GAPDH as reference gene; resulting values were further normalized on day 0. Asterisks denote statistically significant differences between the induced and non-induced groups (****$p < 0.0001$, ** $p < 0.01$). n.d. = not determined.

Quantitative RT-PCR was performed to investigate chondrogenesis induced by immobilized TGF-β3 on mRNA level as well. Chondrogenic marker genes such as aggrecan, collagen II (both hyaline cartilage markers) and Sox9 as well as collagen I as fibrocartilage marker and collagen X as hypertrophic marker were analyzed using qRT-PCR. Sox9 is a marker in the phase of differentiation of BMSCs to chondrocytes, its expression is induced by TGF-β3 [198]. Comparing adsorbed with covalently coupled TGF-β3, Sox9 expression is higher for the coupled TGF-β3 assuming that differentiation was still going on (**Figure 87C**). Aggrecan (ACAN) is one of the main components of the ECM of articular hyaline cartilage that is embedded into a meshwork of collagen II fibres [199]. The upregulation of aggrecan was significant for covalently coupled TGF-β3 as well as exogenous supplemented TGF-β3 compared to blank beads, whereas aggrecan was not upregulated by the adsorbed TGF-β3 (**Figure 87A**). Additionally, collagen II was upregulated by covalently coupled TGF-β3 and exogenous supplemented TGF-β3 with statistical

significance (**Figure 87B**). Expression of collagen I, the marker for fibrocartilage, was upregulated by TGF-β3 supplemented exogenously with statistical significance. Collagen I expression was higher for the adsorbed TGF-β3 sample than for the covalently coupled TGF-β3 sample, but without statistical significance (**Figure 87D**). Collagen X, the hypertrophic marker, was only expressed after induction with exogenously supplemented TGF-β3 with statistical significance (**Figure 87E**).

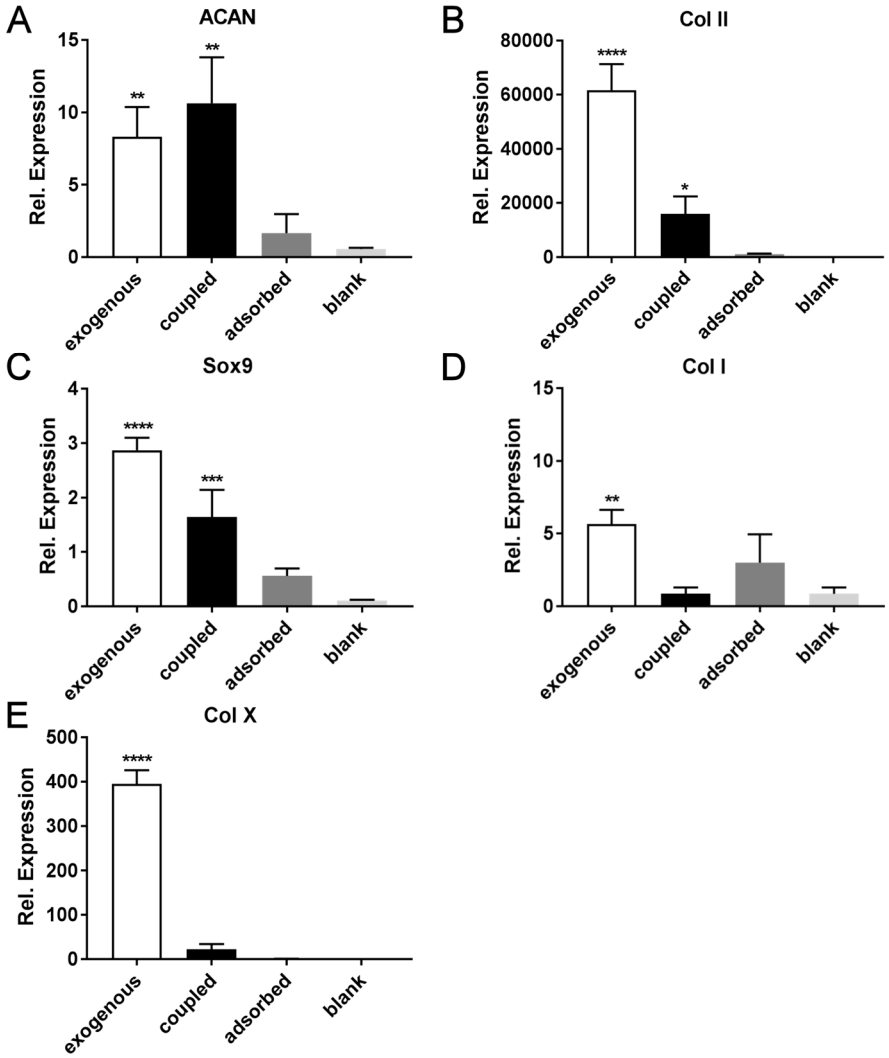

Figure 87: Analysis of chondrogenic marker genes with qRT-PCR. Normalization of gene expression levels on RPL13a as reference gene; resulting values were further normalized on day 0. Exogenous = medium supplemented with TGF-β3 (10 ng/mL, 1 mL each, 9 medium changes → 90 ng TGF-β3); coupled = 78 ng TGF-β3, coupled covalently to PMMA beads, adsorbed = 13 ng TGF-β3 adsorbed to PMMA beads (n = 2); blank = non-treated PMMA- beads. Asterisks denote statistically significant differences between the groups referring to the blank (****$p < 0.0001$, *** $p < 0.001$, ** $p < 0.01$, * $p < 0.05$).

6 Discussion and outlook

As proteins gain more and more importance as therapeutics, there is an urgent need for stable and save protein formulations. Up to date, most proteins are administered parenterally. Due to their poor *in vivo* serum half-life, frequent injections and high doses, which may trigger severe side effects, are needed for effective therapy. Hence, controlled and sustained delivery systems for proteins are required to address these limitations. Although some injectable sustained-release protein formulations are on the market, there is still an urgent need to develop further delivery systems for biologics.

Moreover, it is of paramount importance to understand physico-chemical and biological characteristics of the protein of interest during development of biopharmaceuticals. The macromolecular structure of biologics is sensitive to external conditions making production, formulation and storage challenging. Chemical as well as physical degradation mechanisms need to be known and prevented. During chemical degradation processes such as deamidation, hydrolysis, oxidation and disulfide scrambling occur changes in the chemical structure of the protein whereas during physical degradation processes such as denaturation, aggregation, precipitation and misfolding the chemical structure is unchanged but the physical state of the protein alters [200].

The pH screening and forced degradation study aimed at developing a new injectable formulation for the dimeric fusion protein PR-15, that can be stored at 4 °C. In order to declare expiration date of the developed PR-15 formulation, a long-term stability study at the proposed storage temperature has to be conducted, according to the Q1A (R2) and Q5C Guidelines established by the International Council of Harmonization (ICH). Shelf lives of biological products differ from 0.5 to 5 years making it difficult to draft uniform guidelines regarding the duration of stability study. Former PR-15 formulation was stored at -80 °C or -20 °C because shelf-life of PR-15 at 4 °C was smaller than 6 months [75]. Consequently, we suppose a PR-15 self-life smaller than 1 year at 5 °C ± 3 °C resulting in monthly real-time/real-temperature stability studies for the first 3 months and every 3 months thereafter for at least 12 months. The pH screening study at accelerated conditions (25 °C ± 2 °C) provides additional data for determining expiration date whereas the pH screening under stressed conditions (40 °C ± 2 °C) as well as forced degradation study helped to define test parameters to investigate product stability. Furthermore, forced degradation study helped to monitor potential degradation pathways of PR-15 with the aim be able to prevent degradation during production, shipping and long-term storage and thereby maintain its stability as well as its bioactivity. The performed pH screening study detailed a pH value of 7.0 as the most favorable formulation pH for PR-15. At pH 7.0 the formation of aggregates was just observed under stressed conditions, after 4 weeks 4.9 % aggregates and after 8 weeks 3.6 % aggregates were detected through SEC **(Figures 10D** and **12D)**. However, even at pH 7.0 the chemical degradation

of PR-15 reached a high degree under accelerated as well as stressed conditions. During HIC between 42.9–88.5 % degradation products were detected increasing with temperature and time compared to 6.2 % degradation products in the initial sample (**Figures 13D** and **15D**) requiring further optimization. For this purpose, a Design of Experiments (DoE) was chosen.

During the forced degradation study, mainly thermal stress, acidic conditions and light exposure caused PR-15 degradation and the formation of aggregates. Hence, thermal stress was chosen to stress the 25 different PR-15 formulations, prepared according to the working sheet created by the DoE software MODDE 9.0. The aim of the DoE was to investigate if the used phosphate buffer of the former Revacept® formulation maintained the stability and bioactivity of PR-15 compared to other buffer types. Moreover, we aimed at finding a pH optimum in terms of stability. As pH values smaller than 7.0 failed during pH screening study a pH range from 7.0 to 8.0 was investigated during DoE. Additionally, the influence of Tween® 20 [80, 81] (0.1 %) as stabilizer against protein aggregation and to prevent surface adsorption as well as methionine [82] (20 mM) as reducing agent was analyzed on PR-15 stability. After the performance of DoE and its statistical analysis, the most stable PR-15 formulation was in histidine buffer, at pH 7.813, supplemented with 0.0904 % Tween® 20 and 8.121 mM methionine (**Figures 59–61**). However, a pH variation from ~7.55 – 7.9 with a Tween® 20 concentration from ~0.09 – 0.1 % is possible without exceeding specified maxima of the responses if methionine concentration is ~8 mM and a variation of methionine concentration from ~3 – 15 mM with a Tween® 20 concentration from ~0.09 – 0.1 % is feasible without altering formulation stability if pH is about 7.8. For the imidazole group of histidine a pK_a value of about 6.5 was calculated for a 50 mM histidine buffer at the favored storage temperature of 4 °C [201] and buffers are most effective in the range pH = $pK_a \pm 1$. Hence, a pH value around the center (pH 7.5) is preferred for PR-15 formulation in order to maintain buffer capacity. Choosing a pH value near 7.5 requires a high Tween® 20 concentration and a methionine concentration around the center (**Figures 59-61**). Consequently, we suggest to formulate PR-15 at pH 7.55 with 0.0904 % Tween® 20 and 8.121 mM methionine.

Moreover, PR-15 revealed to degrade by cleavage in the hinge region forming the so-called 90 kDa band containing the monomer and the C-terminus (**Figures 17** and **18, Table 13**). We hypothesize that in the chosen formulation buffers (pH 5-8) the cleavage is located in the upper hinge region ^{256}SCDKTHT (**Figure 17A**) between ^{258}Asp and ^{259}Lys (^{256}SCDKTHT) or ^{261}His and ^{262}Thr (^{256}SCDKTHT). This so-called fragmentation is temperature and pH dependent. At acidic pH (≤ pH 5) the cleavage between ^{258}Asp and ^{259}Lys (^{256}SCDKTHT) by a nucleophilic attack of the ionized side-chain of carboxylate on the protonated carbonyl carbon of the peptide bond followed by the release of the Lys [182, 202] is considerable and at basic pH (> pH 8) the cleavage between ^{256}Ser and ^{257}Cys (^{256}SCDKTHT) by β-elimination [203, 204] is dominant whereas at neutral pH (pH 5–7) cleavage preferably occurs between ^{258}Asp and ^{259}Lys and ^{261}His and ^{262}Thr (^{256}SCDKTHT) [182].

Fragmentation may not only reduce bioactivity of PR-15, but also change aggregation rates and thereby increase immunogenicity of PR-15 formulation. Regarding the results of the DoE study the usage of histidine buffer showed reduced fragmentation rates and aggregation rates compared to the usage of phosphate buffer. The issue of buffer-dependent fragmentation was observed earlier by Salinas et al. [205]. In their study the authors postulated a decrease of antibody flexibility through histidine and thereby a decrease of solvent accessibility and hydrolysis rate. Additionally, Katayama et al. [206] showed that thermal stability of interferon-tau was significantly enhanced by the usage of histidine buffer, compared to phosphate buffer. Histidine was found to stabilize the native state of interferon-tau through non-specific binding and thereby reducing the aggregation rate [206]. In our case, the mechanism behind PR-15 stabilization through histidine was not elucidated and further trials would be necessary to manifest the stabilizing mechanism. Vibrational spectroscopy methods such as FTIR or Raman would be useful tools for investigating protein-excipient interactions [207]. However, a significant enhancement of thermal stability of PR-15 by the usage of histidine instead of phosphate buffer was demonstrated and the adjustment of the former PR-15 formulation by advanceCOR is recommended. Additionally, a long term stability study at 5 °C ± 3 °C for a minimum of 12 months and an accelerated stability study at 25 °C ± 2°C for at least 6 months have to be conducted in order to test the new formulation buffer.

Bioconjugation is a versatile tool for the modification of biomolecules that gained more and more attention over the last years because of the various application possibilities.
Conventional EDC/NHS chemistry is often used for the conjugation of biomaterials with biologics [208]. Unfortunately, inter- and intramolecular crosslinks of the biomaterial as well as within the biologic are an unavoidable disadvantage of this approach. The resulting heterogeneity and covalent aggregates that are inevitable constitute an immunological safety risk for biomedical applications [87]. Another popular bioconjugation reaction is the so-called click reaction [103]. The click reaction or copper catalyzed 1,3-dipolar azide alkyne cycloaddition offers the possibility for site-directed bioconjugation with maximal spatial control and without disadvantages such as inter- and intramolecular crosslinks and immunogenicity because of the heterogeneous product outcome. EDC/NHS chemistry offers simple and rapid modification of nearly every protein, as there are various carboxyl and amino groups available in the protein structure. In contrast, unnatural alkyne or azido groups have to be incorporated into the protein of interest before the performance of click reaction. During this work we chose three strategies of incorporating alkyne or azido groups into the protein structure. First, we incorporated azido groups into SF by the usage of diazonium coupling as described earlier by Murphy et al. with slight modification [93]. Second, we chose FGF-2 as model protein because it bears two unpaired cysteine residues pointing outwards and thus being accessible for thiol PEGylation reaction with an alkyne PEG [209]. Third, we incorporated

the unnatural amino acid propargyl-L-lysine (plk) into IGF-I through genetic engineering during protein translation [210].

SF is predominantly composed of non-reactive amino acids such as alanine and glycine and comprises not many possibilities for functionalization as there exist just few aspartic acid, glutamic acid and tyrosine residues [92]. Diazonium coupling chemistry opens incorporation of functional groups such as amines, alkynes, azides, carboxylic acids or sulfonic acids. Hereby, the 280 tyrosines per SF molecule or rather 1 % of them were modified with a diazonium salt to provide an azido group resulting in an azobenzene derivative with azide functionality as described earlier [87, 211, 212]. The successful modification of SF by diazonium coupling chemistry was visible by a change of the color from colorless to yellow. Additionally, the azobenzene chromophore was verified by UV spectroscopy showing the azobenzene peak at 352 nm with a shoulder at 410 nm (data not shown).

In order to incorporate alkyne functionalities into FGF-2, we chose one favored bioconjuation reaction, the PEG conjugation or PEGylation, targeting free thiols via thiol-reactive iodoacetamide. Conjugating biologics to PEG not only prolongs their half-life but also increases their solubility and decreases their immunogenicity [213]. During synthesis of PEG-protein-conjugates the degree of PEGylation, meaning the number of PEG molecules per protein, and the position of the PEG in the sequence of the protein need to be tightly controlled [39]. Otherwise, random PEGylation of proteins yield isomer mixtures of multiple PEGylated proteins complicating protein purification and resulting into limitations such as potential single isomer toxicity or reproducibility of isomer ratios during manufacturing [214]. Mostly, lysine residues are the target sites used for PEGylation resulting in heterogeneous proteins as there exist more than one lysine residue in the backbone of most proteins. FGF-2 contains 13 lysines, 1 in the receptor binding site (residues 119-128) [215] and 3 in the heparin binding site [216]. Hence, lysine PEGylation would most likely negatively influence receptor as well as heparin binding of FGF-2. In order to reduce the potential target sites and the probability of reduced bioactivity, we chose the amino acid cysteine as target site for FGF-2 and used thio-reactive iodoacetamido-PEG for PEGylation. FGF-2 contains 4 cysteine residues, but no disulfide bridges [188]. Two of the cysteine residues are pointing outwards and two into the protein core and thus are not accessible for PEGylation reaction [188, 216]. Hence, the synthesis of 3 isoforms of PEGylated FGF-2 (monoPEGylated at Cys^{82}, monoPEGylated at Cys^{100}, diPEGylated at Cys^{82} and Cys^{100}) was possible. The results reported here within confirmed this assumption, either one or two PEGs were found per FGF-2 molecule (**Figures 63** and **66, Supplementary Figures 6** and **8**). Moreover, none of these cysteine residues is located either in the heparin binding site or in the receptor binding site, and thus no interactions with receptors are expected for these cysteines [215, 216]. However, heparin affinity of FGF-2 was reduced through PEGylation with long PEG chains with a molecular weight of approximately 10 kDa displaying a faster elution from heparin column during purification (**Supplementary Figure 7**) and bioactivity

was decreased ~ 4-fold (**Figure 68C**) [217]. However, PEGylated FGF-2 was found to bind to heparin, showed moderate bioactivity and exhibited superior heat stability compared to native FGF-2 (**Figure 68B**). Besides, an RP-HPLC method was established to separate FGF-2 from PEGylated FGF-2 and to quantify the purity of PEGylated FGF-2 samples, yielding PEGylated FGF with an overall purity of 89–98 % (**Figure 67**).

After functionalization of SF with azido groups and successful decoration of FGF-2 with alkyne-PEG, click as well as EDC/NHS chemistry were performed in solution with the aim to compare these two common coupling reactions.

However, we were not able to expose the mentioned advantages of click chemistry in relation to EDC/NHS chemistry. On the one hand, the reaction of PEGylated FGF-2 with SF in solution resulted in substantial amounts of side products by both click and EDC/NHS chemistry procedures. On the other hand, coupling efficiency of the FGF-2 to SF was very low as demonstrated by Western Blot analysis (**Figure 69**). The remaining uncoupled PEG-FGF-2 was adsorbed to SF and could not be removed through extensive dialyzing. FGF-2 is a basic protein with an isoelectric point of 9.6 resulting in a net positive charge under physiological conditions [215]. In contrast, SF with an isoelectric point of ~4 bears a net negative charge at pH 7.4 [218], and thus electrostatic interactions between FGF-2 and SF are unavoidable under the chosen reaction conditions. Hence, reaction conditions were optimized to improve conjugation outcome and to remove uncoupled FGF-2. Further optimization trials were performed by the usage of microspheres instead of SF solution. The aim was to remove adsorbed FGF-2 through extensive washing of the microspheres or to prevent FGF-2 adsorption by blocking the microspheres with BSA, coupling at high salt concentrations or at different pH values in order to reduce electrostatic interactions between the microspheres and FGF-2. Even the change from SF to sepharose or PMMA microspheres, respectively, did not prevent FGF-2 adsorption. The carboxyl groups of sepharose as well as carboxylated PMMA with a pK_a value of ~4.9 are likewise negatively charged under all tried reaction conditions. So we were not able to differentiate the measured bioactivities of coupled and adsorbed FGF-2 during proliferation assays, and hence we could not distinguish between EDC/NHS coupled and clicked FGF-2. In order to distinguish between covalently coupled and adsorbed FGF-2, cell culture trials such as bone tissue engineering over 28 days would be required.

In our case bioorthogonal click reaction was performed at one or two positions in PEGylated FGF-2, resulting into product heterogeneity. The approach of genetically introducing unnatural amino acids into the protein of interest at one predefined site prevents product heterogeneity as demonstrated before with myoglobin [210], ubiquitin [219], IL-4 [220] and FGF-2 [189], enabling site-directed protein modification.

Protein delivery is beneficial in the field of regenerative medicine. In order to engineer damaged tissue, different growth factors have to be present at the site of injury to induce cell migration,

adhesion, proliferation, growth as well as differentiation. Unfortunately, there is a lack of appropriate delivery methods that mimic physiological delivery of growth factors and administration of growth factors via injection, intravenously or directly into the tissue of interest, is often ineffective because of the short *in vivo* half-live or causes severe side effects because of high doses, respectively. TGF-β, for example, is secreted as inactive large latent complex (LLC) with latent transforming growth factor β binding protein-1 (LTBP-1) and latency associated peptide (LAP) *in vivo* [221]. Through this LCC that is bound to fibronectin and fibrillin in the ECM via LTBP-1 bioactivity of TGF-β is regulated and somehow preserved. Integrins, proteases and deglycosidases are potential TGF-β activators that release TGF-β from LCC and enable receptor binding if required (**Figure 88**) [222].

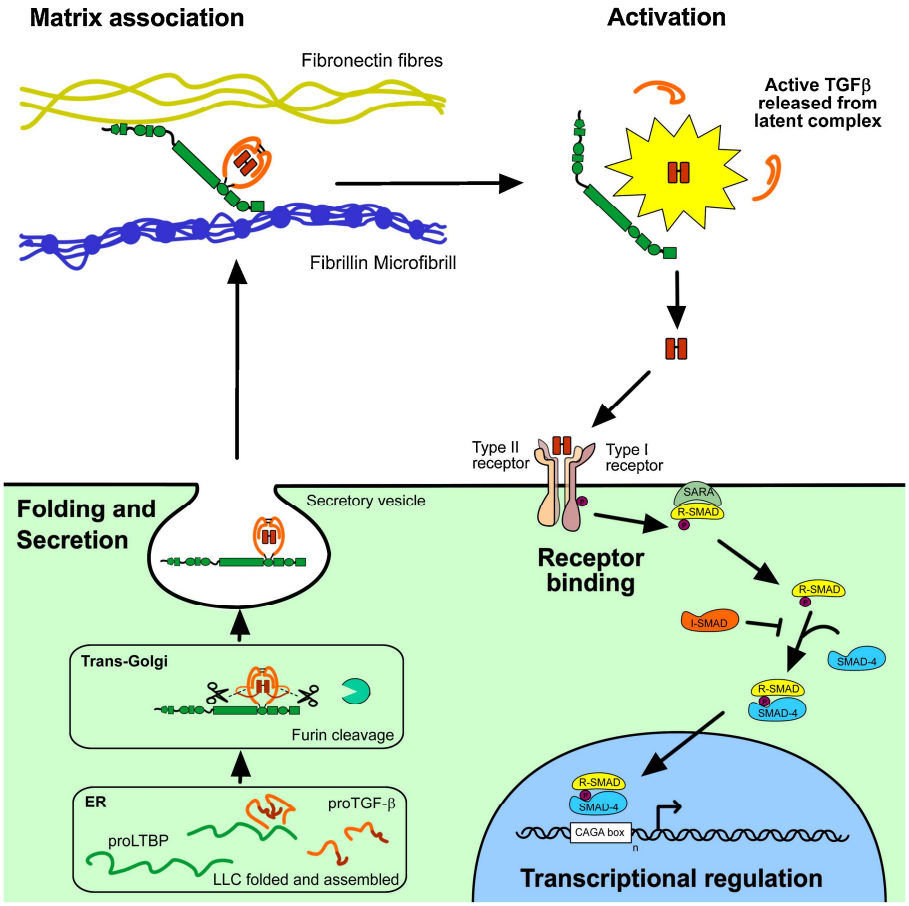

Figure 88: Simplified scheme of TGF-β secretion and signaling. Reprinted from [222], Copyright (2013), with permission from Elsevier.

Site-directed immobilization of the corresponding growth factors to biomaterials with a structure and geometry similar to the engineered tissue is probably one strategy to contribute to this limitation. This concept aimed at the development of a multifunctionalized osteochondral implant for the regeneration of cartilage defects. In order to develop such osteochondral plugs with postulated better healing outcome, the growth factors IGF-I, TGF-β3 and BMP-2 need to be presented spatially restricted on the construct to develop cartilage and bone simultaneously in close

proximity to each other. Such an implant has to meet some requirements like biocompatibility, biodegradability over an appropriate time scale, adequate mechanical properties, a surface that allows cell adhesion and high porosity with an interconnected pore system to allow cell infiltration, nutrient as well as oxygen transport [132]. We chose SF as biomaterial for the implant preparation as it possesses the mentioned qualifications [223] and developed scaffolds with an interconnected pore system. In order to generate bone and cartilage on one scaffold with ideal geometry for each tissue, we developed porous SF scaffolds with two different porosities (**Figure 78**). The suitability of this biphasic scaffold to induce osteogenesis as well as chondrogenesis was assessed in cell culture trials using BMSCs (**Figures 82, 83** and **86**). In further trials, for cartilage tissue engineering the side with the larger pores of the biphasic SF scaffold is intended to be biofunctionalized with IGF-I and TGF-β3, whereas for bone tissue engineering the side with the smaller pores is designated for biofunctionalization with BMP-2 and TGF-β3. The spatially restricted presentation of such growth factors requires chemical modification in order to couple them covalently and site-directed on the SF scaffold. The incorporation of an alkyne or an azido group in the backbone of IGF-I, TGF-β3 as well as BMP-2 by genetic engineering and the equipment of the SF scaffold with azido and alkyne groups, each on opposing sides, represent the ideal solution to finally biofunctionalize the biphasic SF scaffold by click reaction in a site-directed pattern. Following the approach of genetically introducing unnatural amino acids into the protein of interest [210], we designed an IGF-I mutant bearing alkyne functionality as the PEGylation of cysteines or lysines was ineligible for IGF-I. PEGylation of cysteines was not possible because all the 6 occurring cysteines built disulfide bridges [224, 225]. PEGylation of the 3 lysines (Lys^{27}, Lys^{65}, Lys^{68}) was no strategy to pursue due to the formation of a heterologous mixture of randomly PEGylated IGF-I. Previous studies with lysine based PEGylated IGF-I (Lys^{27}, Lys^{65} or Lys^{68}) showed a decreased short-term activity in cell migration with an influence on the P13K/AKT pathway but a maintained long term activity on cell proliferation, myoblast differentiation or motor neuron survival, meaning no or marginally influence on the ERK/MAPK pathway [226]. As the activation of the P13K pathway was supposed to be required for proteoglycan synthesis by chondrocytes [116], the loss of P13K activation would not be acceptable for cartilage tissue engineering. Until now, the role of the 3 lysines in receptor binding is discussed controversially, Zhang et al. postulated that the positive charged amino acids Lys^{27}, Lys^{65} and Lys^{68} play an important role in receptor binding shown by a 10 to 15-fold loss of receptor binding affinity after exchanging the 3 lysines to alanine (Ala) [227]. In contrast, Bayne et al. reported that the deletion of the D-domain has no considerable effect on receptor binding of IGF-I [228]. Moreover, Sivaramakrishnan et al. reported a 10-fold reduced binding affinity of IGF-I to the IGF binding proteins (IGFBP-1–6) through lysine PEGylation (Lys^{27}, Lys^{65}, Lys^{68}) [229] having an influence on IGF-I half-life and tissue distribution [230]. However, steric hindrance by the large PEG chain seems to be the most appropriate and logical explanation for the reduced binding affinity of

PEGylated IGF-I to the receptor or to the binding proteins, respectively. One strategy to maintain native binding affinity of IGF-I after PEGylation is the incorporation of the PEG chain through a cleavable linker. Thereby, we benefit from PEGylation concerning *in vivo* have-life but we have no disadvantages impacting bioactivity because the long PEG chain is already cleaved off before receptor binding. The approach from Nguyen et al. for the incorporation of aliphatic azides and alkynes into proteins via the PylRS/$tRNA_{CUA}$ pair is another strategy to address this limitation [210]. Consequently, an appropriate position in IGF-I sequence was identified for the incorporation of unnatural amino acids bearing alkyne or azide functionality without affecting IGF-I potency. Bayne et al. showed that Tyr^{24} and the residues 28–37 of IGF-I play a critical role in IGF type I receptor binding [228]. As Lys^{27} is located in close proximity to these residues involved in receptor binding, this lysine was excluded for modification. The two residual lysines (Lys^{65} and Lys^{68}) are located in the D-domain of IGF-I and thus outside the IGF type I receptor binding site [214], even if there exist converse opinions in literature [227, 231]. So we chose to exchange Lys^{65} and engineered one IGF-I mutant containing the pyrrolysine analogue plk at position 65. Plk-IGF-I expression was challenging as the yields were very low (**Figures 75** and **77**). Hence, future optimization of plk-IGF-I expression is necessary in order to express plk-IGF-I in a sufficient amount before continuing with site-directed bioconjugation through click chemistry.
Following a similar approach, Tabisz et al. introduced propargyl-L-lysine into BMP-2 at position 3 and obtained a BMP-2 variant with alkyne functionality without altered receptor binding properties and with maintained bioactivity [232]. By the usage of this site-directed approach the orientation of the coupled growth factor is controlled, and thus the receptor binding is improved and consequently growth factor signaling is maximized after immobilization (**Figure 89**) [232]. Hence, clickable BMP-2 is available for developing osteochondral implants. However, for spatial restricted presentation of the growth factors an azide bearing unnatural amino acid such as (S)-2-amino-6-((2-azidoethoxy)carbonylamino) hexanoic acid (Alk) has to be incorporated in BMP-2 or IGF-I as already done for eGFP [150], IL-4 [220] and myoglobin [210] in order to click the two growth factors at different sides of the SF scaffold.

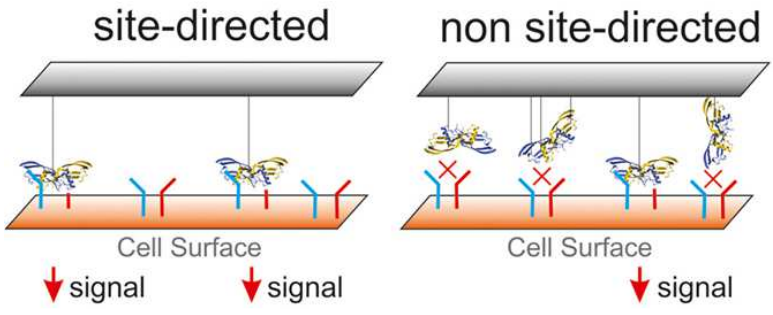

Figure 89: Schematic illustration of difference between site-directed and non site-directed immobilization. Reprinted with permission from [232]. Copyright (2017) American Chemical Society.

Last but not least, we intended to immobilize TGF-β3 on the SF scaffold. For the initiation and maintenance of chondrogenesis TGF-β is essential in an appropriate concentration [233]. To date the optimal TGF-β concentration for *in vivo* chondrogenesis has not been systematically determined, however, 10 ng/mL TGF-β are mostly used for *in vitro* chondrogenesis [109, 233]. Park et al. mixed TGF-β3 physically conjugated with chondroitin sulfate in scaffolds [234], Bian et al. encapsulated TGF-β3 in alginate microspheres within hyaluronic acid hydrogels [235], Morille et al. incorporated TGF-β3 in PLGA-P188-PLGA microcarriers [236] and Bertolo et al. even crosslinked TGF-β1 with EDC/NHS chemistry to collagen microcarriers [86] in order to enhance MSC chondrogenesis. However, the development of TGF-β releasing matrices providing an appropriate TGF-β concentration for chondrogenesis is challenging. Since half-lives of growth factors are short, their covalent immobilization is one strategy to control their local bioavailability. TGF-β3s dimeric structure contains 9 cysteines per monomer building 1 intermolecular and 4 intramolecular disulfide bridges [237]. Hence, its expression in bacterial expression systems is extremely difficult because of its complex secondary and tertiary structure. US Patent 6,057,430 [238] described the expression of biologically active dimeric TGF-β3 in *E. coli* but there was no consideration about success of proper refolding, yield and bioactivity. TGF-β3 expression in *E. coli* presumably results into the proper primary structure but correct folding is still a challenge. Moreover, TGF-β3 is poorly soluble and tends to form large aggregates at physiological pH [239]. As a consequence, we did not venture to express TGF-β3 with its complex structure, as incorporation of unnatural amino acids with specific functional groups possibly fails. Moreover, no free cysteine is present for cysteine PEGylation and lysine PEGylation results in heterologous product outcome as there exist 4 lysines per monomer. Finally, we chose EDC/NHS chemistry for TGF-β3 immobilization despite the number of carboxyl and amino groups bearing amino acids (4 lysines, 5 aspartic acids, 6 glutamic acids per monomer) [240] and approved reduced bioactivity caused by the formation of crosslinks. TGF-β1 [86] as well as other growth factors like VEGF [85] and BMP-2 [84] have been successfully immobilized via EDC/NHS chemistry on matrices for tissue engineering with maintained bioactivity. However, a certain degree of loss of bioactivity will certainly occur, caused by inter- and intramolecular crosslinks of the growth factor and the concomitant inaccessibility to receptors.

Here, TGF-β3 was covalently coupled to biocompatible and biostable PMMA beads in the presence as well as in the absence of coupling reagents with the aim to retain its bioactivity. Subsequently, performed luciferase assay confirmed bioactivity of both covalent coupled and adsorbed TGF-β3 on biomaterials (**Figure 81**). Moreover, we established an ELISA method for the quantification of immobilized TGF-β3 in order to test the influence of EDC/NHS coupling on bioactivity. The total amount of TGF-β3 immobilized on the beads was determined and coupling efficiency was calculated. As expected, coupling efficiency of TGF-β3 with EDC/NHS chemistry (80.6 ± 16.3 %) was significantly higher than without coupling reagents (13.0 ± 4.7 %) (**Figure 80**). With these

results obtained from ELISA we were able to compare the impact of coupled and adsorbed TGF-β3 for cartilage tissue engineering. No difference between covalent immobilized and adsorbed TGF-β3 regarding relative luciferase activities was found, confirming maintained bioactivity (**Figure 81A**). However, we detected a loss of bioactivity presumably caused by the formed crosslinks becoming evident when total and active amount of TGF-β3 on the beads were compared (**Figure 81B** and **C**). Furthermore, we used BMSCs and seeded them together with TGF-β3 coupled beads on SF scaffolds in order to drive them to the chondrogenic lineage. We tested exogenous supplementation of 10 ng/mL TGF-β3, as frequently used for *in vitro* MSC chondrogenesis [241], in comparison to 78 ng covalent coupled TGF-β3 per scaffold and 13 ng adsorbed TGF-β3 per scaffold. The results of our histological and immunohistochemical studies after 21 days in culture showed GAG as well as collagen I and II accumulation to a variable extent (**Figure 84**). All samples supplemented with exogenous TGF-β3 showed strong staining for GAG, collagen I and II, while in the absence of TGF-β3 no staining was visible with a just weak staining for collagen I. Covalent coupled TGF-β3 samples showed stronger staining for GAG and collagen II than adsorbed TGF-β3 but less staining for collagen I. After 21 days in culture a significant GAG as well as collagen deposition compared to blank beads was detected by biochemical assays, but there was no significant differences between covalent coupled TGF-β3 and adsorbed TGF-β3 beads (**Figure 85**). qRT-PCR of gene expression from BMSCs was used to assess cartilage-specific marker genes for investigating the development of fibrocartilaginous and hypertrophic cartilage instead of hyaline cartilage [242] (**Figure 87**). The chondrogenic marker genes aggrecan, collagen II, and Sox9 were upregulated for exogenous supplemented as well as covalent coupled TGF-β3 with statistical significance compared to blank, whereas all three marker genes were downregulated for adsorbed TGF-β3 (**Figure 87A–C**). In contrast, the fibrocartilage marker gene collagen I was upregulated by adsorbed as well as exogenous TGF-β3, for exogenous TGF-β3 with statistical significance, and the hypertrophic marker gene collagen X was upregulated by exogenous supplemented TGF-β3 with statistical significance (**Figure 87D** and **E**). Thus, we draw the conclusion that local delivery of TGF-β3 delivery via PMMA beads prevented formation of fibrocartilaginous and hypertrophic cartilage compared to exogenous supplemented TGF-β3. Even so, at day 21 all chondrogenic marker genes were downregulated by adsorbed TGF-β3 indicating that the entire amount of adsorbed TGF-β3 had already been diffused in the culture medium and removed by media exchanges (**Figure 87**). These results led to the conclusion that covalent immobilized TGF-β3 is superior towards exogenous TGF-β3 supplementation and even towards adsorbed TGF-β3 for articular hyaline cartilage formation despite the demonstrated constraint of bioactivity caused by inter- and intramolecular crosslinks. The covalent coupling of the growth factor to biostable PMMA beads prevents diffusion and loss of the growth factor maintaining a stable and consistent TGF-β3 concentration in the target area. Additionally, TGF-β3s short *in vivo* half-life of smaller than 30 minutes [233] was apparently prolonged through covalent coupling. It is known that

TGF-β3 is internalized with its receptor via clathrin-mediated pathway for promoting signaling or via caveolin-mediated pathway for receptor degradation [243]. Presumably, immobilized TGF-β3 cannot be internalized after recognition by the TGF-receptor, and thus intracellular signaling pathways are activated permanently as already described before by Ito et al. as “artificial juxtacrine stimulation” [244]. The so-called down-regulation meaning the degradation of TGF-β receptors and thereby the turnoff of TGF-β3 signal does not take place without internalization [245]. Our findings confirmed maintenance of growth factors bioactivity. Anyway, future studies are required for evaluating the optimal concentration of covalently coupled TGF-β3 for articular hyaline cartilage formation and to investigate if internalization is needed for full TGF-β3 signaling. This question needs to be addressed for the other growth factors BMP-2 [119], IGF-I [246] and FGF-2 [247] as well.

Coupling of growth factors via cleavable linkers can be one efficient possibility to ascertain the required endocytosis. During osteoarthritis or other pathophysiological conditions matrix metalloproteinases (MMPs) are overexpressed at disease site [248, 249]. Hence, for further assimilation of growth factor delivery to physiological situation a protease cleavable linker can be coupled between the biomaterial and the growth factor developing a bioresponsive delivery system as already shown for Myostatin [250]. The combination of cleavable and non-cleavable linkers provides beneficial effects from both immobilized as well as from soluble growth factors at the site of action.

Due to the positive outcome during cartilage tissue engineering, the PMMA beads with immobilized TGF-β3 are suitable for the development of osteochondral grafts in the future.

As TGF-β3 plays a pivotal role in chondrogenesis [241] as well as in osteogenesis [251], the distribution of PMMA beads with immobilized TGF-β3 in the pores of the entire biphasic SF scaffold is beneficial. On the one hand, TGF-β3 stimulates chondrocyte proliferation and inhibits chondrocyte hypertrophy, and on the other hand, TGF-β3 promotes osteoblast terminal maturation [122, 252].

Finally, almost all building blocks are completed to enable the formation of osteochondral implants by combining the protein modification and coupling methods investigated during this work. Expression of clickable IGF-I has to be optimized in order to increase the yield of clickable IGF-I in the future. Furthermore, the incorporation of (S)-2-amino-6-((2-azidoethoxy)carbonylamino) hexanoic acid (Alk) instead of propargyl-L-lysine (Plk) at position 65 of IGF-I is envisioned in order to have one alkyne bearing growth factor (BMP-2) and one azide bearing growth factor (IGF-I) for spatial restricted presentation of the required growth factors on SF scaffolds. Additionally, one scaffold side will be prepared with azido-SF (small pores) and the other side with alkyne-SF (large pores) in order to couple BMP-2 and IGF-I spatial restricted on the side with the appropriate pore size for bone or cartilage, respectively (**Figure 5**).

This approach of local growth factor presentation on osteochondral implants with site-directed immobilized growth factors (IGF-I and BMP-2) and not site-directed immobilized growth factors (TGF-β3) may improve the maintenance of biological activity of the applied growth factors through prevention of diffusion processes and consequently circumvents the injection of high doses of such growth factors, which causes severe side effects.

7 References

[1] S. Mitragotri, P. A. Burke, and R. Langer, "Overcoming the challenges in administering biopharmaceuticals: formulation and delivery strategies," *Nat Rev Drug Discov*, vol. 13, no. 9, pp. 655-72, Sep, 2014.

[2] G. Walsh, "Biopharmaceutical benchmarks 2014," *Nat Biotechnol*, vol. 32, no. 10, pp. 992-1000, Oct, 2014.

[3] S. S. Usmani, G. Bedi, J. S. Samuel, S. Singh, S. Kalra, P. Kumar, A. A. Ahuja, M. Sharma, A. Gautam, and G. P. S. Raghava, "THPdb: Database of FDA-approved peptide and protein therapeutics," *PLoS One*, vol. 12, no. 7, pp. e0181748, 2017.

[4] P. J. Carter, "Introduction to current and future protein therapeutics: a protein engineering perspective," *Exp Cell Res*, vol. 317, no. 9, pp. 1261-9, May 15, 2011.

[5] R. Anour, "Biosimilars versus 'biobetters'—a regulator's perspective," *Generics and Biosimilars Initiative Journal*, vol. 3, no. 4, pp. 166-167, 2014.

[6] S. Hermeling, D. J. A. Crommelin, H. Schellekens, and W. Jiskoot, "Structure-Immunogenicity Relationships of Therapeutic Proteins," *Pharmaceutical Research*, vol. 21, no. 6, pp. 897-903, 2004.

[7] D. S. Pisal, M. P. Kosloski, and S. V. Balu-Iyer, "Delivery of therapeutic proteins," *J Pharm Sci*, vol. 99, no. 6, pp. 2557-75, Jun, 2010.

[8] B. J. Bruno, G. D. Miller, and C. S. Lim, "Basics and recent advances in peptide and protein drug delivery," *Ther Deliv*, vol. 4, no. 11, pp. 1443-67, Nov, 2013.

[9] J. D. Bos, and M. M. H. M. Meinardi, "The 500 Dalton rule for the skin penetration of chemical compounds and drugs," *Experimental Dermatology*, vol. 9, no. 3, pp. 165-169, 2000.

[10] T. Caon, L. Jin, C. M. Simoes, R. S. Norton, and J. A. Nicolazzo, "Enhancing the buccal mucosal delivery of peptide and protein therapeutics," *Pharm Res*, vol. 32, no. 1, pp. 1-21, Jan, 2015.

[11] J. L. Richardson, and L. Illum, "The vaginal route of peptide and protein drug delivery," *Advanced Drug Delivery Reviews*, vol. 8, no. 2-3, pp. 341-366, 1992.

[12] G. Scheuch, and R. Siekmeier, "Novel approaches to enhance pulmonary delivery of proteins and peptides," *J Physiol Pharmacol*, vol. 58 Suppl 5, no. Pt 2, pp. 615-25, Nov, 2007.

[13] I. Schultz, F. Vollmers, T. Lühmann, J.-C. Rybak, R. Wittmann, K. Stank, H. Steckel, B. Kardziev, M. Schmidt, P. Högger, and L. Meinel, "Pulmonary Insulin-like Growth Factor I Delivery from Trehalose and Silk-Fibroin Microparticles," *ACS Biomaterials Science & Engineering*, vol. 1, no. 2, pp. 119-129, 2015.

[14] Jitendra, P. K. Sharma, S. Bansal, and A. Banik, "Noninvasive routes of proteins and peptides drug delivery," *Indian J Pharm Sci*, vol. 73, no. 4, pp. 367-75, Jul, 2011.

[15] M. Mackay, J. Phillips, and J. Hastewell, "Peptide drug delivery: Colonic and rectal absorption," *Advanced Drug Delivery Reviews*, vol. 28, no. 2, pp. 253-273, 1997.

[16] B. K. Davis, "Control of diabetes with polyacrylamide implants containing insulin," *Experientia*, vol. 28, no. 3, pp. 348-348, 1972.

[17] R. Langer, and J. Folkman, "Polymers for the sustained release of proteins and other macromolecules," *Nature*, vol. 263, no. 5580, pp. 797-800, 1976.

[18] R. Vaishya, V. Khurana, S. Patel, and A. K. Mitra, "Long-term delivery of protein therapeutics," *Expert Opin Drug Deliv*, vol. 12, no. 3, pp. 415-40, Mar, 2015.

[19] A. A. Kaspar, and J. M. Reichert, "Future directions for peptide therapeutics development," *Drug Discov Today*, vol. 18, no. 17-18, pp. 807-17, Sep, 2013.

[20] V. R. Sinha, and A. Trehan, "Biodegradable microspheres for protein delivery," *Journal of Controlled Release*, vol. 90, no. 3, pp. 261-280, 2003.

[21] A. D. Bangham, and R. W. Horne, "Negative staining of phospholipids and their structural modification by surface-active agents as observed in the electron microscope," *Journal of Molecular Biology*, vol. 8, no. 5, pp. 660-IN10, 1964.

[22] L. Sercombe, T. Veerati, F. Moheimani, S. Y. Wu, A. K. Sood, and S. Hua, “Advances and Challenges of Liposome Assisted Drug Delivery,” *Front Pharmacol*, vol. 6, pp. 286, 2015.
[23] J. Swaminathan, and C. Ehrhardt, “Liposomal delivery of proteins and peptides,” *Expert Opin Drug Deliv*, vol. 9, no. 12, pp. 1489-503, Dec, 2012.
[24] J. S. Powell, D. J. Nugent, J. A. Harrison, A. Soni, A. Luk, H. Stass, and E. Gorina, “Safety and pharmacokinetics of a recombinant factor VIII with pegylated liposomes in severe hemophilia A,” *J Thromb Haemost*, vol. 6, no. 2, pp. 277-83, Feb, 2008.
[25] R. Yatuv, M. Robinson, I. Dayan-Tarshish, and M. Baru, “The use of PEGylated liposomes in the development of drug delivery applications for the treatment of hemophilia,” *International Journal of Nanomedicine*, vol. 5, pp. 581-591, 2010.
[26] R. L. Dunn, J. P. English, D. R. Cowsar, and D. P. Vanderbilt, "Biodegradable in-situ forming implants and methods of producing the same," US 4938763 A, Google Patents, 1990.
[27] A. Katdare, and M. Chaubal, *Excipient Development for Pharmaceutical, Biotechnology, and Drug Delivery Systems*: CRC Press, 2006.
[28] R. L. Dunn, J. S. Garrett, H. Ravivarapu, and B. L. Chandrashekar, "Polymeric delivery formulations of leuprolide with improved efficacy," US 20100226954 A1, Google Patents, 2010.
[29] R. Perez-Marrero, and R. C. Tyler, “A subcutaneous delivery system for the extended release of leuprolide acetate for the treatment of prostate cancer,” *Expert Opin Pharmacother*, vol. 5, no. 2, pp. 447-57, Feb, 2004.
[30] M. Oak, and J. Singh, “Controlled delivery of basal level of insulin from chitosan-zinc-insulin-complex-loaded thermosensitive copolymer,” *J Pharm Sci*, vol. 101, no. 3, pp. 1079-96, Mar, 2012.
[31] A. Linderholm, and S. M. Chamow, “Immunoglobulin Fc-Fusion Proteins Part 1: Their Design and Manufacture,” *Bioprocess Intl.*, vol. 12, no. 9, 2014.
[32] S. Schulte, “Half-life extension through albumin fusion technologies,” *Thrombosis Research*, vol. 124, pp. S6-S8, Dec, 2009.
[33] D. Keefe, M. Heartlein, and S. Josiah, “Transferrin Fusion Protein Therapies: Acetylcholine Receptor-Transferrin Fusion Protein as a Model,” pp. 191-199, 2013.
[34] W. R. Strohl, “Fusion Proteins for Half-Life Extension of Biologics as a Strategy to Make Biobetters,” *BioDrugs*, vol. 29, no. 4, pp. 215-39, Aug, 2015.
[35] D. M. Czajkowsky, J. Hu, Z. Shao, and R. J. Pleass, “Fc-fusion proteins: new developments and future perspectives,” *EMBO Mol Med*, vol. 4, no. 10, pp. 1015-28, Oct, 2012.
[36] A. Abuchowski, J. R. McCoy, N. C. Palczuk, T. van Es, and F. F. Davis, “Effect of covalent attachment of polyethylene glycol on immunogenicity and circulating life of bovine liver catalase,” *J Biol Chem*, vol. 252, no. 11, pp. 3582-6, Jun 10, 1977.
[37] S. Jevsevar, M. Kunstelj, and V. G. Porekar, “PEGylation of therapeutic proteins,” *Biotechnol J*, vol. 5, no. 1, pp. 113-28, Jan, 2010.
[38] S. N. S. Alconcel, A. S. Baas, and H. D. Maynard, “FDA-approved poly(ethylene glycol)–protein conjugate drugs,” *Polymer Chemistry*, vol. 2, no. 7, pp. 1442, 2011.
[39] D. Pfister, and M. Morbidelli, “Process for protein PEGylation,” *J Control Release*, vol. 180, pp. 134-49, Apr 28, 2014.
[40] H. A. Lagasse, A. Alexaki, V. L. Simhadri, N. H. Katagiri, W. Jankowski, Z. E. Sauna, and C. Kimchi-Sarfaty, “Recent advances in (therapeutic protein) drug development,” *F1000Res*, vol. 6, pp. 113, 2017.
[41] J. M. Harris, N. E. Martin, and M. Modi, “Pegylation: a novel process for modifying pharmacokinetics,” *Clin Pharmacokinet*, vol. 40, no. 7, pp. 539-51, 2001.
[42] L. Santucci, A. Mencarelli, B. Renga, G. Pasut, F. Veronese, A. Zacheo, A. Germani, and S. Fiorucci, “Nitric oxide modulates proapoptotic and antiapoptotic properties of chemotherapy agents: the case of NO-pegylated epirubicin,” *FASEB J*, vol. 20, no. 6, pp. 765-7, Apr, 2006.
[43] D. C. Roopenian, and S. Akilesh, “FcRn: the neonatal Fc receptor comes of age,” *Nat Rev Immunol*, vol. 7, no. 9, pp. 715-25, Sep, 2007.

[44] R. E. Kontermann, “Strategies for extended serum half-life of protein therapeutics,” *Curr Opin Biotechnol*, vol. 22, no. 6, pp. 868-76, Dec, 2011.
[45] F. Unverdorben, “Immunoglobulin-based strategies for half-life extension of recombinant proteins Immunglobulin-basierte Strategien zur Verlängerung der Halbwertszeit rekombinanter Proteine Felix Unverdorben,” 2015.
[46] D. J. Capon, S. M. Chamow, J. Mordenti, S. A. Marsters, T. Gregory, H. Mitsuya, R. A. Byrn, C. Lucas, F. M. Wurm, J. E. Groopman, and et al., “Designing CD4 immunoadhesins for AIDS therapy,” *Nature*, vol. 337, no. 6207, pp. 525-31, Feb 9, 1989.
[47] "EU Clinical Trials Register - European Medcines Agency," 24.08.2017, 2017; https://www.clinicaltrialsregister.eu/ctr-search/search.
[48] P. Yeh, D. Landais, M. Lemaitre, I. Maury, J. Y. Crenne, J. Becquart, A. Murry-Brelier, F. Boucher, G. Montay, and R. Fleer, “Design of yeast-secreted albumin derivatives for human therapy: biological and antiviral properties of a serum albumin-CD4 genetic conjugate,” *Proceedings of the National Academy of Sciences*, vol. 89, no. 5, pp. 1904-1908, 1992.
[49] M. Nazeef, and J. P. Sheehan, “New developments in the management of moderate-to-severe hemophilia B,” *J Blood Med*, vol. 7, pp. 27-38, 2016.
[50] "FDA approves first coagulation factor-albumin fusion protein to treat patients with hemophilia B," 20.10.2016, 2016; http://www.fda.gov/NewsEvents/Newsroom/PressAnnouncements/ucm489266.htm.
[51] "European approval for CSL's IDELVION," 20.10.2016, 2016; http://biotechdispatch.com.au/news/european-approval-for-csls-idelvion.
[52] E. Santagostino, “PROLONG-9FP clinical development program – phase I results of recombinant fusion protein linking coagulation factor IX with recombinant albumin (rIX-FP),” *Thrombosis Research*, vol. 131, pp. S7-S10, 2013.
[53] X. Chen, H. F. Lee, J. L. Zaro, and W. C. Shen, “Effects of receptor binding on plasma half-life of bifunctional transferrin fusion proteins,” *Mol Pharm*, vol. 8, no. 2, pp. 457-65, Apr 4, 2011.
[54] B. J. Kim, J. Zhou, B. Martin, O. D. Carlson, S. Maudsley, N. H. Greig, M. P. Mattson, E. E. Ladenheim, J. Wustner, A. Turner, H. Sadeghi, and J. M. Egan, “Transferrin fusion technology: a novel approach to prolonging biological half-life of insulinotropic peptides,” *J Pharmacol Exp Ther*, vol. 334, no. 3, pp. 682-92, Sep 1, 2010.
[55] J. Shao, J. L. Zaro, and W. C. Shen, “Proinsulin-Transferrin Fusion Protein Exhibits a Prolonged and Selective Effect on the Control of Hepatic Glucose Production in an Experimental Model of Type 1 Diabetes,” *Mol Pharm*, Jul 11, 2016.
[56] Y. Bai, D. K. Ann, and W. C. Shen, “Recombinant granulocyte colony-stimulating factor-transferrin fusion protein as an oral myelopoietic agent,” *Proc Natl Acad Sci U S A*, vol. 102, no. 20, pp. 7292-6, May 17, 2005.
[57] A. Hawe, M. Wiggenhorn, M. van de Weert, J. H. Garbe, H. C. Mahler, and W. Jiskoot, “Forced degradation of therapeutic proteins,” *J Pharm Sci*, vol. 101, no. 3, pp. 895-913, Mar, 2012.
[58] B. S. Chang, and S. Hershenson, “Practical approaches to protein formulation development,” *Pharm Biotechnol*, vol. 13, pp. 1-25, 2002.
[59] W. Wang, “Instability, stabilization, and formulation of liquid protein pharmaceuticals,” *International Journal of Pharmaceutics*, vol. 185, no. 2, pp. 129-188, 1999.
[60] A. Jaklenec, A. Stamp, E. Deweerd, A. Sherwin, and R. Langer, “Progress in the tissue engineering and stem cell industry "are we there yet?",” *Tissue Eng Part B Rev*, vol. 18, no. 3, pp. 155-66, Jun, 2012.
[61] J. R. Wolter, and R. F. Meyer, “Sessile macrophages forming clear endotheliumlike membrane on the inside of successful keratoprosthesis,” *Graefe's Archive for Clinical and Experimental Ophthalmology*, vol. 222, no. 3, pp. 109-117, 1985.
[62] R. Langer, and J. Vacanti, “Tissue engineering,” *Science*, vol. 260, no. 5110, pp. 920-926, 1993.

[63] J. Henkel, M. A. Woodruff, D. R. Epari, R. Steck, V. Glatt, I. C. Dickinson, P. F. Choong, M. A. Schuetz, and D. W. Hutmacher, "Bone Regeneration Based on Tissue Engineering Conceptions - A 21st Century Perspective," *Bone Res*, vol. 1, no. 3, pp. 216-48, Sep, 2013.

[64] L. Kock, C. C. van Donkelaar, and K. Ito, "Tissue engineering of functional articular cartilage: the current status," *Cell Tissue Res*, vol. 347, no. 3, pp. 613-27, Mar, 2012.

[65] K. Vig, A. Chaudhari, S. Tripathi, S. Dixit, R. Sahu, S. Pillai, V. A. Dennis, and S. R. Singh, "Advances in Skin Regeneration Using Tissue Engineering," *Int J Mol Sci*, vol. 18, no. 4, Apr 7, 2017.

[66] K. Belanger, T. M. Dinis, S. Taourirt, G. Vidal, D. L. Kaplan, and C. Egles, "Recent Strategies in Tissue Engineering for Guided Peripheral Nerve Regeneration," *Macromol Biosci*, vol. 16, no. 4, pp. 472-81, Apr, 2016.

[67] W. J. Zhang, W. Liu, L. Cui, and Y. Cao, "Tissue engineering of blood vessel," *J Cell Mol Med*, vol. 11, no. 5, pp. 945-57, Sep-Oct, 2007.

[68] A. A. Palakkan, D. C. Hay, P. R. Anil Kumar, T. V. Kumary, and J. A. Ross, "Liver tissue engineering and cell sources: issues and challenges," *Liver Int*, vol. 33, no. 5, pp. 666-76, May, 2013.

[69] M. W. Curtis, and B. Russell, "Cardiac tissue engineering," *J Cardiovasc Nurs*, vol. 24, no. 2, pp. 87-92, Mar-Apr, 2009.

[70] A. C. Mitchell, P. S. Briquez, J. A. Hubbell, and J. R. Cochran, "Engineering growth factors for regenerative medicine applications," *Acta Biomater*, vol. 30, pp. 1-12, Jan 15, 2016.

[71] "OP-1 Implant - Stryker," 11.11.2016, 2016; http://www.stryker.com/cn/products/Orthopaedics/BoneSubstitutes/OP-1Implant/020210.

[72] "INFUSE® bone graft - Medtronic," 11.11.2016, 2016; http://www.infusebonegraft.com/healthcare-providers/about-infuse-bonegraft/index.htm.

[73] S. Massberg, I. Konrad, A. Bultmann, C. Schulz, G. Munch, M. Peluso, M. Lorenz, S. Schneider, F. Besta, I. Muller, B. Hu, H. Langer, E. Kremmer, M. Rudelius, U. Heinzmann, M. Ungerer, and M. Gawaz, "Soluble glycoprotein VI dimer inhibits platelet adhesion and aggregation to the injured vessel wall in vivo," *FASEB J*, vol. 18, no. 2, pp. 397-9, Feb, 2004.

[74] M. Ungerer, K. Rosport, A. Bultmann, R. Piechatzek, K. Uhland, P. Schlieper, M. Gawaz, and G. Munch, "Novel antiplatelet drug revacept (Dimeric Glycoprotein VI-Fc) specifically and efficiently inhibited collagen-induced platelet aggregation without affecting general hemostasis in humans," *Circulation*, vol. 123, no. 17, pp. 1891-9, May 3, 2011.

[75] G. Münch, K. Uhland, and S. Neidhold, "Investigational Medicinal Product Dossier (Impd) - Revacept®," advanceCOR GmbH, 2013, pp. 1-139.

[76] R. J. Falconer, C. Chan, K. Hughes, and T. P. Munro, "Stabilization of a monoclonal antibody during purification and formulation by addition of basic amino acid excipients," *Journal of Chemical Technology & Biotechnology*, vol. 86, no. 7, pp. 942-948, 2011.

[77] A. L. Daugherty, and R. J. Mrsny, "Formulation and delivery issues for monoclonal antibody therapeutics," *Adv Drug Deliv Rev*, vol. 58, no. 5-6, pp. 686-706, Aug 7, 2006.

[78] C. Lehermayr, H. C. Mahler, K. Mader, and S. Fischer, "Assessment of net charge and protein-protein interactions of different monoclonal antibodies," *J Pharm Sci*, vol. 100, no. 7, pp. 2551-62, Jul, 2011.

[79] P. Kheddo, M. Tracka, J. Armer, R. J. Dearman, S. Uddin, C. F. van der Walle, and A. P. Golovanov, "The effect of arginine glutamate on the stability of monoclonal antibodies in solution," *Int J Pharm*, vol. 473, no. 1-2, pp. 126-33, Oct 1, 2014.

[80] N. W. Warne, "Development of high concentration protein biopharmaceuticals: the use of platform approaches in formulation development," *Eur J Pharm Biopharm*, vol. 78, no. 2, pp. 208-12, Jun, 2011.

[81] N. W. Warne, P. E. Nichols, and P. J. Loureiro, "Protein formulations with reduced viscosity and uses thereof," Google Patents, 2007.

[82] C. P. Lee, and M. N. L. Huang, "D-optimal designs for second-order response surface models with qualitative factors," *Data Sci*, vol. 9, pp. 139-153, 2011.

[83] C. D. Spicer, and B. G. Davis, "Selective chemical protein modification," *Nat Commun,* vol. 5, pp. 4740, 2014.
[84] V. Karageorgiou, L. Meinel, S. Hofmann, A. Malhotra, V. Volloch, and D. Kaplan, "Bone morphogenetic protein-2 decorated silk fibroin films induce osteogenic differentiation of human bone marrow stromal cells," *J Biomed Mater Res A,* vol. 71, no. 3, pp. 528-37, Dec 1, 2004.
[85] L. L. Chiu, and M. Radisic, "Scaffolds with covalently immobilized VEGF and Angiopoietin-1 for vascularization of engineered tissues," *Biomaterials,* vol. 31, no. 2, pp. 226-41, Jan, 2010.
[86] A. Bertolo, F. Arcolino, S. Capossela, A. R. Taddei, M. Baur, T. Potzel, and J. Stoyanov, "Growth Factors Cross-Linked to Collagen Microcarriers Promote Expansion and Chondrogenic Differentiation of Human Mesenchymal Stem Cells," *Tissue Eng Part A,* vol. 21, no. 19-20, pp. 2618-28, Oct, 2015.
[87] H. Zhao, E. Heusler, G. Jones, L. Li, V. Werner, O. Germershaus, J. Ritzer, T. Luehmann, and L. Meinel, "Decoration of silk fibroin by click chemistry for biomedical application," *J Struct Biol,* vol. 186, no. 3, pp. 420-30, Jun, 2014.
[88] S. Sofia, M. B. McCarthy, G. Gronowicz, and D. L. Kaplan, "Functionalized silk-based biomaterials for bone formation," *J Biomed Mater Res,* vol. 54, no. 1, pp. 139-48, Jan, 2001.
[89] Y. Wang, H. J. Kim, G. Vunjak-Novakovic, and D. L. Kaplan, "Stem cell-based tissue engineering with silk biomaterials," *Biomaterials,* vol. 27, no. 36, pp. 6064-82, Dec, 2006.
[90] G. H. Altman, F. Diaz, C. Jakuba, T. Calabro, R. L. Horan, J. Chen, H. Lu, J. Richmond, and D. L. Kaplan, "Silk-based biomaterials," *Biomaterials,* vol. 24, no. 3, pp. 401-16, Feb, 2003.
[91] J. Melke, S. Midha, S. Ghosh, K. Ito, and S. Hofmann, "Silk fibroin as biomaterial for bone tissue engineering," *Acta Biomater,* vol. 31, pp. 1-16, Feb, 2016.
[92] A. R. Murphy, and D. L. Kaplan, "Biomedical applications of chemically-modified silk fibroin," *J Mater Chem,* vol. 19, no. 36, pp. 6443-6450, Jun 23, 2009.
[93] A. R. Murphy, P. St John, and D. L. Kaplan, "Modification of silk fibroin using diazonium coupling chemistry and the effects on hMSC proliferation and differentiation," *Biomaterials,* vol. 29, no. 19, pp. 2829-38, Jul, 2008.
[94] N. Budisa, "Prolegomena to future experimental efforts on genetic code engineering by expanding its amino acid repertoire," *Angew Chem Int Ed Engl,* vol. 43, no. 47, pp. 6426-63, Dec 3, 2004.
[95] S. Eger, M. Scheffner, A. Marx, and M. Rubini, *Formation of Ubiquitin Dimers via Azide-Alkyne Click Reaction - Chaper 41*, Totowa, NJ: Humana Press, 2012.
[96] T. Yang, "PEGylation-Successful Approach for Therapeutic Protein Conjugation," *Modern Chemistry & Applications,* vol. 01, no. 04, 2013.
[97] M. J. Roberts, M. D. Bentley, and J. M. Harris, "Chemistry for peptide and protein PEGylation," *Advanced Drug Delivery Reviews,* vol. 64, no. SUPPL., pp. 116-127, 2012.
[98] G. Pasut, and F. M. Veronese, "State of the art in PEGylation: the great versatility achieved after forty years of research," *J Control Release,* vol. 161, no. 2, pp. 461-72, Jul 20, 2012.
[99] N. M. Aljamali, "Review in Azo Compounds and its Biological Activity," *Biochemistry & Analytical Biochemistry,* vol. 04, no. 02, 2015.
[100] J. Conde, J. T. Dias, V. Grazu, M. Moros, P. V. Baptista, and J. M. de la Fuente, "Revisiting 30 years of biofunctionalization and surface chemistry of inorganic nanoparticles for nanomedicine," *Front Chem,* vol. 2, no. JUNE 2014, pp. 48, 2014.
[101] R. A. Young, "Transcription termination in the Escherichia coli ribosomal RNA operon rrnC," *J Biol Chem,* vol. 254, no. 24, pp. 12725-31, Dec 25, 1979.
[102] H. C. Kolb, M. G. Finn, and K. B. Sharpless, "Click Chemistry: Diverse Chemical Function from a Few Good Reactions," *Angewandte Chemie International Edition,* vol. 40, no. 11, pp. 2004-2021, 2001.
[103] V. V. Rostovtsev, L. G. Green, V. V. Fokin, and K. B. Sharpless, "A Stepwise Huisgen Cycloaddition Process: Copper(I)-Catalyzed Regioselective "Ligation" of Azides and

Terminal Alkynes," *Angewandte Chemie International Edition*, vol. 41, no. 14, pp. 2596-2599, 2002.
[104] J. Lam, S. Lu, F. K. Kasper, and A. G. Mikos, "Strategies for controlled delivery of biologics for cartilage repair," *Adv Drug Deliv Rev*, vol. 84, pp. 123-34, Apr, 2015.
[105] C. Chung, and J. A. Burdick, "Engineering cartilage tissue," *Adv Drug Deliv Rev*, vol. 60, no. 2, pp. 243-62, Jan 14, 2008.
[106] L. Danisovic, I. Varga, R. Zamborsky, and D. Bohmer, "The tissue engineering of articular cartilage: cells, scaffolds and stimulating factors," *Exp Biol Med (Maywood)*, vol. 237, no. 1, pp. 10-7, Jan, 2012.
[107] E. Mevel, L. E. Monfoulet, C. Merceron, V. Coxam, Y. Wittrant, L. Beck, and J. Guicheux, "Nutraceuticals in joint health: animal models as instrumental tools," *Drug Discov Today*, vol. 19, no. 10, pp. 1649-58, Oct, 2014.
[108] S. Oussedik, K. Tsitskaris, and D. Parker, "Treatment of articular cartilage lesions of the knee by microfracture or autologous chondrocyte implantation: a systematic review," *Arthroscopy*, vol. 31, no. 4, pp. 732-44, Apr, 2015.
[109] T. A. Ahmed, and M. T. Hincke, "Strategies for articular cartilage lesion repair and functional restoration," *Tissue Eng Part B Rev*, vol. 16, no. 3, pp. 305-29, Jun, 2010.
[110] C. Vinatier, C. Bouffi, C. Merceron, J. Gordeladze, J. M. Brondello, C. Jorgensen, P. Weiss, J. Guicheux, and D. Noel, "Cartilage tissue engineering: towards a biomaterial-assisted mesenchymal stem cell therapy," *Curr Stem Cell Res Ther*, vol. 4, no. 4, pp. 318-29, Dec, 2009.
[111] R. Kelc, J. Naranda, M. Kuhta, and M. Vogri, "Novel Therapies for the Management of Sports Injuries," 2013.
[112] S. Boeuf, and W. Richter, "Chondrogenesis of mesenchymal stem cells: role of tissue source and inducing factors," *Stem Cell Res Ther*, vol. 1, no. 4, pp. 31, 2010.
[113] R. W. Matheny, Jr., and B. C. Nindl, "Loss of IGF-IEa or IGF-IEb impairs myogenic differentiation," *Endocrinology*, vol. 152, no. 5, pp. 1923-34, May, 2011.
[114] L. C. Davies, E. J. Blain, S. J. Gilbert, B. Caterson, and V. C. Duance, "The potential of IGF-1 and TGFbeta1 for promoting "adult" articular cartilage repair: an in vitro study," *Tissue Eng Part A*, vol. 14, no. 7, pp. 1251-61, Jul, 2008.
[115] L. Longobardi, L. O'Rear, S. Aakula, B. Johnstone, K. Shimer, A. Chytil, W. A. Horton, H. L. Moses, and A. Spagnoli, "Effect of IGF-I in the chondrogenesis of bone marrow mesenchymal stem cells in the presence or absence of TGF-beta signaling," *J Bone Miner Res*, vol. 21, no. 4, pp. 626-36, Apr, 2006.
[116] B. G. Starkman, J. D. Cravero, M. Delcarlo, and R. F. Loeser, "IGF-I stimulation of proteoglycan synthesis by chondrocytes requires activation of the PI 3-kinase pathway but not ERK MAPK," *Biochem J*, vol. 389, no. Pt 3, pp. 723-9, Aug 1, 2005.
[117] D. W. Walsh, C. Godson, D. P. Brazil, and F. Martin, "Extracellular BMP-antagonist regulation in development and disease: tied up in knots," *Trends Cell Biol*, vol. 20, no. 5, pp. 244-56, May, 2010.
[118] D. Chen, M. Zhao, and G. R. Mundy, "Bone morphogenetic proteins," *Growth Factors*, vol. 22, no. 4, pp. 233-41, Dec, 2004.
[119] H. Alborzinia, H. Schmidt-Glenewinkel, I. Ilkavets, K. Breitkopf-Heinlein, X. Cheng, P. Hortschansky, S. Dooley, and S. Wolfl, "Quantitative kinetics analysis of BMP2 uptake into cells and its modulation by BMP antagonists," *J Cell Sci*, vol. 126, no. Pt 1, pp. 117-27, Jan 1, 2013.
[120] S. Scarfi, "Use of bone morphogenetic proteins in mesenchymal stem cell stimulation of cartilage and bone repair," *World J Stem Cells*, vol. 8, no. 1, pp. 1-12, Jan 26, 2016.
[121] J. Yang, P. Shi, M. Tu, Y. Wang, M. Liu, F. Fan, and M. Du, "Bone morphogenetic proteins: Relationship between molecular structure and their osteogenic activity," *Food Science and Human Wellness*, vol. 3, no. 3-4, pp. 127-135, 2014.
[122] J. Shen, S. Li, and D. Chen, "TGF-beta signaling and the development of osteoarthritis," *Bone Res*, vol. 2, no. January, pp. 14002-14002, 2014.

[123] A. S. Patil, R. B. Sable, and R. M. Kothari, "An update on transforming growth factor-beta (TGF-beta): sources, types, functions and clinical applicability for cartilage/bone healing," *J Cell Physiol,* vol. 226, no. 12, pp. 3094-103, Dec, 2011.
[124] K. W. Finnson, Y. Chi, G. Bou-Gharios, A. Leask, and A. Philip, "TGF-b signaling in cartilage homeostasis and osteoarthritis," *Front Biosci (Schol Ed),* vol. 4, pp. 251-68, 2012.
[125] X. Li, C. Wang, J. Xiao, W. L. McKeehan, and F. Wang, "Fibroblast growth factors, old kids on the new block," *Semin Cell Dev Biol,* vol. 53, pp. 155-67, May, 2016.
[126] N. Itoh, and D. M. Ornitz, "Evolution of the Fgf and Fgfr gene families," *Trends Genet,* vol. 20, no. 11, pp. 563-9, Nov, 2004.
[127] A. Kharitonenkov, "FGFs and metabolism," *Curr Opin Pharmacol,* vol. 9, no. 6, pp. 805-10, Dec, 2009.
[128] M. A. Nugent, and R. V. Iozzo, "Fibroblast growth factor-2," *Int J Biochem Cell Biol,* vol. 32, no. 2, pp. 115-20, Feb, 2000.
[129] A. Bikfalvi, S. Klein, G. Pintucci, and D. B. Rifkin, "Biological roles of fibroblast growth factor-2," *Endocr Rev,* vol. 18, no. 1, pp. 26-45, Feb, 1997.
[130] Z. Cao, C. Dou, and S. Dong, "Scaffolding Biomaterials for Cartilage Regeneration," *Journal of Nanomaterials,* vol. 2014, pp. 1-8, 2014.
[131] S. Hofmann, S. Knecht, R. Langer, D. L. Kaplan, G. Vunjak-Novakovic, H. P. Merkle, and L. Meinel, "Cartilage-like tissue engineering using silk scaffolds and mesenchymal stem cells," *Tissue Engineering,* vol. 12, no. 10, pp. 2729-2738, Oct, 2006.
[132] L. Meinel, S. Hofmann, V. Karageorgiou, L. Zichner, R. Langer, D. Kaplan, and G. Vunjak-Novakovic, "Engineering cartilage-like tissue using human mesenchymal stem cells and silk protein scaffolds," *Biotechnol Bioeng,* vol. 88, no. 3, pp. 379-91, Nov 5, 2004.
[133] C. Wang, Q. Yan, H. B. Liu, X. H. Zhou, and S. J. Xiao, "Different EDC/NHS activation mechanisms between PAA and PMAA brushes and the following amidation reactions," *Langmuir,* vol. 27, no. 19, pp. 12058-68, Oct 4, 2011.
[134] G. Lewis, "Viscoelastic properties of injectable bone cements for orthopaedic applications: state-of-the-art review," *J Biomed Mater Res B Appl Biomater,* vol. 98, no. 1, pp. 171-91, Jul, 2011.
[135] K. Klemm, "Gentamicin-PMMA-beads in treating bone and soft tissue infections," *Zentralbl Chir,* vol. 104, no. 14, pp. 934-42, 1979.
[136] D. Correa, and S. A. Lietman, "Articular cartilage repair: Current needs, methods and research directions," *Semin Cell Dev Biol,* vol. 62, pp. 67-77, Feb, 2017.
[137] D. Schaefer, I. Martin, P. Shastri, R. F. Padera, R. Langer, L. E. Freed, and G. Vunjak-Novakovic, "In vitro generation of osteochondral composites," *Biomaterials,* vol. 21, no. 24, pp. 2599-2606, 2000.
[138] I. Martin, S. Miot, A. Barbero, M. Jakob, and D. Wendt, "Osteochondral tissue engineering," *J Biomech,* vol. 40, no. 4, pp. 750-65, 2007.
[139] J. F. Mano, and R. L. Reis, "Osteochondral defects: present situation and tissue engineering approaches," *J Tissue Eng Regen Med,* vol. 1, no. 4, pp. 261-73, Jul-Aug, 2007.
[140] C. M. Murphy, M. G. Haugh, and F. J. O'Brien, "The effect of mean pore size on cell attachment, proliferation and migration in collagen-glycosaminoglycan scaffolds for bone tissue engineering," *Biomaterials,* vol. 31, no. 3, pp. 461-6, Jan, 2010.
[141] J. J. Klawitter, J. G. Bagwell, A. M. Weinstein, and B. W. Sauer, "An evaluation of bone growth into porous high density polyethylene," *J Biomed Mater Res,* vol. 10, no. 2, pp. 311-23, Mar, 1976.
[142] S. Yamane, N. Iwasaki, Y. Kasahara, K. Harada, T. Majima, K. Monde, S. Nishimura, and A. Minami, "Effect of pore size on in vitro cartilage formation using chitosan-based hyaluronic acid hybrid polymer fibers," *J Biomed Mater Res A,* vol. 81, no. 3, pp. 586-93, Jun 1, 2007.
[143] D. H. Rosenzweig, E. Carelli, T. Steffen, P. Jarzem, and L. Haglund, "3D-Printed ABS and PLA Scaffolds for Cartilage and Nucleus Pulposus Tissue Regeneration," *Int J Mol Sci,* vol. 16, no. 7, pp. 15118-35, Jul 03, 2015.

[144] L. Uebersax, H. Hagenmuller, S. Hofmann, E. Gruenblatt, R. Muller, G. Vunjak-Novakovic, D. L. Kaplan, H. P. Merkle, and L. Meinel, "Effect of scaffold design on bone morphology in vitro," *Tissue Eng*, vol. 12, no. 12, pp. 3417-29, Dec, 2006.
[145] M. Hasija, L. Li, N. Rahman, and S. F. Ausar, "Forced degradation studies: an essential tool for the formulation development of vaccines," *Vaccine: Development and Therapy*, vol. 3, pp. 11-33, 2013.
[146] M. K. Joubert, Q. Luo, Y. Nashed-Samuel, J. Wypych, and L. O. Narhi, "Classification and characterization of therapeutic antibody aggregates," *J Biol Chem*, vol. 286, no. 28, pp. 25118-33, Jul 15, 2011.
[147] C. Dionex, "Monitoring Monoclonal Antibody Stability by Cation-Exchange Chromatography, Application Note 128," *Sunnyvale, CA, USA*, 2009, pp. 1-7.
[148] L. Eriksson, *Design of Experiments: Principles and Applications*: Umetrics, 2008.
[149] "ExPASy ProtParam tool," 11.11.2014, 2014; http://web.expasy.org/protparam/.
[150] G. Wandrey, J. Wurzel, K. Hoffmann, T. Ladner, J. Buchs, L. Meinel, and T. Luhmann, "Probing unnatural amino acid integration into enhanced green fluorescent protein by genetic code expansion with a high-throughput screening platform," *J Biol Eng*, vol. 10, pp. 11, 2016.
[151] G. V. Born, and M. J. Cross, "The Aggregation of Blood Platelets," *J Physiol*, vol. 168, no. 1, pp. 178-95, Aug, 1963.
[152] F. H. Niesen, H. Berglund, and M. Vedadi, "The use of differential scanning fluorimetry to detect ligand interactions that promote protein stability," *Nat Protoc*, vol. 2, no. 9, pp. 2212-21, 2007.
[153] E. Wenk, A. J. Meinel, S. Wildy, H. P. Merkle, and L. Meinel, "Microporous silk fibroin scaffolds embedding PLGA microparticles for controlled growth factor delivery in tissue engineering," *Biomaterials*, vol. 30, no. 13, pp. 2571-81, May, 2009.
[154] M. E. Gasparian, P. A. Elistratov, N. I. Drize, I. N. Nifontova, D. A. Dolgikh, and M. P. Kirpichnikov, "Overexpression in Escherichia coli and purification of human fibroblast growth factor (FGF-2)," *Biochemistry (Mosc)*, vol. 74, no. 2, pp. 221-5, Feb, 2009.
[155] C. H. Squires, J. Childs, S. P. Eisenberg, P. J. Polverini, and A. Sommer, "Production and characterization of human basic fibroblast growth factor from Escherichia coli," *J Biol Chem*, vol. 263, no. 31, pp. 16297-302, Nov 05, 1988.
[156] M. W. Pantoliano, R. A. Horlick, B. A. Springer, D. E. Van Dyk, T. Tobery, D. R. Wetmore, J. D. Lear, A. T. Nahapetian, J. D. Bradley, and W. P. Sisk, "Multivalent ligand-receptor binding interactions in the fibroblast growth factor system produce a cooperative growth factor and heparin mechanism for receptor dimerization," *Biochemistry*, vol. 33, no. 34, pp. 10229-48, Aug 30, 1994.
[157] D. H. Doherty, M. S. Rosendahl, D. J. Smith, J. M. Hughes, E. A. Chlipala, and G. N. Cox, "Site-specific PEGylation of engineered cysteine analogues of recombinant human granulocyte-macrophage colony-stimulating factor," *Bioconjug Chem*, vol. 16, no. 5, pp. 1291-8, Sep-Oct, 2005.
[158] O. Germershaus, I. Schultz, T. Luhmann, M. Beck-Broichsitter, P. Hogger, and L. Meinel, "Insulin-like growth factor-I aerosol formulations for pulmonary delivery," *Eur J Pharm Biopharm*, vol. 85, no. 1, pp. 61-8, Sep, 2013.
[159] C. Leibiger, N. Kosyakova, H. Mkrtchyan, M. Glei, V. Trifonov, and T. Liehr, "First molecular cytogenetic high resolution characterization of the NIH 3T3 cell line by murine multicolor banding," *J Histochem Cytochem*, vol. 61, no. 4, pp. 306-12, Apr, 2013.
[160] L. Eiselleova, K. Matulka, V. Kriz, M. Kunova, Z. Schmidtova, J. Neradil, B. Tichy, D. Dvorakova, S. Pospisilova, A. Hampl, and P. Dvorak, "A complex role for FGF-2 in self-renewal, survival, and adhesion of human embryonic stem cells," *Stem Cells*, vol. 27, no. 8, pp. 1847-57, Aug, 2009.
[161] H. E. Gottlieb, V. Kotlyar, and A. Nudelman, "NMR chemical shifts of common laboratory solvents as trace impurities," *Journal of Organic Chemistry*, vol. 62, no. 21, pp. 7512-7515, Oct 17, 1997.

[162] A. van Kimmenade, M. W. Bond, J. H. Schumacher, C. Laquoi, and R. A. Kastelein, "Expression, renaturation and purification of recombinant human interleukin 4 from Escherichia coli," *Eur J Biochem*, vol. 173, no. 1, pp. 109-14, Apr 5, 1988.
[163] N. D. Wangsa-Wirawan, B. K. O'Neill, and A. P. Middelberg, "Physicochemical characteristics of LR3-IGF1 protein inclusion bodies: electrophoretic mobility studies," *Biotechnol Prog*, vol. 17, no. 4, pp. 786-90, Jul-Aug, 2001.
[164] U. K. Laemmli, "Cleavage of Structural Proteins during the Assembly of the Head of Bacteriophage T4," *Nature*, vol. 227, no. 5259, pp. 680-685, 1970.
[165] V. Neuhoff, N. Arold, D. Taube, and W. Ehrhardt, "Improved staining of proteins in polyacrylamide gels including isoelectric focusing gels with clear background at nanogram sensitivity using Coomassie Brilliant Blue G-250 and R-250," *Electrophoresis*, vol. 9, no. 6, pp. 255-62, Jun, 1988.
[166] P. Jeno, T. Mini, S. Moes, E. Hintermann, and M. Horst, "Internal sequences from proteins digested in polyacrylamide gels," *Anal Biochem*, vol. 224, no. 1, pp. 75-82, Jan 1, 1995.
[167] J. Rosenfeld, J. Capdevielle, J. C. Guillemot, and P. Ferrara, "In-gel digestion of proteins for internal sequence analysis after one- or two-dimensional gel electrophoresis," *Analytical Biochemistry*, vol. 203, no. 1, pp. 173-179, 1992.
[168] D. S. Bischoff, N. S. Makhijani, and D. T. Yamaguchi, "Constitutive expression of human telomerase enhances the proliferation potential of human mesenchymal stem cells," *Biores Open Access*, vol. 1, no. 6, pp. 273-9, Dec, 2012.
[169] L. J. C. Jonk, S. Itoh, C.-H. Heldin, P. ten Dijke, and W. Kruijer, "Identification and Functional Characterization of a Smad Binding Element (SBE) in theJunBPromoter That Acts as a Transforming Growth Factor-β, Activin, and Bone Morphogenetic Protein-inducible Enhancer," *Journal of Biological Chemistry*, vol. 273, no. 33, pp. 21145-21152, 1998.
[170] I. Tesseur, K. Zou, E. Berber, H. Zhang, and T. Wyss-Coray, "Highly sensitive and specific bioassay for measuring bioactive TGF-beta," *BMC Cell Biol*, vol. 7, no. 1, pp. 15, 2006.
[171] D. Eyrich, H. Wiese, G. Maier, D. Skodacek, B. Appel, H. Sarhan, J. Tessmar, R. Staudenmaier, M. M. Wenzel, A. Goepferich, and T. Blunk, "In vitro and in vivo cartilage engineering using a combination of chondrocyte-seeded long-term stable fibrin gels and polycaprolactone-based polyurethane scaffolds," *Tissue Eng*, vol. 13, no. 9, pp. 2207-18, Sep, 2007.
[172] R. Farndale, D. Buttle, and A. Barrett, "Improved quantitation and discrimination of sulphated glycosaminoglycans by use of dimethylmethylene blue," *Biochimica et Biophysica Acta (BBA) - General Subjects*, vol. 883, no. 2, pp. 173-177, 1986.
[173] J. F. Woessner, "The determination of hydroxyproline in tissue and protein samples containing small proportions of this imino acid," *Archives of Biochemistry and Biophysics*, vol. 93, no. 2, pp. 440-447, 1961.
[174] A. P. Hollander, T. F. Heathfield, C. Webber, Y. Iwata, R. Bourne, C. Rorabeck, and A. R. Poole, "Increased damage to type II collagen in osteoarthritic articular cartilage detected by a new immunoassay," *J Clin Invest*, vol. 93, no. 4, pp. 1722-32, Apr, 1994.
[175] K. Wittmann, K. Storck, C. Muhr, H. Mayer, S. Regn, R. Staudenmaier, H. Wiese, G. Maier, P. Bauer-Kreisel, and T. Blunk, "Development of volume-stable adipose tissue constructs using polycaprolactone-based polyurethane scaffolds and fibrin hydrogels," *J Tissue Eng Regen Med*, vol. 10, no. 10, pp. E409-E418, Oct, 2016.
[176] D. Arzenšek, *Dynamic light scattering and application to proteins in solutions*, 2010.
[177] B. Granvogl, M. Ploscher, and L. A. Eichacker, "Sample preparation by in-gel digestion for mass spectrometry-based proteomics," *Anal Bioanal Chem*, vol. 389, no. 4, pp. 991-1002, Oct, 2007.
[178] M. Getie, C. E. Schmelzer, and R. H. Neubert, "Characterization of peptides resulting from digestion of human skin elastin with elastase," *Proteins*, vol. 61, no. 3, pp. 649-57, Nov 15, 2005.
[179] D. T. McLachlin, and B. T. Chait, "Analysis of phosphorylated proteins and peptides by mass spectrometry," *Curr Opin Chem Biol*, vol. 5, no. 5, pp. 591-602, Oct, 2001.

[180] "ExPASy Compute pI/Mw tool," 11.11.2014, 2014; http://web.expasy.org/compute_pi/.
[181] B. Testa, and J. M. Mayer, *Hydrolysis in Drug and Prodrug Metabolism*: Wiley, 2003.
[182] J. Vlasak, and R. Ionescu, "Fragmentation of monoclonal antibodies," *mAbs,* vol. 3, no. 3, pp. 253-263, 2014.
[183] A. J. Cordoba, B. J. Shyong, D. Breen, and R. J. Harris, "Non-enzymatic hinge region fragmentation of antibodies in solution," *J Chromatogr B Analyt Technol Biomed Life Sci,* vol. 818, no. 2, pp. 115-21, Apr 25, 2005.
[184] Y. Miura, T. Takahashi, S. M. Jung, and M. Moroi, "Analysis of the interaction of platelet collagen receptor glycoprotein VI (GPVI) with collagen. A dimeric form of GPVI, but not the monomeric form, shows affinity to fibrous collagen," *J Biol Chem,* vol. 277, no. 48, pp. 46197-204, Nov 29, 2002.
[185] A. Hawe, M. Sutter, and W. Jiskoot, "Extrinsic fluorescent dyes as tools for protein characterization," *Pharm Res,* vol. 25, no. 7, pp. 1487-99, Jul, 2008.
[186] M. Correia, M. T. Neves-Petersen, P. B. Jeppesen, S. Gregersen, and S. B. Petersen, "UV-light exposure of insulin: pharmaceutical implications upon covalent insulin dityrosine dimerization and disulphide bond photolysis," *PLoS One,* vol. 7, no. 12, pp. e50733, 2012.
[187] A. a. S. Shipway. "CalcTool: Protein size calculator," 8.01.2016, 2016; http://www.calctool.org/CALC/prof/bio/protein_size.
[188] D. Estape, J. van den Heuvel, and U. Rinas, "Susceptibility towards intramolecular disulphide-bond formation affects conformational stability and folding of human basic fibroblast growth factor," *Biochem J,* vol. 335 (Pt 2), no. 2, pp. 343-9, Oct 15, 1998.
[189] T. Lühmann, G. Jones, M. Gutmann, J.-C. Rybak, J. Nickel, M. Rubini, and L. Meinel, "Bio-orthogonal Immobilization of Fibroblast Growth Factor 2 for Spatial Controlled Cell Proliferation," *ACS Biomaterials Science & Engineering,* vol. 1, no. 9, pp. 740-746, 2015.
[190] "Protein Fluorescence," *Principles of Fluorescence Spectroscopy*, J. R. Lakowicz, ed., pp. 529-575, Boston, MA: Springer US, 2006.
[191] X. Wu, X. Li, Y. Zeng, Q. Zheng, and S. Wu, "Site-directed PEGylation of human basic fibroblast growth factor," *Protein Expr Purif,* vol. 48, no. 1, pp. 24-7, Jul, 2006.
[192] K. S. Masters, "Covalent growth factor immobilization strategies for tissue repair and regeneration," *Macromol Biosci,* vol. 11, no. 9, pp. 1149-63, Sep 9, 2011.
[193] H. Friebolin, *Ein- und zweidimensionale NMR-Spektroskopie: Eine Einführung*: Wiley, 2013.
[194] R. A. Hart, P. M. Lester, D. H. Reifsnyder, J. R. Ogez, and S. E. Builder, "Large Scale, In Situ Isolation of Periplasmic IGF–I from E. coli," *Bio/Technology,* vol. 12, no. 11, pp. 1113-1117, 1994.
[195] D. Hartinger, S. Heinl, H. E. Schwartz, R. Grabherr, G. Schatzmayr, D. Haltrich, and W. D. Moll, "Enhancement of solubility in Escherichia coli and purification of an aminotransferase from Sphingopyxis sp. MTA144 for deamination of hydrolyzed fumonisin B(1)," *Microb Cell Fact,* vol. 9, pp. 62, 2010.
[196] "Prokaryotic Expression Overview," 15.05.2014, 2014; http://wolfson.huji.ac.il/expression/novagen_ProkExp.pdf.
[197] "ExPASy PeptideMass tool," 15.05.2014, 2014; http://web.expasy.org/peptide_mass/.
[198] L. Quintana, N. I. zur Nieden, and C. E. Semino, "Morphogenetic and regulatory mechanisms during developmental chondrogenesis: new paradigms for cartilage tissue engineering," *Tissue Eng Part B Rev,* vol. 15, no. 1, pp. 29-41, Mar, 2009.
[199] J. Schneevoigt, C. Fabian, C. Leovsky, J. Seeger, and M. Bahramsoltani, "In Vitro Expression of the Extracellular Matrix Components Aggrecan, Collagen Types I and II by Articular Cartilage-Derived Chondrocytes," *Anat Histol Embryol,* vol. 46, no. 1, pp. 43-50, Feb, 2017.
[200] M. C. Manning, D. K. Chou, B. M. Murphy, R. W. Payne, and D. S. Katayama, "Stability of protein pharmaceuticals: an update," *Pharm Res,* vol. 27, no. 4, pp. 544-75, Apr, 2010.
[201] "Biological Buffers - Reach Devices," 15.10.2015, 2015; http://www.reachdevices.com/Protein/BiologicalBuffers.html.

[202] A. B. Joshi, M. Sawai, W. R. Kearney, and L. E. Kirsch, "Studies on the mechanism of aspartic acid cleavage and glutamine deamidation in the acidic degradation of glucagon," *J Pharm Sci*, vol. 94, no. 9, pp. 1912-27, Sep, 2005.

[203] S. L. Cohen, C. Price, and J. Vlasak, "Beta-elimination and peptide bond hydrolysis: two distinct mechanisms of human IgG1 hinge fragmentation upon storage," *J Am Chem Soc*, vol. 129, no. 22, pp. 6976-7, Jun 6, 2007.

[204] J. R. Whitaker, "Changes Occuring in Proteins in Alkaline Solution," vol. 123, pp. 145-163, 1980.

[205] B. A. Salinas, H. A. Sathish, A. U. Shah, J. F. Carpenter, and T. W. Randolph, "Buffer-dependent fragmentation of a humanized full-length monoclonal antibody," *J Pharm Sci*, vol. 99, no. 7, pp. 2962-74, Jul, 2010.

[206] D. S. Katayama, R. Nayar, D. K. Chou, J. J. Valente, J. Cooper, C. S. Henry, D. G. Vander Velde, L. Villarete, C. P. Liu, and M. C. Manning, "Effect of buffer species on the thermally induced aggregation of interferon-tau," *J Pharm Sci*, vol. 95, no. 6, pp. 1212-26, Jun, 2006.

[207] T. J. Kamerzell, R. Esfandiary, S. B. Joshi, C. R. Middaugh, and D. B. Volkin, "Protein-excipient interactions: mechanisms and biophysical characterization applied to protein formulation development," *Adv Drug Deliv Rev*, vol. 63, no. 13, pp. 1118-59, Oct, 2011.

[208] Z. Grabarek, and J. Gergely, "Zero-length crosslinking procedure with the use of active esters," *Analytical Biochemistry*, vol. 185, no. 1, pp. 131-135, 1990/02/15, 1990.

[209] F. M. Veronese, "Peptide and protein PEGylation," *Biomaterials*, vol. 22, no. 5, pp. 405-417, 2001.

[210] D. P. Nguyen, H. Lusic, H. Neumann, P. B. Kapadnis, A. Deiters, and J. W. Chin, "Genetic encoding and labeling of aliphatic azides and alkynes in recombinant proteins via a pyrrolysyl-tRNA Synthetase/tRNA(CUA) pair and click chemistry," *J Am Chem Soc*, vol. 131, no. 25, pp. 8720-1, Jul 1, 2009.

[211] S. Das, D. Pati, N. Tiwari, A. Nisal, and S. Sen Gupta, "Synthesis of silk fibroin-glycopolypeptide conjugates and their recognition with lectin," *Biomacromolecules*, vol. 13, no. 11, pp. 3695-702, Nov 12, 2012.

[212] S. Sampaio, T. M. R. Miranda, J. G. Santos, and G. M. B. Soares, "Preparation of silk fibroin-poly(ethylene glycol) conjugate films through click chemistry," *Polymer International*, vol. 60, no. 12, pp. 1737-1744, 2011.

[213] J. M. Harris, and R. B. Chess, "Effect of pegylation on pharmaceuticals," *Nat Rev Drug Discov*, vol. 2, no. 3, pp. 214-21, Mar, 2003.

[214] F. Metzger, W. Sajid, S. Saenger, C. Staudenmaier, C. van der Poel, B. Sobottka, A. Schuler, M. Sawitzky, R. Poirier, D. Tuerck, E. Schick, A. Schaubmar, F. Hesse, K. Amrein, H. Loetscher, G. S. Lynch, A. Hoeflich, P. De Meyts, and H. J. Schoenfeld, "Separation of fast from slow anabolism by site-specific PEGylation of insulin-like growth factor I (IGF-I)," *J Biol Chem*, vol. 286, no. 22, pp. 19501-10, Jun 03, 2011.

[215] J. D. Zhang, L. S. Cousens, P. J. Barr, and S. R. Sprang, "Three-dimensional structure of human basic fibroblast growth factor, a structural homolog of interleukin 1 beta," *Proc Natl Acad Sci U S A*, vol. 88, no. 8, pp. 3446-50, Apr 15, 1991.

[216] Z. Shahrokh, V. Sluzky, P. R. Stratton, G. A. Eberlein, and Y. J. Wang, "Disulfide-Linked Oligomerization of Basic Fibroblast Growth-Factor - Effect of Sulfated Compounds," *Formulation and Delivery of Proteins and Peptides*, vol. 567, pp. 85-99, 1994.

[217] X. Wu, X. Liu, Y. Xiao, Z. Huang, J. Xiao, S. Lin, L. Cai, W. Feng, and X. Li, "Purification and modification by polyethylene glycol of a new human basic fibroblast growth factor mutant-hbFGF(Ser25,87,92)," *J Chromatogr A*, vol. 1161, no. 1-2, pp. 51-5, Aug 17, 2007.

[218] X. Wang, X. Hu, A. Daley, O. Rabotyagova, P. Cebe, and D. L. Kaplan, "Nanolayer biomaterial coatings of silk fibroin for controlled release," *J Control Release*, vol. 121, no. 3, pp. 190-9, Aug 28, 2007.

[219] S. Eger, M. Scheffner, A. Marx, and M. Rubini, "Synthesis of defined ubiquitin dimers," *J Am Chem Soc*, vol. 132, no. 46, pp. 16337-9, Nov 24, 2010.

[220] T. Luhmann, V. Spieler, V. Werner, M. G. Ludwig, J. Fiebig, T. Muller, and L. Meinel, "Interleukin-4 clicked surfaces drive M2 macrophage polarization," *Chembiochem*, Sep 5, 2016.
[221] I. B. Robertson, M. Horiguchi, L. Zilberberg, B. Dabovic, K. Hadjiolova, and D. B. Rifkin, "Latent TGF-beta-binding proteins," *Matrix Biol*, vol. 47, pp. 44-53, Sep, 2015.
[222] I. B. Robertson, and D. B. Rifkin, "Unchaining the beast; insights from structural and evolutionary studies on TGFbeta secretion, sequestration, and activation," *Cytokine Growth Factor Rev*, vol. 24, no. 4, pp. 355-72, Aug, 2013.
[223] R. Nazarov, H. J. Jin, and D. L. Kaplan, "Porous 3-D scaffolds from regenerated silk fibroin," *Biomacromolecules*, vol. 5, no. 3, pp. 718-26, May-Jun, 2004.
[224] R. M. Cooke, T. S. Harvey, and I. D. Campbell, "Solution structure of human insulin-like growth factor 1: a nuclear magnetic resonance and restrained molecular dynamics study," *Biochemistry*, vol. 30, no. 22, pp. 5484-5491, 1991.
[225] I. Schultz, J. Wurzel, and L. Meinel, "Drug delivery of Insulin-like growth factor I," *Eur J Pharm Biopharm*, vol. 97, no. Pt B, pp. 329-37, Nov, 2015.
[226] M. Sivaramakrishnan, A. S. Kashyap, B. Amrein, S. Saenger, S. Meier, C. Staudenmaier, Z. Upton, and F. Metzger, "PEGylation of lysine residues reduces the pro-migratory activity of IGF-I," *Biochim Biophys Acta*, vol. 1830, no. 10, pp. 4734-42, Oct, 2013.
[227] W. Zhang, T. A. Gustafson, W. J. Rutter, and J. D. Johnson, "Positively charged side chains in the insulin-like growth factor-1 C- and D-regions determine receptor binding specificity," *J Biol Chem*, vol. 269, no. 14, pp. 10609-13, Apr 08, 1994.
[228] M. L. Bayne, J. Applebaum, D. Underwood, G. G. Chicchi, B. G. Green, N. S. Hayes, and M. A. Cascieri, "The C-Region of Human Insulin-Like Growth-Factor (Igf)-I Is Required for High-Affinity Binding to the Type-1 Igf Receptor," *Journal of Biological Chemistry*, vol. 264, no. 19, pp. 11004-11008, Jul 5, 1989.
[229] M. Sivaramakrishnan, T. I. Croll, R. Gupta, D. Stupar, D. R. Van Lonkhuyzen, Z. Upton, and G. K. Shooter, "Lysine residues of IGF-I are substrates for transglutaminases and modulate downstream IGF-I signalling," *Biochim Biophys Acta*, vol. 1833, no. 12, pp. 3176-85, Dec, 2013.
[230] D. R. Clemmons, W. H. Busby, T. Arai, T. J. Nam, J. B. Clarke, J. I. Jones, and D. K. Ankrapp, "Role of insulin-like growth factor binding proteins in the control of IGF actions," *Progress in Growth Factor Research*, vol. 6, no. 2-4, pp. 357-366, 1995.
[231] A. Denley, L. J. Cosgrove, G. W. Booker, J. C. Wallace, and B. E. Forbes, "Molecular interactions of the IGF system," *Cytokine Growth Factor Rev*, vol. 16, no. 4-5, pp. 421-39, Aug-Oct, 2005.
[232] B. Tabisz, W. Schmitz, M. Schmitz, T. Luehmann, E. Heusler, J. C. Rybak, L. Meinel, J. E. Fiebig, T. D. Mueller, and J. Nickel, "Site-Directed Immobilization of BMP-2: Two Approaches for the Production of Innovative Osteoinductive Scaffolds," *Biomacromolecules*, Feb 17, 2017.
[233] H. Madry, A. Rey-Rico, J. K. Venkatesan, B. Johnstone, and M. Cucchiarini, "Transforming growth factor Beta-releasing scaffolds for cartilage tissue engineering," *Tissue Eng Part B Rev*, vol. 20, no. 2, pp. 106-25, Apr, 2014.
[234] J. S. Park, H. J. Yang, D. G. Woo, H. N. Yang, K. Na, and K. H. Park, "Chondrogenic differentiation of mesenchymal stem cells embedded in a scaffold by long-term release of TGF-beta 3 complexed with chondroitin sulfate," *J Biomed Mater Res A*, vol. 92, no. 2, pp. 806-16, Feb, 2010.
[235] L. Bian, D. Y. Zhai, E. Tous, R. Rai, R. L. Mauck, and J. A. Burdick, "Enhanced MSC chondrogenesis following delivery of TGF-beta3 from alginate microspheres within hyaluronic acid hydrogels in vitro and in vivo," *Biomaterials*, vol. 32, no. 27, pp. 6425-34, Sep, 2011.
[236] M. Morille, T. Van-Thanh, X. Garric, J. Cayon, J. Coudane, D. Noel, M. C. Venier-Julienne, and C. N. Montero-Menei, "New PLGA-P188-PLGA matrix enhances TGF-beta3 release from pharmacologically active microcarriers and promotes chondrogenesis of mesenchymal stem cells," *J Control Release*, vol. 170, no. 1, pp. 99-110, Aug 28, 2013.

[237] N. D. Cerletti, G. K. D. Mcmaster, D. D. Cox, A. D. Schmitz, and B. D. Meyhack, "Process for the production of biologically active protein (e.g. TGF)," Google Patents, 1991.
[238] N. Cerletti, "Process for the production biologically active dimeric protein," Google Patents, 2000.
[239] J. Pellaud, U. Schote, T. Arvinte, and J. Seelig, “Conformation and self-association of human recombinant transforming growth factor-beta3 in aqueous solutions,” *J Biol Chem*, vol. 274, no. 12, pp. 7699-704, Mar 19, 1999.
[240] P. ten Dijke, K. K. Iwata, C. Goddard, C. Pieler, E. Canalis, T. L. McCarthy, and M. Centrella, “Recombinant transforming growth factor type beta 3: biological activities and receptor-binding properties in isolated bone cells,” *Mol Cell Biol*, vol. 10, no. 9, pp. 4473-9, Sep, 1990.
[241] Q. O. Tang, K. Shakib, M. Heliotis, E. Tsiridis, A. Mantalaris, U. Ripamonti, and E. Tsiridis, “TGF-beta3: A potential biological therapy for enhancing chondrogenesis,” *Expert Opin Biol Ther*, vol. 9, no. 6, pp. 689-701, Jun, 2009.
[242] K. Pelttari, E. Steck, and W. Richter, “The use of mesenchymal stem cells for chondrogenesis,” *Injury*, vol. 39 Suppl 1, pp. S58-65, Apr, 2008.
[243] C. Le Roy, and J. L. Wrana, “Clathrin- and non-clathrin-mediated endocytic regulation of cell signalling,” *Nat Rev Mol Cell Biol*, vol. 6, no. 2, pp. 112-26, Feb, 2005.
[244] Y. Ito, G. Chen, and Y. Imanishi, “Artificial juxtacrine stimulation for tissue engineering,” *J Biomater Sci Polym Ed*, vol. 9, no. 8, pp. 879-90, 1998.
[245] Y. G. Chen, “Endocytic regulation of TGF-beta signaling,” *Cell Res*, vol. 19, no. 1, pp. 58-70, Jan, 2009.
[246] J. C. Chow, “Insulin-like Growth Factor-I Receptor Internalization Regulates Signaling via the Shc/Mitogen-activated Protein Kinase Pathway, but Not the Insulin Receptor Substrate-1 Pathway,” *Journal of Biological Chemistry*, vol. 273, no. 8, pp. 4672-4680, 1998.
[247] A. Wiedlocha, and V. Sorensen, “Signaling, internalization, and intracellular activity of fibroblast growth factor,” *Curr Top Microbiol Immunol*, vol. 286, pp. 45-79, 2004.
[248] J. Martel-Pelletier, D. J. Welsch, and J. P. Pelletier, “Metalloproteases and inhibitors in arthritic diseases,” *Best Pract Res Clin Rheumatol*, vol. 15, no. 5, pp. 805-29, Dec, 2001.
[249] C. J. Malemud, “Matrix metalloproteinases (MMPs) in health and disease: an overview,” *Front Biosci*, vol. 11, pp. 1696-701, May 01, 2006.
[250] A. C. Braun, M. Gutmann, R. Ebert, F. Jakob, H. Gieseler, T. Luhmann, and L. Meinel, “Matrix Metalloproteinase Responsive Delivery of Myostatin Inhibitors,” *Pharm Res*, vol. 34, no. 1, pp. 58-72, Jan, 2017.
[251] M. Wu, G. Chen, and Y. P. Li, “TGF-beta and BMP signaling in osteoblast, skeletal development, and bone formation, homeostasis and disease,” *Bone Res*, vol. 4, pp. 16009, 2016.
[252] M. E. Joyce, A. B. Roberts, M. B. Sporn, and M. E. Bolander, “Transforming growth factor-beta and the initiation of chondrogenesis and osteogenesis in the rat femur,” *J Cell Biol*, vol. 110, no. 6, pp. 2195-207, Jun, 1990.

8 Summary

During the last decades the number of biologics increased dramatically and several biopharmaceutical drugs such as peptides, therapeutic proteins, hormones, enzymes, vaccines, monoclonal antibodies and antibody-drug conjugates conquered the market. Moreover, administration and local delivery of growth factors has gained substantial importance in the field of tissue engineering. Despite progress that has been made over the last decades formulation and delivery of therapeutic proteins is still a challenge. Thus, we worked on formulation and delivery strategies of therapeutic proteins to improve their biological performance.

Phase I of this work deals with protein stability with the main focus on a liquid protein formulation of the dimeric fusion protein PR-15, a lesion specific platelet adhesion inhibitor. In order to develop an adequate formulation ensuring the stability and bioactivity of PR-15 during storage at 4 °C, a pH screening, a forced degradation and a Design of Experiments (DoE) was performed. First the stability and bioactivity of PR-15 in 50 mM histidine buffer in relation to pH was evaluated in a short-term storage stability study at 25 °C and 40 °C for 4 and 8 weeks using different analytical methods. Additionally, potential degradation pathways of PR-15 were investigated under stressed conditions such as heat treatment, acidic or basic pH, freeze-thaw cycles, light exposure, induced oxidation and induced deamidation during the forced degradation study. Moreover, we were able to identify the main degradation product of PR-15 by performing LC/ESI-MS analysis. Further optimization of the injectable PR-15 formulation concerning pH, the choice of buffer and the addition of excipients was studied in the following DoE and finally an optimal PR-15 formulation was found.

The growth factors BMP-2, IGF-I and TGF-β3 were selected for the differentiation of stem cells for tissue engineering of cartilage and bone in order to prepare multifunctionalized osteochondral implants for the regeneration of cartilage defects.

Silk fibroin (SF) was chosen as biomaterial because of its biocompatibility, mechanical properties and its opportunity for biofunctionalization. Ideal geometry of SF scaffolds with optimal porosity was found in order to generate both tissues on one scaffold.

The growth factors BMP-2 and IGF-I were modified to allow spatially restricted covalent immobilization on the generated porous SF scaffolds. In order to perform site-directed covalent coupling by the usage of click chemistry on two opposite sides of the scaffold, we genetically engineered BMP-2 (not shown in this work; performed by Barbara Tabisz) and IGF-I for the introduction of alkyne or azide bearing artificial amino acids. TGF-β3 was immobilized to beads through common EDC/NHS chemistry requiring no modification and distributed in the pores of the entire scaffold.

For this reason protein modification, protein engineering, protein immobilization and bioconjugation are investigated in **phase II**. Beside the synthesis the focus was on the characterization of such modified proteins and its conjugates. The field of protein engineering offers a wide range of possibilities to modify existing proteins or to design new proteins with prolonged serum half-life, increased conformational stability or improved release rates according to their clinical use.

Site-directed click chemistry and non-site-directed EDC/NHS chemistry were used for bioconjugation and protein immobilization with the aim to underline the preferences of site-directed coupling.

We chose three strategies for the incorporation of alkyne or azide functionality for the performance of click reaction into the protein of interest: diazonium coupling reaction, PEGylation and genetic engineering. Azido groups were successfully introduced into SF by implementation of diazonium coupling and alkyne, amino or acid functionality was incorporated into FGF-2 as model protein by means of thiol PEGylation. The proper folding of FGF-2 after PEGylation was assessed by fluorescence spectroscopy, WST-1 proliferation assay ensured moderate bioactivity and the purity of PEGylated FGF-2 samples was monitored with RP-HPLC. Moreover, the modification of native FGF-2 with 10 kDa PEG chains resulted in enhanced thermal stability.

Additionally, we genetically engineered one IGF-I mutant by incorporating the unnatural amino acid propargyl-L-lysine (plk) at position 65 into the IGF-I amino acid sequence and were able to express hardly verifiable amounts of plk-IGF-I. Consequently, plk-IGF-I expression has to be further optimized in future studies in order to generate plk-IGF-I with higher yields.

Bioconjugation of PEGylated FGF-2 with functionalized silk was performed in solution and was successful for click as well as EDC/NHS chemistry. However, substantial amounts of unreacted PEG-FGF-2 were adsorbed to SF and could not be removed from the reaction mixture making it impossible to expose the advantages of click chemistry in relation to EDC/NHS chemistry. The immobilization of PEG-FGF-2 to microspheres was a trial to increase product yield and to remove unreacted PEG-FGF-2 from reaction mixture. Bound PEG-FGF-2 was visualized by fluorescence imaging or flow cytometry and bioactivity was assessed by analysis of the proliferation of NIH 3T3 cells. However, immobilization on beads raised the same issue as in solution: adsorption caused by electrostatic interactions of positively charged FGF-2 and negatively charged SF or beads. Finally, we were not able to prove superiority of site-directed click chemistry over non-site-directed EDC/NHS.

The skills and knowledge in protein immobilization as well as protein characterization acquired during phase II helped us in **phase III** to engineer cartilage tissue in biofunctionalized SF scaffolds. The approach of covalent immobilization of the required growth factors is relevant because of their short in vivo half-lives and aimed at controlling their bioavailability. So TGF-β3 was covalently coupled by means of EDC/NHS chemistry to biocompatible and biostable PMMA beads. Herein,

we directly compared bioactivity of covalently coupled and adsorbed TGF-β3. During the so-called luciferase assay bioactivity of covalent coupled as well as adsorbed TGF-β3 on PMMA beads was ensured. In order to investigate the real influence of EDC/NHS chemistry on TGF-β3's bioactivity, the amount of immobilized TGF-β3 on PMMA beads was determined. Therefore, an ELISA method was established. The assessment of total amount of TGF-β3 immobilized on the PMMA beads allowed as to calculate coupling efficiency. A significantly higher coupling efficiency was determined for the coupling of TGF-β3 via EDC/NHS chemistry compared to the reaction without coupling reagents indicating a small amount of adsorbed TGF-β3. These results provide opportunity to determine the consequence of coupling by means of EDC/NHS chemistry for TGF-β3 bioactivity. At first sight, no statistically significant difference between covalent immobilized and adsorbed TGF-β3 was observed regarding relative luciferase activities. But during comparison of total and active amount of TGF-β3 on PMMA beads detected by ELISA or luciferase assay, respectively, a decrease of TGF-β3's bioactivity became apparent. Nevertheless, immobilized TGF-β3 was further investigated in combination with SF scaffolds in order to drive BMSCs to the chondrogenic lineage. According to the results obtained through histological and immunohistochemical studies, biochemical assays as well as qRT-PCR of gene expression from BMSCs after 21 days in culture immobilized TGF-β3 was able to engineer cartilage tissue. These findings support the thesis that local presentation of TGF-β3 is superior towards exogenous TGF-β3 for the development of hyaline cartilage. Furthermore, we conclude that covalent immobilized TGF-β3 is not only superior towards exogenously supplemented TGF-β3 but also superior towards adsorbed TGF-β3 for articular hyaline cartilage tissue engineering. Diffusion processes were inhibited through covalent immobilization of TGF-β3 to PMMA beads and thereby a stable and consistent TGF-β3 concentration was maintained in the target area.

With the knowledge acquired during phase II and III as well as during the studies of Barbara Tabisz concerning the expression and purification of plk-BMP-2 we made considerable progress towards the formation of multifunctionalized osteochondral implants for the regeneration of cartilage defects. However, further studies are required for the translation of these insights into the development of multifunctionalized osteochondral SF scaffolds.

9 Zusammenfassung

In den letzten Jahrzehnten stieg die Zahl der Biologika dramatisch an und mehrere biopharmazeutische Arzneimittel wie Peptide, therapeutische Proteine, Hormone, Enzyme, Impfstoffe, monoklonale Antikörper und Antikörper-Wirkstoff-Konjugate eroberten den Markt. Darüber hinaus hat die Applikation und lokale Verabreichung von Wachstumsfaktoren im Bereich des Tissue Engineerings eine wesentliche Bedeutung erlangt. Trotz der in den letzten Jahrzehnten erzielten Fortschritte ist die Formulierung und Verabreichung therapeutischer Proteine noch immer eine Herausforderung. Daher haben wir uns in dieser Arbeit mit der Formulierung und Verabreichung therapeutischer Proteine beschäftigt und Strategien entwickelt, um deren biologische Wirkung zu verbessern.

In **Phase I** dieser Arbeit konzentrieren wir uns auf die Stabilität des dimeren Fusionsproteins PR-15, einem Inhibitor der Adhäsion von Plättchen an arterielle Gefäßläsionen. Um eine geeignete flüssige Formulierung zu entwickeln, welche die Stabilität und Bioaktivität von PR-15 während der Lagerung bei 4 °C sicherstellt, wurde ein pH Screening, eine Forced Degradation Studie und ein Design of Experiments (DoE) durchgeführt. Zuerst wurde die Stabilität und Bioaktivität von PR-15 bei verschiedenen pH Werten in 50 mM Histidinpuffer in einer Kurzzeitstabilitätsstudie bei 25 °C und 40 °C nach 4 und 8 Wochen mit Hilfe verschiedener analytischer Methoden beobachtet. Des Weiteren wurden mögliche Abbauwege von PR-15 unter Stressbedingungen wie erhöhter Temperatur, saurem oder basischem pH-Wert, Einfrier-Auftau-Zyklen, Lichteinwirkung, induzierter Oxidation sowie induzierter Deamidierung während der Forced Degradation Studie untersucht. Darüber hinaus konnten wir das Hauptabbauprodukt von PR-15 durch LC/ESI-MS Analysen identifizieren. Im folgenden DoE wurde die injizierbare PR-15 Formulierung weiter optimiert und bezüglich pH, der Wahl des Puffers sowie der Zugabe von Hilfsstoffen analysiert, bis letztendlich eine optimale PR-15-Formulierung gefunden wurde.

Die Wachstumsfaktoren BMP-2, IGF-I und TGF-β3 wurden zur Differenzierung von Stammzellen für das Tissue Engineering von Knochen und Knorpel ausgewählt, um multifunktionalisierte osteochondrale Implantate zur Regeneration von Knorpeldefekten herzustellen. Seidenfibroin (SF) wurde aufgrund seiner Biokompatibilität, seiner mechanischen Eigenschaften und seiner Möglichkeiten zur Biofunktionalisierung als Biomaterial gewählt. Zuerst wurden SF-Scaffolds mit idealer Geometrie und optimaler Porosität erzeugt, um sowohl Knochen also auch Knorpel auf einem Scaffold herzustellen. Um eine räumlich begrenzte kovalente Immobilisierung der Wachstumsfaktoren BMP-2 und IGF-I auf den porösen SF-Scaffolds zu ermöglichen, wurden diese mit unnatürlichen Aminosäuren genetisch modifiziert. Das Einführen von Alkin- bzw. Azidresten in die Aminosäuresequenz von BMP-2 (in dieser Arbeit nicht gezeigt; von Barbara Tabisz durchgeführt) und IGF-I erlaubt unter Verwendung der Click-Chemie eine ortsgerichtete kovalente Kopplung der Wachstumsfaktoren an zwei gegenüberliegenden Seiten der Scaffolds. TGF-β3

wurde durch gewöhnliche EDC/NHS-Chemie, welche keine Modifikation erforderte, kovalent an Mikrosphären immobilisiert und in den Poren des gesamten SF-Scaffolds verteilt.
Daher beschäftigen wir uns in **Phase II** mit der Modifikation von Proteinen, dem Protein Engineering, der Immobilisation von Proteinen und mit Biokonjugation. Neben der Synthese lag der Fokus auf der Charakterisierung modifizierter Proteine und deren Konjugaten. Das Gebiet des Protein Engineerings bietet eine Vielzahl von Möglichkeiten, bestehende Proteine zu modifizieren oder neue Proteine mit verlängerter Serumhalbwertszeit, erhöhter konformativer Stabilität oder verbesserten Freisetzungsraten entsprechend der klinischen Anwendung zu entwickeln.
Die ortsspezifische Click-Chemie und die nicht-ortsspezifische EDC/NHS-Chemie wurden für die Biokonjugation und die Immobilisierung von Proteinen verwendet mit dem Ziel, die Vorzüge der ortsgerichteten Kopplung hervorzuheben. Für den Einbau der für die Durchführung der Click-Reaktion erforderlichen Alkin- bzw. Azidfunktionalität in das betreffende Protein wurden drei Strategien ausgewählt: die Azokupplung, die PEGylierung und die gentechnische Modifizierung. Azidgruppen wurden mittels Azokupplung erfolgreich in SF eingebaut und die Alkin-, Amino- oder Säurefunktionalität wurde mittels PEGylierung der Cysteine in das Modellprotein FGF-2 integriert. Die korrekte Faltung von FGF-2 nach erfolgreicher PEGylierung wurde durch Fluoreszenzspektroskopie bestätigt, im WST-1 Proliferationsassay wurde eine angemessene Bioaktivität festgestellt und die Reinheit von PEGylierten FGF-2 wurde mittels RP-HPLC analysiert. Darüber hinaus führte die Modifikation von nativem FGF-2 mit 10 kDa PEG-Ketten zu einer erhöhten thermischen Stabilität.
Des Weiteren wurde ein IGF-I-Mutant gentechnisch hergestellt, indem die unnatürliche Aminosäure Propargyl-L-Lysin (Plk) an Position 65 in die IGF-I-Sequenz eingebaut wurde. Da letztendlich lediglich kaum nachweisbare Mengen an Plk-IGF-I exprimiert werden konnten, muss die Plk-IGF-I-Expression in anschließenden Studien weiter optimiert werden, um Plk-IGF-I mit höheren Ausbeuten erzeugen zu können.
Die Biokonjugation von PEGyliertem FGF-2 und funktionalisierter Seide wurde sowohl mittels Click- als auch mittels EDC/NHS-Chemie erfolgreich durchgeführt. Allerdings wurden erhebliche Mengen PEG-FGF-2 lediglich an SF adsorbiert und nicht kovalent gekoppelt und konnten schlussendlich nicht aus dem Reaktionsgemisch entfernt werden. Die anschließende Immobilisierung von PEG-FGF-2 an Mikrosphären, war ein Versuch die Ausbeute der Reaktion zu erhöhen und adsorbiertes PEG-FGF-2 leichter zu entfernen. Immobilisiertes PEG-FGF-2 wurde mittels Fluoreszenzmikroskopie und/oder Durchflusszytometrie nachgewiesen und die Bioaktivität wurde durch die Analyse der Proliferation von NIH-3T3-Zellen ermittelt. Die Immobilisierung auf Mikrosphären führte jedoch zu demselben Problem wie in Lösung: Adsorption von positiv geladenem FGF-2 an negativ geladenes SF bzw. negativ geladenen Mikrosphären durch elektrostatische Wechselwirkungen. Schließlich waren wir nicht in der Lage, die Überlegenheit der ortsgerichteten Click-Chemie gegenüber der nicht-ortsgerichteten EDC/ NHS-Chemie zu beweisen.

Die während Phase II erworbenen Fähigkeiten und Kenntnisse im Bereich der Immobilisierung und Charakterisierung von Proteinen halfen uns in **Phase III** Knorpelgewebe in biofunktionalisierten SF-Scaffolds zu erzeugen. Der Ansatz der kovalenten Immobilisierung, der für das Tissue Engineering von Knorpel erforderlichen Wachstumsfaktoren, ist aufgrund ihrer kurzen *in vivo* Halbwertszeiten von Bedeutung und zielt darauf ab, ihre Bioverfügbarkeit zu kontrollieren. So wurde TGF-β3 mittels EDC/NHS-Chemie kovalent an biokompatible und biostabile PMMA-Mikrosphären gekoppelt. Mit Hilfe des sogenannten Luciferase-Assays wurden die Bioaktivitäten von kovalent gekoppeltem sowie von adsorbiertem TGF-β3 auf PMMA-Mikrosphären ermittelt. Um die Kopplungseffizienz zu berechnen und den tatsächlichen Einfluss der EDC/NHS-Chemie auf die Bioaktivität von TGF-β3 zu untersuchen, wurde die Menge an immobilisiertem TGF-β3 auf PMMA-Mikrosphären mittels ELISA bestimmt. Für die Kopplung von TGF-β3 mittels EDC/NHS-Chemie wurde eine signifikant höhere Kopplungseffizienz im Vergleich zu der Reaktion ohne Kopplungsreagenzien, welche eine geringe Menge an adsorbiertem TGF-β3 zeigte, bestimmt. Bei alleiniger Betrachtung der Ergebnisse des Luciferase-Assays, bei welchem kein statistisch signifikanter Unterschied zwischen kovalent immobilisiertem und adsorbiertem TGF-β3 bezüglich der relativen Luciferase-Aktivität beobachtet wurde, scheint es als hätte die EDC/NHS-Kopplung keinen Einfluss auf die Bioaktivität von TGF-β3. Beim Vergleich der mittels ELISA bestimmten TGF-β3 Gesamtmenge und der mittels Luciferase-Assay bestimmten Menge an aktivem TGF-β3 auf den PMMA-Mikrosphären, wurde jedoch ein Verlust der Bioaktivität von TGF-β3 durch die EDC/NHS-Kopplung deutlich. Ungeachtet dessen, wurde immobilisiertes TGF-β3 genutzt, um Knorpelgewebe in SF-Scaffolds aus BMSCs zu generieren. Nach den Ergebnissen der histologischen und immunhistochemischen Untersuchungen, der biochemischen Assays sowie der qRT-PCR der Genexpression von BMSCs nach 21 Tagen in Kultur, gelang es uns unter Verwendung von immobilisiertem TGF-β3 Knorpelgewebe aufzubauen. Diese Ergebnisse unterstützen die These, dass die lokale Präsentation von TGF-β3 gegenüber exogen zugegebenem TGF-β3 für die Entwicklung von hyalinem Knorpel überlegen ist. Außerdem schließen wir daraus, dass kovalent immobilisiertes TGF-β3 nicht nur gegenüber exogen zugegebenem TGF-β3 für die Entwicklung von hyalinem Knorpelgewebe überlegen ist, sondern auch gegenüber adsorbiertem TGF-β3. Diffusionsprozesse konnten durch kovalente Immobilisierung von TGF-β3 an PMMA-Mikrosphären verhindert werden und damit eine stabile und gleichmäßige TGF-β3-Konzentration am Wirkort aufrechterhalten werden.

Mit den in Phase II und III gewonnenen Erkenntnissen und den Untersuchungen von Barbara Tabisz zur Expression und Aufreinigung von plk-BMP-2 haben wir erhebliche Fortschritte bei der Entwicklung multifunktionaler osteochondraler Implantate zur Regeneration von Knorpeldefekten gemacht. Für die Umsetzung dieser Erkenntnisse zur Herstellung multifunktionaler osteochondraler SF-Scaffolds sind jedoch weitere Studien erforderlich.

10 Appendix

10.1 Supplementary data

Exp No	*Run Order*	*Buffer*	*pH*	*Tween® 20 [%]*	*Methionine [mM]*
1	4	Phosphate	7.0	0	6.667
2	1	Phosphate	7.0	0.1	13.333
3	2	Phosphate	7.0	0.033	0
4	3	Phosphate	7.0	0.067	20

Table 18: Run order of sample preparation in phosphate buffer pH 7.0.

Exp No	*Run Order*	*Buffer*	*pH*	*Tween® 20 [%]*	*Methionine [mM]*
5	1	Phosphate	8.0	0	13.333
6	2	Phosphate	8.0	0.1	6.667
7	3	Phosphate	8.0	0.067	0
8	4	Phosphate	8.0	0.033	20

Table 19: Run order of sample preparation in phosphate buffer pH 8.0.

Exp No	*Run Order*	*Buffer*	*pH*	*Tween® 20 [%]*	*Methionine [mM]*
9	2	Phosphate	7.667	0	0
11	1	Phosphate	7.667	0.1	0

Table 20: Run order of sample preparation in phosphate buffer pH 7.667.

Exp No	*Run Order*	*Buffer*	*pH*	*Tween® 20 [%]*	*Methionine [mM]*
10	1	Phosphate	7.333	0	20
12	2	Phosphate	7.333	0.1	20

Table 21: Run order of sample preparation in phosphate buffer pH 7.333.

Exp No	*Run Order*	*Buffer*	*pH*	*Tween® 20 [%]*	*Methionine [mM]*
13	3	Histidine	7.0	0	0
15	2	Histidine	7.0	0.1	0
17	1	Histidine	7.0	0	20
19	4	Histidine	7.0	0.1	20

Table 22: Run order of sample preparation in histidine buffer pH 7.0.

Exp No	*Run Order*	*Buffer*	*pH*	*Tween® 20 [%]*	*Methionine [mM]*
14	4	Histidine	8.0	0	0
16	2	Histidine	8.0	0.1	0
18	3	Histidine	8.0	0	20
20	1	Histidine	8.0	0.1	20

Table 23: Run order of sample preparation in histidine buffer pH 8.0.

Exp No	*Run Order*	*Buffer*	*pH*	*Tween® 20 [%]*	*Methionine [mM]*
21	3	Histidine	7.5	0.05	10
22	2	Histidine	7.5	0.05	10
23	4	Histidine	7.5	0.05	10
24	5	Histidine	7.5	0.05	10
25	1	Histidine	7.5	0.05	10

Table 24: Run order of sample preparation in histidine buffer pH 7.5.

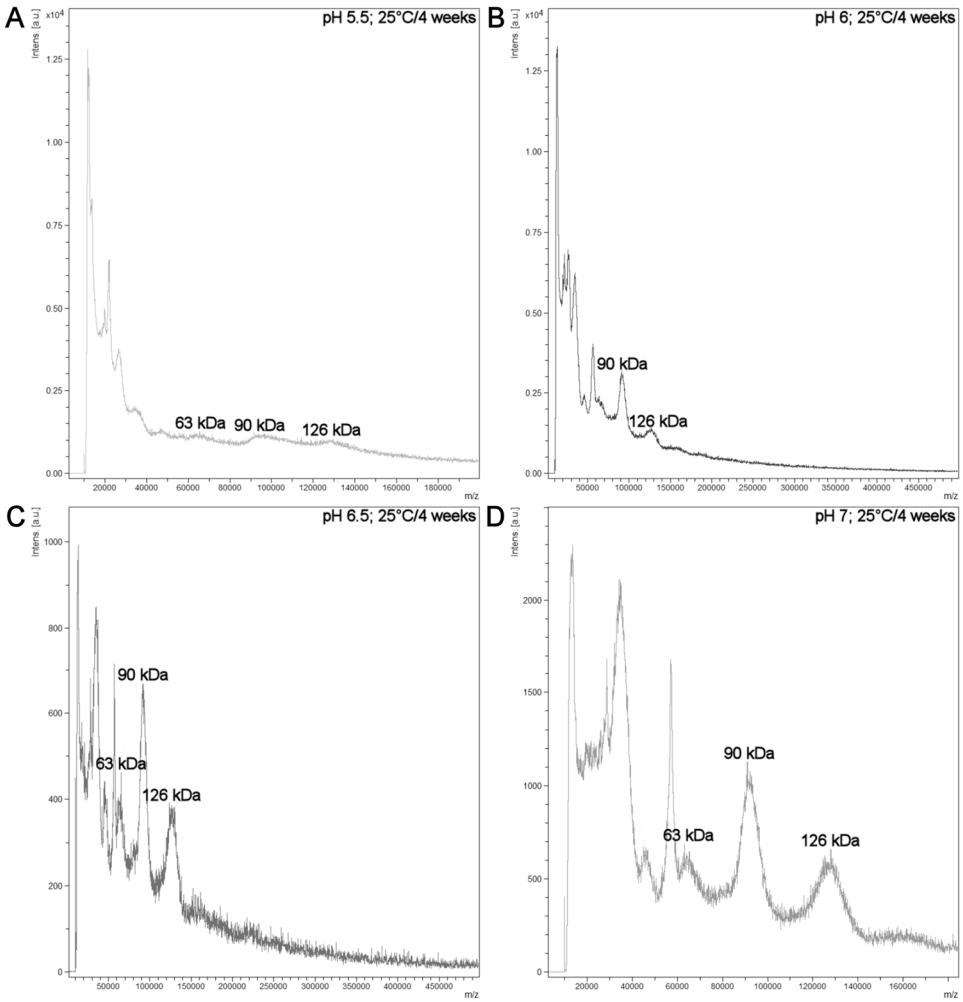

Supplementary Figure 1: MALDI-TOF MS spectra of PR-15 samples after incubation at 25 °C for 4 weeks at (A) pH 5.5, (B) pH 6.0, (C) pH 6.5 and (D) pH 7.0.

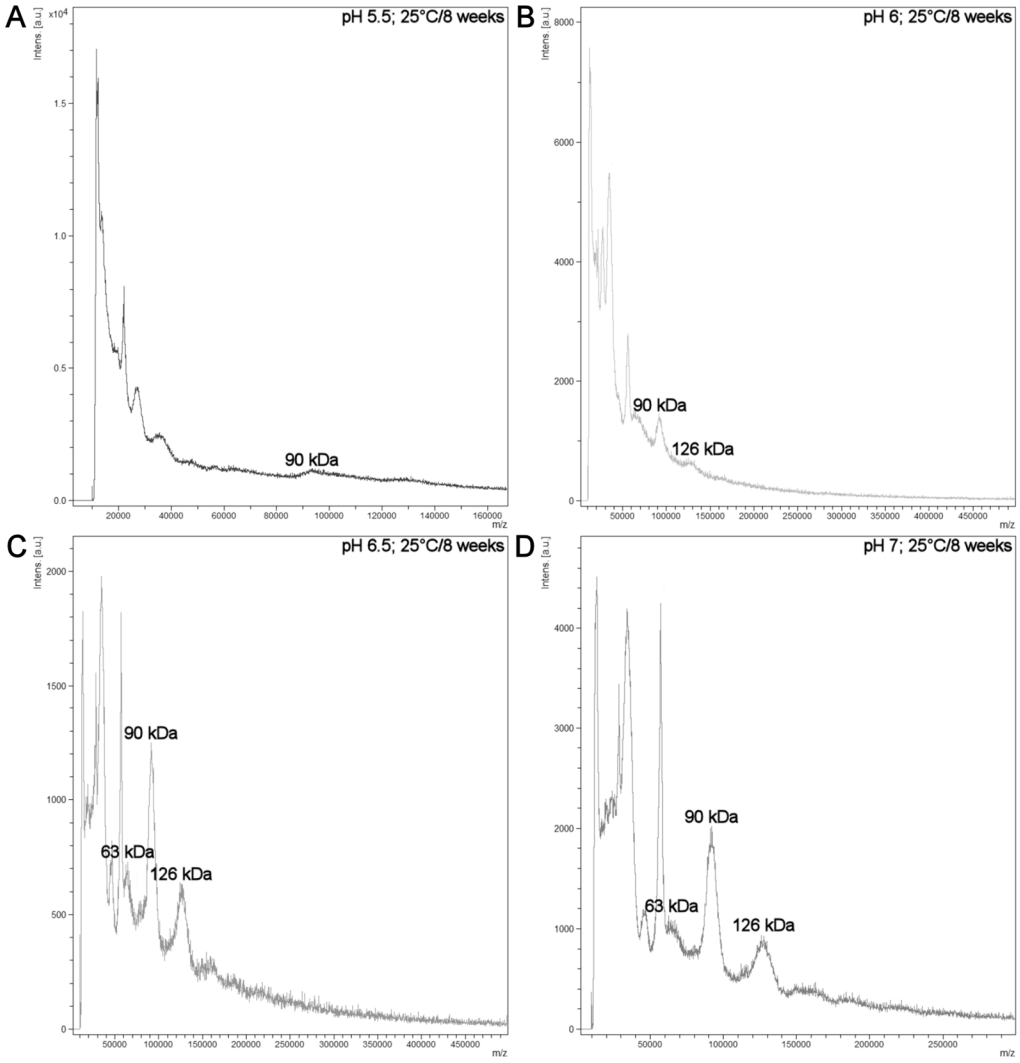

Supplementary Figure 2: MALDI-TOF MS spectra of PR-15 samples after incubation at 25 °C for 8 weeks at (A) pH 5.5, (B) pH 6.0, (C) pH 6.5 and (D) pH 7.0.

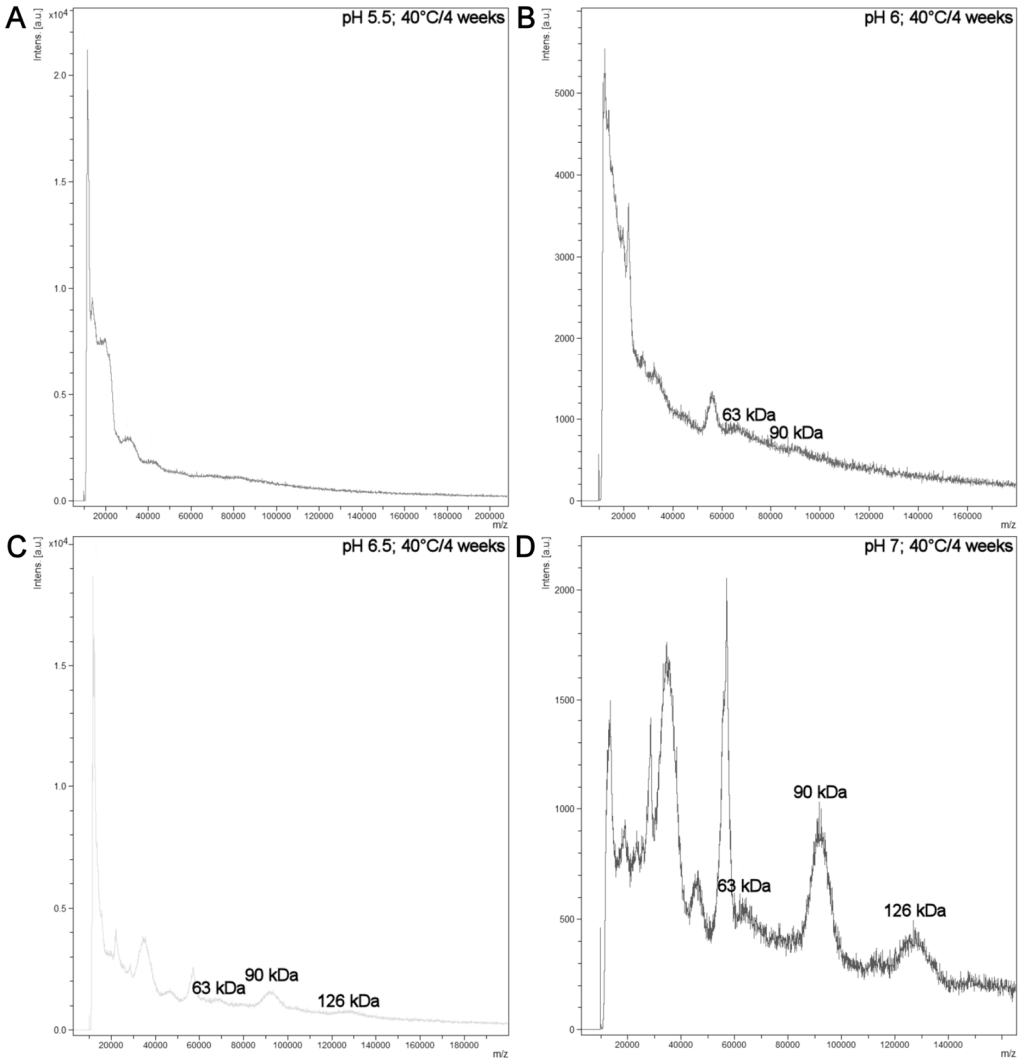

Supplementary Figure 3: MALDI-TOF MS spectra of PR-15 samples after incubation at 40 °C for 4 weeks at (A) pH 5.5, (B) pH 6.0, (C) pH 6.5 and (D) pH 7.0.

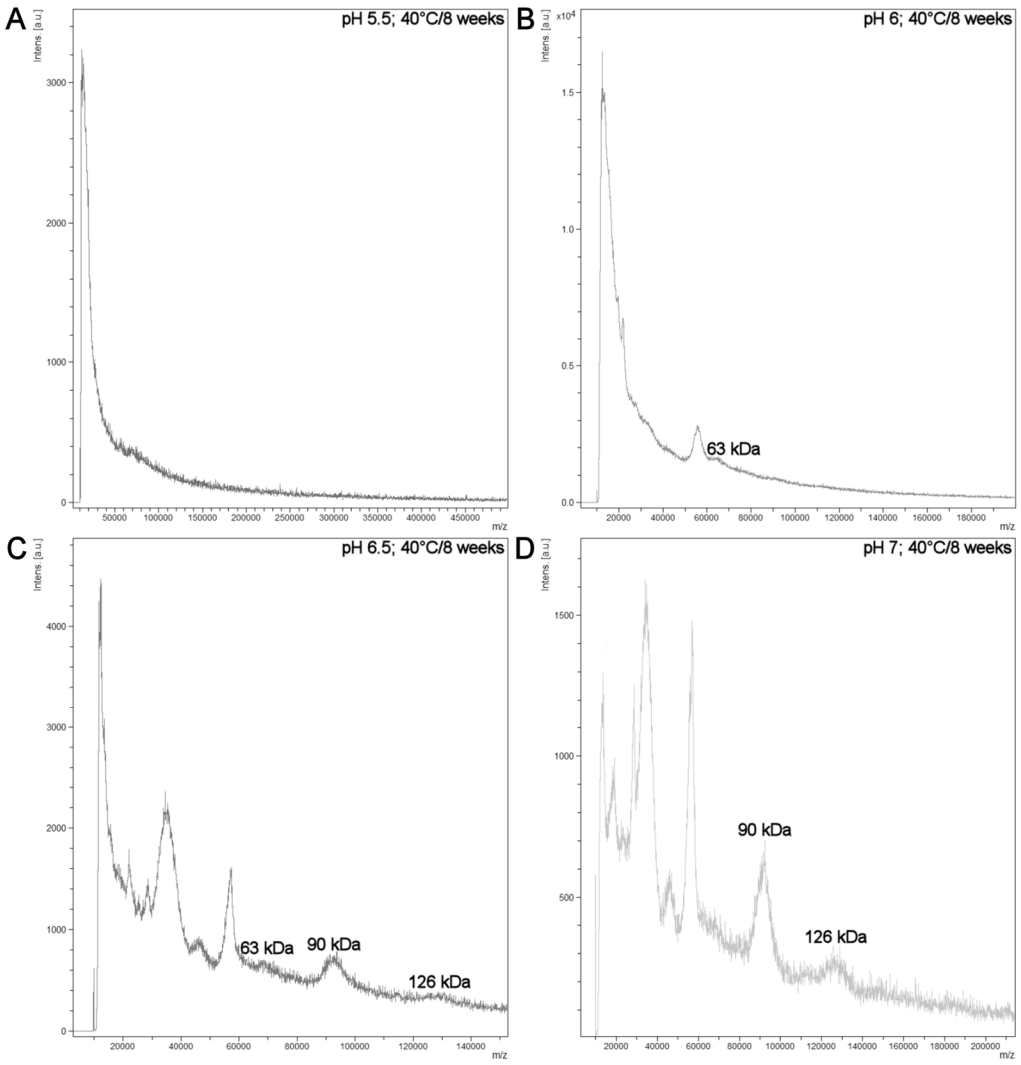

Supplementary Figure 4: MALDI-TOF MS spectra of PR-15 samples after incubation at 40 °C for 8 weeks at (A) pH 5.5, (B) pH 6.0, (C) pH 6.5 and (D) pH 7.0.

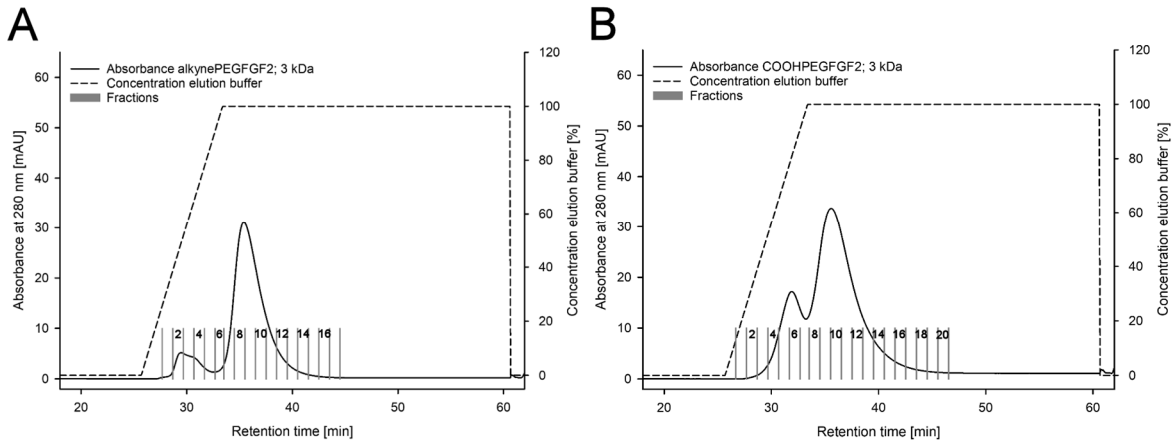

Supplementary Figure 5: Elution chromatogram of (A) 3 kDa alkyne-PEG-FGF-2 (fractions 6–14) and (B) 3 kDa COOH-PEG-FGF-2 (fractions 8–17) from heparin column.

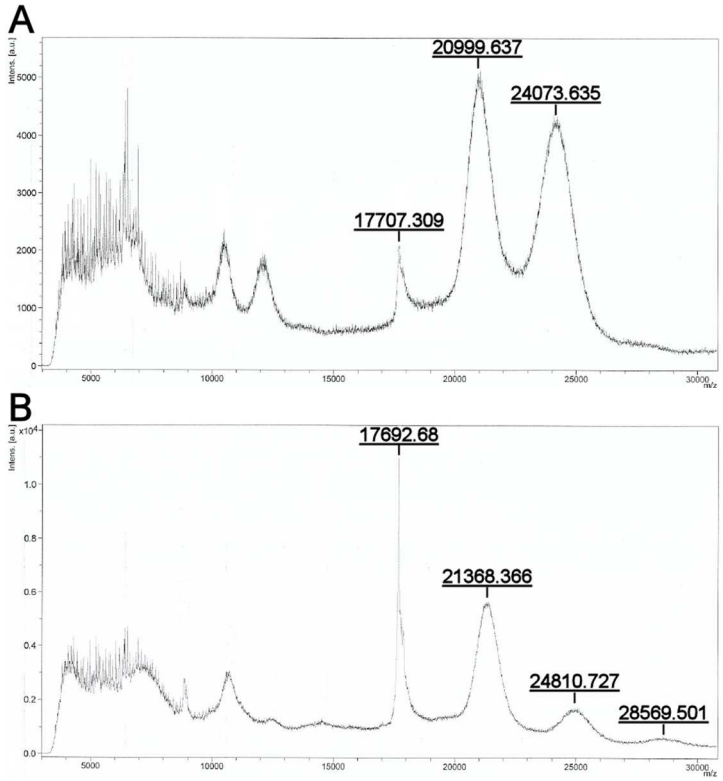

Supplementary Figure 6: MALDI-TOF MS spectra of FGF-2 after (A) PEGylation with iodoacetamido-PEG-alkyne (3 kDa) and (B) after PEGylation with iodoacetyl-PEG-acid (3 kDa). Reprinted from [87], Copyright (2014), with permission from Elsevier.

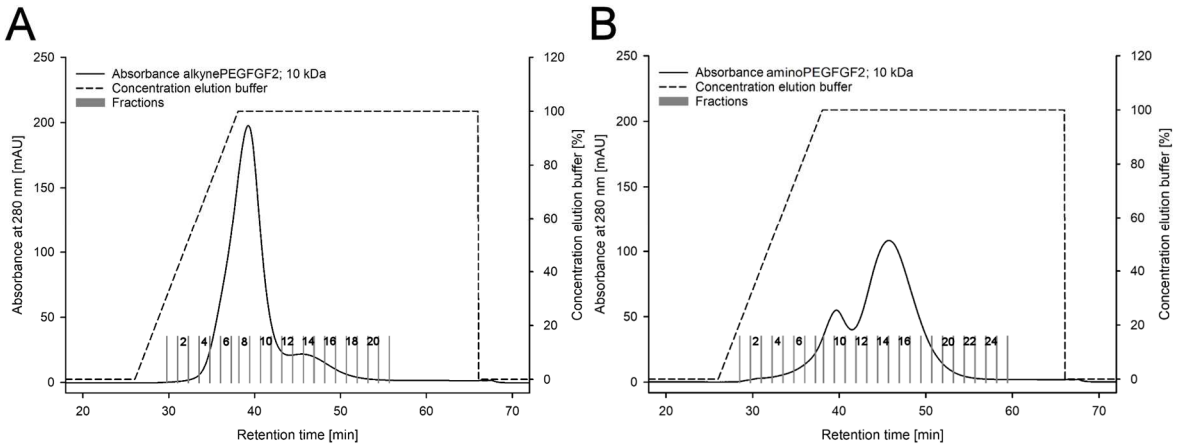

Supplementary Figure 7: Elution chromatogram of (A) 10 kDa alkyne-PEG-FGF-2 (fractions 1–10) and (B) 10 kDa amino-PEG-FGF-2 (fractions 1–9) from heparin column.

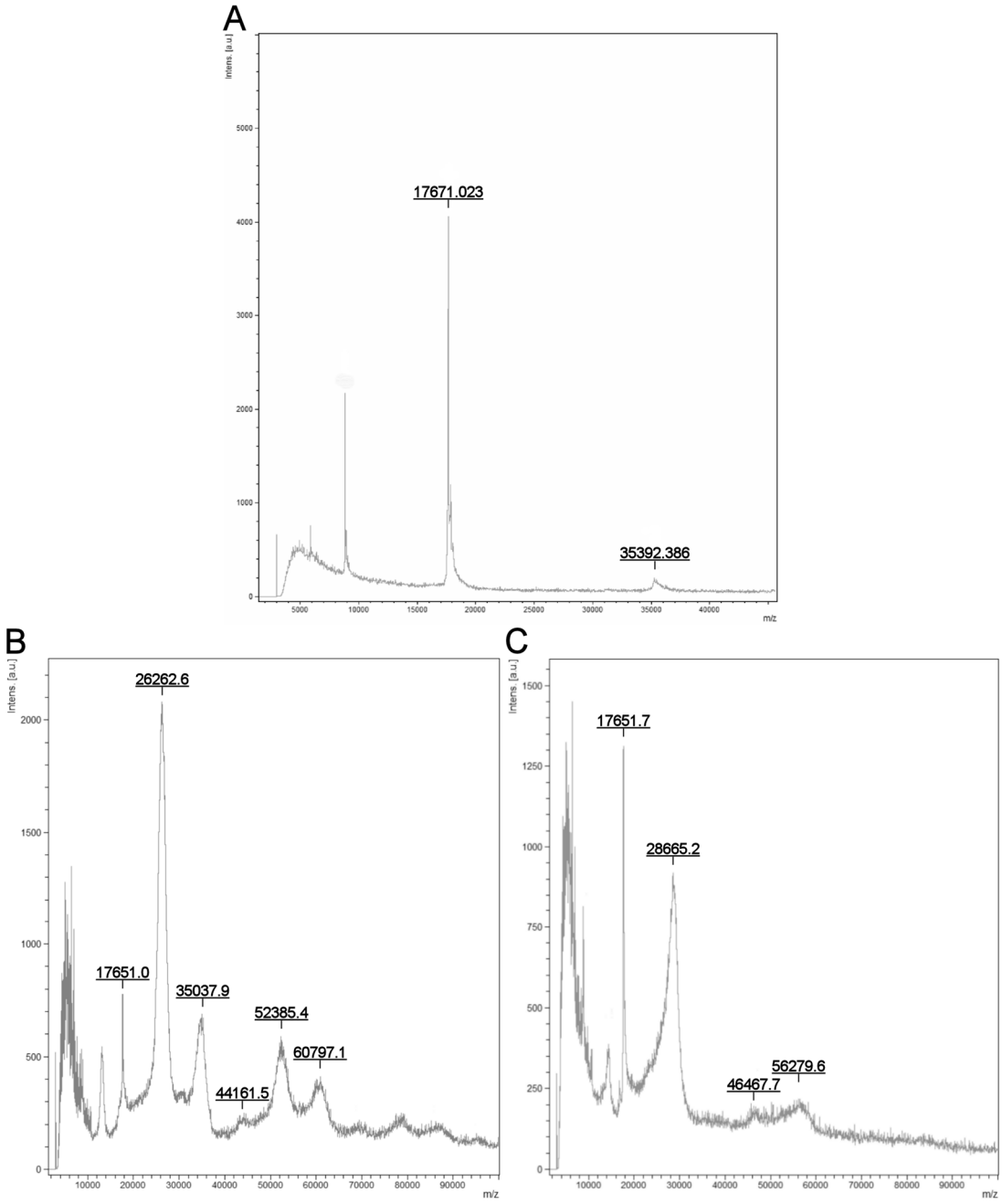

Supplementary Figure 8: MALDI-TOF MS spectra of (A) FGF-2 reference, (B) FGF-2 after PEGylation with 10 kDa iodoacetamido-PEG-alkyne and (C) FGF-2 after PEGylation with 10 kDa iodoacetamido-PEG-amid.

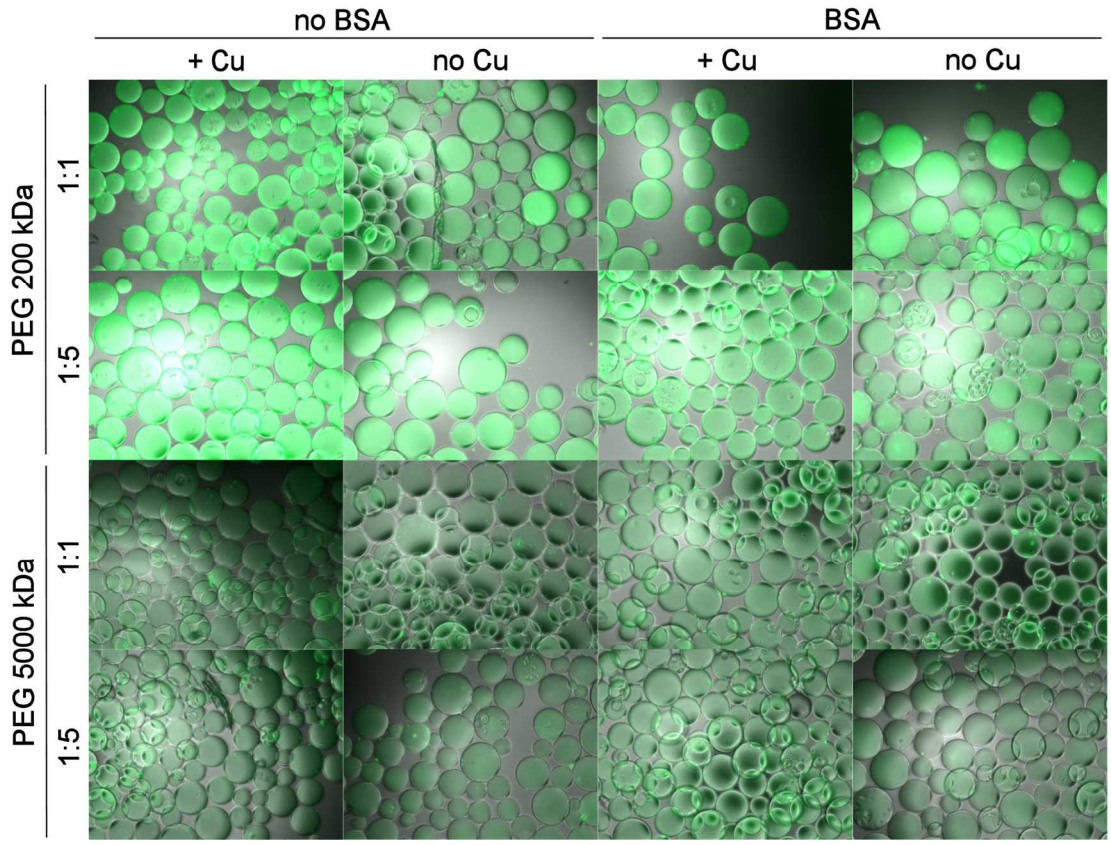

Supplementary Figure 9: Fluorescence images of sepharose beads after FGF-2 immobilization and incubation with primary FGF-2 and secondary FITC labelled antibody.

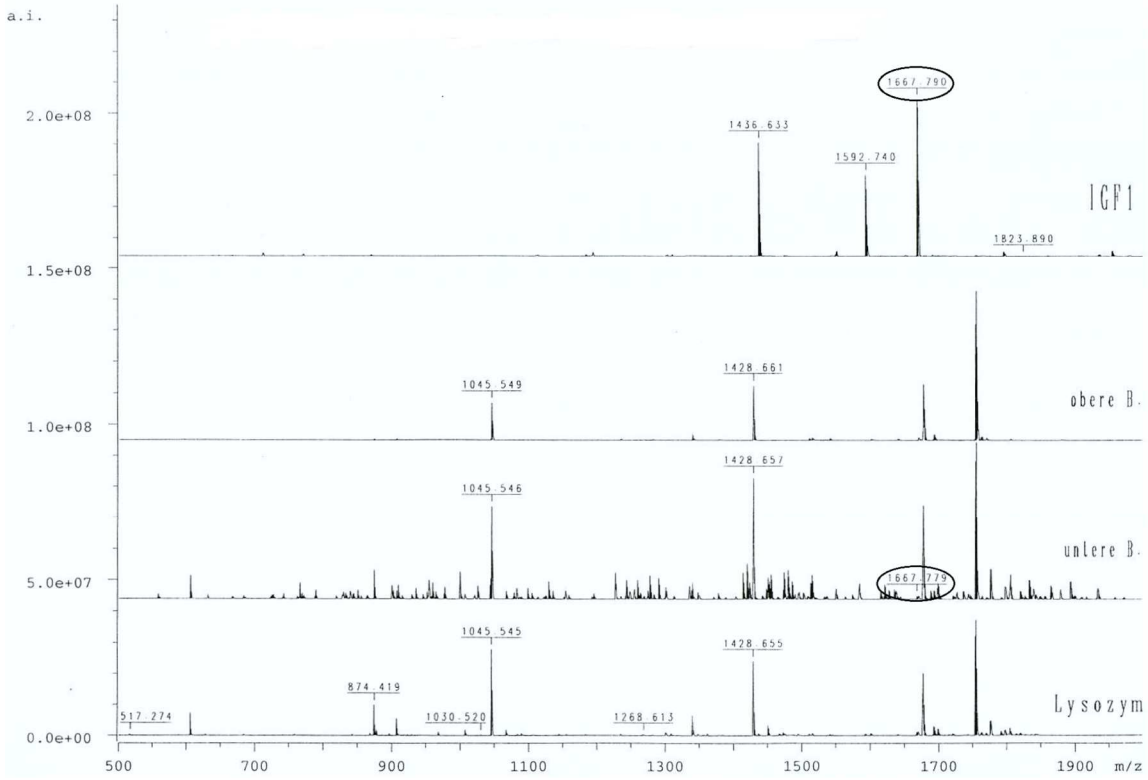

Supplementary Figure 10: ESI/MS spectra of IGF-I reference, lysozyme and two cut bands in close proximity to each other at the height of IGF-I reference after in-gel tryptic digestion.

10.2 Supplementary information

NMR

Propargyl-L-lysine

Molecular formula: $C_{10}H_{16}N_2O_4$ (+ $C_2HF_3O_2$)

Molecular weight: 228.25 g/mol (+ 114.02 g/mol Trifluoroacetic acid)

^{1}H-NMR (D_2O, δ [ppm], J [Hz]): 4.70 (d, 2H, $^4J_{H,H}$ = 1.9 Hz, Nr. 3), 3.88 (t, 1H, $^3J_{H,H}$ = 6.2 Hz, Nr. 9), 3.19 (t, 2H, $^3J_{H,H}$ = 6.8 Hz, Nr. 5), 2.93 (t, 1H, $^4J_{H,H}$ = 1.9 Hz, Nr. 1), 2.06–1.83 (m, 2H, Nr. 6/7), 1.66–1.53 (m, 2H, Nr. 8), 1.53–1.36 (m, 2H, Nr. 6/7).

^{13}C-NMR (DMSO-d_6, δ [ppm], J [Hz]): 173.9 (Nr. 10), 157.6 (Nr. 4), 78.6 (Nr.1), 75.6 (Nr. 2), 54.1 (Nr. 3), 52.7 (Nr. 9), 40.0 (Nr. 5), 29.8 (Nr. 6/7), 28.4 (Nr. 8), 21.5 (Nr. 6/7).

DNA sequences of human IGF-I

ATGGGAAAAA TCAGCAGTCT TCCAACCCAA TTATTTAAGT GCTGCTTTTG TGATTTCTTG
AAGGTGAAGA TGCACACCAT GTCCTCCTCG CATCTCTTCT ACCTGGCGCT GTGCCTGCTC
ACCTTCACCA GCTCTGCCAC GGCTGGACCG GAGACGCTCT GCGGGGCTGA GCTGGTGGAT
GCTCTTCAGT TCGTGTGTGG AGACAGGGGC TTTTATTTCA ACAAGCCCAC AGGGTATGGC
TCCAGCAGTC GGAGGGCGCC TCAGACAGGC ATCGTGGATG AGTGCTGCTT CCGGAGCTGT
GATCTAAGGA GGCTGGAGAT GTATTGCGCA CCCCTCAAGC CTGCCAAGTC AGCTCGCTCT
GTCCGTGCCC AGCGCCACAC CGACATGCCC AAGACCCAGA AGGAAGTACA TTTGAAGAAC
GCAAGTAGAG GGAGTGCAGG AAACAAGAAC TACAGGATGT AG

signal peptide propeptide IGF-I chain E-peptide lysine 65

10.3 List of Abbreviations

A	Absorbance
ACN	Acetonitrile
AGC	Automatic gain control
ATCC	American Type Cultured Collection
BMP-2	Bone morphogenetic protein 2
B. mori	Bombyx mori
BSA	Bovine serum albumin
cDNA	Complementary deoxyribonucleic acid
CCD	Central composite design
CME	Cellulose mixed ester
CRP	Collagen related peptide
CRP-XL	Cross-linked collagen-related peptide
CuAAC	Cu(I)-catalyzed azide-alkyne cycloaddition
DLS	Dynamic light scattering
DMEM	Dulbecco’s Modified Eagle Medium
DMMB	Dimethylmethylene blue
DMSO	Dimethyl sulfoxide
DNA	Deoxyribonucleic acid
DoE	Design of Experiments
DPBS	Dulbecco’s phosphate buffered saline
DSF	Differential scanning fluorimetry
DTT	Dithiothreitol
ECM	Extracellular matrix
E. coli	Escherichia coli
EDC	N-ethyl-N’-(3-(dimethylamino)propyl)carbodiimide
EDTA	Ethylenediaminetetraacetate
ELISA	Enzyme-linked immunosorbent assay
ESI	Electronspray ionization
FACS	Fluorescence-activated cell sorting
FBS	Fetal bovine serum
FCS	Fetal calf serum
FD	Forced degradation
FGF-2	Fibroblast growth factor 2
FPLC	Fast protein liquid chromatography
GAG	Glycosaminoglycans

GM-CSF	Granulocyte-macrophage colony-stimulating factor
Gln	Glutamine
GP VI	Glycoprotein
HIC	Hydrophobic interaction chromatography
hMSC	human mesenchymal stem cells
HRP	Horse radish peroxidase
ICH	International Council of Harmonization
IGF-I	Insulin-like growth factor I
IgG	Immunoglobulin G
IPTG	Isopropyl β-D-1-thiogalactopyranoside
IL-4	Interleukin 4
LB	Lysogeny broth
LC/ESI-MS	Liquid chromatography/Electrospray ionization mass spectrometry
mAB	monoclonal antibody
MALDI MS	Matrix-assisted laser desorption/ionization mass spectrometry
MALDI-TOF MS	Matrix-assisted laser desorption ionization time-of-flight mass spectrometry
MES	2-(N-morpholino)ethanesulfonic acid
mRNA	Messenger ribonucleic acid
MS	Mass spectrometry
MSC	Mesenchymal stem cells
MWCO	Molecular weight cut-off
m/z	mass to charge ratio
NH_4HCO_3	Ammonium hydrogen carbonate
NHS	N-hydroxysuccinimide
oCPC	ortho-cresolphthalein complexone
OD	Optical density
PBS	Phosphate buffered saline
PCL	Polycaprolactone
PCR	Polymerase chain reaction
PdI	Polydispersity index
PEG	Poly(ethylene glycol)
PEI	Polyethylenimine
Pen/Strep	Penicillin and streptomycin
pERK	Phosphorylated extracellular signal-regulated kinase
PES	Polyethersulfone
PGA	Poly(glycolic acid)

pI	Isoelectric point
PLA	Poly(lactic acid)
PLGA	Poly(lactic-coglycolic acid)
Plk	Propargyl-L-lysine
PMMA	Poly(methyl methacrylate)
PMSF	Phenylmethylsulfonyl fluoride
PNGase	Peptide-N-glycosidase
PS	Polystyrene
PS	Penicillin-streptomycin
R^2	Coefficient of determination
RNA	Ribonucleic acid
RP-HPLC	Reversed-phase high performance liquid chromatography
RSM	Response surface methodology
RT	Room temperature
RT-PCR	Reverse transcription polymerase chain reaction
SBE	SMAD binding element
SDS	Sodium dodecylsulfate
SDS-PAGE	Sodium dodecylsulfate polyacrylamide gel electrophoresis
SEC	Size exclusion chromatography
SEI	Secondary electron imaging
SEM	Scanning electron microscopy
SF	Silk fibroin
SOC	Super Optimal Broth
TAE	Tris-acetate-EDTA
TB	Terrific broth
TBTA	Tris(benzyltriazolylmethyl)amine
TEMED	Tetramethylenediamine
TERT	Telomerase reverse transcriptase
TFA	Trifluoracetic acid
TGF-β3	Transforming growth factor beta 3
TLC	Thin-layer chromatography
TMB	Tetramethylbenzidine
UV	Ultraviolet
VEGF	Vascular endothelial growth factor
VIS	Visible
WST	Water soluble tetrazolium salt

10.4 Buffers and solutions

50 mM Histidine buffer, adjusted to the appropriate pH

L-histidine Reagent Plus® ≥ 99 % (TLC)	7.78 g
Ultrapure water	ad 1 L

50 mM Phosphate buffer, pH 7.0

Sodium dihydrogen phosphate	0.6343 g
Disodium hydrogen phosphate	1.0241 g
Ultrapure water	ad 250 mL

50 mM Phosphate buffer, pH 7.333

Sodium dihydrogen phosphate	0.3809 g
Disodium hydrogen phosphate	1.3239 g
Ultrapure water	ad 250 mL

50 mM Phosphate buffer, pH 7.667

Sodium dihydrogen phosphate	0.2044 g
Disodium hydrogen phosphate	1.5327 g
Ultrapure water	ad 250 mL

50 mM Phosphate buffer, pH 8.0

Sodium dihydrogen phosphate	0.1024 g
Disodium hydrogen phosphate	1.6533 g
Ultrapure water	ad 250 mL

5 mM Citrate buffer, pH 3.8

Citric acid * H_2O	0.3677 g
Sodium citrate * 2 H_2O	0.2206 g
Ultrapure water	ad 500 mL

Mercapto-Strip-Buffer

10 % SDS	20 mL
0.5 M Tris HCl, pH 6.8	12.5 mL
Ultrapure water	67.5 mL
β-Mercaptoethanol	800 µL

10x Western blot buffer

Trizma base	30.3 g
Glycin	144.1 g
Ultrapure water	ad 1 L

1x Western blot buffer

10x WB buffer	100 mL
Water	500 mL
Methanol	200 mL
Ultrapure water	ad 1 L

10x TBS (pH 7.6)

Trizma base	18.62 g
NaCl	80.06 g
Ultrapure water	ad 1 L

1x TBST

10x TBS	100 mL
10 % Tween 20	10 mL
Ultrapure water	ad 1 L

APS solution

Ammonium persulfate	10 %

Coomassie Brilliant Blue staining solution

Coomassie Brilliant Blue (Bio-Rad)	1 g
Methanol	500 mL
Glacial acetic acid	100 mL
Ultrapure water	400 mL

Coomassie destaining solution

Glacial acetic acid	10 % (v/v)
Methanol	20 % (v/v)

Reducing SDS sample buffer (6x)

SDS	1 g
Glycerol	3 mL
1 M Tris, pH 6.8	3.5 mL
Bromophenol blue	1.2 mg
DTT	0.93 g
Ultrapure water	ad 10 mL

Non-reducing Laemmli sample buffer (4x)

1 M Tris pH 6.8	2.4 mL
SDS pellets	0.8 g
Glycerol 100 %	4 mL
Bromophenol blue	0.01 %
Ultrapure water	3.8 mL

4x reducing Laemmli sample buffer

1 M Tris pH 6.8	2.4 mL
SDS pellets	0.8 g
Glycerol 100 %	4 mL
Bromophenol blue	0.01 %
β-mercaptoethanol	1 mL
Ultrapure water	2.8 mL

Tris acetate SDS running buffer

20x Novex Tris-acetate-SDS running buffer	50 mL
Ultrapure water	ad 1 L

SDS electrophoresis buffer

Tris	25 mM
Glycine	192 mM
SDS	1 %

Transfer buffer

Tris	25 mM
Glycine	192 mM
Methanol	20 % (v/v)

Stacking gel buffer (4x), pH 6.8

Tris	500 mM
SDS	0.4 %

Separating gel buffer (4x), pH 8.8

Tris	1.5 M
SDS	0.4 %

Acrylamide/bisacrylamide solution 30 % / 0.8 %

Acrylamide	30 % (w/v)
N,N'-methylenebisacrylamide	0.8 %

Separating gel (12 %)

Acrylamide/bisacrylamide solution 30%/0.8%	6.0 mL
Separating gel buffer (4x), pH 8.8	3.75 mL
Ultrapure water	5.25 mL
APS solution	0.05 mL
TEMED	10 µL

Separating gel (15 %)

Acrylamide/bisacrylamide solution 30%/0.8%	7.5 mL
Separating gel buffer (4x), pH 8.8	3.75 mL
Ultrapure water	3.75 mL
APS solution	0.05 mL
TEMED	10 µL

Stacking gel (3.9 %)

Acrylamide/bisacrylamide solution 30%/0.8%	0.65 mL
Stacking gel buffer (4x), pH 6.8	1.25 mL
Ultrapure water	3.05 mL
APS solution	25 µL
TEMED	5 µL

Eluent A, pH 7.4 (purification FGF-2)

Disodium hydrogen phosphate	10 mM
Sodium dihydrogen phosphate	2 mM
Sodium chloride	300 mM

Eluent B, pH 7.4 (purification FGF-2)

Disodium hydrogen phosphate	10 mM
Sodium dihydrogen phosphate	2 mM
Sodium chloride	1.5 M

PBS buffer, pH 7.4

Sodium chloride	80 g
Potassium chloride	2 g
Disodium hydrogen phosphate	6.09 g
Potassium dihydrogen phosphate	2 g
Ultrapure water	ad 1 L

Lysogeny broth (LB) medium, pH 7,2

Tryptone	10 g
Sodium chloride	5 g
Yeast extract	5 g
Magnesium sulfate heptahydrate	5 g
Glucose	1 g
Ultrapure water	ad 1 L

Terrific broth (TB) medium

Tryptone	12 g
Yeast extract	24 g
Glycerine	4 mL
Ultrapure water	ad 900 mL

TAE buffer, pH 8.5

Tris	40 mM
Glacial acetic acid	0.11 % (v/v)
EDTA	2 mM

SOC medium

Yeast extract	0.5 % (w/v)
Tryptone	2 % (w/v)
Sodium chloride	10 mM
Potassium chloride	2.5 mM
Magnesium chloride	10 mM
Magnesium sulfate	10 mM
Glucose	20 mM

Agar medium, pH 7.5

Agar	1.4 %
Sodium chloride	0.8 %
Tryptone	1 %
Yeast extract	0.5 %
Glucose	0.5 % (w/v)

LB glycerol medium

Glycerin	20 % (v/v)
LB medium	

10.5 Curriculum Vitae

10.6 Publications und poster presentations

Publications

Tabisz, B., Schmitz, W., Schmitz, M., Luehmann, T., **Heusler, E**., Rybak, J., Meinel, L., Fiebig, J. E., Mueller, T. D., Nickel, J. (2017). "Site-Directed Immobilization of BMP-2: Two Approaches for the Production of Innovative Osteoinductive Scaffolds." Biomacromolecules, 18(3), 695–708.

Zhao, H., **Heusler, E**., Jones, G., Li, L., Werner, V., Germershaus, O., Ritzer, J., Luehmann, T., Meinel, L. (2014). „Decoration of silk fibroin by click chemistry for biomedical application." J Struct Biol, 186(3): 420-30.

Poster presentations

Heusler, E.*, Krähnke, M.*, Blunk, T., Meinel, L. (2015). "Multifunktionalisierte osteochondrale Implantate." *Poster presentation*, IZKF Retreat, Kloster Banz, Bad Staffelstein, Germany.
* corresponding authors

Heusler, E., Jones, G., Zhao, H., Luehmann, T., Meinel, L. (2014). "Synthesis and characterization of 'clickable' alkyne-PEGylated FGF-2 and its site-directed immobilization to azide modified microspheres via click chemistry." *Poster presentation*, DPhG Annual Meeting, Frankfurt, Germany.

Krähnke, M., **Heusler, E.**, Böck, T., Blunk, T., Meinel, L. (2013). "Multifunktionalisierte Osteochondrale Implantate – Chondrogene und Osteogene Differenzierung von Mesenchymalen Stammzellen in Seidenfibroin-Scaffolds." *Poster presentation*, Deutscher Kongress für Orthopädie und Unfallchirurgie (DKOU), Berlin, Germany.

Krähnke, M., **Heusler, E.**, Böck, T., Blunk, T., Meinel, L. (2013). "Towards Engineering Osteochondral Implants – Chondrogenic and Osteogenic Differentiation of Mesenchymal Stem Cells in Silk Fibroin Scaffolds." *Poster presentation*, World Conference on Regenerative Medicine, Leipzig, Germany.

Krähnke, M., **Heusler, E.**, Blunk, T., Meinel, L. (2012). "Multifunktionalisierte osteochondrale Implantate." *Poster presentation*, IZKF Retreat, Kloster Banz, Bad Staffelstein, Germany.

10.7 Acknowledgements

First of all, I would like to express my deepest gratitude to Prof. Dr. Dr. Lorenz Meinel for giving me the opportunity to join his research group and work in this interesting field of research. I appreciated his wide scientific skills, his engagement for providing excellent equipment conditions and his helpful advice and support.
I sincerely thank my supervisor Dr. Tessa Lühmann for her dedicated guidance and encouragement during my PhD. I am very grateful for her constant support and for her most valuable and honest scientific advice.
Furthermore, I would like to express my gratitude to Prof. Dr. Petra Högger and Prof. Dr. Torsten Blunk for being my referee.
Many thanks go to Dr. Susanne Neidhold from advanceCOR GmbH for the great collaboration in Phase I and the opportunity to include these results in my PhD thesis.
Special thanks go to Prof. Dr. Torsten Blunk and Martin Krähnke from the Department of Trauma, Hand, Plastic and Reconstructive Surgery of Würzburg for their contribution to Phase III and the harmonic collaboration.
I am very grateful for the support of Dr. Joachim Nickel from the Chair of Tissue Engineering and Regenerative Medicine of Würzburg during cloning of IGF-I in Phase II and the opportunity to perform cloning experiments in his research group. He offered me his expertise and time.
I am further indebted to advanceCOR, Martin Krähnke, Alexandra Braun, Gabriel Jones, Markus Gutmann, Dr. Jennifer Ritzer, Johannes Wiest and the group of Prof. Schlosser for the performance of experiments that were beneficial for my work and made the results more meaningful.
HHAC GmbH is kindly acknowledged for the possibility to use their climate chamber TCS-301 Ph for light exposure experiments during forced degradation study of PR-15 in phase I.
Furthermore, I acknowledge the financial support of the Interdisciplinary Center for Clinical Research (IZKF) of Würzburg, grant number D-218, and the Federal Ministry of Education and Research (BMBF).
I would like to thank my PhD colleagues and the whole group for their practical as well as mental support. Christine Schneider, Dr. Sasche Zügner and Doris Moret basically supported me concerning organization as well as the supervision of students. Georg Walter, Matthias Völker and Karl Vollmuth always helped when technical problems occurred. Gabriel Jones, Isabel Schultz, Marika Kutscher, Sebastian Puhl and Joel Wurzel ensured having an enjoyable and fun time both during working and during our free time. Thank you all.
Special thanks goes to my colleague and close friend Gabriel Jones for proof-reading this thesis.
Moreover, I want to thank my brother, my parents-in-law and my close friends for their help, advices and assurances during the whole time.

Naturally, I want to deeply thank my parents for their infinite support and their constant encouragement throughout this exciting time with many ups and downs. Thank you that you always believed in me and motivated me.
Last but not least, I want to thank my husband for his constant support, his encouragement and his patience. Thank you for always being there for me and for being a valuable balance to my scientific adventure.

10.8 Documentation of experimental work not done by me

All experimental work described in this thesis was done by me, except the following:

Operator	*Institute*	*Chapter*
Dr. Jennifer Ritzer	Department of Pharmaceutical Technology and Biopharmacy, University of Würzburg, Germany	4.1.4.6 acquired MALDI-TOF MS spectra of prepared samples 4.2.2.3.2 acquired MALDI-TOF MS spectra of prepared samples
Stephanie Lamer	Rudolf Virchow Center for Experimental Biomedicine, University of Würzburg, Germany	4.1.4.7 performed trypsin digest of the excised bands and performed LC/ESI-MS analysis
Dr. Susanne Neidhold	advanceCOR GmbH, Martinsried, Germany	4.1.4.8 performed SDS-PAGE analysis 4.1.4.9 determined biological activity by collagen ELISA 4.1.4.10 determined biological activity by inhibition of platelet aggregation
Gabriel Jones	Department of Pharmaceutical Technology and Biopharmacy, University of Würzburg, Germany	4.2.2.1 expressed and purified FGF-2 4.2.2.3.4 evoked unfolding of FGF-2 and recorded emission spectrum of unfolded FGF-2
Marcus Gutmann	Department of Pharmaceutical Technology and Biopharmacy, University of Würzburg, Germany	4.2.2.1 expressed and purified FGF-2
Johannes Wiest	Institute for Pharmacy and Food Chemistry, University of Würzburg, Germany.	4.2.3.2 acquired NMR spectra
Werner Schmitz	Department of Biochemistry and Molecular Biology, University of Würzburg, Germany	4.2.3.12 acquired ESI-MS spectra
Alexandra Braun	Department of Pharmaceutical Technology and Biopharmacy, University of Würzburg, Germany	4.3.7 performed Luciferase assay to determine bioactivity of immobilized TGF-β3
Martin Krähnke	Department of Trauma, Hand, Plastic and Reconstructive Surgery, University of Würzburg, Germany	4.3.8 Isolation and culture of BMSCs 4.3.9 Culture of MSC-SF scaffold constructs and chondrogenic and osteogenic differentiation of BMSCs 4.3.10 Histology and immunohistochemistry 4.3.11 Biochemical analysis 4.3.12 RNA isolation and quantitative real-time PCR